



## **University of Huddersfield Repository**

Akowua, Kwame D.B

Integration of On-Machine Surface Metrology and Machining Process Prediction

### **Original Citation**

Akowua, Kwame D.B (2018) Integration of On-Machine Surface Metrology and Machining Process Prediction. Doctoral thesis, University of Huddersfield.

This version is available at <http://eprints.hud.ac.uk/id/eprint/35006/>

The University Repository is a digital collection of the research output of the University, available on Open Access. Copyright and Moral Rights for the items on this site are retained by the individual author and/or other copyright owners. Users may access full items free of charge; copies of full text items generally can be reproduced, displayed or performed and given to third parties in any format or medium for personal research or study, educational or not-for-profit purposes without prior permission or charge, provided:

- The authors, title and full bibliographic details is credited in any copy;
- A hyperlink and/or URL is included for the original metadata page; and
- The content is not changed in any way.

For more information, including our policy and submission procedure, please contact the Repository Team at: [E.mailbox@hud.ac.uk](mailto:E.mailbox@hud.ac.uk).

<http://eprints.hud.ac.uk/>

University of Huddersfield  
School of Computing and Engineering  
Centre for Precision Technologies (CPT)

**INTEGRATION OF ON-MACHINE  
SURFACE METROLOGY AND  
MACHINING PROCESS PREDICTION**

Kwame Dente Baffour Akowua

A thesis submitted to the University of Huddersfield in partial fulfilment of  
the requirements for the degree of

Doctor of Philosophy

November 2018

## **Copyright Statement**

1. The author of this thesis (including any appendices and/or schedules to this thesis) owns any copyright in it (the “Copyright”) and s/he has given The University of Huddersfield the right to use such copyright for any administrative, promotional, educational and/or teaching purposes.
2. Copies of this thesis, either in full or in extracts, may be made only in accordance with the regulations of the University Library. Details of these regulations may be obtained from the Librarian. This page must form part of any such copies made.
3. The ownership of any patents, designs, trademarks and any and all other intellectual property rights except for the Copyright (the “Intellectual Property Rights”) and any reproductions of copyright works, for example graphs and tables (“Re- productions”), which may be described in this thesis, may not be owned by the author and may be owned by third parties. Such Intellectual Property Rights and Reproductions cannot and must not be made available for use without the prior written permission of the owner(s) of the relevant Intellectual Property Rights and/or Reproductions

## **Abstract**

As the demand for manufactured parts increase tremendously due to the short life span of products as well as mass production in this era; one of the most challenging problems faced production and quality departments is to ensure that the quality of manufactured parts is not compromised over quantity.

In order to avoid excess downtime during quality assessments, on-line or on-machine inspection is becoming preferred over off-line inspection. For dimensional inspection, on-machine probing can be adopted to reduce the need for manual or CMM based inspection. For typical surfaces produced on CNC machine tools used in advanced manufacturing industries, there is currently no on-machine measurement solution. To ensure high surface quality as well as high throughput on a typical shop floor; this thesis presents two approaches to enhance the chances of right-first-time manufacturing.

The first is a new methodology that exploits the characteristics of a 2D laser line scanner for fast, on-machine areal surface measurement at the micro-scale level. A commercial low-cost laser triangulation instrument is improved and utilised to obtain a high resolution and wider measurement area suitable for the identification of a range of areal roughness parameters on machined parts produced using a typical milling process.

Crucially, the traceability for the new methodology is also established. This includes reports of the measurement uncertainties associated with each of its metrological characteristics (MCs) and the combined uncertainty of each of its axes. The MCs that were considered include measurement noise, residual flatness, linearity deviation, perpendicularity deviation and amplification coefficient. A comparison of the novel technique with conventional lab-based surface metrology instrument shows a high correlation (99 %) between parameters as well as its ability to identify key features on a machined part such as scratches. The inspected surfaces had  $S_a$  ( $0.3 - 6 \mu m$ ) which covers most of the advanced manufacturing industries such as aerospace, automotive and civil nuclear.

The second approach involves the development of a novel method for enhancing

surface quality and machining parameter prediction on the manufacturing shop floor. A proposed artificial neural networks (ANN) model is utilised to predict the quality of the surface of manufactured parts based on the machining conditions as a preliminary or ‘pre-process’ tool before manufacturing. Pilot investigations leading to the selection of the appropriate parameters other than only  $S_a$  to be used as the output of the model is conducted. Also, other investigations that improve the robustness of the developed model to ensure that accurate prediction can be made were conducted.

Finally, the proposed model is shown to compare favourably to alternative models in literature with different network architectures, training and learning algorithms. The model was validated for a range of conditions and was confirmed to have an accuracy of  $S_q$  (91%),  $S_{al}$  (93%) and  $S_a$  (91%) even for process parameters that were outside of the range used for training the model.

## **Acknowledgements**

With God all things are possible; therefore, all thanks and praises are due to God for his love, grace and blessings that has made possible, the completion of this work. I would like to thank all my supervisors; Dr. Simon Fletcher, Professor Andrew Longstaff and Dr. Naeem Mian for helping and directing me in every stage of my research. They have not only guided me but also trusted and believed in me at each phase of my research. Thank you to all of my colleagues at the Centre for Precision Technologies. The opportunity to work with not just diverse, but knowledgeable and skilled group of people has been a thing of joy. Great thanks to my parents; Mr. & Mrs Dente Baffour – Akowua and my pastor; Pastor Rebecca Siyolwe, for the love, support and care. I will forever be grateful to you. Thank to my sisters; Mrs Akosua Dardey, Miss Regina Akua Boakyiwaa and Miss Akosua Abrafi, for their love.

# Contents

<i>Abstract</i> .....	<i>ii</i>
<i>Acknowledgements</i> .....	<i>iv</i>
<i>Contents</i> .....	<i>v</i>
<i>List of Tables</i> .....	<i>ix</i>
<i>List of Figures</i> .....	<i>xi</i>
<i>List of nomenclature</i> .....	<i>xiv</i>
<i>List of acronyms</i> .....	<i>xviii</i>
Chapter 1                          Introduction.....	1
<b>1.1         Inspection in manufacturing process</b> .....	<b>2</b>
<b>1.2         Surface metrology</b> .....	<b>4</b>
<b>1.3         Research motivation</b> .....	<b>5</b>
<b>1.4         Research aims and objectives</b> .....	<b>6</b>
<b>1.5         Scope of research</b> .....	<b>7</b>
<b>1.6         The structure of this thesis</b> .....	<b>9</b>
Chapter 2                          Literature review .....	11
<b>2.1         Metrology in manufacturing processes</b> .....	<b>11</b>
<b>2.2         Branches of metrology in manufacturing industries</b> .....	<b>13</b>
2.2.1 <i>Dimensional metrology</i> .....	14
2.2.2 <i>Geometrical metrology</i> .....	15
2.2.3 <i>Surface metrology</i> .....	16
<b>2.3Instrumentation for surface metrology</b> .....	<b>16</b>
2.3.1 <i>Interferometry-Based techniques for surface metrology</i> .....	17
2.3.2 <i>Non-Interferometry techniques for surface metrology</i> .....	22
<b>2.4         Requirements for on-machine surface metrology instrumentation in manufacturing</b> .....	<b>24</b>
<b>2.5Modelling methods in surface metrology</b> .....	<b>27</b>
2.5.1 <i>Principle-based models</i> .....	30

2.5.2	<i>Empirical-based models</i> .....	33
<b>2.6</b>	<b>Summary of review and gaps.....</b>	<b>37</b>
2.6.1	<i>Measurement .....</i>	37
2.6.2	<i>Predictive model.....</i>	38
Chapter 3 .....		40
<b>3.1</b>	<b>General description of laser triangulation .....</b>	<b>40</b>
<b>3.2</b>	<b>Laser line scanner –Keyence LJ -V7000.....</b>	<b>42</b>
3.2.1	<i>Description of the identified instrument .....</i>	42
3.2.2	<i>Specification of the identified instrument .....</i>	43
3.2.3	<i>Benefits of blue laser over red laser in metrology.....</i>	46
3.2.4	<i>Data type obtained from the laser line scanner .....</i>	47
3.2.5	<i>Selection of sampling frequency for on-machine surface metrology .....</i>	47
<b>3.3</b>	<b>Improving lateral resolution in profile axis of LJ-V7020K.....</b>	<b>52</b>
3.3.1	<i>Procedure for performing MDS of areal measurement.....</i>	53
3.3.2	<i>Effect of perpendicularity deviation error on MDS techniques .....</i>	60
<b>3.4</b>	<b>Simulation of noise compensation using MDS for surface measurement .....</b>	<b>62</b>
3.4.1	<i>Simulation of ideal face-milled surface topology .....</i>	63
3.4.2	<i>Quantification of environmental noise on height measurement.....</i>	65
3.4.3	<i>Simulation of ideal face-milled surface topology plus noise .....</i>	72
<b>3.5</b>	<b>Summary of chapter .....</b>	<b>75</b>
Chapter 4 .....		77
<b>4.1</b>	<b>Calibration procedures .....</b>	<b>78</b>
4.1.1	<i>Development of a cross-grating artefact suitable for calibrating MDS .....</i>	80
4.1.2	<i>Measurement noise of MDS technique.....</i>	84
4.1.3	<i>Residual flatness of MDS technique .....</i>	88
4.1.3	<i>Amplification coefficient and linearity deviation of MDS technique .....</i>	91
4.1.4	<i>Perpendicularity deviation .....</i>	99
<b>4.3</b>	<b>Measurement of uncertainty associated with MDS measurement .....</b>	<b>100</b>
4.3.1	<i>Scale contribution .....</i>	101
4.3.2	<i>Perpendicularity contribution .....</i>	102
4.3.3	<i>Noise contribution.....</i>	102

<b>4.4</b>	<b>Comparison with another surface metrology instrument .....</b>	<b>103</b>
4.4.1	<i>Rules of comparison .....</i>	103
4.4.2	<i>Benchmark instrument .....</i>	105
4.4.3	<i>Samples used for comparison.....</i>	105
4.4.4	<i>Results from comparison.....</i>	106
<b>4.5</b>	<b>Summary of chapter.....</b>	<b>110</b>
Chapter 5 .....		111
<b>5.1</b>	<b>Best measurement area to represent a milled surface .....</b>	<b>112</b>
<b>5.2</b>	<b>Controlling degradation of the tool tip during face-milling ..</b>	<b>114</b>
<b>5.3</b>	<b>Appropriate areal parameters to distinguish milled parts with different surface topologies .....</b>	<b>121</b>
5.3.1	<i>Procedure for selection of best areal parameter .....</i>	122
5.3.2	<i>Results and discussion; selection of appropriate areal parameter .....</i>	124
<b>5.4</b>	<b>Influence of machining conditions on areal parameters.....</b>	<b>126</b>
5.4.1	<i>Analysis of variance(ANOVA) .....</i>	127
5.4.2	<i>Main effects of cutting parameters on areal parameters .....</i>	129
<b>5.5</b>	<b>Summary of chapter.....</b>	<b>131</b>
Chapter 6 .....		133
<b>6.1</b>	<b>Artificial Intelligence (AI) methods.....</b>	<b>134</b>
6.1.1	<i>Basic introduction to ANN .....</i>	135
6.1.2	<i>Selecting the right network structure and functions for ANN model .....</i>	136
6.1.3	<i>Quality assessment of developed models .....</i>	138
<b>6.2</b>	<b>Development of the ANN .....</b>	<b>139</b>
6.2.1	<i>Conventional surface topography predictive model .....</i>	140
6.2.2	<i>Enclosed multiple network model for surface topography prediction....</i>	142
<b>6.3</b>	<b>Validation of chosen models .....</b>	<b>143</b>
<b>6.4</b>	<b>Comparison of results for models with measured results .....</b>	<b>146</b>
<b>6.5</b>	<b>Summary of chapter.....</b>	<b>149</b>
Chapter 7 .....		150
<b>7.1</b>	<b>Thesis summary .....</b>	<b>150</b>

<b>7.2</b>	<b>Contribution and novelty.....</b>	<b>158</b>
<b>7.3</b>	<b>Future works .....</b>	<b>159</b>
 References .....		161
<b>Appendices.....</b>		172
	<i>Appendix A ..... Surface Metrology Parameters.....</i>	172
A.1	<i>Profile Parameters .....</i>	172
A.2	<i>Surface texture Areal Parameters .....</i>	174
<i>Appendix B..... Data sheet of Keyence LJ-V7020K sensor head .....</i>		193
B.1	<i>Specifications LJ-V7020K sensor head.....</i>	193
B.2	<i>Dimensions of LJ-V7020K sensor head. Reproduced from Keyence [119].</i>	194
<i>Appendix C.....Results from Optiv_Classic CMM.....</i>		195
C.1	<i>Results obtained from measuring distance between groove .....</i>	195
C.2	<i>Results obtained from measuring the optical dimensional standard 200</i>	
<i>Appendix D .....Images and topologies .....</i>		201
D.1	<i>Mitutyo SFM 001 .....</i>	201
D.2	<i>Rough sample face milled surface .....</i>	202
D.3	<i>Smooth sample face milled surface.....</i>	204
<i>Appendix E..... Cross-correlation table.....</i>		206
<i>Appendix F..... Cutting Parameters, corresponding surface Roughness, and Their S/N .....</i>		207

# List of Tables

1.1	Specification of target instrument . . . . .	8
1.2	Range of cutting parameters used . . . . .	9
2.1	Comparison between selected instruments.....	27
2.2	Comparison between principle-based and data-driven models .....	36
3.1	R <sub>z</sub> and its corresponding Sq value .....	65
3.2	Height variation as a result of white noise in a machine tool .....	69
4.1	Estimation of total uncertainty associated with cross grating artefact .....	84
4.2	Sq <sub>noise</sub> ( $\mu\text{m}$ ) using the subtraction technique.....	88
4.3	Sq <sub>noise</sub> ( $\mu\text{m}$ ) using the averaging technique.....	88
4.4	Results obtained from calibrating of the z-axis of MDS using step heights. .	95
4.5	Results obtained from calibrating of the x-axis of MDS using cross grating artefact.....	97
4.6	Results obtained from calibrating of the y-axis of MDS using cross grating artefact.....	97
4.7	Results of the MDS error calculation in the diagonal direction.....	99
4.8	Uncertainty budget for scale contribution.....	101
4.9	Standard measurement uncertainties associated with MDS calibration of the z-axis scale.....	101
4.10	Standard measurement uncertainties associated with MDS calibration of the x-axis.....	102
4.11	Standard measurement uncertainties associated with MDS calibration of the y-axis.....	102
4.12	Uncertainty budget for noise contribution .....	103
4.13	Parametric comparison of artefacts; Sa in $\mu\text{m}$ .....	107
4.14	Parametric comparison of machined blocks; Sa in $\mu\text{m}$ .....	107
5.1	Results of different topology on the same machined workpiece.....	113
5.2	Mechanical properties of the workpiece (AL 6061) .....	115
5.3	Composition (wt.%) of workpiece (AL 6061) .....	116
5.4	Cutting parameters with levels .....	127
5.5	Analysis of variance for Sq ( $\mu\text{m}$ ).....	128
5.6	Analysis of variance for Sal ( $\mu\text{m}$ ).....	128
5.7	Analysis of variance for Sa ( $\mu\text{m}$ ) .....	129
6.1	Best Models (Conventional Model 3 - X <sub>1</sub> - 3) Based on their R <sub>MSE</sub> Values.....	141
6.2	Best Models (Conventional Model 3 – X <sub>1</sub> – X <sub>2</sub> – 3) Based on their R <sub>MSE</sub> Values .....	141
6.3	Best Networks for the prediction of only Sa .....	142

6.4	Best Networks for the prediction of only Sq.....	143
6.5	Best Networks for the prediction of only Sal .....	143
6.6	Cross-verification cutting parameter .....	144
6.7	Performances of selected conventional model for prediction of surface texture parameters.....	145
6.8	Performances of selected networks for Enclosed multiple network Model for prediction of surface texture parameters .....	145

# List of Figures

2.1	Branches of metrology in manufacturing and workpiece properties . . .	13
2.2	Components of Michelson's interferometer.....	17
2.3	Measurement of a USAF1951 test target with a confocal microscope (10 objective, NA = 0.3). (a) Measurement in standard operating conditions. (b) Measurement with a thin oil film between the microscope and the test target.....	26
2.4	Influencing factors for surface roughness of machined component .....	28
3.1	Laser triangulation for dimensional measurement .....	41
3.2	LJ-V7020K sensor head .....	42
3.3	LJ V7020K set on CMM of step height measurement in a clean room; arrow pointing the sensor head of the laser line scanner.....	44
3.4	Profile measurement obtained from red and blue laser .....	46
3.5	CNC machine with Keyence mounted on for in machine surface measurement. 1;Keyence Scanning Head, 2. Specimen Block 3. Rotary worktable of 5-axis CNC machine tool .....	49
3.6	Topography of step height measured using line scanner LJ-V7020K ..	49
3.7	Residual error bar chart of the step height measurement against different sampling frequencies .....	50
3.8	First data obtained from both the 1st and 2nd scan during MDS surface measurement over an area.....	53
3.9	Images captured after initial importing datasets in MATLAB.....	54
3.10	Images of datasets in MATLAB after resizing.....	55
3.11	Dataset with slope affecting two axes.....	56
3.12	Dataset with slope affecting only one axis.....	57
3.13	Dataset after applying slope removal algorithm.....	57
3.14	MDS initial dataset captured in MATLAB .....	58
3.15	MDS final dataset captured in MATLAB.....	58
3.16	A simulated ideal surface topology.....	59
3.17	Induced missing data in the ideal surface topology .....	59
3.18	Reconstructed surface topology using the data manipulation after induced missing data.....	60
3.19	Deviation from Sq values against error induced MDS .....	61
3.20	Simulated profile for a face-milled surface .....	64
3.21	Simulation of surface topology of milled surface.....	65
3.22	Environmental temperature variations recorded over 3 days .....	68
3.23	Experimental setup to measure vibration during MDS measurement; red arrow pointing to accelerometer in both figures .....	71
3.24	Frequency spectrum obtained when the accelerometer is attached to the spindle .....	71

3.25	Vibration signal analysis obtained when the accelerometer is attached to the worktable.....	72
3.26	Surface plot of residual error in Sq by scanning perpendicular to the surface lays .....	74
3.27	Surface plot of residual error in Sq by scanning parallel to the surface lays	75
3.28	Surface plot of residual error in Sq by using MDS .....	75
4.1	Design of cross-grating artefact	81
4.2	Final grinding process of locally made cross grating.....	82
4.3	The NPL optical dimensional standard.....	83
4.4	Optical flat for the calibration of MDS .....	87
4.5	Flow chart for the flatness deviation threshold method .....	90
4.6	Effect of increasing the number of averaged measurement of a flat.....	91
4.7	Example of an instrument response curve—: a- actual input quantities, b- measured quantities, 1- ideal response curve, 2-actual response curve of the instrument, 3-line from which the amplification coefficient is derived, 4-local linearity deviation .....	92
4.8	Calibration of Z-axis of MDS using gauge blocks .....	94
4.9	Bar Error chart of residual error obtained from MDS for calibration of its z-axis.....	95
4.10	Lateral and diagonal direction measurements using image processing algorithm; red line represents data along the same profile axis, blue line represents data along the same time axis and green line represents data in diagonal direction.....	96
4.11	Bar error chart of residual error obtained from MDS for calibration of its x-axis.....	98
4.12	Bar error chart of residual error obtained from MDS for calibration of its y-axis.....	98
4.13	Bar error chart of residual error obtained from MDS for calibration (diagonal).....	99
4.14	Topologies and image of Microsurf 336, Sample N4.....	108
5.1	Effect of the tilted cutter on the surface topography .....	112
5.2	Different topology obtained from the same face milled workpiece .....	113
5.3	Images of inserts; from the alicona software and microscope .....	117
5.4	Effect of fine face milling on tool inserts as the number of samples increase..	119
5.5	Effect of Rough face milling on tool inserts as the number of samples increase.....	120
5.6	Image - checking tool degradation using a digital indicator; arrow pointing to tool holder during the checking process .....	121
5.7	Faced-milled blocks with different surface topography; The rough sample on the left had an $S_a$ value of $5.7 \mu\text{m}$ whiles the fine face milled sample on the right had an $S_a$ value of $1.2 \mu\text{m}$ .....	123
5.8	Significance vs areal parameters between fine and rough face-milled surface ..	124
5.9	Main effects plot for $S_q$ .....	129
5.10	Main effects plot for $S_a$ .....	130
5.11	Main effects plot for $S_{al}$ .....	131

6.1	Structure of feed-forward neural network with four layers, one input layer, two hidden layers and one output layer.....	135
6.2	Structure of enclosed multiple network model.....	139
6.3	Bland-Altman plot for the chosen models against measured Sa value.....	147
6.4	Bland-Altman plot for the chosen models against measured Sal value ....	147
6.5	Bland-Altman plot for the chosen models against measured Sq value .....	148

# List of nomenclature

d	Measurement range of the instrument
$f(x)$	Activation function
$l_x$	Linearity deviation; x-axis
$l_y$	Linearity deviation; y-axis
$l_z$	Linearity deviation; z-axis
$net_j^k$	Output of the element j in layer k
r	Coefficient of correlation
$r_{FR}$	Cross-correlation coefficient between the two face-milled surfaces
$u_{x\text{-axis}}$	Total uncertainties in x-axis
$u_{y\text{-axis}}$	Total uncertainties in y-axis
$u_{z\text{-axis}}$	Total uncertainties in z-axis
$u_{err}$	Uncertainties associated with measurement error
$u_{machP}$	Uncertainties associated with machine performance
$u_{NF}$	Uncertainties associated with noise contribution
$u_{opticalplate}$	Uncertainties associated with optical dimensional standard
$u_{repeat}$	Uncertainties associated with repeatability
$u_{reprod}$	Uncertainties associated with reproducibility
$u_{temp}$	Uncertainties associated with thermal variation
$u_{total}$	Combined standard uncertainty
$u_{trac}$	Uncertainties associated with traceability
$x_i$	Measured surface parameter
$y_i$	Predicted surface parameter by ANN
Al	Aluminium
$C_i$	Calibrated values
Cr	Chromium
Cu	Copper
D	Diameter of input beam
F	Focal length
Fe	Iron
$F_z$	Feed per tooth vector
$I_i$	Measured values

L	The distance between a reference point on the light detector and the source of light
Mg	Magnesium
Mn	Manganese
O <sup>j</sup> <sub>k</sub>	Output of the j <sup>th</sup> neuron in the k <sup>th</sup> layer.
R	The distance between the laser and the near end of the measurement range
Ra	Arithmetical mean deviation of the assessed profile
Rc	Mean height of profile elements of the assessed profile
Rku	Kurtosis of the assessed profile
Rp	Maximum profile peak height
Rq	Root mean Square deviation of the assessed profile
Rsk	Skewness of the assessed profile
RSm	Mean width of profile elements of the assessed profile
Rt	Total height of the assessed profile
Rv	Maximum profile valley depth height
Rz	Maximum height of the assessed profile
S <sub>5z</sub>	Five-point pit height of the assessed areal surface
Sa	Arithmetical mean height of the assessed areal surface
Sal	Auto-correlation length
Sdq	Root mean square gradient of the assessed areal surface
Sdr	Developed interfacial area ratio
S <sup>F,i</sup>	Surface topography parameter fine milled surface
Si	Silicon
S <sub>i</sub>	Significance of a parameter
SIM <sub>t</sub>	The area of defects
Sk	Core roughness depth of the assessed areal surface
Sku	Kurtosis of the assessed areal surface
Smr1	Valley material portion of the assessed areal surface
Smr2	Peak material portion of the assessed areal surface
Sp	Maximum peak height of the assessed areal surface
Spk	Reduced peak height of the assessed areal surface
Sq	Root mean square height of the assessed areal surface
Sq <sub>flat</sub>	Sq value of a flat
Sq <sub>i</sub>	Sq value of the simulated surface topology

$Sq_{MDS}$	Sq of the MDS surface topology
$Sq_n$	Sq value of surface topology with induced noise
$Sq_{noise}$	The measurement noise
$S^{R,i}$	Surface topography parameter rough milled surface
$S_s$	Spot size
$Ssk$	Skewness of the assessed areal surface
$Str$	Texture aspect ratio
$Sv$	Maximum pit height of the assessed areal surface
$Svk$	Reduced dale height, reduced valley depth
$S_v$	A surface topography parameter
$Sz$	Maximum height of the assessed areal surface
$Sz_{flatness}$	$Sz$ value of a flat
$P$	Profile element
$Ti$	Titanium
$Vmc$	Core material volume of the assessed areal surface
$Vmp$	Reduced peaks volume of the assessed areal surface
$Vvc$	Core void volume of the assessed areal surface
$Vvv$	Dale void volume of the assessed areal surface
$W^k_{ji}$	Weight between the $i^{\text{th}}$ neuron in the $(k-1)^{\text{th}}$ layer
$X_{ith}$	Number of neurons in the $ith$ -hidden layer
$Zn$	Zinc
$\Delta d$	Distance between the surface of the object to be measured and the near end of the measurement range
$\Delta L$	Distance between the reflected light and the source of the light
$\alpha_x$	Amplification coefficient; x-axis
$\alpha_y$	Amplification coefficient; y-axis
$\alpha_z$	Amplification coefficient; z-axis
$\beta$	Angle of inclination of cutter
$\delta_{err}$	Measurement error
$\delta_{repeat}$	Repeatability
$\delta_{reprod}$	Reproducibility
$\delta_{trac}$	Traceability

$\lambda$	Wavelength
$\mu^F$	Mean of the sample on a fine surface
$\mu^R$	Mean of the sample on a rough surface
$\omega$	Beam waist radius
%RE	Percentage residual error

# List of acronyms

<b>Acronym</b>	<b>Meaning</b>
ADC	Analog to Digital Converter
AFM	Atomic Force Microscope
AI	Artificial Intelligence
ANFIS	Adaptive Neuro-Fuzzy Inference System
ANN	Artificial Neural Network
ANOVA	Analysis of variance
AOTF	Acousto Optical Tuneable Filter
BS	British Standards
CAD	Computer-Aided Design
CCD	Charge-Coupled Device
CCI	Coherence Correlation Interferometry
CMM	Coordinate Measuring Machine
CMOS	Complementary Metal Oxide Semiconductor
CNC	Computer Numerical Control
CSI	Coherence Scanning Interferometry
DAQ	Data Acquisition
EMN	Enclosed Multiple Network

FFT	Fast Fourier transform
FV	Focus Variation
GA	Genetic Algorithm
GD&T	Geometric Dimensioning and Tolerancing
GPS	Geometrical Product Specification and Verification
HI	Heterodyne Interferometry
IEPE	Integrated Electronics Piezo-Electric
ISO	International Organization for Standardization
LabVIEW	Laboratory Virtual Instrument Engineering Workbench
MATLAB	Matrix Laboratory
MC	Metrological Characteristic
MDS	Multi Directional Scanning
MWLI	Multi-Wavelength Interferometry
NA	Numerical Aperture
NaN	Not a number
NI	National Instruments
NMI	National Measurement Institute
NPL	National Physical Laboratory
OEM	Original Equipment Manufacturer
OPD	Optical Path Difference
PAF	Point Autofocus

PC	Personal Computer
PSI	Phase Shifting Interferometry
R2R	Roll to Roll
RMSE	Root Mean Square Error
RSM	Response Surface Methodology
SNR	Signal to Noise Ratio
SPM	Scanning Probe Microscopes
UK	United Kingdom
USA	United State of America
USB	Universal Serial Bus
WLI	White Light Interferometry
WSI	Wavelength Scanning Interferometry

# Chapter 1

## Introduction

A noticeable trend over the past few decades confirm that as human population increases, the demand for manufactured products also rises tremendously. These products are used in various sectors such as construction, transportation, energy, and oil and gas industries all over the world. The majority of these products are produced through a series of machining processes, which transform the raw materials into a desirable shape, form, and size. Examples of conventional subtractive machining processes include milling, grinding and honing.

The advancement of technology has played a key role in meeting up with the demands of manufactured products. As most industries are considering a move towards automated processes which involve incorporating advanced technologies such as robotics into the manufacturing process to reduce labour as well as increase productivity. However, the demands of manufacturing products are still not satisfied because most manufacturing companies, especially small and medium companies are still having some of their process on conventional machines.

An alternative way often used in sectors that require a high volume of manufactured products is to employ services of multiple manufacturing companies i.e. creating a supply chain. Since it has been discovered that productivity increases when each manufacturing company is assigned batch production of a unique part of the overall product. The manufactured parts from all the manufacturing companies are then assembled to obtain a complete product. This method has many benefits apart from increasing productively. That is, parts can be used for other products as well, making manufacturing and storage very easy.

However, to guarantee an increase in production with reduced rejects, all manufacturing companies involved should have the same quality assurance scheme. The total effort made in ensuring that products conform to a detailed set of standards and specifications is known as quality assurance. Some of these standards include dimensional, surface finish and functional tolerances. Everyone involved with the manufacturing process is responsible for quality assurance of the product. The customer is responsible for communicating effectively with the designer; covering all expected attributes of the product, then from the designer to the manufacturer.

The manufacturing level is often the most expensive of the whole process. Therefore, to eliminate errors that will lead to rejection of products after this level, techniques such as optimisation of the manufacturing process and effective inspection are employed to ensure the consumer is satisfied or delighted.

## **1.1 Inspection in manufacturing process**

The approach for performing inspections can be grouped under three main categories which are; in-process, on-machine and post- process [1].

Post-process inspection is the most common inspection approach used in advanced manufacturing sectors. This involves movement of the machined part into a controlled environment to reduce the influence of contaminants that affect the measurement procedure. Post-process inspection is practised in many industries due to the difficulties in achieving the requisite efficiency and measurement uncertainty when using manual instruments on the machine or locally in the shop floor environment. Most high precision coordinate measurement instruments, such as Coordinate Measurement Machines (CMMs), are quite sensitive to temperature variation or such dirty environments. The presence of lubricants, swarf and mechanical vibrations in a shop floor contribute to the reasons most industries requiring inspection of components with tight tolerances prefer post-process measurement. Post process inspections typically require time and skilful

alignment procedures if re-machining is required. Using this type of inspection technique increases the manufacturing process' idle time, which reduces production efficiency in general. Also, there is a lower success rate in attempts of re-machining parts if any defect is detected due to the alignment procedures.

Online inspection technique is the direct opposite of post-process technique. It involves obtaining measurements from machined parts during the machining process. This implies that the measurement instrument is exposed to the harsh machining environment during measurement. The machined parts, however, remain in the same position. This removes the need for any alignment procedure as the machined part is held firmly on the machine tool throughout the inspection process. This is the most challenging technique because of the environmental disturbances such as abnormal temperature changes, lubrication and vibration which have high tendencies to affect most measurement instruments. However, from a theoretical stand point [1], this technique is the fastest and will reduce inspection time and increase productivity when compared to post process inspection because it is part of the machine tool. Ideally, the concept of in-process inspection compensates for the performance of the instrument to increase productivity.

On-machine inspection technique also known as in-situ in other publications [2], [3] is a bridge between the aforementioned inspection methods. It seems to combine the advantages from both in-process and post-process techniques. On-machine technique involves measuring the machined part on the machine after the machining process. Since the machining process is completed during on-machine measurement, most of the environmental disturbances will have reduced. The remaining disturbances could be easily compensated for by the use of a sophisticated instrument. Such instrument is expected to have the capability to resist the disturbances on the shop floor. The time consumption for on-machine inspections can be better when compared to post-process inspections. Also, since inspection is performed on the shop floor the need to move machined parts is eliminated.

In general, there has been a significant switch in the approach of inspections in the last decade. Much attention has been given to in-process and on-machine inspection instead

of post-process. This is only true for dimensional inspections but for surface inspections there is a desire to switch however, there are no economical solutions available.

In-process will only be possible for applications where the uncontrolled environment is still suitable for the measurement instrument due to the sensitivity of most instruments. On the other hand, there is a higher chance of success for implementation of on-machine measurement instrument in manufacturing. The instrument is required to have a reasonable size. This will help to allow flexible mounting and ease in operation within the machine tool workspace.

## 1.2 Surface metrology

The surface of an object is defined as the boundary between the object and its surrounding environment. In the context of surface metrology in manufacturing, the object is the machined part. Surface metrology in manufacturing can therefore be described as a science of measurement which mainly focuses on the measurement of the deviations of the surface of a machined part from its proposed shape defined on the initial engineering drawing [4]. It could also be defined as “the science of measuring small-scale geometrical features on surfaces: the topography of the surface”[5].

For the past few centuries, dating back even to the First World War, manufacturing engineers have not been in total ignorance of the link between the surface of a product and its quality. As pioneers such as Amonton, Coulomb and da Vinci emphasized that friction and worn properties of manufactured parts are as a result of the surface of the product in the sixteenth century [5]. The history of surface metrology and the various changes that have occurred over the years can be found in [5], [6].

Advancement in this field and the knowledge about its importance in relation with other disciplines have increased tremendously during the last two decades [5]. Most of the advancements link to the discovery that the influences of functional surface can affect the quality of the manufactured parts. It has been proven in practice that 90 percent of all failures in engineering component are surface initiated through mechanisms such as

fatigue cracking and adhesive wear [7].

During this era, researchers and industrial engineers have been able to make innovations such as using the surface texture to monitor the state of a machine tool and manufacturing process, and also identifying the relationship between the surface texture and the optical, tribological, biological, aerodynamic and many other properties of the manufactured component [8]. Henceforth, a confirmation of the success of using information from surface texture as an indicator for quality assessment.

Parameters deduced from a surface topology dataset can either be profile (line) based or an areal (area) based analysis. Profile related parameters are commonly used because it is straightforward to compute and relatively quick to measure as well. However, profile parameter of a machined part does not give much information about the measured part due to its small data size. Areal related parameters give more details about the measured part and are accepted by most surface metrology researchers. However, many industries have yet to adopt areal measurement for inspection, partly because many standards in GD&T (Geometric Dimensioning and Tolerancing) don't require such detailed measurement [9] and partly because rapid measurement of an area usually requires optical instruments which can be expensive or require special environments to operate. Hence, areal parameters are considered in this thesis to enhance the integration of areal surface metrology on the shop floor and on the machine. **Appendix A** explains in detail some of the commonly used surface metrology parameters.

### 1.3 Research motivation

This research was motivated by an existing challenge for manufacturers, which is, ensuring that high quality products are manufactured whilst not compromising on the speed or efficiency of the manufacturing process. At the moment, most industries prefer inspection of the quality of machined part offline regardless of the disadvantages outlined earlier. However, as part of the European FP7 Nanomend project [10], research has proven the success of fully integrating a surface measurement instrument in a roll-

2-roll manufacturing environment for on-line detection of manufacturing defects [11]. It has therefore confirmed the possibility of using areal surface parameters as indicators for defect in the manufacturing process at the nanoscale level.

This research follows suit by integrating a surface metrology instrument into a typical shop floor machine tool for on-machine inspection at the microscale level ensuring data captured are not contaminated due to the environment. This includes levels of surface finish often required in the advanced manufacturing sectors. This is discussed in section 1.5.

This resolves the issue associated with moving large parts to a controlled-environment for surface measurement. And brings in end-users such as civil nuclear where very large parts require inspection, including surface measurements, but they cannot be moved easily and traditional portable profilometry provides limited information.

After on-machine calibration of the chosen instrument for the above task, the manufacturing process is improved using the captured surface topology with the assistance of artificial intelligence techniques.

## **1.4 Research aims and objectives**

The main aim of this thesis is;

*"to employ advanced techniques for increasing the quality of face-milled parts using areal surface roughness parameters obtained efficiently using on-machine surface measurement."*

This can further be broken down into;

1. Investigating the potential for embedding a surface measurement instrument into a milling machine for on-machine surface metrology.
2. Predicting quality of face milled surfaces from machine conditions using intelligent techniques.

In order to achieve the above aims, this research work has come up with the following objectives: Objectives for aim 1 includes

- I. To investigate available surface metrology techniques suitable for on-machine surface measurement for face milling process on a typical shop floor.
- II. To develop a novel method to enhance the quality of measurement obtained from the identified technique for successful on-machine measurement.
- III. To validate the measurement technique for on-machine surface measurement to establish traceability.

Objectives for aim 2 includes

- IV. To investigate the appropriate areal surface parameters for representing the face-milling process.
- V. To investigate the relationship between machining conditions and the selected areal surface parameters.
- VI. To develop different neural network models with different training algorithms, learning algorithms, transfer function for each layer and network architectures.
- VII. To identify the model that is best in predicting areal surface roughness parameters for a face milling process.

## **1.5 Scope of research**

It is important to state that the scope of this research was limited to development or selection of a robust technique for on-machine measurement of the surface topography of machined parts from a normal milling process, as well as develop techniques to utilise

the acquired surface topography to improve the manufacturing process.

To achieve that, the specification of the selected/developed technique should be better or same as the outline target specification in table 1.1.

**Table 1.1:** Specification of target instrument

<b>Parameter</b>	<b>Targeted Specification</b>
Measurement Time	< 1.0 min
Measurement Area	> 6.0 mm x 6.0 mm
Vertical Resolution	$\leq 0.5 \mu m$
Lateral Resolution	$\leq 5 \mu m$
Size of instrument	< 200 mm x 200 mm x 200 mm
Accuracy	$\leq 0.5 \mu m$

It should be mentioned here that the target specifications, especially the resolution were chosen based on interviews with precision manufacturing industries such as Reliance Precision Limited in Huddersfield and the Nuclear Advanced Manufacturing Research Centre. It was concluded that the typical fine surface finish for the target industries for this research was of Ra between 0.8 to  $1.6 \mu m$ . This would also satisfy the kind of requirements applied in the civil nuclear industry which typically specify an Ra between 1.8 to  $3.2 \mu m$ .

Also, the second factor which was considered was the range of cutting conditions. The machining process used throughout this thesis was face-milling and the range of cutting parameters used throughout this research is shown in table 1.2. The properties of the cutting tools used will be described later. Based on the range of cutting conditions and the properties the spacing between the trails of the machining process is confirmed to be between 31–166  $\mu m$ . The spacing between the trails can be related to the feed per tooth which can be computed using the formula below [12].

$$\text{Feed per tooth} = \frac{\text{Feed rate}}{\text{Cutting speed} \times \text{Number of teeth}} \quad (1.1)$$

These range of cutting parameters were considered after consulting with machinists in

the industry to ensure they all fall within the recommended cutting parameters provided by the manufacturer's technical guide for end milling.

**Table 1.2:** Range of cutting parameters used

Parameter	Minimum	Maximum
<b>Cutting Speed (RPM)</b>	4000.00	8000.00
<b>Feed Rate (mm/min)</b>	750.00	2000.00
<b>Depth of Cut (mm)</b>	0.20	1.70

## 1.6 The structure of this thesis

The structure of this thesis is given as follows:

**Chapter 1:** The previous sections of this chapter have presented background on surface metrology and its relation to inspection in manufacturing. Also, the motivation, aims and objectives of this research have been clarified. The scope of research, which encompasses the target specification of the instrument to be used, has also been outlined.

**Chapter 2** presents a review of literature relating to surface metrology techniques as well as models for surface roughness parameters prediction. Subjects reviewed include the principle-based models, empirical-based models, and predictive models. Studies relating to the requirement of on-machine surface metrology has also been conducted. A comparison of the reviewed surface metrology techniques is also given which leads to selection of the appropriate technique for this research.

**Chapter 3** discusses the identified instrument in detail. It presents a novel technique to increase its specifications to meet the targeted specifications in table 1.1. Results obtained from the novel technique when purely simulation generated dataset are used is also presented as well as results from the simulated dataset with controlled noise levels to examine its robustness.

**Chapter 4** presents the on-machine calibration of the novel technique using

metrological characteristics (MCs). The MCs covered include measurement noise, residual flatness, amplification coefficient, linearity deviation and perpendicularity deviation after which an attempt to estimate the measurement uncertainty using MCs is unveiled. In conclusion, results of on-machine measurements using the novel technique is compared with another commercial instrument.

**Chapter 5** presents a series of investigations leading to the development of a robust model. These include; appropriate section to be used to represent a face milled surface to maintain consistencies, appropriate areal parameters in order to distinguish milled surfaces, appropriate technique to employed to avoid the impact of tool degradation during face milling samples and then influence of machining conditions on areal parameters.

In **chapter 6**, different models are developed and verified. Results are compared, and the model with the highest accuracy of prediction is selected.

In **chapter 7** shows summary of the thesis results, conclusion and potential recommended topics for further research being discussed.

Several appendices are provided in this thesis document; containing information that is more detailed, calibration certificate and tables of results.

# Chapter 2

## Literature review

The addition of metrology into the manufacturing chain allows easy and fast checks for right size, shape and finish of machined parts to specified tolerances. In this chapter, a general overview of metrology in manufacturing process is presented, followed by the requirement of on-machine surface metrology technique. This chapter also reviews and appraises current on-machine and in-process metrology techniques. The chapter concludes with a comparison of potential surface metrology techniques in order to identify the best instrument or technique that fits the specifications in chapter 1.

### 2.1 Metrology in manufacturing processes

In the past, metrology in manufacturing processes had been branded to be luxurious and had the stigma of being non-productive [13].

The reason given was that, integrating metrology into a manufacturing process will not improve the throughput of the process or ‘add value’ to the product. In other words, the number of parts machined within a defined period will not increase by adding metrology to the process. It was contended that the choice to incorporate metrology would increase the overall manufacturing cycle time, hence diminish the throughput. The increase in overall manufacturing time was attributed to the time spent to perform the metrology

process whilst the machine tool is idle. This gave rise to questions about the importance of metrology in the manufacturing industry. Below are some of the benefits of metrology

in manufacturing that has been discovered over time.

1. Metrology enhances effective communication between machinist, designers, suppliers, and customers. In fast-growing industries with high demands and customization such as the automotive industries where different sub-contractors or branches usually manufacture parts at different locations; measurement of features of produced parts is relevant. In most situations, the final product is an assembly of parts manufactured from other production sites. To achieve quality products from all the industries and simultaneously satisfy the customer's desire, metrological parameters can be used to communicate between all parties involved effectively. Customer rejects/returns rate will reduce as manufacturers for all location aim to achieve the customer's specification using parameters obtained from metrology as indicators.
2. Metrology gives rise to parameters that reflect the link between the geometrical and functional properties of the product. Simply put, parameters such as roundness and surface roughness average, which are obtained from metrology can easily be related to the functional performance and the form of the product. For example, the surface roughness average of a product can be related to the friction a product produces when in operation [14].

Another benefit of metrology when embedded into manufacturing process is that it reduces scrap rates. By integrating metrology into manufacturing process, operators can quickly identify when parts being manufactured are going out of tolerance. This is very useful in batch production, as in the case of any deviation in tolerance, subsequent parts will not be affected. This is because the operator will rectify or adjust manufacturing parameters to obtain the defined acceptable tolerance. In some cases, the out of tolerance product can be re-machined to achieve the pre-defined tolerance hence reducing scrap rate. The above stated benefits of integrating metrology into manufacturing process can be found in extant literature [13], [15], [16]. These benefits

have revealed that metrology can be used to achieve high efficiency, reduced scrap rates, high product reliability and increased productivity in manufacturing industries. These qualities are often the key goals of modern industries due to the high demand in industrial marketing.

## 2.2 Branches of metrology in manufacturing industries

Metrology has been defined earlier as the science of measurement. In manufacturing, several properties of manufactured parts can be measured. These include temperature, weight, shape and surface integrity of the part. In order to eliminate confusion and maintain uniformity internationally, the Geometrical Product Specification and Verification (GPS) of the International Organization for Standardization (ISO) has identified nine geometrical properties which could be used to describe a machined part and are listed in BS ISO 14638:2015 [ 17 ].

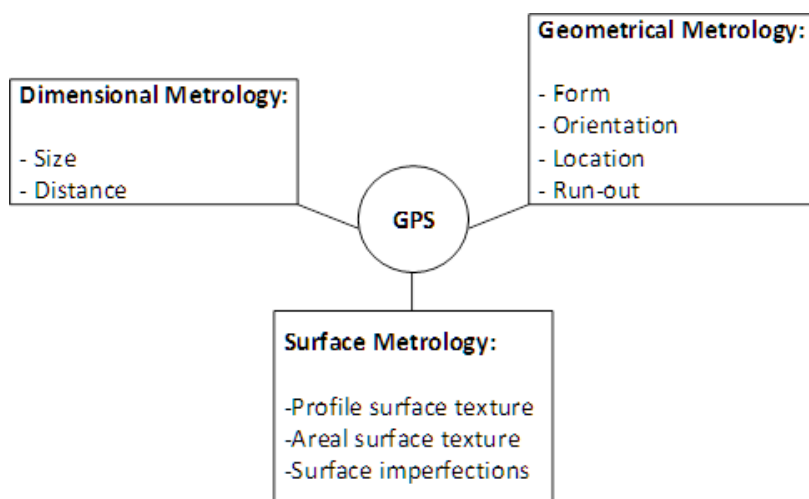


**Figure 2.1:** Branches of metrology in manufacturing and workpiece properties.

Reproduced from [17], [18]

These properties can further be grouped under three main headings referred to as the three

main branches of metrology in manufacturing in this thesis as well as other publication [18]. Figure 2.1 represents the selected geometrical properties extracted from ISO 14638:2015 and the metrology group they fall under at the time of writing this thesis.

### **2.2.1 Dimensional metrology**

Based on reviewed literatures, dimensional metrology has been propelled to the forefront in most investigations of metrology related research and Journal. In other words, more literatures are available compared to geometrical or surface metrology. This might be because most customers require manufactured parts to undergo dimensional and geometrical tolerance tests. This request has led engineers and researchers applying various techniques to obtain dimensional metrology information of machined part within a short frame of time (nanosecond range).

The coordinate measurement machines (CMM) is one of the most common systems for obtaining dimensional properties of a machined part. CMMs are systems mainly made up of a movable probe device in three or more axes, within a specified workspace. The workspace is mapped by high precision linear transducers, one for each axis.

By the machine following a precise manual or programmed path, the probe moves until it is in contact with surface of the machine part to be measured. The probe then sends a signal to a computer, which, in turn, allows for the memorization of that exact contact point coordinate. A control unit then utilizes the gathered coordinates to formulate a mathematical representation of the measured surface (associated geometrical elements) from which dimensions, the form and position tolerances, inter axes and hole diameters are obtained [19]. There is a possibility as well for the CMM to be programmed in order to generate a complete dimensional test certificate.

Yang *et al.* developed a high precision micro-CMM [20]. The micro-CMM moving volume was  $160\text{ mm} \times 160\text{ mm} \times 100\text{ mm}$  (XYZ), and they concluded to have achieved 50 nm measurement uncertainty with a measuring volume of  $30\text{ mm} \times 30\text{ mm} \times 10\text{ mm}$

(XYZ). CMMs, however, are susceptible and need to be operated in controlled environments in order to obtain reliable results.

Optical methods have likewise been successfully used in dimensional metrology; for instance, in the measurement of length, displacement interferometry or laser triangulation could be utilised. And for angular measurements, optical encoders or autocollimators could be employed [21]. Other instruments such as laser tracker [22] and x-ray computed tomography [23], [24] have also been employed for dimensional metrology.

Dimensional metrology can further be divided into three based on the scales; nano-scale dimensional metrology, micro-scale dimensional metrology [25] and large-scale dimensional metrology [26].

To obtain nano-scale information, techniques such as scanning probe microscopy (SPM) [27] and atomic force microscopy (AFM) [28] have been considered in dimensional metrology.

### **2.2.2 Geometrical metrology**

Geometrical metrology gives a better description of a machined part compared to dimensional metrology. Unlike dimensional metrology, geometrical metrology focuses on capturing adequate information that can be used to represent all the features of a machined part and not just a single point-to-point estimation as in the case of dimensional metrology. However, it can be said that a series of dimensional datasets of a machined part can be used to obtain respective geometrical datasets. Due to this relationship, all instruments or techniques that can be employed to obtain geometrical datasets can be used to obtain dimensional datasets as well. Also, some dimensional metrology instruments with high specifications have a higher chance of being successful in geometrical metrology. Typical examples of instruments that have been used for both dimensional and geometrical metrology are the CMM and x-ray computed tomography

[29].

One of the trending application of geometrical metrology is in reverse engineering [30]. That is reproducing a mimic of the component from its geometrical dataset.

### **2.2.3 Surface metrology**

Surface metrology dataset usually has a higher resolution compared to geometrical dataset. Ideally, both dimensional and geometrical dataset could be extracted for surface metrology dataset. However, the measurement area or coverage area of surface metrology datasets are usually very small compared to dimensional and geometrical dataset. Therefore, there would not be sufficient data to achieve such an aim. This thesis is centred on this branch of metrology, thus more details of this branch will be clarified in other sections of this thesis. Section 1.2 has already given an introduction to surface metrology and the following sections give more details about this branch of metrology.

## **2.3 Instrumentation for surface metrology**

One of the most critical decisions in metrology regardless of the measurement process type is the instrument/technique to be utilized for measurement. Instrumentation therefore plays a vital role in metrology process and affects key properties of the acquired dataset such as the quality and size of the dataset. Also, the degree to which the dataset is influenced by external factors such as vibration and thermal variations has a high correlation with the robustness of the instrument/technique used. This section reviews available commercial instruments, as well as, techniques that have been employed surface metrology.

This review does not consider contact methods due to their demerits. These include, but not limited to damaging of delicate measurands, and their slowness during measurement compared to the non-contact methods. Other groups that were also not considered is the

microscopes which include scanning probe microscopes (SPMs) and atomic force microscope (AFM), because of their sensitivity and slowness in nature. Bhushan [31] declares them unsuitable for in-process or on-machine measurement on a typical manufacturing shop floor.

This review is focused on optical methods suitable for in-process/on-machine surface metrology measurement. Optical methods, in general, can be categorized or divided into two; techniques based on the principle of interferometry and the non-interferometry techniques.

### **2.3.1 Interferometry-Based techniques for surface metrology**

Interferometry is a measurement technique that extracts properties of measurands by using the phenomenon of interference of waves such as light and sound waves. Albert A. Michelson developed the first instrument that utilized light interference as a measuring

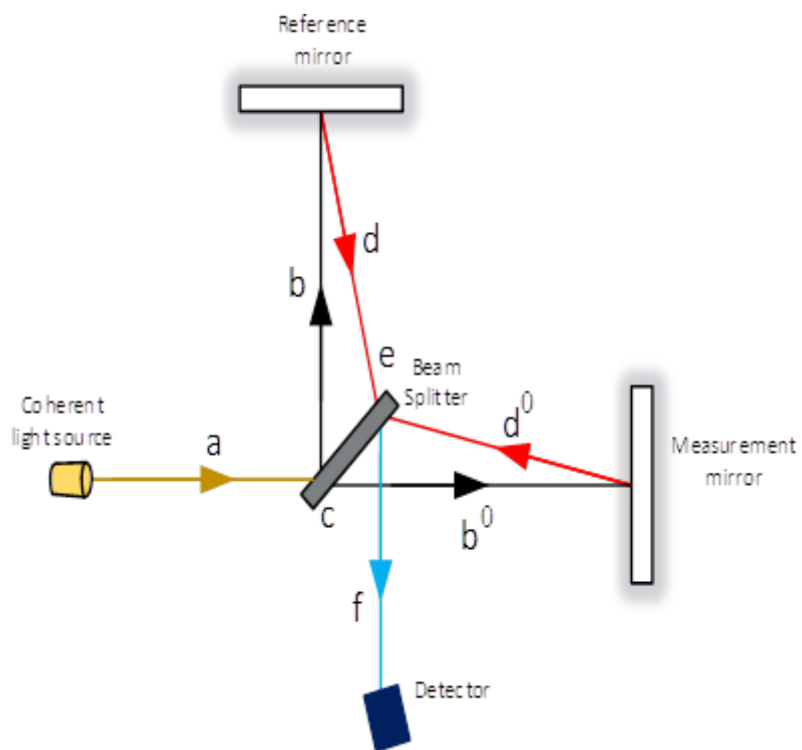


**Figure 2.2:** Components of Michelson's interferometer

tool in the 1880's. Michelson's interferometer was made up of a beam splitter (half-silvered mirror), a detector and two mirrors as shown in figure 2.2. The principle of operation of Michelson's interferometer is explained as follows.

A beam of light ('a' in figure 2.2) is projected from a coherent light source towards a beam splitter. As its name suggests, the beam splitter splits beam 'a' into two beams ('b' and 'b<sub>0</sub>') at point 'c' and directs their paths towards the two mirrors. One of the mirrors represent the reference surface whiles the other mirror represents the measurands surface. The two beams ('b' and 'b<sub>0</sub>') are reflected to the beam splitter at point 'e' as beam ('d' and 'd<sub>0</sub>'). The two reflective beams ('d' and 'd<sub>0</sub>') are recombined again to form beam 'f' at point 'e' on the splitter and sent to the detector. The path difference between beams ('b + d' and 'b<sub>0</sub> + d<sub>0</sub>') cause a phase difference in beam 'f', which creates an interference fringe pattern. By processing beam 'f' received by the detector, the surface properties of the measurand, as well as other properties, can be obtained.

This system has been modify over the years to obtain more robust instruments that can be widely employed in metrology. By using laser instead of a coherent light source, a charge-coupled device (CCD) as a dictator and a computer for analyses; the application of interferometry is found in high-resolution metrology applications. However, it is essential to note that techniques that make use of optical interferometry are very sensitive to noise from the environment such as mechanical vibration; thermal variations and air turbulence [32]. In an attempt to resolve these errors and improve the quality of the results several modifications an adjustment have been made to the ideal setup shown above. These are well documented in extant literature [33]. Below are some that have found their application in metrology.

- **Phase Shifting Interferometry (PSI)**

In PSI, the phase shift of the interference fringe pattern is controlled during the interferometry measurement. This can be achieved with or without mechanical assistance. Creath [34] suggests the use of rotating polarizers, moving diffraction

gratings, mirrors translation or glass slides tilting to achieving the controlled phase shift. Also, electro-optic, acousto-optic and photoelastic devices were outlined by Izatt and Chama [35] for phase modulation in PSI without any mechanical aid. PSI is preferred over other Interferometry techniques in metrology because it can achieve both resolution and a repeatability less than 1 nm in relation to the field of view. This is as a result of the surface heights being directly proportional to the interference phase [8], and hence the benefit of controlling the phase shift. However, due to the constant attempt to control the phase in the interference fringes, the measurement rate is meagre, hence increasing the exposure of the measurement results to environmental disturbances such as vibrations.

4D Technology has commercialized this technique for on-machine metrology (NanoCam Sq) [36]. The available brochure on the instrument confirms shorter acquisition time which makes measuring possible on a shop floor despite vibration [37].

- **Heterodyne Interferometry (HI)**

HI is achieved by introducing a frequency shift between two interferometer beams. The frequency shifting can be achieved either mechanically or non-mechanically just as in the case of PSI [38]. This is performed to obtain a smaller optical path difference (OPD) lesser than the observed spectral bands. By reducing the OPD, measurement has a better SNR (signal to noise ratio) [39] at the same time giving the ability to measure with nanometre accuracy. However, the major drawback of HI is the  $2\pi$  phase ambiguity, limiting the OPD measurement range to half the light source wavelength.

- **White Light Interferometry (WLI)**

This interferometry technique uses a white light laser as a source of light. White light lasers are used because they have a short coherence length and a wide bandwidth. There are two requirements for a white light interferometry to achieve high resolution and stable measurement. That is to ensure that the position of the zero-order interference fringe and the spacing of the interference fringes must be

independent of the wavelength of the light source [40]. Wyant [40] elaborates on different types of white light interferometers that are used in surface metrology. Taylor-Hobson Ltd. has commercialized a type of white light interferometry referred to as the coherence correlation interferometry (CCI). The CCI 6000 has a vertical resolution of 0.01 nm, and a standard measurement range is 100  $\mu\text{m}$  [41], [42]. One significant advantage of WLIs is their ability to measure non-continuous surfaces without phase ambiguity. However, they also face similar demerits as PSI; very expensive, sensitive to vibration and slow during measurement, hence not suitable for on-machine metrology.

- **Multi-Wavelength Interferometry (MWLI)**

This system is made up of more than one interferometer to obtain a high-quality measurement. One interferometer is allocated as a reference to compensate for environmental disturbances while others are used for the measurements, multiplexing two light sources having different wavelengths will effectively extend the measurement range of the method. Its robustness has been considered for on-machine measurement, and its stability has been confirmed in literature [43]. Luphos GmbH has also commercialized it. Other merits of utilizing this technique includes the ability to measure optically rough surfaces which has been a challenge for other interferometric techniques [44]. However, the main disadvantage of MWLI is the cost involved in building it.

- **Wavelength Scanning Interferometry (WSI)**

The WSI can be related to coherence scanning interferometry (CSI), a type of WLI. This is because both techniques eliminate the  $2\pi$  phase ambiguity error by combining multiple-wavelength. However, CSI suffers from slowness in measurement due to the high interference of environmental disturbances. Which is caused by the mechanical components used for phase shifting. WSI, on the other hand, achieves phase shifting by the variation of the illumination of the light source in the interferometer. The changing of the illumination is achievable in WSI

because it comprises of a tuneable wavelength laser diode utilized as a light source, an interferometer in a Linnik configured interferometer and a camera with CCD. The tuning range of a typical laser diode employed in WSI is usually several nanometers, which is achieved by modulating the injection current [45]–[47]. Early challenges faced by this technique as reviewed by various publications [48]–[50] were highlighted as the hopping problems; which exist in laser diodes, and the narrow scanning range. This greatly affected the measurement accuracy of WSI. However, research has indicated that by combining the WSI with other techniques such as HI [51] and PSI [52], the accuracy is improved. Also, the hopping problems of a laser diode could be rectified by an external cavity laser diode [53]. Newer developments like the AOTF (acousto-optical-tuneable-filter) allow for the designing of fast scanning, wideband tuneable sources.

Fortunately, a combination of the WSI with other techniques will not only increase the accuracy but also reduce the resistance of the system to environmental disturbance. Moreover, during the last decade, compensational circuitry has been added to the WSI in order to introduce it to on-machine measurements [54]. Elrawemi *et al.*, [55] demonstrated the possibility of capturing areal surface dataset on-machine using a WSI. Their WSI could detect defects down to  $3\text{ }\mu\text{m}$  in the lateral dimension. They compared the results obtained from a roll-to-roll manufacturing environment to an offline CCI in a controlled environment and concluded that they had good correlation. Henceforth their WSI can be integrated onto R2R platforms as a quality assurance tool. The WSI obtained quality measurement due to the robustness of the compensation system and the complexity of the measurement algorithms as well as high computing processors used for fast measurement. They also employed an active servo mechanism control system which serves as a tool for phase-compensation in eliminating environmental noise effects. This is presented in details by Jiang *et al.* [56]. This technique will be further considered for its possibility to be implemented for on-

machine metrology on a typical shop floor in this thesis.

### **2.3.2 Non-Interferometry techniques for surface metrology**

- **Focus Variation (FV)**

In focus variation technique, two primary steps are employed to obtain surface metrology dataset over an area.

1. Vertical scanning by mechanical translation of the optical head or the whole optics over the sample to obtain a stack of images of the sample at the same position.
2. Application of image processing algorithms to the captured images to construct 3D topographical dataset based on the changes of the focus or sharpness of the image.

It is one of the profoundly ingrained methods in surface metrology with an allied ISO standard for calibration [57]. Details of the principle of FV can be found in literature [57]–[59]. The FV technique is known for its ability to achieve very high axial resolutions (10 nm) [60]. Range for its vertical scan depends also on the objective working distance, ranging from a few mm to about 20 mm or more. However, the drawback of FV is linked to the slowness of vertical scanning as it makes the measurement results subjected to environmental disturbances such as vibration. In addition, this technique also struggles with measuring transparent samples because they have focus curves without dominant peaks.

Regardless of all the above limitations, Alicona has commercialized FV for on-machine metrology. Alicona claims their IF-SensorR25 [61] and IF-Portable [62] measurement kits employ FV, and are suitable for integration with machine tools on a shop floor. Hence, this technique will be further considered for its possibility to be implemented for on-machine metrology on a typical shop floor in this thesis.

- **Point Autofocus (PAF)**

In PAF, the surface topography of the sample to be measured is obtained by automatically focusing a laser beam at a small spot on sample surface and capturing the height information of the surface. With assistance from a moving XY scanning stage, the area surface height information of the scan can be obtained by traversing over the area of interest. The lateral resolution is determined by the laser beam spot size and the traversing speed used during the measurement [63]. Mitaka kohki co. Ltd. has commercialized this technique. MITAKA MLP - 3SP (size;  $129\text{ mm} \times 90\text{ mm} \times 162\text{ mm}$ ) is claimed to have a moving range (XYZ) of  $120\text{ mm} \times 120\text{ mm} \times 130\text{ mm}$  with a scale resolution of 10 nm. According to the manufacturers dataset [64], it is suitable for in-line areal measurement when integrated into a finishing machine. This claim is questionable because one of the most significant limitations of PAFs is that it takes a long time to scan which exposes the captured dataset to environmental disturbances such as vibration. Moreover, because the traversing stage is usually controlled using mechanical translations, the immunity of the technique to environmental disturbances will require a very sophisticated compensatory system.

- **Laser Triangulation**

Laser triangulation uses the concept of trigonometry to obtain height information from a sample. The critical parameters needed for laser triangulation are the incident angle of a beam of laser projected over a sample and two known lengths. The distance between the light detector and the surface of the sample, and the distance between the laser light source and the light detector are the lengths required to obtain metrology information when using laser triangulation. It is one of the most common techniques in metrology and has been used for dimensional measurements [65], geometrical measurements [66] as well as surface imperfection measurement [67]. Commercial instruments that employ this technique for metrology include but not limited to Nextengine's 3D scanners,

ShapeGrabber's SG100 and Keyence LV7000 series. Review of the performance of these instruments are presented in extant literature [68].

This technique is very robust and less costly compared to other methods. It has also been used for in-situ applications not excluding obtaining a measurement from a shop floor [66], [69]. Also, because of its robustness, it has been integrated with robots for metrology purposes [70]. However, these are typically for form measurement and has so far not been used for surface finish measurement (at the time this review was conducted). This instrument will be further considered for its possibility to be implemented for on-machine surface texture metrology on a typical shop floor in this thesis. The reason is because some of the latest systems, from manufacturers such as Keyence and Micro-Epsilon, use a blue light source which provides a shorter wavelength, and which results in an improved resolution and lower noise when measuring shiny surfaces. These new characteristics are fundamental for measuring surface topography features at the micro-scale.

Throughout the literature survey work very few academic publications on novel surface metrology instrument suitable for on-machine measurement were found.

## **2.4 Requirements for on-machine surface metrology instrumentation in manufacturing**

The aim of this thesis includes the integration of a surface metrology instrument on a machine tool to capture surface topography of machined part in the micro-scale level. This act is expected to improve the throughput by reducing the number of scrapped parts as well as allowing re-machining of out of tolerance parts. For this aim to be achieved, the selected instrument must meet majority of the following requirements;

1. **Size** – This size of the instrument needs to be considered. Integrating a bulky

instrument will not be realistic. The size of the instrument can pose a challenge on where to retrofit it in the existing machine tools platform.

**2. Measurement Speed**-With the aim of increasing throughput by on-machine metrology, the time spent during the measurement process can affect the aim in two main ways. If the measurement speed is slow;

- The time spent could absurdly increase the idle time of the machine tool. Hence would not be considered prudent to use the technique when compared to off-line measurement.
- The impact of the environmental disturbances on the measurement increases as the measurement time increases.

The ideal measurement time spent should be at least less than one minute to achieve benefits from on-machine metrology.

**3. Measurement range** – As stated in chapter 1, the expected measurement area of the instrument should be at least  $6\text{ mm} \times 6\text{ mm}$  and the vertical range of at least 1 mm. The selected instrument is expected to provide at least sub-micron resolution and repeatability. Since the target surfaces are face-milled parts, the selected instrument is also expected to have the ability to measure very rough surfaces.

**4. Robustness and cost** – Some sophisticated instruments can be expensive due to their design, perhaps incorporating stable light sources, advanced optics or high frequency mechanical control systems for adaptive compensation. The selected instrument should be robust enough to resist environmental disturbances such as vibration, temperature, pressure, humidity and the presence of lubricants or cooling fluids.

Most manufacturing processes use cooling fluids during the subtractive machining

process. Therefore, in order to capture quality datasets on the machine, it is expedient to use an instrument that will not be affected by the fluid during the on-machine measurement or robust enough to capture good data after air blast cleaning which will remove swarf and coolant but residues of coolant and oil may persist. An experiment performed by Mueller *et al.* [71] proves that microscopes may struggle to obtain quality measurement under such influence. By applying an oil film on an object and measuring it, they discovered that the disturbance affected the performance of the instrument by making the measurement very blurry as shown in figure 2.3.

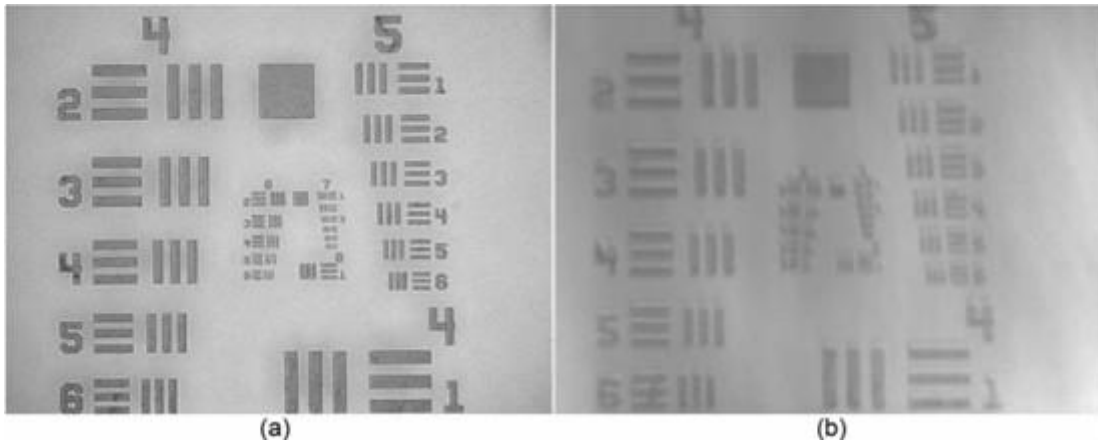


**Figure 2.3:** Measurement of a USAF1951 test target with a confocal microscope (10 objective, NA = 0.3). (a) Measurement in standard operating conditions. (b) Measurement with a thin oil film between the microscope and the test target. Reproduced from [71].

In section 2.3, a review of optical surface metrology techniques were presented. Based on their limitations, merits, and previous results or applications for on-machine metrology, the following techniques were selected and compared based on the requirements outlined earlier in this section. Table 2.1 shows the comparison between the selected instruments.

The importance of the role of surface metrology in manufacturing industry cannot be overlooked as high demands, and high quality parts are expected as industries evolve. On-machine metrology is one of the techniques that can be used to monitor the quality of a machined part to meet specifications of consumers. However, even though

information obtained for on-machine metrology can be used for re-machining of the part if it is out of tolerance, it can be debated that this will not be possible if the part is smaller than specified.

**Table 2.1:** Comparison between selected instruments

		<b>Laser Triangulation (Keyence LV7000)</b>	<b>Focus Variation (Alicona IF- sensor R25)</b>	<b>Wavelength Scanning Interferometer (lens dependent) *</b>
1	Size of the instrument (XYZ) /mm	111x 103 x 42	126 x 153 x 249	*
2	Measurement time /sec	**	<1	<1
3	Cost /£	9,900.00	36,000.00	*

\* It is in the process of being commercialized by IBS precision as Arinna

\*\*Depending on the speed of mechanics employed to move the instrument across the area of interest. However, it takes < 32  $\mu$ s to capture a single profile.

Controlling the specifications of a machined part from the beginning of a manufacturing process could be made possible by employing predictive models in manufacturing. These can be used to avoid initial errors in the machining process by selecting the right manufacturing conditions. A combination of on-machine measurement and a good model that describes the relationship between the surface texture and the cutting conditions increases the possibility of right-first-time during the manufacturing process.

## 2.5 Modelling methods in surface metrology

Models can be referred to as functions that describe the state of a system based on the relationship between two corresponding datasets; one set as input and the other as output

dataset. In this thesis, the output of the models that will be considered are surface texture parameters and the inputs are factors on the shop floor that affect the surface texture. Numerous factors can influence the surface texture of machined parts during manufacturing. Examples of these factors adopted from [72] and [73] are presented in figure 2.4.

Due to the complexity of the relationship between these factors in the figure 2.4 and the surface texture of machined parts, a significant amount of research has been dedicated to it in the last few decades.

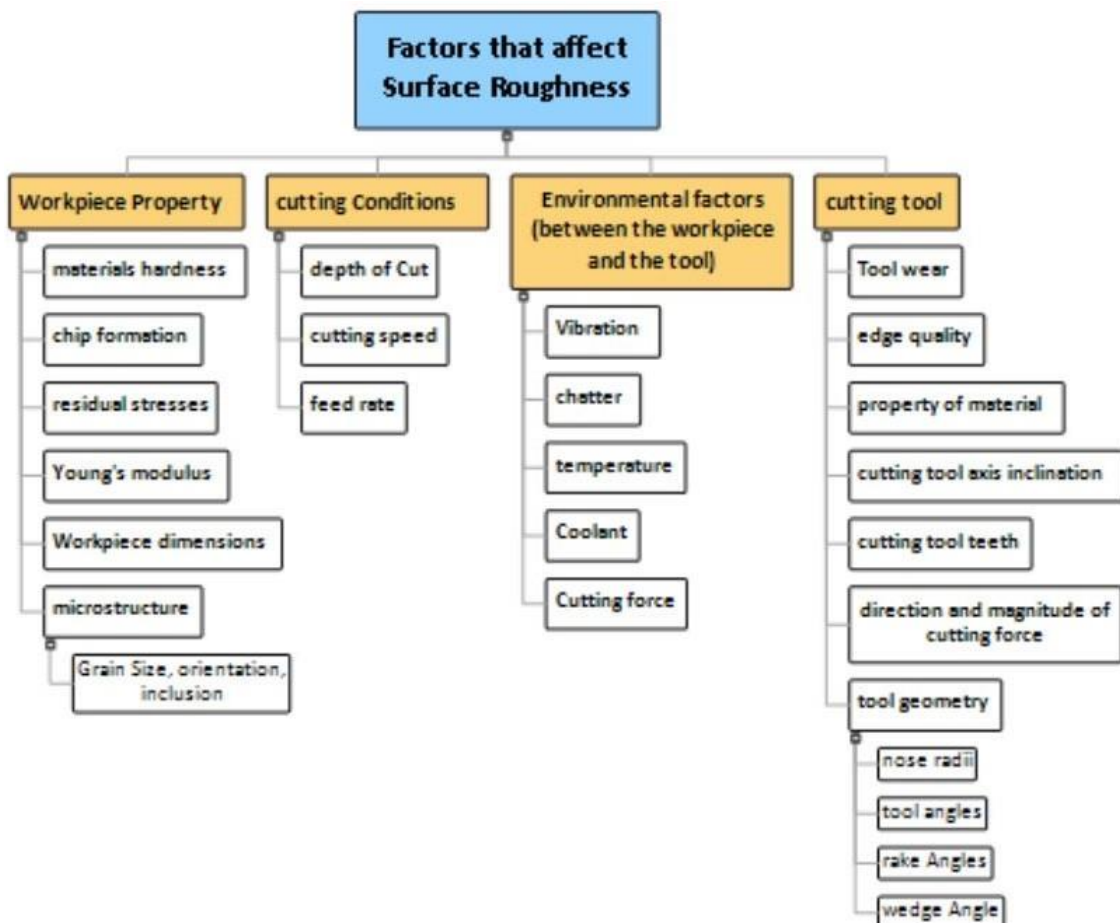


**Figure 2.4:** Factors that influence the surface roughness of machined parts

Models, in general, can be developed by either theoretical or experimental approach or in some cases a hybrid of both. Theoretical models are developed from already

established theories or first principles and are expressed in space differential equations to simulate the relationship between the output parameters (surface texture) and the input parameters to the model. They are also referred to as white-box models in other publications. These models maybe less costly to develop in terms of experimentation but the designer is expected to have a broad knowledge of the system to be modelled and there could be significant modeling work involved (for example physic modeling). The knowledge should comprise of the mathematical relation of the input and output as well as the operational principle of the system. It can be concluded that the designer's mathematical understanding of the system plays a vital role in the model's accuracy. That is, the closeness of the model to the real system depends on the mathematical understanding of the designer about the system. The accuracy is usually assessed by a comparison of results from both the model and the real system when using the same input dataset. An up to date review of theoretical models for surface roughness has been presented in [73].

The disadvantage of theoretical models is that, it is challenging and sometimes impossible to develop a theoretical model when the input and output do not have any existing proven relationship or the system under study is very complicated to analyse using first principles. In such scenario, experimental methods can be employed to acquire lots of data from the system. The data can be used to develop a model for the system.

Data-driven models are very costly in terms of time and money. This is because the system needs to be operated using different inputs to obtain a set of corresponding outputs for both training and validation of the model. That is, based on the two datasets obtained (the input dataset and its corresponding output dataset), the model is developed. The set of data used to develop the model is referred to as the training dataset. Data-driven models, unlike theoretical models, are not based on physical equations but on the experimental dataset, hence the name data-driven model. It has also be referred to as black box model or empirical-based models in other publications. Techniques employed

to obtain data-driven models can be grouped into two categories: statistical techniques, which includes regression methods, and artificial intelligence techniques, which include Artificial Neural Networks (ANNs) and fuzzy systems. A review of data-driven surface roughness models is presented in the following subsection.

Models can also be developed from both experimental dataset and first principle physical equations of a system. This is referred to as a grey model. In other words, a grey model combines outputs from a data-driven model and theoretical model to obtain a more accurate model hence, is referred to as a hybrid model in other publications. A typical example of such model for surface roughness is presented by He *et al.* [74]. He *et al.* developed a model that incorporates both theoretical and empirical techniques in predicting the machined parts surface roughness of a single point diamond turning process. The theoretical side of the model used equations to describe the effects of the kinematics and minimum undeformed chip thickness on surface roughness while the empirical side of the model utilized ANN to handle the uncertain components such as the material spring back, plastic side flow and micro defects on the cutting edge of diamond tool associated with surface roughness.

The following sub-sections review relevant literature on models of surface roughness related to this thesis.

### **2.5.1 Principle-based models**

Felhő *et al.* [75] developed a theoretical model to predict surface profile parameters such as Ra and Rz in a face milling process. Based on previous mathematical equations presented in reviews by Arrazola *et al.* [76] and Peters *et al.* [77] on the roughness of a machined surface, Felhő and his team claim to have developed a model that consider the geometry of the inserts used, axial and radial run-out of inserts as well as cutting parameters; cutting depth and feed rate. Their model is supported by the theory that a milling process can be characterized as the main motion being produced by axial rotation of the milling tool while the movement of the part perpendicularly to the axis of the

cutter produces the auxiliary motion. This process creates a structured pattern on the milled part representing the surface finish on the part after milling. They concluded that the calculated theoretical surface roughness parameters ;Ra and Rz (see **Appendix A** for definitions) achieved by their model have a good correlation i.e.  $R^2$  of 0.978 and 0.969 respectively with the measured roughness. A confocal chromatic surface measurement equipment was used to measure Ra and Rz of machined parts. Four different samples were machined with four different tool insert shapes; square, octagonal, circular and dodecagonal using different feed rates and were used in determining the accuracy of their model.

Even though the average of three measurements was taken on each sample during the evaluation analysis, the number of samples could be considered low for such analysis. This is because by using four samples, in this case, the authors prevent readers from knowing the ability of the model to truly identify different shapes of inserts as well as the different levels of feed rate and their influence on the surface roughness. A paradoxical argument could also emerge when considering the pairing of the two variable parameters; the shape of the insert and the feed rate for each cutting trial. Lastly, face milled topographies are made up of height and spacing features. The evaluation of the model only highlights two height parameters and neglects spacing parameters. This does not show readers the model's ability to predict spacing parameters. In such analysis, it is expedient for authors to consider varying one input parameter at a time to determine the true accuracy of the model. Also, other spacing parameters should be considered.

Muñoz-Escalona and Maropoulos [78] considered most of the suggestions made above about Felhő *et al.*'s [75] model, when developing their model. Muñoz-Escalona and Maropoulos developed a geometrical model for face-milled part using only square inserts. Based on the already established mathematical relationship between surface roughness of a milled surface and machine tools kinematics properties adopted from Baek *et al.*[79] , Wang *et al.* [80] and the cutting tools geometrical parameters from

Franco *et al.* [81], a more accurate model was developed. In addition to the previously established relationships, Muñoz-Escalona and Maropoulos also considered the impact of tool run outs and axial tool deviation on the height values of the surface roughness. They concluded that their model had an accuracy of 98% based on the relative error obtained from the theoretical Ra (predicted values from the model) and real Ra (measured results from a surface measurement instrument, a non-contact white lamp profilometer ProScan2000). An L<sub>36</sub> Taguchi experimental design was employed; which ensured effective variation of the feed per tooth, cutting speed, the axial cut depth and the radius of the tool nose during their testing trials. Hence 36 samples were machined for the evaluation of the model. Unfortunately, they also did not demonstrate the ability of the model to predict spacing parameters.

Tomov *et al.*, [82] also presented a theoretical model which was developed based on the profile obtained from the kinematics of the cutting process and geometry of the tool insert. The cutting tool conditions used to develop the profile was feed rate, tool radius and tool angles. To adequately validate the model, twenty different cutting conditions were used to machine different samples for analysis by varying cutting speed, feed rate, tool nose radius and depth of cut. The real surface roughness of the machined samples was measured using Mitutoyo Surf test at five locations that are equally spaced around the sample's circumference. Height parameters Ra and Rz were compared as well as spacing parameter Rsm (see **Appendix A** for definitions).

Other white box models for the prediction of the profile of machined surface can also be found in [73]. As it was expressed in chapter 1, this thesis is geared towards areal parameters of machined surfaces due to their benefits over profile parameters. Below are examples of theoretical models for prediction of areal surface texture parameter.

At the time of writing this thesis, only a few models were reported to have such ability. Tavares [83] reviewed and evaluated three white box models for prediction of areal surface texture. The three models were developed based on principles extracted from Greenwood and Williamson [84], Chang [85] and Zhao [86]. Tavares extracted areal

surface parameters such as  $S_a$ ,  $S_q$ ,  $S_t$  and  $S_{sk}$  (see **Appendix A** for definitions) from the output of the analysis of the model. He then gave a full description of the model's ability to predict both spacing parameters and height parameters. With a stylus instrument applied in a raster mode, the surface topography of a real machined part was obtained for analysis. The evaluation area was 2 mm x 2 mm.

The model developed by Felhő *et al.* [75], for predicting  $R_a$  and  $R_z$  was also revised to predict areal surface parameters in Felhő *et al.* [87]. The enhancement was made possible by using a CAD simulator to assist in creating the topography of a surface based on the results from their previous profile model [75]. Both visual and parametric comparison was shown to demonstrate the accuracy of the model. The areal surface topography was obtained by measuring samples with an optical instrument. Compared to their previous model, they only considered one insert shape and varied the feed rate during the evaluation process. They concluded that their models obtained a good accuracy by using the same cutting conditions as the experimental conditions in the simulation. The size of the evaluation area was 4 mm x 4 mm.

### **2.5.2 Empirical-based models**

As explained earlier, the empirical-based model can be further divided into two: statistical models and artificial intelligence (AI) models. Due to the complexity of the relationship between the surface texture of a machined part and the cutting conditions used in machining, many data-driven models have been developed compared to theoretical models. Data-driven statistical models that utilise regression and response surface methodology (RSM) techniques have been considered in most literature, as well as AI models; genetic algorithm (GA), fuzzy logic algorithm, and artificial neural network (ANN) likewise [88]. It should be mentioned that there are hybrid models that combine two data-driven techniques to develop more accurate models. A typical example is adaptive neuro-fuzzy inference system (ANFIS) model which combines the

concept of artificial neural network and fuzzy logic algorithm. In addition, most data-driven models are developed with assistance from high level programming packages such as MATLAB or statistical software packages such as Minitab, making them easier to develop compared to theoretical models, hence the difference in preference.

Yang *et al.*,[89] presented a mathematical model which employed response surface methodology (RSM) for prediction of surface quality in a turning process. In order to reduce the cost involved in developing the model, three-factor central composite design of experiment (CCD) was used. CCD reduces the number of experiments required for training the model which results in a reduction of cost. The input to their model were cutting speed, feed rate and depth of cut which was used to predict the profile surface roughness ( $R_a$ ) and the contour lines of the surface texture on the machined part (titanium alloy was the material used in their work). The accuracy of their model was verified using a one-way ANOVA, and they claimed that their model had high credibility. However, the validation process was based on a prediction of three samples which were also used for the training process, hence making the accuracy of the model questionable. Vallejo *et al.* [90], also developed an RSM model based on CCD datasets for predicting  $R_a$  in a high-speed milling operation. Feed rate, tool diameter, radial depth of cut and the curvature of the geometry of the cutting tool were used as the input to their model. They claimed their model showed excellent performance with an average percentage error of 14.3 % between the measured and predicted  $R_a$ . The verification dataset were all new cutting conditions and were different from the training dataset.

Vishwakarma *et al* [91], developed a regression model to predict surface roughness ( $R_a$ ) for electric discharge machining considering current, pulse time, duty cycle, gap voltage and flushing pressure as the input. Their results show that the flushing pressure has a minimum effect on the surface roughness for steel alloy. They claim their model had an average percentage error of prediction of 6.4 %. Unfortunately, the validation and training datasets were the same. Hence, the average percentage error might increase if new datasets are used for the validation process.

A genetic algorithm has also been used for developing models for the prediction of the surface texture of a machined part [92]–[94]. GA models mimic the process of natural evolution by integrating the “survival of the fittest” philosophy. Zain *et al.* [93] presents a GA surface roughness (Ra) model with the radial rake angle of the tool, combined with speed and feed rate cutting conditions as the input parameter. The model was compared with RSM model, and they claimed their model was more accurate.

Another AI technique that has been used in prediction of surface texture parameters is fuzzy logic [95], [96]. In Ali *et al.* [95] a total of 16 input variables were used to develop a surface predictive model in a grinding process. This is the largest number of inputs for a data-driven model that has been reviewed in this thesis.

ANN turns out to be one of the most commonly used AI techniques in developing a data-driven model. ANN surface roughness predictive models have been developed for different machining processes. This includes but is not limited to lathing process [97], end milling [98]–[100], high speed turning [101], hard turning [102], drilling [103], honing [104] and face milling [105]. The main reasons for the mass patronage of ANN is the ease of development and high accuracy compared to other data-driven models. For example, Paturi *et al.* [106] developed a regression model and ANN model with the same training dataset. They confirmed that the correlation coefficients between the predicted results and the experimental results of the ANN model and regression model were 0.998 and 0.978 respectively. Also, Asiltürk *et al.* [107], worked on similar research in a turning process and had similar findings. That is, ANN models are more accurate than regression models. A comparative study of ANN and RSM conducted by Patel *et al.* [108] for the prediction of surface roughness also proves that ANN is more effective than RSM. ANN have similarly been proven to be more accurate than fuzzy presented by Verma *et al* [109].

Hybrid models such as ANFIS have also been developed to predict the surface roughness for machining processes such as milling [110], [111] and turning [[112], [113]]. Also, when the accuracy of ANFIS was compared with ANN by Verma *et al* [109], they

confirmed ANFIS had more accuracy than ANN when the two models were created from grinding process dataset.

Other hybrid models include but are not limited to, integrating of ANN and GA to develop a model for predicting the surface roughness in milling [114] and electric discharge machining [115]. Also, an GA coupled with RSM model has also been developed by Sangwan [116].

Table 2.2 presents a comparison between principle-based and data-driven models.

From table 2.2, its can be seen that the benefits of data-driven models out ways that of deriving models from first principles. Models based on first principles to predict the surface topology will not be considered in this thesis because of barriers such as cost, time and skills required to develop such models.

**Table 2.2** Comparison between principle-based and data-driven models; taken from [117]

	<b>Principle-based modelling</b>	<b>Empirical-based modelling</b>
<b>1. Data reliance</b>	Small data	Big data to train upon
<b>2. Domain expertise reliance</b>	High reliance upon deep domain expertise	Can provide useful results with little domain knowledge
<b>3. Adaptability and deployability</b>	Requires complex and time-consuming derivation to account for new relations	Rapidly adapt to the circumstances of a specific problem instance
<b>4. Interpretability</b>	Consistent, physically meaningful link between parameters	Physics agnostic surrogate, limited by the rigidity of the model functional form.

## 2.6 Summary of review and gaps

### 2.6.1 Measurement

One of the aims of this thesis is to create a new system and methodology which will be suitable for on-machine surface metrology in a face-milling machining process. Section 2.3 reviews most of the available techniques that have been considered in surface metrology in general. The review highlighted the advantages and the disadvantages of these techniques. A comparison was then made between three techniques. These techniques were chosen based on previous research and the datasheet specification of commercialized instruments that employ the techniques which confirm that they satisfy most of the requirement of on-machine measurement stated in section 2.4. The Keyence LV7000 series, which utilises laser triangulation technique, seems more promising from on-machine metrology compared to the others. Unfortunately, the following are still unknown about this instrument and needs to be explored:

- **Performance for on-machine surface measurement for face-milling manufacturing process** - Most of the available literature on the identified instrument confirms its possibility to be used for on-machine form and dimensional measurement as well as surface imperfection detection. This increases the confidence to integrate this instrument for on-machine surface metrology. However, there is no record of it being used for surface metrology even in an off-line set up. Therefore, this gap needs to be explored due to the instrument's low cost and robustness compared to other surface metrology instruments.
- **Environmental Influence**- On a typical shop floor, the instrument will be subjected to noise as a result of the impact of the environmental factors such as temperature and vibrations. As there is no record for using this instrument for surface metrology at the time of writing this thesis, there is also no record of its

ability to reduce environmental noise or compensate for errors associated with environmental variations. Therefore, investigations must be conducted to confirm the robustness of the identified instrument as well as develop techniques for improving the quality of results captured when using the identified instrument for surface metrology.

- **Calibration of the instrument-** During the active period of this thesis, the standard for calibration of areal surface instrument was being drafted [118]. Only a few techniques have fully-approved ISO standards for calibrations. Unfortunately, laser triangulation is not one of them. In other words, there is no knowledge of the calibration process to employ when utilizing the Keyence LV7000 for areal surface measurement. This gap also needs to be investigated into.

### **2.6.2 Predictive model**

To increase right-first-time in a milling process, the second aim of this thesis is geared towards employing optimization techniques to assist in predicting surface metrology information of machined surfaces based on the cutting conditions. Section 2.5 reviews both theoretical and data-driven surface roughness prediction models. The review reveals that the main factors affecting the surface texture of a machined parts are the kinematic properties of the cutting process. That is, the cutting speed, feed rate and depth of cut. Also, it was discovered from the review that using AI techniques for developed surface roughness model produces a more reliable and accurate model compared to other techniques. Hence, an AI model is considered in this thesis to assist the on-machine surface metrology to increase right-first-time machining on a shop floor. Unfortunately, the following areas have not been addressed in previous literature which create gaps in knowledge that need to be investigated.

- **Areal surface roughness model -** All the available AI models had profile

surface parameters as output. Even though areal surface parameters give more accurate representation of a surface compared to profile parameters, none of the available AI models considers it as an output to the model. This is most likely due to the cost and time involved to obtain areal surface measurement as well as the availability of instrument. Hence developing a model for areal surface roughness parameters will be a novel contribution to knowledge and exploits the first aim of the project which will readily provide areal data sets.

- **Appropriate surface parameter** - Numerous surface texture parameters can be obtained from a single areal measurement (See **Appendix A**). Some of the areal parameters have a great link with the functional performance of the machined surface. Hence, it is appropriate to investigate the right surface parameters that should be used to represent finishes obtained from face milling process. All the reviewed literature has paid no attention to selecting the appropriate surface roughness parameter that best describes machined part. This has created a gap in knowledge as there is no literature on surface parameters that best describes surfaces obtained from milling process.
- **Measurement area** – The area on the sample which is measured plays a key role in the measurement process especially on surfaces that do not have uniform structure of texture. This is because measuring different areas on such samples will produce different surface metrology information even though it was machined with the same cutting conditions. An investigation will also be considered to select the best area on a milled surface to best represent the whole surface under study.

# Chapter 3

## Laser triangulation for on-machine areal surface measurement

This thesis employs a low-cost laser triangulation line scanner for on-machine surface measurement. The overview of various techniques suitable for in-process and on-machine surface measurement and the specifications of new systems, described in the previous chapter, indicated that laser triangulation has the potential of being utilised for surface measurement of micro-scale level topography on machined parts.

The primary target for the application of the technique is on-machine metrology, specifically for the measurement of the surface texture of face-milled parts directly on the machine tool.

This chapter gives a detailed description of the instrument identified in the literature review and the logical justification. A series of experimental and simulation analyses are conducted to fine-tune the instrument. A new method for obtaining surface measurement using the laser line scanner instrument is then introduced to achieve high resolution and accuracy for rapid areal surface metrology.

### 3.1 General description of laser triangulation

The process of triangulation originated from trigonometry; a branch of mathematics that deals with the relationships between lengths and angles of triangles.

Triangulation can be defined as a process of finding unknown properties based on some known properties, provided that all the properties have a triangular relation. In reality, the unknown property can be the distance between two locations or the angle between three locations. Today, triangulation is found in applications such as surveying, navigation systems and metrology instrumentation.

In metrology, by setting up a laser diode and a light detector in the right order, the principle of triangulation has been used to develop non-contact displacement

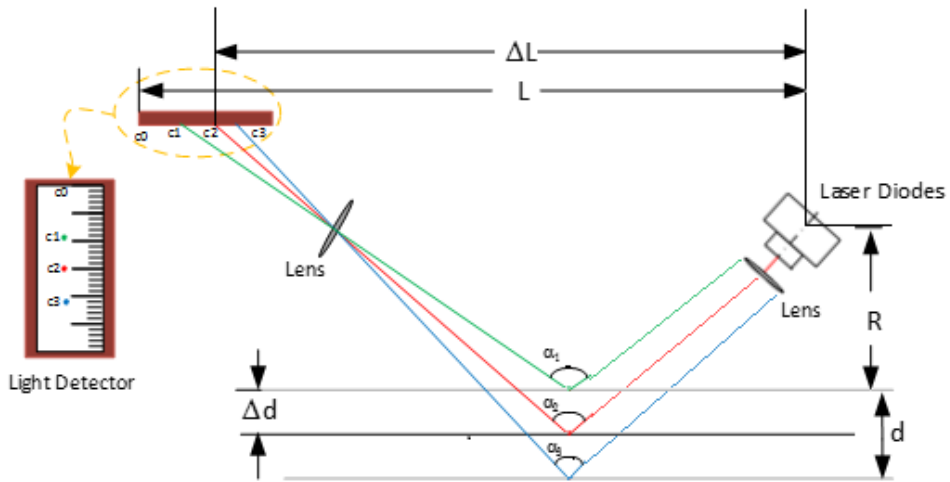


**Figure 3.1:** Laser triangulation for dimensional measurement

measurement as shown in figure 3.1. The measurement range of the instrument is denoted as  $d$  in figure 3.1.  $R$  is the distance between the laser and the near end of the measurement range.  $\Delta d$ , the distance between the surface of the object to be measured and the near end of the measurement range.  $\Delta d$  is the unknown distance in most cases. With assistance from the grading on the light detector, the distance between the reflected light and the source of the light (laser diode) is determined, labelled as  $\Delta L$ .

$\Delta L$  is the difference between  $L$  (a known distance from the laser diode to a known point ( $c_0$ ) on the graded light detector) and the point on the light detector where the reflected light is incident. Based on the point of incidence on the detector (for example,  $c_2$ ), the angle of reflection ( $\alpha_2$ ) is computed using  $C_1$  and  $\alpha_1$  or  $C_3$  and  $\alpha_3$ .

Some examples of laser triangulation applied in metrology applications and their merit over other techniques are reviewed in section 2.3.2. A laser line scanner, namely Keyence LJ V7000, which also utilised this technique is selected for further exploration for its potential to be used for on-machine surface metrology. At the time of this investigation, it was a new model with excellent specifications in terms of resolution and utilizes blue laser for low noise on shiny (machined) surfaces.

## 3.2 Laser line scanner –Keyence LJ -V7000

### 3.2.1 Description of the identified instrument

The Keyence LJ – V7000 series is a group of sensor heads developed by Keyence Cooperation Ltd for obtaining inline 2D and 3D form measurements. These sensor heads are classified under laser line scanners because;

- (i) they employ a laser triangulation measurement technique to capture data
- (ii) they traverse over the area of measurement to capture the data

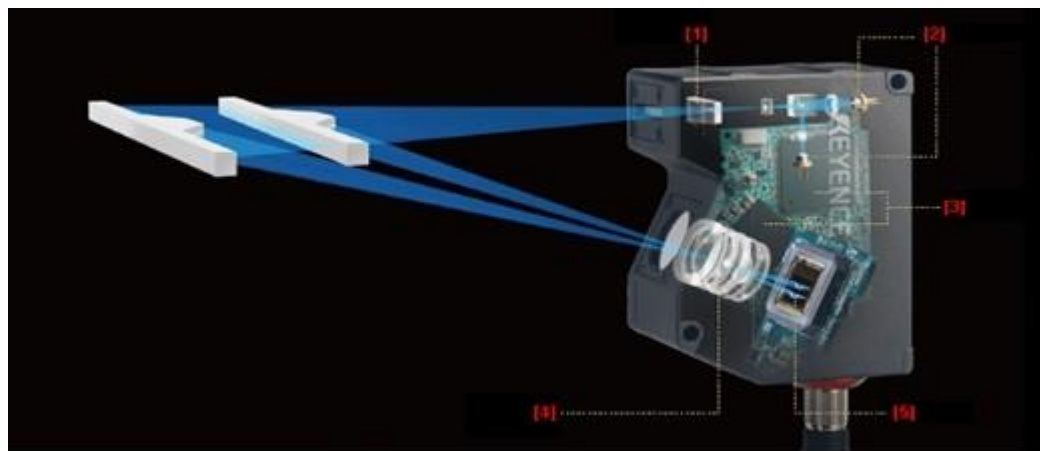


**Figure 3.2:** LJ-V7020K sensor head, taken from [119]

In other words, either the sample to be measured or the sensor head is kept in constant motion over the measurement area during the measurement process. The sensor head that was used in this thesis is the LJ-V7020K, and its primary components are shown in

figure 3.2. The datasheet of the chosen sensor head is presented in **Appendix B**. The sensor head shown in figure 3.2 comprise of;

- (1) Cylindrical lens
- (2) Semiconductor lasers
- (3) Processor
- (4) 2D ernostar lens
- (5) High-speed enhanced eye emulation complementary metal–oxide–semiconductor; HSE3 CMOS which serves as the light detector. The main noticeable enhancement comparing LJ-V7020K to the generic setup shown in figure 3.1 is the additional processor. This processor increases the rate at which the data is captured for high-speed measurement, handles imaging and generation of the data and checks whether or not the measurement is within tolerance (or in the field of view) before saving for post-process analysis.

### **3.2.2 Specification of the identified instrument**

The specification of LJ V7020K is presented in its dataset presented in **Appendix B**. However, some specifications are worth mentioning because they are the anchors of further discussions in this thesis. These include the spatial resolution, the measurement resolution and the range. The resolution in the profile axis (the direction of the laser scan line, which in the recorded data displays as x-axis) is  $10 \mu\text{m}$  over a length of 8 mm. In other words, every profile measured when using the LJ V7020K covers a length of 8 mm and consists of 800 evenly spaced sampling points, hence has a resolution of  $10 \mu\text{m}$ . Unfortunately, the length cannot be increased over 8 mm. In order to measure an area with width that exceeds 8 mm, multiple scans can be obtained in a raster mode and the captured dataset stitched together for analysis as considered by Nygaard [67].

The measurement resolution is  $0.1 \mu\text{m}$  in the z-axis direction i.e. the direction perpendicular to the surface being measured. The standoff distance from the sensor head to the surface is in the region 26.5 mm to 21.9 mm. Hence, the measurement range in the

z-axis is 4.6 mm. The resolution and the range in the z-axis cannot be altered.

The resolution in the time-axis (y-axis) is dependent on the speed of travel of the sensor over the surface and the sampling frequency during the measurement process. Equation 3.1 shows the relationship between the resolution in the time-axis, the sampling frequency and the speed of travel.

$$\text{Resolution in time - axis } (\mu\text{m}) = \frac{\text{Speed of travel } (\mu\text{m per second})}{\text{Sampling frequency } (\text{Hz})} \quad (3.1)$$

From equation 3.1, it can be deduced that by reducing the speed of travel and increasing the sampling frequency, the resolution in the time axis can be increased tremendously. A realistic example is if the sensor head is set to a sampling rate of 100 Hz and mounted on a CMM machine (as shown in figure 3.3) which is programmed to move at 1 mm/min across a known length, the resolution of the time-axis will be 1.67  $\mu\text{m}$ , calculation shown below.



**Figure 3.3:** LJ V7020K set on CMM for step height measurement in a clean room; arrow pointing the sensor head of the laser line scanner

$$\text{Sampling Frequency (Hz)} = 100 \text{ Hz}$$

$$\text{Speed of travel } (\mu\text{m/second}) = 10 \text{ mm/min} = 166.67 \mu\text{m/second}$$

Resolution in the time – axis ( $\mu\text{m}$ ) =  $166.67 / (100) = 1.67 \mu\text{m}$

However, it should be noted that moving at an extremely low speed and/or sampling at a very high frequency would greatly contribute to the level of contamination in the captured data. Therefore, it is expedient to find the optimized speed and sampling frequency to be used in every application i.e. identify the appropriate sampling frequency and speed of travel using the laser line scanner for on-machine surface metrology. Also, the minimum resolution is dependent on the beam waist radius of the laser or the spot size. The beam waist radius,  $\omega$ , is given by;

$$\omega = \left(\frac{2\lambda}{\pi}\right)\left(\frac{F}{D}\right) \quad (3.2)$$

Where ‘ $\lambda$ ’ is wavelength, ‘F’ is the focal length of the lens and ‘D’ is the input beam diameter. The spot size, ‘ $S_s$ ’ is also given by

$$S_s = 2\omega \quad (3.3)$$

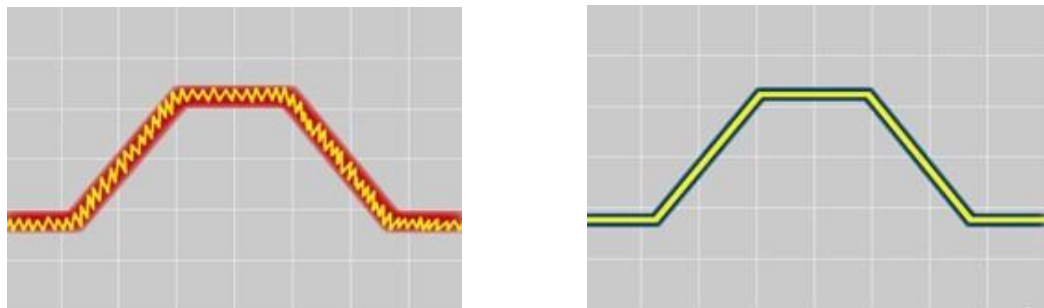
Therefore;

$$S_s = \left(\frac{4\lambda}{\pi}\right)\left(\frac{F}{D}\right) \quad (3.4)$$

From the dataset of the identified instrument in **Appendix B**, the spot size of the Keyence LV7020K is  $35 \mu\text{m}$ . This enables features of half the spot size to be measured [120]. Recall the expected spacing between the key features (machine trails) on the face-milled parts, stated in chapter 1 ( $31 - 166 \mu\text{m}$ ); the selected instrument should be capable of capturing these features during measurement.

### 3.2.3 Benefits of blue laser over red laser in metrology

The lateral resolution of the identified instrument is expected to be higher than other commercial laser line scanners. This is because most commercial laser line scanners utilise red lasers (wavelength,  $\lambda$ , between 740 – 625 nm [121]) while the LJ-V7020K uses a blue laser [119] (wavelength is 405 nm according to the data sheet in **Appendix B**). Based on the magnitude of the two wavelengths obtained from red and blue lasers and from equation 3.4, the identified instrument should guarantee sharp profiles as shown in figure 3.4. Due to the spot size, blue lasers have lower intensity compared to the red laser and so they penetrate less significantly into the sample being measured. Due to the high penetrations of red lasers, the light defuses, resulting in a spot that is defocused on the target surface. This gives rise to a blurred spot reflected onto the detector, meaning that an exact distance cannot be defined by the sensor. On the other hand, due to the reduced intensity and wavelength, the blue laser does not penetrate into the target object but it produces a focused laser point on the detector, providing precise and stable measurement results.



**(a)** With a conventional red laser, the beam that formed the image is thick, resulting in the generation of variation in the profile    **(b)** With a blue laser (LJ – V 7020K), the image forming beam becomes sharp to enable the measurement of shapes

**Figure 3.4:** Profile measurement obtained from red and blue laser taken from [122]

The shorter wavelength also performs better on glossy or highly polished/machined surfaces. A shiny surface distorts a red laser, resulting in a “speckle” effect. This produces an increase in the signal noise on the detector and as a result, the accuracy is lost during measurement. On the other hand, the shorter wavelength of the blue laser

performs better with much less speckling, resulting in much lower level of noise, typically by a factor between two and three when compared to red lasers for surfaces similar to those being considered in this research [122].

### **3.2.4 Data type obtained from the laser line scanner**

Data obtained from 3D scanners can be in either a point cloud or grid format. In point cloud format, the dataset is saved in reference to coordinates. Simply put, the dataset is a three-columned table consisting of x, y and z coordinates where each row represents a measured feature or sampling point. The grid format, on the other hand, presents the height values (z-axis coordinate) of the measured feature in a “large matrix”. The row and column in refer to the “large matrix” can be used to compute for its resolution as well as the x and y coordinates of the measured feature. Instruments that are designated for large volume scanning usually employ point cloud format while instruments that are used for obtaining height differences over surfaces usually utilise grid data format. The data obtained from the LV-J7020K is in a grid format. The rows represents all the measured profiles along the time-axis. 800 columns are obtained from measurements when using the LV-J7020K. This is because height differences are captured in 800 bins to obtain a profile. As explained earlier, the resolution in the profile axis is  $10 \mu\text{m}$  due to the 800 bins evenly spaced over 8 mm and the time axis is dependent on the sampling frequency and the speed of measurement. Unlike the speed of measurement that can be varied over a wide range depending on the specification of the motion axis (in this case the feed rate of a CNC machine tool axis), the sampling frequency is limited by the manufacturer to nine different levels. In order to select the appropriate sampling frequency, an investigation was conducted.

### **3.2.5 Selection of sampling frequency for on-machine surface metrology**

It is important to mention that, based on available literature at the time of this work, the

application of a laser line scanner to obtain areal surface topography measurement had not been performed therefore no guidelines for parameter selection existed.

For the time-axis direction, a travel length of 8 mm was considered in order to obtain a square area as the measured area (8 mm is the fixed length of the profile axis). That also helps to achieve a larger coverage area than the stated targeted area in chapter 1, and one which is significantly larger than many areal surface measurement systems.

To find the best sampling frequency, three arbitrary travelling speeds; 10, 20 and 30 mm/min, were used to measure a step height of 999.90  $\mu\text{m}$  with an uncertainty of 0.1  $\mu\text{m}$  from the artefacts calibration record. This was carried out first in a controlled environment and then on a shop floor. The speeds were carefully chosen, this is because the benefits of taken measurement with the identified instrument when the travelling speed is lesser than 10 mm/min is outwaded by the spot size of the instrument. Also, the target resolution in the time-axis cannot be met if the travelling speed is above 30 mm/min.

In the controlled environment (Coordinate Metrology Room), the room temperature was set to  $20^\circ\text{C} \pm 0.5^\circ\text{C}$ , the LJ-V7020K was mounted on a CMM (having passive vibration isolation) as shown in figure 3.3. For the second test, it was attached to a CNC machine spindle on the shop floor as shown in figure 3.5. The machine tool is a typical small 5-axis CNC milling machine. It has 3 Cartesian axes have an average traverse range of 600 mm and two rotary axes on which a 300 mm rotary work table is mounted. The test sample is clamped securely in a vice on the table. This is a very common CNC machine type and a typical setup for a component being manufactured on the machine, therefore the test is representative of the situation of in-process measurement we are trying to achieve.



**Figure 3.5:** CNC machine with Keyence mounted on for in machine surface measurement.  
1. Keyence Scanning Head 2. Specimen Block 3. Rotary worktable of 5-axis CNC machine tool

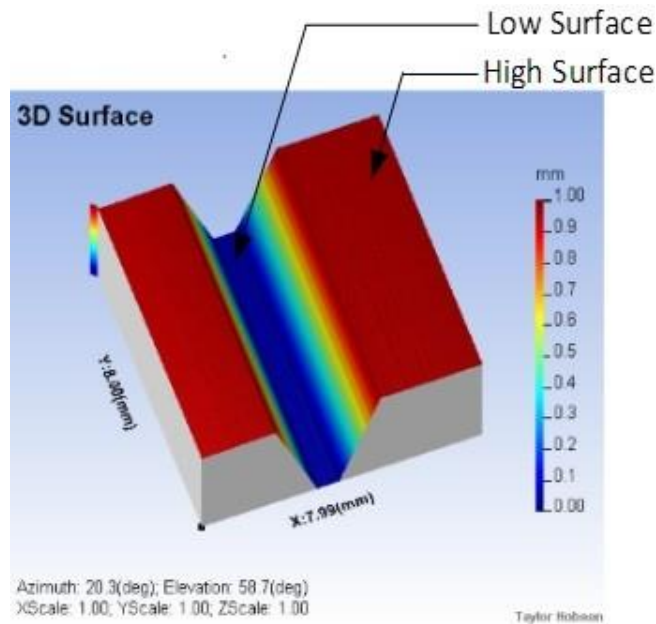


**Figure 3.6:** Topography of step height measured using line scanner LJ-V7020K

The nominal characteristic of the step height was obtained from the captured datasets by the following steps;

1. Average of high surface datasets was computed; ‘H’
2. Average of low surface datasets was computed; ‘L’
3. The difference between the two average values was computed; ‘n’.

Where ‘n’ is the expected nominal value of the step height ( $999.90 \mu\text{m}$ ). Figure 3.6 shows the topography of the step height obtained using the identified instrument. Measurements were performed three times for each sampling frequency, and the mean expected nominal value was considered. The error, which is the difference between the step height calibrated value and the measured value was obtained. Figure 3.7 shows a residual error from measuring the step height in both environmental conditions. The error bar depict the variations of the residual error whiles varying the travelling speed.

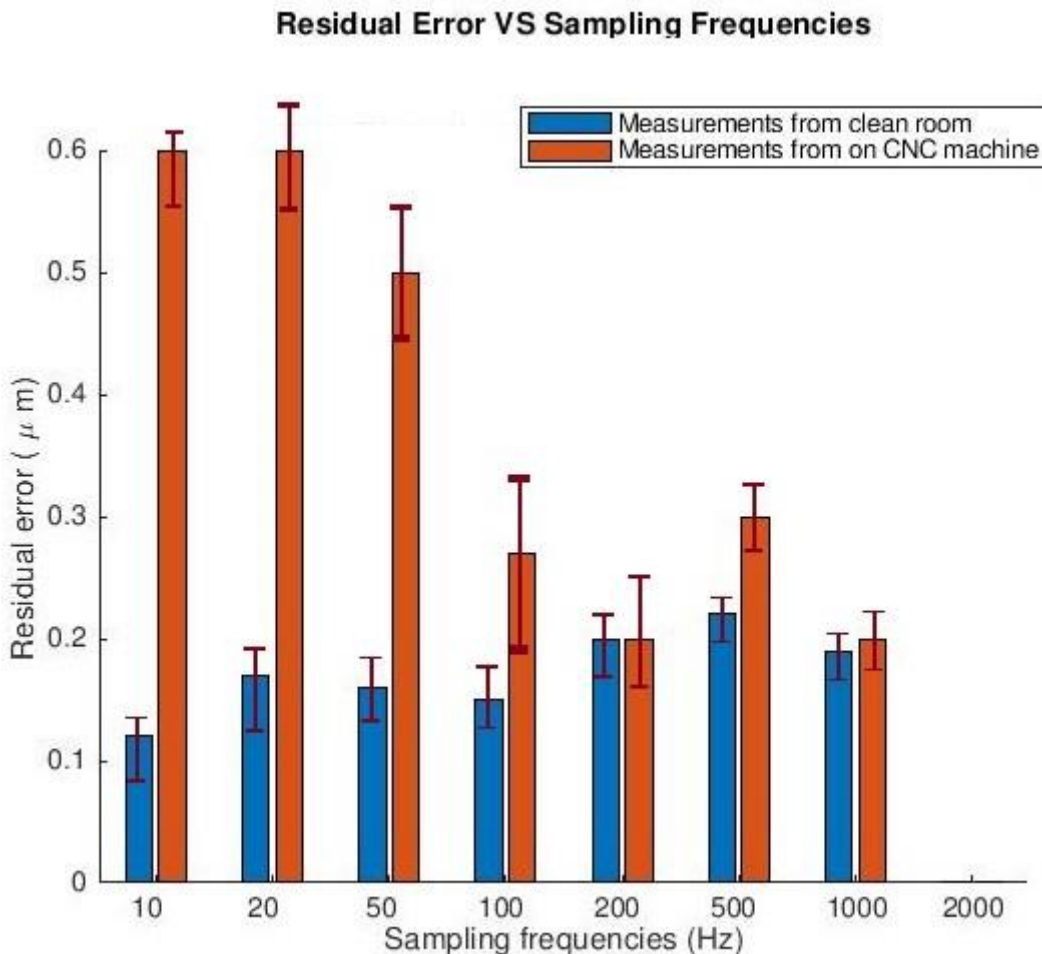


**Figure 3.7:** Residual error bar chart of the step height measurement against different sampling frequencies

It can be observed from figure 3.7 that the error bar at 2000 Hz has no width, indicating measuring with such sampling frequency is immune to errors associated with scanning speed at all levels. Unfortunately, it is not so, during the analysis of the captured dataset, a great challenge arose, which is to process measurements with more than 30,000 profiles. This issue could have been resolved by using a supercomputer with higher processing power than a typical desktop PC. Supercomputers were not considered because of availability and cost in relation to the scope of this thesis. Hence, datasets obtained while sampling frequency at 2000 Hz and scanning speed of 10 and 20 mm/min are not represented on the error bar chart. Likewise, at 1000 Hz only measurement obtained from 10 mm/min is presented. From figure 3.7, it can be deduced that measurements taken in a clean room are less subjected to the scanning speed variations compared to the measurements obtained on the CNC machine. The error associated with the measurements as a result of the variations of scanning speed was observed to be  $0.15 \pm 0.03 \mu\text{m}$  for a clean room and  $0.27 \pm 0.11 \mu\text{m}$  on a typical CNC machine.

This result also gives an insight into the instrument's noise and the on-machine measurement noise. Further experiments carried out will be discussed in chapter 4 to vindicate the instrument's noise and the on-machine measurement noise by utilising a novel scanning routine introduced in section 3.3.

It is also clear from figure 3.7 that, on a typical CNC machine in a shop floor environment, sampling at a high frequency reduces the residual error in the measurement. However, on a CMM in a clean room, the sampling frequency does not have a clear relation with the residual error.

100 Hz was selected as the sampling frequency and was utilised throughout the remainder of thesis for the following reasons:

1. Datasets obtained while sampling at 100 Hz and scanning at lower speeds such as 10 mm/ min is more manageable (33 Megabyte per scan), this makes processing of the measurement acceptable given the available time in the research and the

large number of machined samples anticipated for the research and validation phases.

2. Residual error, at three different speeds, is relatively small compared to measurement using other sampling frequencies in the case of both on-machine and clean room measurement.

It is important to mention that the line scanner used in the thesis provides an option to filter the captured dataset in both the time axis and profile axis. None of the inbuilt filtering features were used, this is to prevent key features of the surface topography being filtered out.

### **3.3 Improving lateral resolution in profile axis of LJ-V7020K**

As stated in chapter 1, the chosen approach for on-machine surface metrology is expected to have a lateral resolution  $< 5 \mu\text{m}$ . The identified instrument is limited to a lateral resolution of  $10 \mu\text{m}$  in the profile-axis. In order to improve the resolution in the profile axis as well as minimising the effect of shop floor vibration, a new mode of using the laser line scanner is explored; referred to as multidirectional scanning technique (MDS). MDS is one of the novel contributions of this thesis and has been published [123]. The multidirectional laser line scanning technique has the ability to capture a large measurement area ( $8 \text{ mm} \times 8 \text{ mm}$ ) without data-stitching in a single scan within a short time period ( $< 1 \text{ min}$ ). The large measurement area is sufficient to detect any irregularities on all face-milled parts considered in this thesis. This conclusion was made based on recommendation in BS ISO 4288:1998 [124] and ISO 25178-3:2010 [125] for selecting sampling size when measuring periodic surfaces. However, the following assumptions were made since both standards were for profile measurements and not areal;

1. The surface structure of the machined parts is homogenous and periodic.

$$2. RSm \approx Fz$$

Where;  $RSm$  is the profile elements ( $P$ ) average width as it indicates average value of the length of the profile element ( $P$ ) along the sampling length.  $Fz$  is the Feed per tooth vector of the face-milled surface where the profile element ( $P$ ) is perpendicular to the lays of the face-milled surface.

### 3.3.1 Procedure for performing MDS of areal measurement

To perform MDS, a small 5 Axis CNC machine tool (as shown in figure 3.5) is used to facilitate automated cycles and provide a constant lateral velocity across the measurement area on the face-milled part size (30 mm x 30 mm x 20 mm) during measurement. Detailed description of the face-milled part used in this thesis is given in chapter 5. The surface to be evaluated is scanned in two directions as shown in figure 3.8. The two directions are perpendicular but have a common datum (the first bin as shown in Figure 3.8), which is achieved to within 10 microns using the CNC machine. In other words, with assistance from the rotary axis of the CNC machine, two scans over the same surface (measurement area) is possible, however, perpendicular to each other in relation to their first profile.

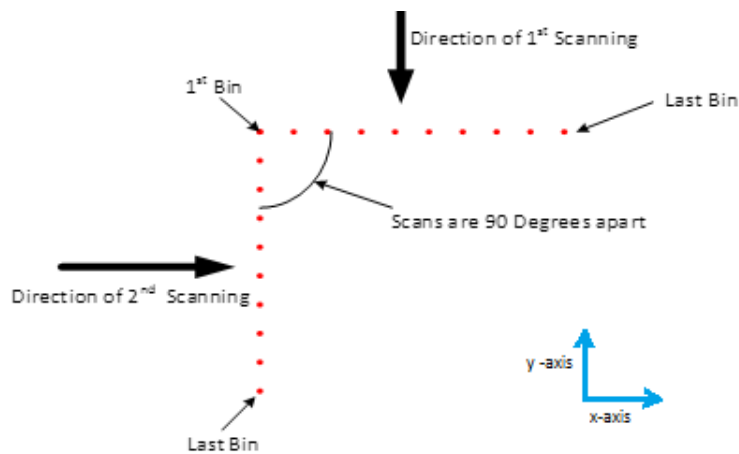


**Figure 3.8:** First data obtained from both the 1st and 2nd scan during MDS surface measurement over an area

A single profile scan takes  $< 32 \mu\text{s}$  to capture dataset which is a vector consisting of 800 elements (see datasheet in **Appendix B**). The short time spent minimises the effect of machine vibration i.e. any vibration having a frequency lower than  $\approx 15 \text{ kHz}$  will not affect the 800 points in a scan. This covers machine vibration experienced in this research. Subsequent scans are also unaffected relative to the line scan but are affected in an absolute sense over a scanned surface comprising many lines in the time axis. By rotating the sample, the direction, which was susceptible to vibration, is now measured by the line scan and thus is now immune. By combining the two datasets, it was envisaged that a robust 2.5D result could be obtained with good robustness against the inevitable vibration anticipated in on-machine measurement. Further analysis on the effect of vibration on MDS technique is included in section 3.4.

The merging of the two datasets are processed in the following order, explained using simulated datasets. Due to small errors in the machine, the plane of the surface being measured is not parallel to the plane described by the motion axis and the laser sweep axis. This ‘tilt’ error would affect this technique which requires the two data sets to be merged. This is easily achieved using a slope removal algorithm, so that any form of tilt on the surface that is captured during scanning is removed before merging the two datasets. The slope removal algorithm is applied to each dataset separately before the merging process. Section 3.3.1.4 includes the detailed method for this step of the new process.

### **3.3.1.1 Step 1: Importing datasets into MATLAB software**

The two datasets are imported into MATLAB and assigned with names for easy identification. In this description, scan 1 and scan 2 are used as the names for clarification propose (see figure 3.8). It should be mentioned that datasets obtained from the Keyence LV7020K scanner comprises of a header file and the dataset. Only the raw dataset is imported into MATLAB for MDS. Figure 3.9 shows two images captured after the simulated datasets are imported into MATLAB.



**Figure 3.9:** Images captured after initial importing datasets in MATLAB

From figure 3.9, the axis labelled with a red arrow is the y axis with reference to the surface of the sample being measurement on the machine tool and green arrow; the x axis. The change in axes observed from the two datasets shown in figure 3.9 is due to the 90-degree rotation explained in section 3.3.1.

### 3.3.1.2 Step 2: Rotation of 2nd scan

The 2nd scan is rotated 90-degree anticlockwise. This is to ensure that the orientation of the 2 datasets are with reference to the axes of the surface being measured and not to the instrument's axes (time and profile axes). Figure 3.10 shows a rotated form of scan

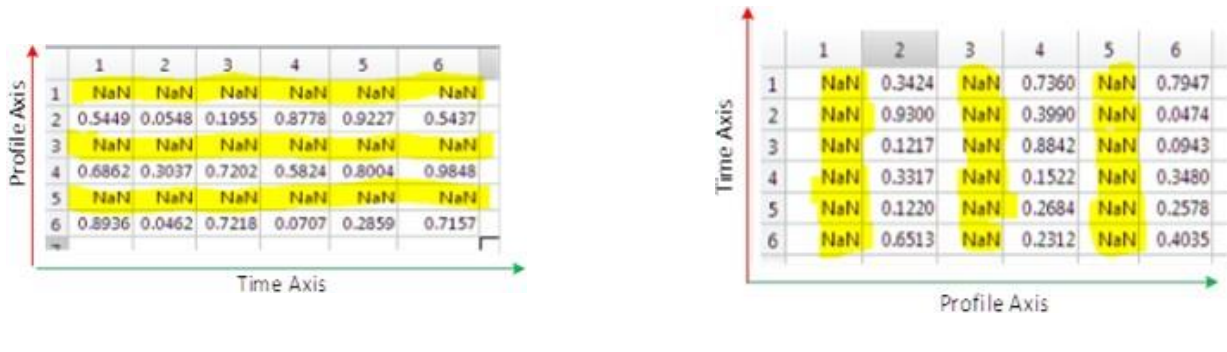


**Figure 3.10:** Images of datasets in MATLAB after resizing

### 3.3.1.3 Step 3: Resizing into square ‘matrices’

As it was stated earlier in section 3.3, the coverage area of the measured surface is square. However, the captured data is usually not a square matrix due to the difference in resolutions on the time and profile axes. In order to ensure the captured datasets are

presented as a square matrix, (looking as if the resolutions on the time and profile axes are the same) empty rows or/and columns are embedded into the captured dataset as shown in figure 3.10.

### 3.3.1.4 Step 4: Least square slope removal

A typical dataset obtained from scanning a surface might have slope embedded in the dataset. This is usually caused by tilting of the surface as explained earlier. Figure 3.11 shows a plot of such dataset. It can be observed from figure 3.11 that the impact of the slope on the dataset is in both X and Y axis.

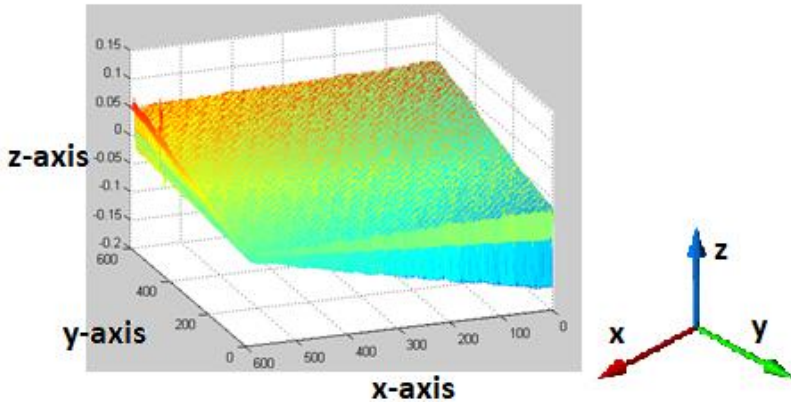


**Figure 3.11.** Dataset with slope affecting two axes

In order to resolve this, a slope removal algorithm is applied to both axes. The algorithm first fits a best-fit plane through the entire captured dataset using the least squared method. A transformation to move the best-fit plane to the origin is obtained and applied to the dataset. The angle between the best-fit plane and the X-Y plane about the X-axis is then computed. The angle obtained is used to rotate all the points in the captured dataset. The outcome is displayed in Figure 3.12.

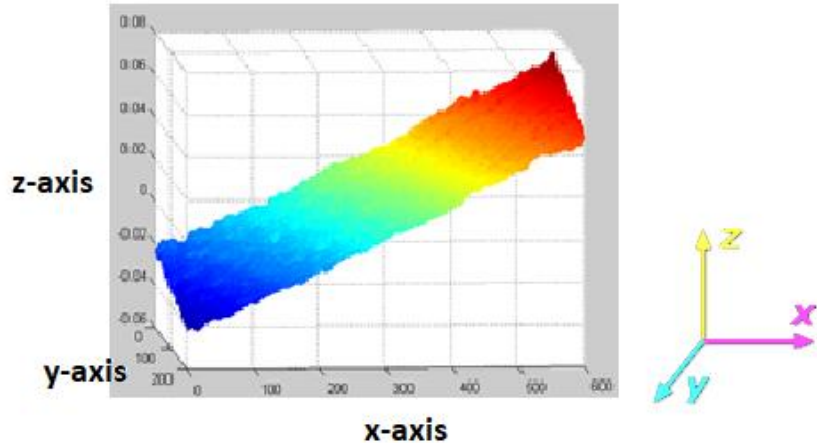


Figure 3.12: Dataset with slope affecting only one axis

The slope in figure 3.12 is along only one axis. In order to remove the slope in figure 3.12, the same rotation procedure is followed as explained above but rotation about the Y-axis plane with the calculated angle is done instead of rotation about the X-axis. The outcome after the translation and rotation procedures on the dataset is shown in figure 3.13.

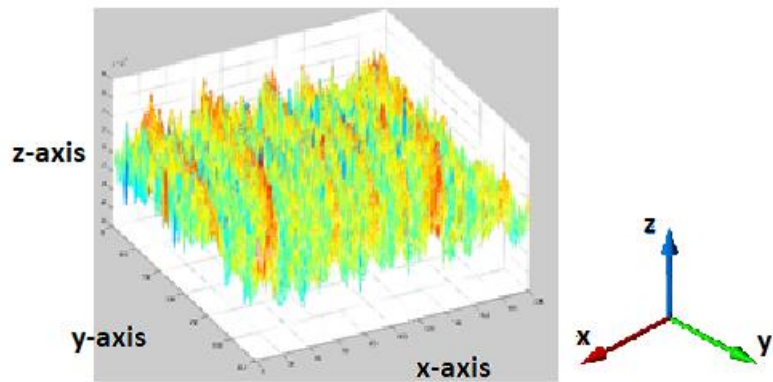


Figure 3.13: Dataset after applying slope removal algorithm

### 3.3.1.5 Step 5: Merging the datasets

Since the two datasets are now having the same size and have the same axes orientation which is with reference to the surface that was measured, an averaging technique is

employed to join the datasets. The result is the MDS dataset and is shown in figure 3.14.

	1	2	3	4	5	6
1	NaN	0.3424	NaN	0.7360	NaN	0.7947
2	0.5449	0.4924	0.1955	0.6384	0.9227	0.2955
3	NaN	0.1217	NaN	0.8842	NaN	0.0943
4	0.6862	0.3177	0.7202	0.3673	0.8004	0.6664
5	NaN	0.1220	NaN	0.2684	NaN	0.2578
6	0.8936	0.3488	0.7218	0.1510	0.2859	0.5596

**Figure 3.14:** MDS initial dataset captured in MATLAB

It should be mentioned that the MDS dataset does not have any reference to the axis of the measurement instrument (that is, it has no time or profile axes) and its axes are with reference to the actual surface of the sample that was measured.

### 3.3.1.6 Step 6: Filling in the empty cells

With the assistance of an advance data manipulation MATLAB algorithms, the missing data (observed as NaN in both figure 3.10 and 3.14) are estimated and filled as shown in figure 3.15.

	1	2	3	4	5	6
1	0.5364	0.3424	0.2735	0.7360	1.0264	0.7947
2	0.5449	0.4924	0.1955	0.6384	0.9227	0.2955
3	0.4282	0.1217	0.4869	0.8842	0.8585	0.0943
4	0.6862	0.3177	0.7202	0.3673	0.8004	0.6664
5	0.5806	0.1220	0.4420	0.2684	0.4374	0.2578
6	0.8936	0.3488	0.7218	0.1510	0.2859	0.5596

**Figure 3.15:** MDS final dataset captured in MATLAB

The data manipulation algorithm operates in the following manner;

- i. Searches for the location of the missing data (NaN) in the topology (MDS dataset).
- ii. Identifies the size of missing data clustered in the location by finding the nearest neighbouring numerical values, both horizontally (x-axis or row) and vertically

(y-axis or column).

- iii. Generate a plane having the size of the cluster of missing data. The height variation in the plane is obtained using interpolation of the values extracted from the nearest neighbouring numerical values to the cluster of missing data.
- iv. The data in the plane is used to fill in the missing data.

A header is then attached to the final dataset and saved as a .csv file which is easily accessible using surface metrology software packages such as Surfstand.

In order to confirm the robustness of the data manipulation algorithm the following topologies (figure 3.16, 3.17 and 3.18) were parameterized and compared.

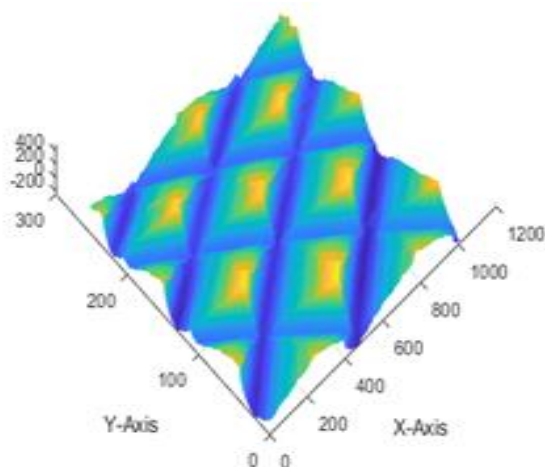


**Figure 3.16** A simulated ideal surface topology

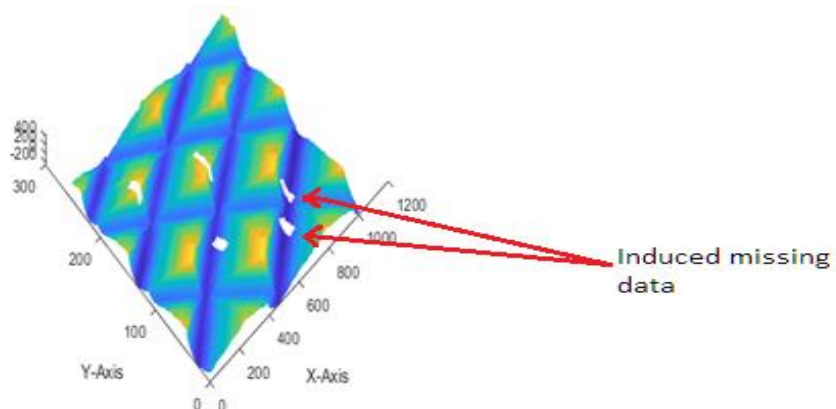


**Figure 3.17** Induced missing data in the ideal surface topology

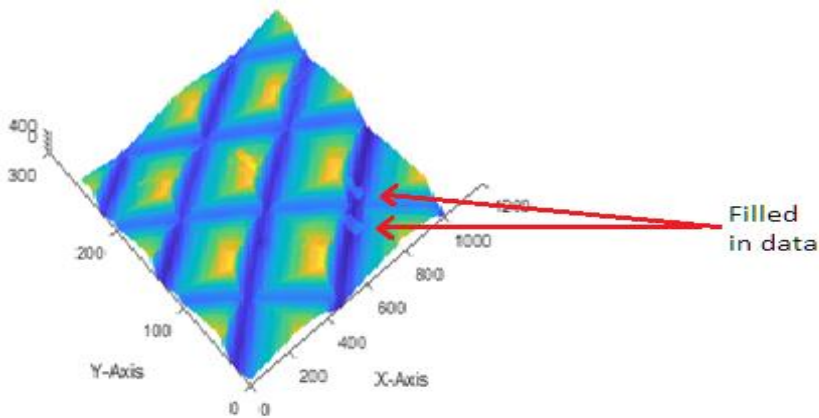


**Figure 3.16** Reconstructed surface topology using the data manipulation after induced missing data

The Sa values of the ideal topology, the induced missing data topology, and the restored missing data topology were 3.5  $\mu\text{m}$ , 2.8  $\mu\text{m}$  and 3.6  $\mu\text{m}$  respectively. The difference between the Sa value of the ideal topology (figure 3.16) and the induced missing data topology (figure 3.17) was 0.7  $\mu\text{m}$  whilst the difference between Sa value of the ideal topology and the restored missing data topology (figure 3.18) when using the data manipulation algorithm was less than 0.1  $\mu\text{m}$ .

It was also discovered that the differences between the ideal and restored missing data topologies were dependant on the cluster size. This is a limitation of this technique. In other words, this technique will struggle with large cluster size of missing data. However, since the data manipulation algorithm was used for only one missing data at a time during the MDS and the cluster size in a typical MDS data is very small, the error of deviation from the ideal topography will be negligible.

### 3.3.2 Effect of perpendicularity deviation error on MDS techniques

The fundamental concept of the MDS technique is based on the ability to capture two separate surface topology measurements of the same area but perpendicular to each other's starting point using a laser line scanner. Although a CNC machine tool rotary

axis is very accurate, there will be deviations from the 90 degrees rotation during MDS therefore perpendicularity deviation as a result of the rotation process may introduce errors into the final merged topology.

In order to understand the effect of the perpendicularity deviation, an experiment was conducted aimed at exploring the degree of error likely to be introduced into the MDS surface metrology final topology due to this deviation. A calibrated artefact that is, SFM 001; image can be found in **Appendix D.1.1** with  $S_q$  value of  $5.6 \mu\text{m}$  and homogeneously spaced surface structure was considered as the surface to be measured in this experiment.

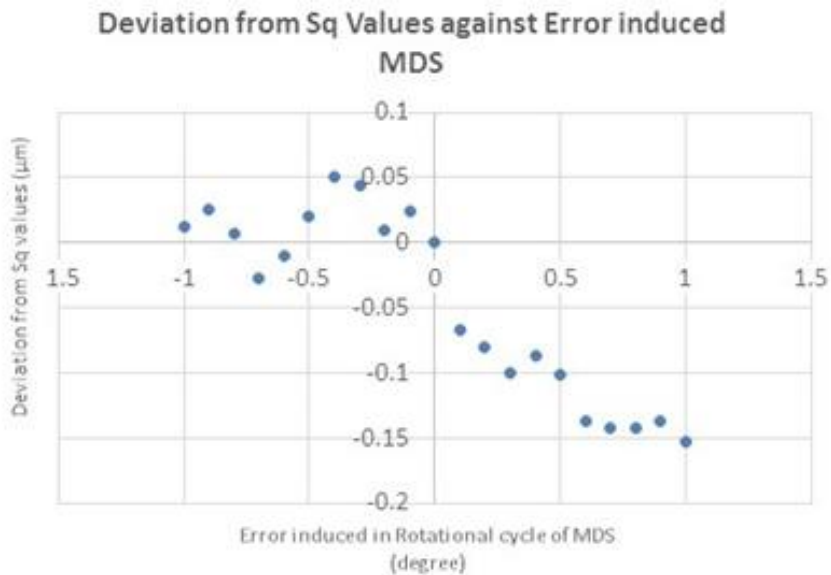


**Figure 3.19:** Deviation from  $S_q$  values against error induced MDS

With assistance of the rotary axis of the machine tool (resolution of 0.01 degree) perpendicularity deviation error was self-induced into the MDS technique in unit steps of 0.1 degree to  $\pm 1$  degree. This range covers rotary positioning errors in any type of CNC rotary axis on a shop floor and perhaps also lower precision indexing tables if they were to be used. Figure 3.19 shows the effects of the induced error on  $S_q$  parameters. From figure 3.19, it can be deduced that positive error induced in the rotational cycle of the MDS has a linear relationship with the impacted error on the  $S_q$  value whilst negative induced errors showed no relationship.

The cause of the difference in values is due to the fact that; a change in the angle for the measurement, changes the angle between the scanning line and the lays of the surface. Hence, there is a likelihood of missing key topography data during the measurement of the surface. The ideal recommended angle is 90 degree according to ISO standard. Changing the angle also changes the angle of refection of the laser triangulation instrument and hence, increase the chance of large variations. Another reason could be that, the change in the angle will also change the exposal of light to the surface being measured and this too can have an impact on the quality of the results. In any case, the overall effect is negligible for anticipated errors on CNC machine tool i.e. < 0.1 degrees proving that the method is robust against this potential error source.

It should be mentioned that tilt of surface is bound to happen, which could also have an impact of the accuracy of the measured topology when using MDS. The cause of the tilt of the surface could be associated with two main factors;

- (1) Inability to replace the machined sample at the exact location it was machined due to uneven base of the sample.
- (2) Loose grip of the machined sample on the worktable of the machine tool due to improper tightening of machine vice during the cutting process as well as the measurement process.

In order to avoid or reduce the above factors from affecting the measurement used in this thesis, the base of all samples were flatten and also a further inspection was conducted by the machinist to confirm the sample was firmly gripped in the worktable's vice.

### **3.4 Simulation of noise compensation using MDS for surface measurement**

In order to determine whether the MDS technique can reduce the impact of

environmental noise such as machine tool vibration, a series of simulations and experiments were conducted. The first experiment involved identifying height variations in measured results due to the impact of the environmental noise on the shop floor as well as in the machine tool. Secondly, an ideal surface topology for a milled surface was generated and with assistance from surface metrology software package, the  $Sq$  value of the simulated surface topology is obtained. This is referred to as ' $Sq_i$ '. Finally, based on the results obtained from the first experiment, different levels of white noise were induced into the simulated surface topology to obtain different surface topology with induced noise. The  $Sq$  of these surface topologies were also retrieved and are referred to as ' $Sq_n$ '. The  $Sq$  of the MDS surface topology,  $Sq_{MDS}$ , was also obtained after merging two surface topologies, both of which had white noise induced in them. The noise were induced in different axes directions, i.e. due to the different scan directions.

It can be recalled from the explanation in section 3.3 that the same degree of noise affects the line scanner in its profile axis because the time spent to capture a single profile is  $< 32 \mu\text{s}$ , sufficiently short that the deviation in the noise level during the scan of a single profile is negligible. Hence, the same level of noise affects the dataset in the same profile axis. However, the time-axis is subjected to different levels of environmental noise hence, the potential for a high level of inconsistencies when using a line scanner for surface metrology in its normal operating mode.

In these experiments  $Sq$  was chosen as an indicator because of its high sensitivity to height variation compared to other height related areal surface parameters (See **Appendix A**).

### **3.4.1 Simulation of ideal face-milled surface topology**

While the vibration levels measured are not very significant, the results obtained from the MDS method indicate a degree of immunity or averaging that occurs due to the different effects of noise in the time axis and the profile axis. In order to fully understand

this effect, simulations have been performed using ideal and noisy data. The following assumptions were made in the generation of the ideal surface topology;

1. The surface topology of a face-milled part can be represented in a periodic form. Hence a continuous sinusoidal form is considered.
2. The ideal surface topology is not affected by any other factor except the tool geometry. Factors such as tool wear, the effect of coolant and other cutting conditions were not considered in the simulation. The tool is made up of a round tip insert, hence a cycloid effect is used to represent the generated surface, where the radius of the cycloid effect is the radius of the tool inserts. The peaks also represent the feed per tooth vector. Figure 3.20 shows a cycloid for the simulation of a profile for a face-milled surface.

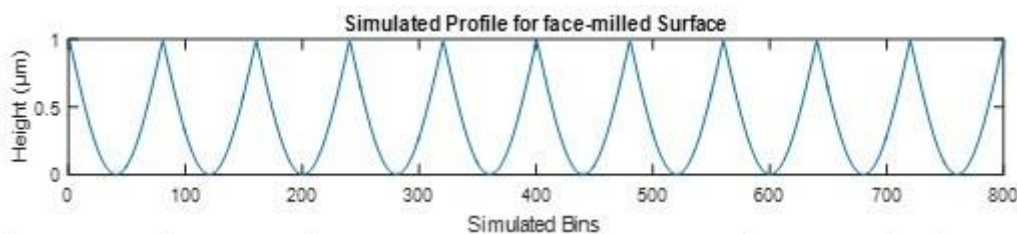


**Figure 3.20:** Simulated profile for a face-milled surface

Rz, the distance between the maximum and minimum point on the profile, which can be calculated using measurement from the vertical distance from the lowest valley to the highest peak within five sampling lengths, then averaging these distances is the same as the amplitude of the cycloid.

A surface topology is generated using the simulated profiles in figure 3.20. A compilation of multiple simulated profiles is used to obtain the simulated surface topology which mimics the results from the laser line scanner when scanned over face-milled parts. The outcome depicts a surface consisting of height maps which is similar to dataset obtained from the LV7020K instrument. The final dataset is imported into Surfstand [126] a commercial and incorporates the relevant areal surface ISO standard

calculations for parameterization in order to obtain the Sq of the ideal simulated surface topology.

It should be mentioned that Rz is varied to cover the full range of surface finish grades this research targets. 0.5, 1.0, 3.0, 6.0, and 8.0  $\mu\text{m}$  Rz values were considered. Five different surface topologies were generated using the above Rz values and parameterized to obtain their corresponding Sq values. During the parameterisation process, no filtering technique was employed.

Figure 3.21 shows the simulation of surface topology of a milled surface using multiple stacks of profiles (1600 profiles). Table 3.1 shows the Sq values obtained from all the Rz values considered. It can be seen from table 3.1 that as Rz increases, the corresponding Sq also increases as expected.

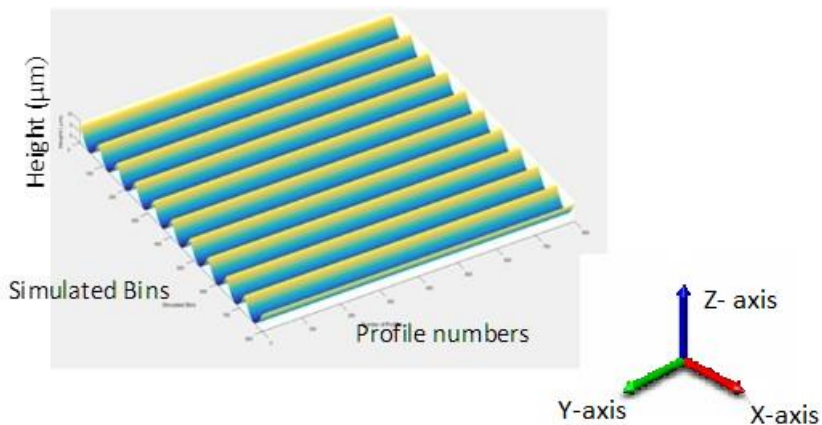


**Figure 3.21:** Simulation of surface topology of milled surface

**Table 3.1:** Rz and its corresponding Sq value

Rz ( $\mu\text{m}$ )	Sq ( $\mu\text{m}$ )
0.50	0.15
1.00	0.31
3.00	0.92
6.00	1.85
8.00	2.47

### 3.4.2 Quantification of environmental noise on height measurement

There is a huge variation of shop floor environmental conditions in different manufacturing industries. Factors such as the size of the shop floor, foundations (type and thickness), types of machines used, the proximity of the machines to each other, ventilation systems and the geographical location of the shop floor play an important role in environmental conditions on a shop floor. It is obvious that multiple machine tools could induce high temperature and vibrations with high amplitudes when the machines are all in operation compared to a shop floor with a single machine tool.

We also cannot neglect the fact that, the floor vibrations; vibrations from active component of machines, passive vibrations on the shop floor and other sources of vibration will have different magnitudes on different shop floors. Zhang *et al.* [127] confirmed that on a typical machine in a shop floor, the vibration frequency range could cover from  $\approx 12$  Hz to  $\approx 12$  kHz.

Apart from isolating the vibration in order to avoid its influence on the measurements, instruments used for on-machine surface metrology are expected to be robust to rapid temperature changes which is one of the main factors that effects on-machine metrology. Multiple sources of heat can be identified on a typical shop floor, which contributes to a large range of variance of the ambient temperature in a shop floor. These sources include heat generated from machine parts such as bearings, gears, and motors. Other sources of heat on the shop floor are also from the machining process itself or external sources (example, heat from outside the workshop when a door is open). It is very difficult to control most of these heat sources, henceforth; it is expedient that the identified instrument for the on-machine measurement is verified for its immunity to temperature variance during measurement.

The shop floor considered in this thesis is within an academic machine tool workshop with several CNC machine tools operational. A series of studies were conducted to establish the feasibility for on-machine measurement on this shop floor. Finally, height variations caused due to the influence of the environmental noise on the shop floor is also measured.

### 3.4.2.1 Impact of temperature on surface metrology

In this analysis, the main aim is to find out if the variation of temperature on the shop floor will affect the surface measurement obtained using MDS technique. In other words, the influence of temperature on the performance of the LV7020K based on the instrument's specification when in operation in a shop floor is analysed. A check on the effect of any significant expansion of workpiece materials during the measurement procedure on the shop floor is also performed. The following metals were considered: aluminium, steel, and titanium and their coefficients of linear thermal expansion are  $23.1 \times 10^{-6}/\text{K}$ ,  $12 \times 10^{-6}/\text{K}$ , and  $8.5 \times 10^{-6}/\text{K}$  respectively.

In order to discovery the variation in temperature on the machine tool which the surface measurement procedure will be carried out, multiple temperature sensors were placed at vantage points around the machine tool. The sensors were attached to the following parts; the surface of the machined part (in this case aluminium), the surface of the worktable of the machine tool, the machine's main cast iron structure and two sensors positioned arbitrarily inside the machine tool to measure the ambient temperature inside the working volume of the machine where the instrument (LV7020K) was mounted. The experiment was conducted over a 3-day period for any notable temperature change.

Figure 3.22 was generated from the captured temperature data from the sensors. Figure 3.22 shows experimental thermal profiles obtained for three days in a typical shop floor environment. The overall temperatures varied by approximately  $\pm 2^{\circ}\text{C}$  in the head assembly and approximately  $\pm 0.5^{\circ}\text{C}$  at the bed (base structure of the machine) during the 3-day period. This result confirms that temperature change over a short period ( $< 1$  minute) will not have any significant impact on the surface measurement of the machined part. The maximum and minimum recorded temperature captured over the experimental period were  $25.5^{\circ}\text{C}$  and  $21.3^{\circ}\text{C}$  respectively as it can be seen in figure 3.22. According to the specification of the instrument; LJ-V7020K (see **Appendix B**), the temperature sensitivity is  $0.01\%$  of FS/  $^{\circ}\text{C}$ . Due to the fact that the range of the measurement FS is so small for this application, typically  $< 10 \mu\text{m}$ , the maximum temperature effect would be negligible ( $0.0001 \times 10 \times 4.2 = 0.0042 \mu\text{m}$ ).

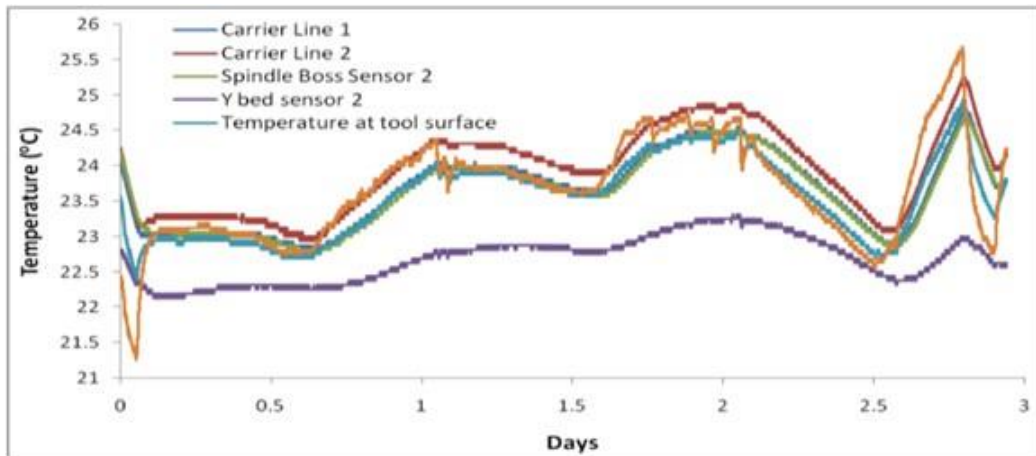


**Figure 3.22:** Environmental temperature variations recorded over 3 days

### 3.4.2.2 Impact of vibration on surface metrology

In this section, the vibration which is generated by the machine tool and the local shop floor environment during the MDS technique is measured using an external instrument and compared with the acceptable vibrational frequency range and its corresponding amplitudes of the LV7020K. Vibrations are generated by various rolling and sliding elements of the drive system on the machine tool while the worktable is usually traversing. Any ancillary equipment such as pumps and any external machinery operating during the MDS scans also generates vibration. Analysis conducted in this section aims to expose the frequencies and amplitudes of these vibrations on the machine tool prone to affect the MDS method. The experiments conducted in this section was further divided into two; the impact of vibration on the vertical axis and lateral axis of MDS.

#### ***Impact of vibration on vertical z-axis direction of MDS***

In this section, noise (vibration in a machine tool and the surrounding environment on the shop floor likely to be systematic and sinusoidal due to rotating motors, bearings, other machinery, structural resonances and other factors which may include the existences of random vibration as well) which affects the raw dataset captured during

on-machine surface metrology was measured. The noise is characterized as a variation of height which will be used in later simulations to determine how the variation is handled by the MDS. In order to achieve this, a single point laser triangulation instrument (LK-H022); with very high resolution of  $0.01 \mu\text{m}$  was used to record changes in height readings of a flat artefact. The resolution of this instrument is 10 times better than the z-axis resolution ( $0.1 \mu\text{m}$ ) of the laser line scanner. Three sets of environmental conditions were considered which are outlined below.

- (i) Performing the routine for the MDS procedure (in the machine tool)
- (ii) Inside the machine tool (whiles the instrument is idle)
- (iii) Outside the machine tool but on the shop floor (on a bench closer to the machine tool).

The range between the captured data and standard deviation was computed and tabulated in table 3.2. It could be concluded from the results that measurements on the machine tool are less affected by noise and vibration compared to measurements obtained on the shop floor. This reduction of noise might be due to the inbuilt vibration absorption system of the machine tool. This reduces the amplitudes of the noise to almost half its magnitude if compared to measurement on the shop floor.

**Table 3.2:** Height variation as a result of white noise in a machine tool

	Range ( $\mu\text{m}$ )	Standard deviation ( $\mu\text{m}$ )
<b>On machine tool,in motion</b>	0.25	$2.91 \times 10^{-5}$
<b>On machine tool, idle</b>	0.37	$3.55 \times 10^{-5}$
<b>On the shop floor</b>	0.59	$0.89 \times 10^{-4}$

Another observable difference between the measurements when the machine tool was stationary and when in motion depicts that, the on-machine measurement without utilizing the machine tool axes increases the noise level unless the machine tool is completely turned off. However, this condition (measuring the noise when the machine tool is completely turned off and assuming some other system (for example a robot arm)

performs the motion for MDS) was not captured in table 3.2 because it is beyond the scope of this research.

### ***Impact of vibration on lateral-axis of MDS***

It is also important to consider the impact of vibration on the lateral -axis of captured data when using the MDS measurement technique as well. This vibration measurements were conducted with an industrial tri-axial accelerometer (type IMI ICP model 629A11) using a single NI 9234 data acquisition (DAQ) hardware unit. The sensitivity and measurement range of the accelerometer used were 100 mV/g and  $\pm$  50 g respectively. The data acquisition system had the following parts; NI 9234 IEPE ADC for capturing data in x, y and z-axes, an NI 9172 USB interface and a LabVIEW based data acquisition interface.

Two pairs of vibration capturing experiments were conducted in this section. In the first experiment; the accelerometer was attached to the spindle (as shown in figure 3.23a) in order to measure the vibration that will affect the surface metrology instrument. The vibration data was captured whiles the machine tool performs the sequences for MDS. With the same set up (shown in figure 3.23a) a second experiment is conducted while the machine tool is stationary but not powered off. This forms the first pair of experiments.

Another pair of experiments are conducted whiles the accelerometer is attached to the worktable as shown in figure 3.23b. Vibration data was also captured for both stationary and in motion states of the machine tool. It can be noticed that, two separate experiments have been conducted and one can be used to represent the natural inherent vibration frequency of the machine tool since the machine was not in motion. The second also represents vibration generated because of the axial traverse motion of the CNC machine.



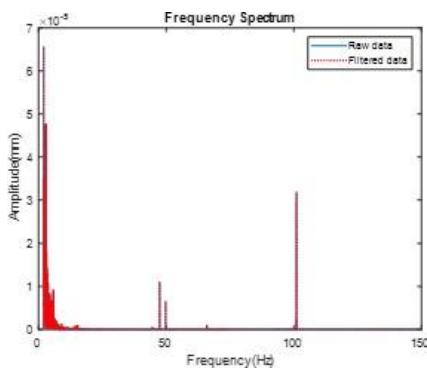
**(a)** Accelerometer attached to the spindle during MDS measurement



**(b)** Accelerometer attached to the worktable during MDS measurement

**Figure 3.23:** Experimental setup to measure vibration during MDS measurement; red arrow pointing to accelerometer in both figures

It should be mentioned that by finding the double integral of the data captured from the accelerometer (acceleration); a displacement value is obtained which has direct relation to the surface metrology data captured when using LV7020K. In this experiment, the displacement value along the lateral axis of the laser line scanner, captured with the accelerometer, was considered as the error induced in the measurement by the vibration of the machine tool.



**(a)** Frequency spectrum obtained when the machine is idle **(b)** Frequency spectrum obtained when during MDS measurement

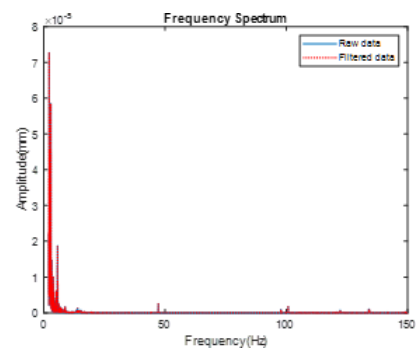


**Figure 3.24:** Frequency spectrum obtained when the accelerometer is attached to the spindle

Figure 3.24 and figure 3.25 provide the frequency spectrums of the data captured with the accelerometer when attached to the spindle and worktable respectively. These were obtained by using Fast Fourier transform (FFT). From both results, it can be deduced

that the machine tool generates more noise (vibration frequencies) while it is stationary compared to when it is in motion. This was an unexpected results. Also, by converting the acceleration axis of a normal frequency spectrum of a vibration signal to displacement, it can clearly be seen that the displacement caused by vibration during MDS measurement is within the vibration tolerance of the laser line scanner.

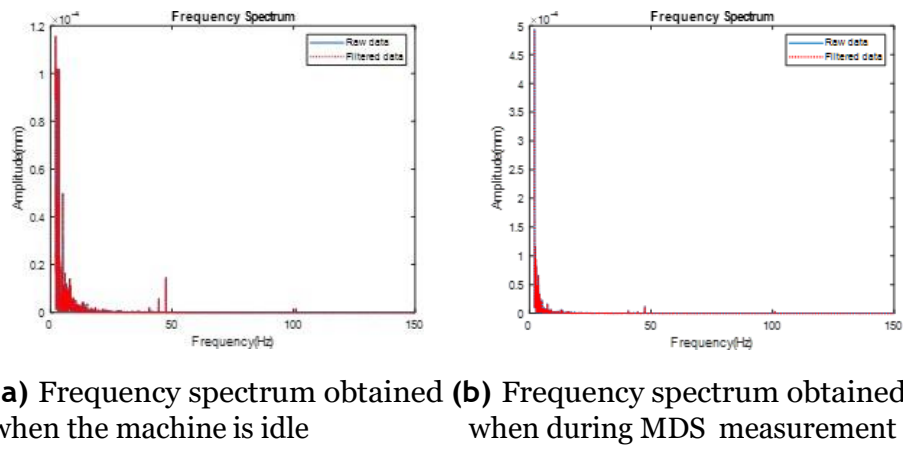


**Figure 3.25:** Vibration signal analysis obtained when the accelerometer is attached to the worktable

Since all the dominant vibration frequencies shown in the frequency spectrum are less than half the sampling frequency of the MDS (100 Hz) the possibility of the results from MDS being immune to the vibrations is high.

### 3.4.3 Simulation of ideal face-milled surface topology plus noise

This section explores the variation in  $S_q$  value when noise is induced in a simulated surface topology. The simulated topologies used in this section consist of the aforementioned ideal structure (figure 3.21) and embedded self-induced noise. The magnitude of the induced noise was ensured to cover the experimentally determined ranges in the results in table 3.2. The noise was applied in the following manner;

1. The same level of noise affects datasets along the same profile axis. Since it has been established that the time taken to capture a single profile data is short enough

to avoid the data being affected by different levels of noise.

2. The effect of the noise on datasets along the same time axis fluctuates randomly.

Multiple simulations were conducted with five different maximum amplitudes of the induced noise; 0.05, 0.10, 0.15, 0.20 and 0.25  $\mu\text{m}$ . At each noise level, the Rz, of the ideal surface topology was also varied.

### **3.4.3.1 Simulation of face-milled surface topology considering MDS effects**

During the MDS, the same surface is scanned twice; that is, if the topology shown in figure 3.21 is to be obtained using MDS, the first scan's profile axis will be say parallel to the lays of the surface (y-axis) and the second scan's profile axis will be perpendicular to the lays of the surface (x-axis). This means the manner in which the noise influences the two scans differs. That is, for the first scan, the variation of noise will be induced on the x-axis while the constant level of noise will be in the y-axis with reference to figure 3.21. This is opposite in the case of the second scan. The variation of noise is expected to affect the y-axis while the constant level of noise; the x-axis with reference to figure 3.21. Hence, Sq obtained from noise-induced surface topology will be referred to as  $Sq_{n1}$  and  $Sq_{n2}$  where n1 and n2 denote first and second simulated scanned dataset respectively.

### **3.4.3.2 Results; different noise levels in surface topology simulations**

Figure 3.26 shows a surface plot of the percentage residual error when the variation of noise is perpendicular to the ideal surface topology. The percentage residual error (%RE) is given by;

$$\%RE = \frac{Sq_n - Sq_i}{Sq_i} \quad (3.5)$$

Where  $Sq_n$  is the Sq obtained from a surface topology with an induced noise,  $Sq_i$  is obtained from the ideal surface topology and the two topologies were generated with the

same Rz.

From Figure 3.23, it can be deduced that at low Rz, which is from 0.5 to approximately  $3 \mu\text{m}$ , the influence of the noise is relatively high compared to higher Rz values. Also, higher Rz values; Rz value above  $3 \mu\text{m}$ , turn out to be almost immune to the low level of noise  $< 0.1 \mu\text{m}$ .

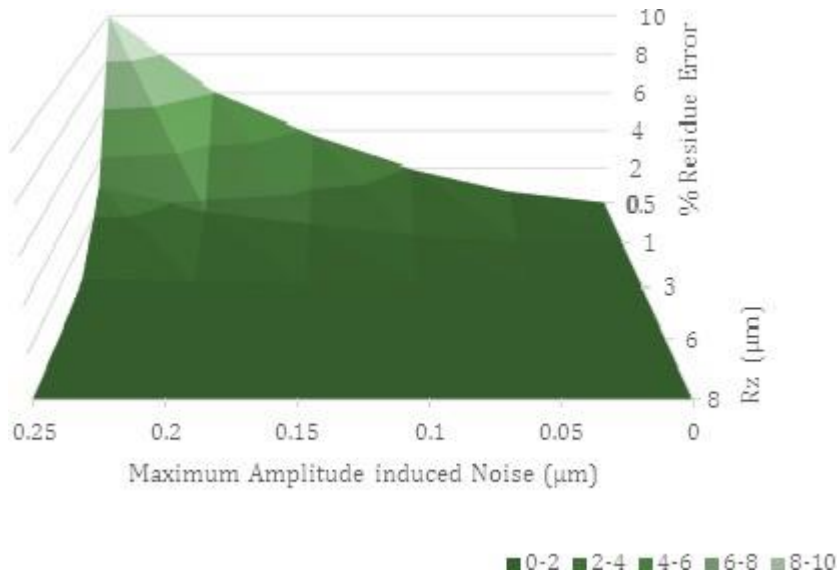


**Figure 3.26:** Surface plot of residual error in  $\text{Sq}$  by scanning perpendicular to the surface lays

Figure 3.27 shows a surface plot of the percentage residual error when the variation of noise is parallel to the ideal surface topology lay. The relationship between the impact of induced noise and the Rz values remains the same in both cases (that is in figure 3.26 and 3.27).

Even though there was a reduction in the residual error (approximately about 1%) at the lowest Rz value ( $0.5 \mu\text{m}$ ) when the maximum amplitude of the induced noise was at its highest ( $0.25 \mu\text{m}$ ), most of the other features of the two results are similar. Figure 3.28 presents a surface plot of the residual error obtained using the new MDS technique.

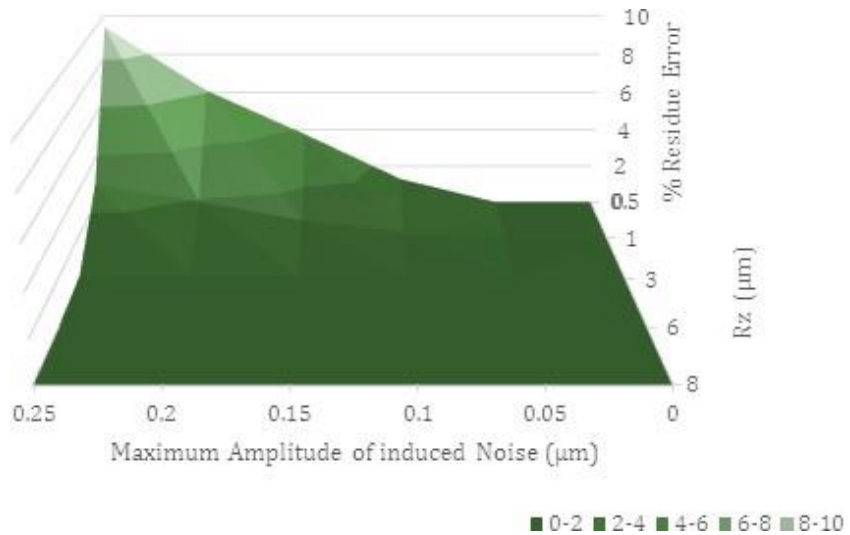


**Figure 3.27:** Surface plot of residual error in  $S_q$  by scanning parallel to the surface lays

Comparing the three surface plots (figure 3.26, 3.27 and 3.28), it can be seen that there is a significant reduction in the level of residual error when the MDS technique is used. This can be due to the fact that, averaging multiple measurements of the same measurand but with different sensitivity due to the sampling rate, reduces the level of induced noise significantly. Hence, this demonstrates the possibility of the MDS reducing the level of noise.

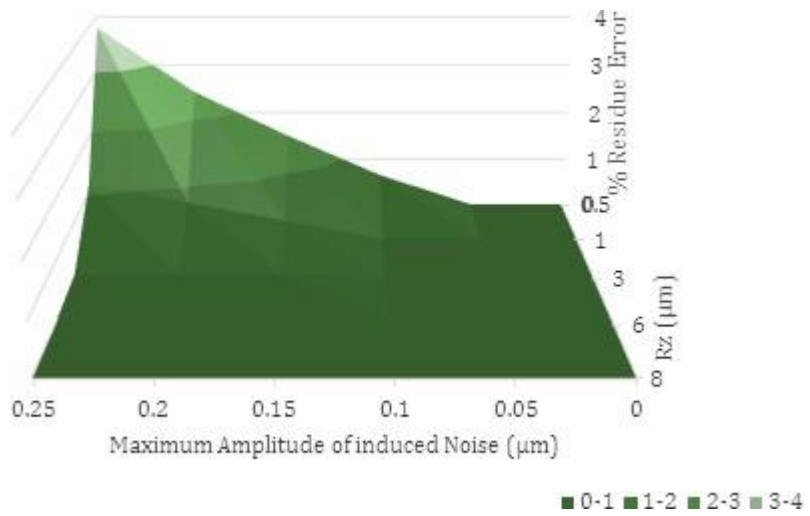


**Figure 3.28:** Surface plot of residual error in  $S_q$  by using MDS

### 3.5 Summary of chapter

The chapter has introduced the basics of laser triangulation and its application in

metrology. This chapter also gives the description of the identified instrument and its benefit over other instruments. The lateral resolution of the instrument is  $10 \mu\text{m}$  in the profile axis and for the time axis depends on the sampling frequency and speed of travel. The resolution in the z-axis is  $0.1 \mu\text{m}$  making it more suitable for micro-scale measurement. The benefit of the identified instruments includes variable sampling frequency.

In this chapter, with the assistance of a step height artefact, it was proven that sampling at 100 Hz, was the most suitable setting to achieve quality measurement in the targeted application without the height resolution being significantly affected by external noise. Merits of this selection include but not limited to not capturing a prohibitively large data size which is difficult to process and avoids very slow speeds scans which are subjected to a wider range of noise. The maximum amplitude of noise on the machine tool used in this thesis was found to be  $0.17 \mu\text{m}$ .

This chapter also presents a novel approach referred to as Multidirectional Scanning technique as a solution for the low resolution in the profile axis compared to the time-axis and z-axis of captured data when using the selected instrument. This technique increases the resolution of the profile axis to match up with that of the time-axis. This is achieved by measuring the same area of evaluation twice with the same scanning parameters but perpendicular to each other with reference to their first scanned profile and fusing the two datasets together. It was revealed that the Multidirectional Scanning technique does not only increase the lateral resolutions but also significantly reduces the level of induced noise into the data by the environmental condition. This has been confirmed in this chapter with a series of simulations; where the noise was reduced from  $0.25 \mu\text{m}$  to approximately  $0.1 \mu\text{m}$ .

With such high expectation from the developed technique, the next chapter of the thesis considers the calibration of the multidirectional scanning technique as well as extensive validation of the results obtained using this technique.

# Chapter 4

## **Calibration and verification of MDS technique for areal surface topography measurement**

The previous chapter demonstrated the possibility of employing a commercially available laser triangulation device for on-machine surface metrology of machined (using milling processes) parts in a typical shop floor environment. This was successful by utilizing a new method that fuses two measurements obtained over the same area, but perpendicular to each other. The method enriches the lateral resolution of the measurement and reduces the influence of external vibration significantly.

This technique for on-machine surface topography is novel, therefore its measurement results need to be compared with other instruments for full validation. It should be possible to calibrate the instrument/method as you would with any measurement system applied in the quality chain. Hence, this chapter is divided into two main parts. The first part presents an attempt to calibrate the new technique and the second; a comparison of measurement results between MDS, and another high specification, and commercial surface metrology instrument. The main aim of this chapter focuses on maintaining the traceability of measurement obtained from the novel technique as well as an attempt to estimate the uncertainty associated with the measurement. The factors that influence the traceability of surface metrology can be divided into two; hardware

related (the instrument-surface interaction) and software related (analysis algorithms and parameter calculations) [118]. In this thesis, the impact on traceability posed by software related factors were not considered because only one surface parameterization software (Surfstand version 6.0) is used throughout. This software has been calibrated and validated in other publication [128], [129]. Hence, calibration in this chapter will solely focus on the impact that instrument-surface interaction poses on traceability of the measurement result. This could be achieved by calibrating the operation axes of the technique and its spatial frequency responses.

Calibration of measurement techniques can be performed using traceable, primary or secondary instruments with very low uncertainties which are usually kept by National Measurement Institutes (NMIs) or accredited laboratories. Calibration can also be performed using calibration artefacts. These artefacts are referred to as material measures in other publications (mainly ISO standards) and are usually used in the absence of suitable primary instruments. In addition, some calibration artefacts can be used in ‘harsh’ environments such as shop floor due to their robustness. Moreover, the cost of obtaining calibration artefacts is relatively lower compared to acquiring services of a primary instrument. However, the uncertainty of artefacts are typically higher than their equivalent primary or secondary instruments. Due to the above merits; artefacts were considered in the calibration of the MDS surface measurement technique. In addition, the application of artefacts for calibrating surfaces is normal practice.

## 4.1 Calibration procedures

It is important to mention that the term calibration used in this thesis is defined as [130]; “Operation that, under specified conditions, in a first step establishes a relation between the quantity values with measurement uncertainties provided by measurement standards and corresponding indications with associated measurement uncertainties and, in a second step, uses this information to establish a relation for obtaining a measurement

from an indication.”

And, ought not to be mistaken for adjustment; which is also defined as [130];

“Set of operations carried out on a measuring system so that it provides prescribed indications corresponding to given values of a quantity to be measured.”

In simple words, calibration involves finding the relations between a measurement instrument or technique and a measurement standard whilst adjustment involves tuning measurement instrument or technique in order to have the same relation in magnitude with a measurement standard. By measuring a calibration artefact on an instrument, the metrological characteristics (MCs) of the measurement technique or instrument are obtained.

ISO 25178 – 600 [131], defines the set of MCs that can be used to calibrate all types of surface topography measurement technique that captures areal topography. Unfortunately, at the time of writing this thesis, the ISO working group; TC213-WG16 were still debating on developing the appropriate procedures for calibrating of different surface metrology techniques. Only a few of these calibration procedures have published which includes, but is not limited to, ISO 25178-601 [125]; contact (stylus) instruments and ISO 25178-606 [57]; non-contact (focus variation) instruments.

Most MCs are determined using unique calibration artefacts such as optical flats and cross-gratings. Commercial surface metrology instrument manufacturers such as Taylor Hobson, Mitutoyo and Alicona, usually provide customized calibration artefact sets for the calibration of their instruments when purchased. Independent manufacturers such as Rubert and Co. Ltd in the UK also provides calibration artefacts for calibration of areal surface metrology instruments. A typical example of such artefacts is the “Bento Box” developed by the National Physical Laboratory (NPL) [130]. The calibration procedures undertaken in this thesis are divided into two; selection of the appropriate calibration artefacts and the selection of the appropriate step for calibrating the X, Y and Z axes of the MDS. It should be mentioned that, based on the following reasons, different calibration artefacts developed by different manufacturers were used to achieve different MC of the MDS technique because a ‘one size fits all’ solution could not be found;

1. The manufacturer's intended use of the identified instrument is not for surface metrology, neither is it for multi-directional scanning. Hence, the original equipment manufacturer (OEM), namely Keyence, did not provide any areal calibration artefact for the instrument.
2. Not every commercial calibration artefact set could be suitable for obtaining the MCs of MDS measurement technique. This is due to the properties of the material used in making most artefacts. A typical example is, the flatness of a transparent glass optical flat could not be measured using a laser triangulation instrument.
3. Most of the available calibration artefacts were developed for calibrating nano-scaled resolution instruments. Hence, making it difficult to employ them for a micro-scale technique such as MDS.

Taking into consideration the above challenges and by reviewing of calibration procedures of other established techniques with similar operational characteristic as the MDS, the MCs of MDS were obtained in the following subsection. Also, other relevant publications [118], [132]–[134] which gives more insight on the calibration of areal surface topography instrument were considered in the process. For clarity, under each MC, the following is discussed; the definition of the MC, the calibration artefact employed, the procedure used and the results.

Furthermore, in situations where the available artefacts are not suitable for obtaining a particular MC, a locally manufactured artefact is developed and calibrated. A typical example is the lateral amplification of MDS, which the developed artefact is presented in the section 4.1.1.

#### **4.1.1 Development of a cross-grating artefact suitable for calibrating MDS**

A cross-grating artefact is required to obtain the following MCs of the MDS technique; lateral amplification coefficient, linearity deviation, and perpendicularity deviation. All the available commercial cross-grating artefact were not suitable for calibrating MDS.

Reasons are as stated earlier in previous section. Another challenge that compelled the development of a new cross-grating artefact was the measurement area to be calibrated. The MDS captures an area of 8 mm x 8 mm size, hence the cross-grating artefact used for the calibration is expected to cover at least the measurement area. To overcome these challenges, a low-cost artefact was developed and calibrated through a primary instrument at NPL. The appropriate procedures for designing and manufacturing of the artefact as well as its calibration were extracted from [135].

#### **4.1.1.1 Procedures used for developing the cross-grating artefact**

Due to the absence of an appropriate commercial calibration artefact to determining the lateral amplification coefficient and linearity deviation of the MDS measurement technique; a new, low-cost cross-grating equivalent artefact was developed.

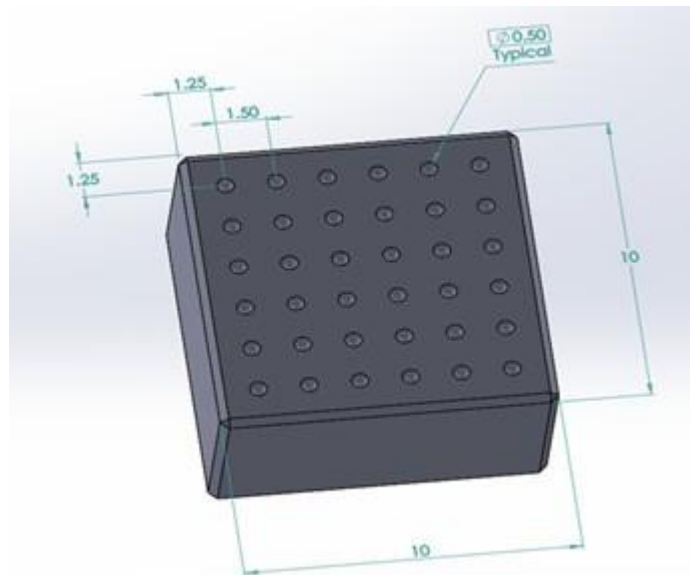


**Figure 4.1:** Design of cross-grating artefact

The developed artefact is made of a steel cubic block. It contains thirty-six hemispherical groove features with 0.5 mm nominal diameter on one face of the cubic block and 1.50 mm nominal distance between two features as shown in figure 4.1. The thirty-six groove features are in the form of a 6 x 6 grid and cover an area of 8 mm x 8 mm. The steps used to develop and calibrate the cross-grating artefact is as follows.

1. The proposed design as described above is first modelled using a computer-aided design (CAD) software package (as shown in figure 4.1). This gives the designer more control and understanding of the nominal distances between the grooves on the artefact. These nominal distances were used throughout the calibration process.
2. Using a cutting speed and feed rate of 3750 RPM and 750 mm/min respectively, a cubic stainless steel block is first manufactured using face milling process. The diameter of the cutter used was 22 mm. All the faces of the cubic block were flatten.
3. The top face of the cubic steel block; that is the face where the u-groove features will be machined; is further smoothed using a grinding process. With the aim of achieving a surface roughness of  $\approx 100$  nm . The surface roughness was confirmed using a stylus instrument (Bruker). The grinding wheel used was 1200 grit CBN vitreous bonded. Feed rate was varied between 5 and 31 mppm, scaled to achieve a constant surface speed. The spindle speed was set to be 48 RPM.
4. After the grinding process, the cubic steel block is then returned to the milling machine to machine the u-groove features using a 0.5 mm diameter milling tool with spindle speed and federate of 12000 RPM and 25 mm/min respectively. The spindle speed and feed rate were carefully selected to avoid tool breakage.



**Figure 4.2:** Final grinding process of locally made cross grating

5. The grinding process is repeated after machining the u-groove features using the same spindle speed and feed rate in step 3 to achieve the final surface topography as well as to remove any burs as a result of step 4. This can be seen in figure 4.2.

#### **4.1.1.2 Calibration of the developed artefact**

The developed artefact was calibrated using an optiv\_classic non-contact coordinate measuring machine (CMM) which is traceable via an optical dimensional standard shown in figure 4.3. The calibration was based on the distances between the centres of paired u-grooves feature on the cross-grating artefact.

The traceability of the calibration results is established using a substitution measurement method (See **Appendix C** for measurements results with CMM) of the optical dimensional standard plate. The detail of the uncertainty estimation for the distances on the cross-grating artefact and the combined uncertainty is shown in table 4.1.



**Figure 4.3:** The NPL optical dimensional standard. Reproduced from [136]

Influential factors considered included, the volumetric error, alignment error and optical path error. Other factors that were also considered in estimating the uncertainty of the measurement were influence factor due to thermal variation and error of coefficient thermal expansion of the measured part.

**Table 4.1:** Estimation of total uncertainty associated with cross grating artefact

Sources	Values/ $\mu\text{m}$	Description
$u_{machP}$	0.200	Influence factors considering the machine performance which includes the volumetric error, alignment error and optical path error. ( <b>Type A</b> )
$u_{temp}$	0.005	Influence factor due to thermal variation and error of coefficient thermal expansion of the cross- gratings artefact ( <b>Type B</b> )
$u_{opticalplate}$	0.050	Influence factors from the measurement of the calibrated optical dimensional standard ( <b>Type B</b> )
$u_{total}$	0.206	Combined standard uncertainty

### 4.1.2 Measurement noise of MDS technique

#### 4.1.2.1 Definition of measurement noise

Measurement noise is defined as the noise added to the output signal during the typical utilization of the instrument. It includes the instrument noise as well as noise arising from the environment (thermal, vibration, air turbulence) and other sources [131]. It is the major error along the z-axis i.e. for the height measurement.

#### 4.1.2.2 Procedure to obtain the measurement noise

To obtain the measurement noise of a surface topology technique, there are two methods that can be employed. They are referred to as the subtraction technique and averaging technique. Regardless of the procedure employed, the areal surface topography parameter,  $S_q$ , is used as the indicator. Below is the procedure for the subtraction technique;

1. Measure the same area twice under the same conditions, that is

- The measurements should be in quick succession
- The same instrument and operator should be used for both measurements

2. One of the raw datasets obtained from step 1 is subtracted from the other, and the resulting dataset is expected to be dataset containing information regarding the measurement noise.

3. The topology data which contains only the information about the measurement noise is parameterized using a surface topology analytical software to obtain the  $Sq$  value.

4. Since the method of subtraction joins the variances of two identical probability distributions that each describe the instrument noise; the measurement noise  $Sq_{noise}$  can therefore be estimated by;

$$Sq_{noise} = \frac{Sq}{\sqrt{2}} \quad (4.1)$$

For the other method of obtaining the measurement noise (averaging method), the suspicion that the noise contribution in a measurement diminishes while averaging numerous measurements over the same area of a sample is considered. The following are steps to obtain  $Sq_{noise}$  when using the averaging technique.

1. The  $Sq_{flat}$  of the calibration artefact (flat surface) is obtained from the artefact calibration's datasheet.
2. The flat is measured and  $Sq$  is obtained from the captured topology. It should be mentioned the  $Sq$  (measured flat) has a relationship with the measurement noise ( $Sq_{noise}$ ) and  $Sq_{flat}$ , which is;

$$Sq = \sqrt{Sq_{flat}^2 + Sq_{noise}^2} \quad (4.2)$$

3. Multiple measurements (n) of the flat at the same area is captured, and the RMS height of the averaged surface topography ( $Sq_n$ ) is obtained.

4. As per the fundamental assumption, the contribution of the measurement noise into the  $Sq$  value decreases as 'n' increases and their relationship is presented as;

$$Sq_n = \sqrt{Sq_{flat}^2 + \frac{Sq_{noise}^2}{n}} \quad (4.3)$$

$Sq_{noise}$  can then be deduced from the equation 4.2 and equation 4.3 as

$$Sq_{noise} = \sqrt{\frac{Sq^2 - Sq_n^2}{1 - \frac{1}{n}}} \quad (4.4)$$

There is no recommended number of repeated measurements (n), however, to confirm the reduction in the measurement noise as n increases, averaging of 2, 4, 8, and 16 measurements are usually considered.

#### 4.1.2.3 Calibration artefact used for obtaining measurement noise of MDS technique

The optical flat shown in figure 4.4 was used in this thesis for obtaining the measurement noise of MDS. The artefact had a flatness of less than 20 nm. It was obtained from the bento box artefacts; manufactured and calibrated by NPL. According to its calibration certificate (cert ref: 2013110351/1), it had an expanded uncertainty of 9.8 nm at a coverage probability of 95% and coverage factor k = 2.

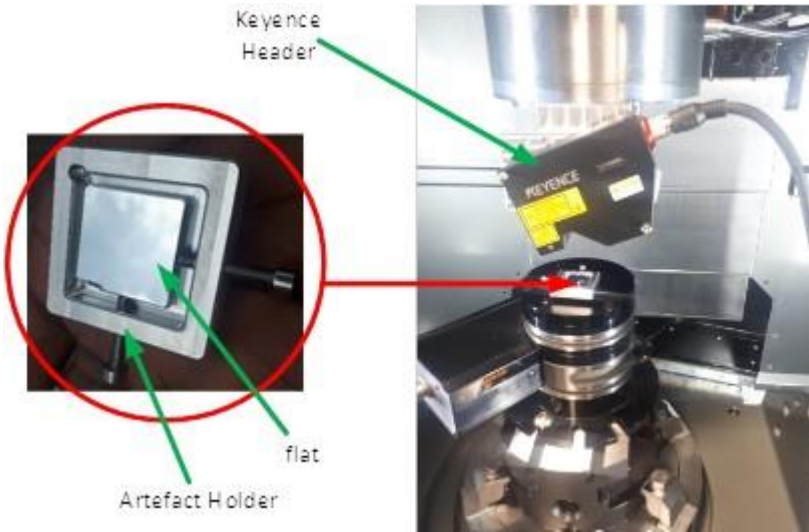


**Figure 4.4:** Optical flat for the calibration of MDS

#### 4.1.2.4 Results; measurement noise

To characterise the noise level variation of the MDS surface measurement technique over its vertical range, the noise measurements are repeated in 3 distinct positions. They were above the recommended position (top), below the recommended position (bottom) and at the recommended position (centre). These ranges are important because the triangulation method has a ‘sweet’ spot in the centre of the detector, probably due to the optimal focal length. The top and bottom positions are approximately 2 mm off the recommended distances between the measurement instrument and the surface whilst the centre position is the recommended distances given by the manufacturer (see **Appendix B**). This was performed with a specific end goal to check noise level variation in the instrument’s entire field of view. The results from the subtraction technique and the averaging technique can be seen in table 4.2 and table 4.3 respectively.

The moderate deviation from the subtraction values (see table 4.2) implies that only one subtraction between two surface measurements is sufficient to estimate measurement noise of MDS technique.

A similar conclusion can also be made regarding the averaging method; i.e. averaging two or four measurements could be sufficient in estimating the measurement noise using the averaging method.

**Table 4.2:**  $Sq_{noise}$  ( $\mu\text{m}$ ) using the subtraction technique

Approx. z-position /mm	$Sq_{noise}$ ( $\mu\text{m}$ )		
	2 (Top)	0 (Centre)	-2 (Bottom)
<b>Subtraction Run</b>			
1	0.99	0.06	0.98
2	1.13	0.04	1.08
3	1.15	0.05	1.09
4	1.10	0.07	1.08
5	1.21	0.07	1.01
<b>Mean</b>	1.12	0.06	1.07
<b>St. dev</b>	0.073	0.012	0.051

**Table 4.3:**  $Sq_{noise}$  ( $\mu\text{m}$ ) using the averaging technique

Approx. z-position /mm	$Sq_{noise}$ ( $\mu\text{m}$ )		
	2 (Top)	0 (Centre)	-2 (Bottom)
<b>Number of Averaged measurement</b>			
2	1.14	0.08	1.10
4	1.11	0.06	1.10
8	1.11	0.05	1.09
16	1.10	0.05	1.08
<b>Mean</b>	1.11	0.06	1.09
<b>St. dev</b>	0.015	0.002	0.008

Both subtraction and averaging methods are successful in estimating the measurement noise of the MDS technique. It was noticed from both methods that the measurement noise increases if the distance between the instrument and the surface is not at the recommended distance by the manufacturer. It can therefore be concluded that the measurement noise of the MDS technique is  $0.06 \mu\text{m}$  since the range required to perform surface measurement is relatively small, and it is easy to use the machine tool to set-up the device in its optimal position.

#### 4.1.3 Residual flatness of MDS technique

#### **4.1.3.1 Definition of residual flatness**

This MC expresses the quality of the areal reference of the technique and is defined [57] as; “the flatness of the areal reference”.

It shows the effect of waviness induced into the measurement by vibration or optical effects such as stray reflections and optical speckles. Its main potential error is along the z-axis and therefore affect the height measurement.

#### **4.1.3.2 Procedure to obtain the residual flatness**

1. Ten measurements are taken arbitrarily over a reference flat surface. The purpose is to reduce the influence of undesirable factors such as scratches or dirt on the flat affecting the Sz value.
2. The measurements are levelled using a high order polynomial to remove the form.
3. Optical spikes are also removed from the measurements by setting threshold values.
4. An averaged topology is obtained from the processed measurements.
5. Sz is obtained from the averaged topology.

The same artefact used for obtaining the MCs of the measurement noise is also used in this section. It should be mentioned that the flat surface from the NPL areal calibration set came with a traceable Sz value of  $7.2 \text{ nm} \pm 10.3 \text{ nm}$  with a 95% confidence (coverage factor k equal 2).

#### **4.1.3.3 Results; residual flatness**

Ten arbitrary measurements were obtained using the MDS at different locations on the artefact according to the recommendation of VDI/VDE 2655 [8]. The form and the residual surface were obtained using a 12<sup>th</sup> order polynomial form removal. An inbuilt feature, part of the parameterization software package used in this thesis (SURFSTAND V6.0) was used for both form removal and setting the threshold values. Images at each

stage are shown in figure 4.5. It should be mentioned, figure 4.5 focuses on showing the process and not necessarily the scales and axis labels.

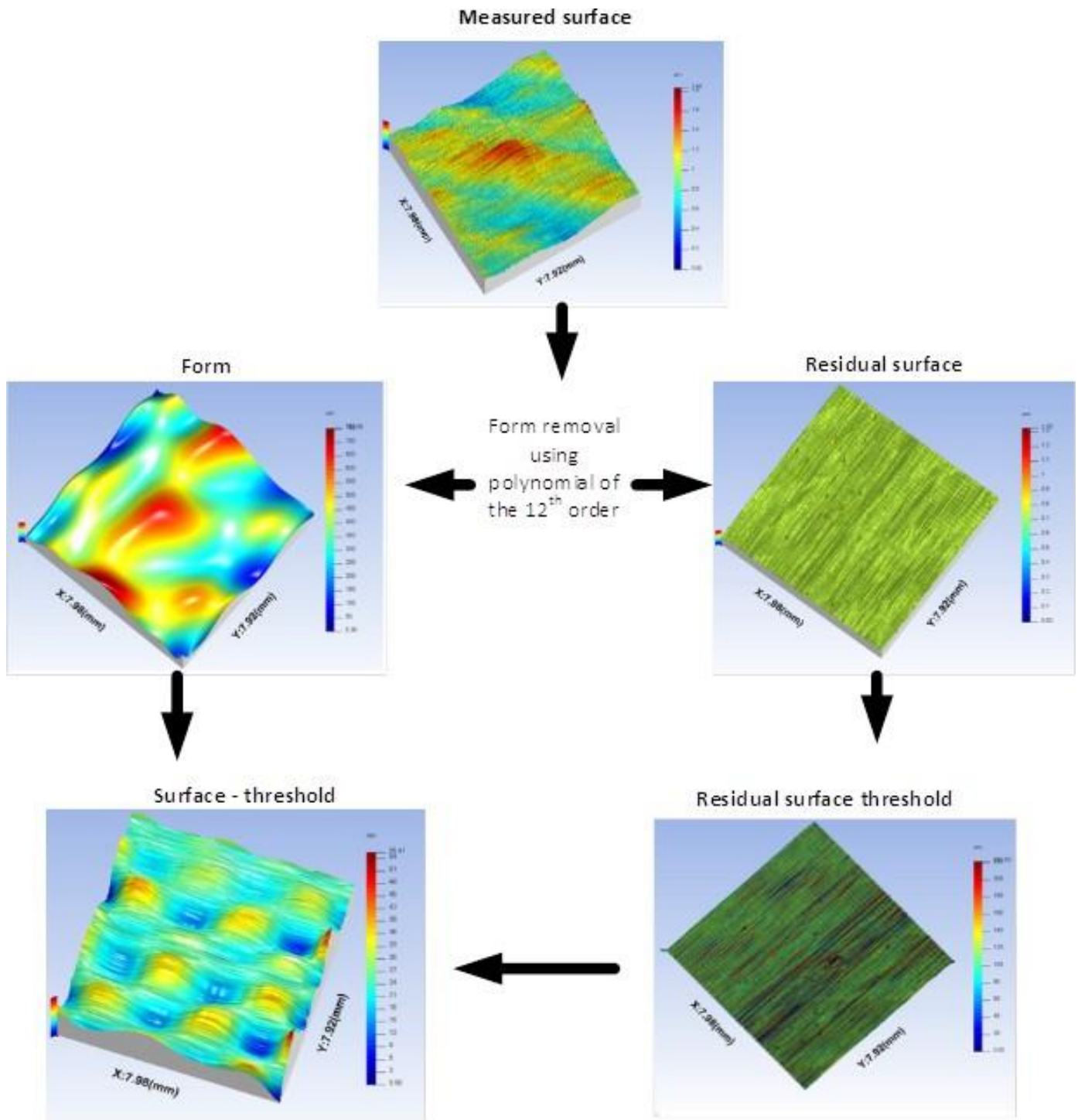


**Figure 4.5:** Flow chart for the flatness deviation threshold method

Selection of appropriate threshold is critical because an incorrect threshold will underestimate the magnitude of the  $Sz$  value of the measurement. The challenge of

finding the appropriate threshold was overcome by setting the thresholds of the peaks and valleys of the residual surfaces so that they are 3 times larger than the Sq value of the residual surface.

The final topology obtained when all the 10 measurements are averaged cumulatively is shown in figure 4.6. The  $Sz_{flatness}$  of the averaged topology was found to be 229 nm. Figure 4.6 shows the  $Sz_{flatness}$  value as the number of averaged measurements increases.

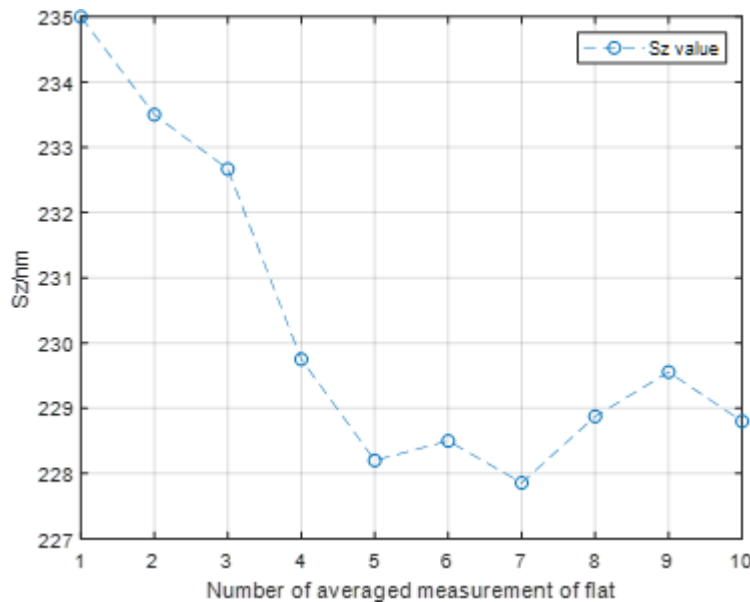


**Figure 4.6:** Effect of increasing the number of averaged measurement of a flat

### 4.1.3 Amplification coefficient and linearity deviation of MDS technique

#### 4.1.3.1 Definition of amplification coefficient and linearity deviation

1. The amplification coefficient can be defined as “the slope of the linear regression curve obtained from the response curve”[131] as shown in figure 4.7.
2. The linearity is defined as “the maximum local difference between the line, from which the amplification coefficient is derived, and the response curve” [131] as shown in figure 4.7. Their main potential error is along the x, y and z-axis.

It is important to mention that the amplification coefficient and linearity deviation could be obtain for both the lateral axes and the vertical axis for a surface measurement instrument. Therefore, the following sub-section is in two parts; the first focuses on finding the amplification coefficient and linearity deviation of the vertical axis of the MDS technique, then the second, focuses on the lateral axes.

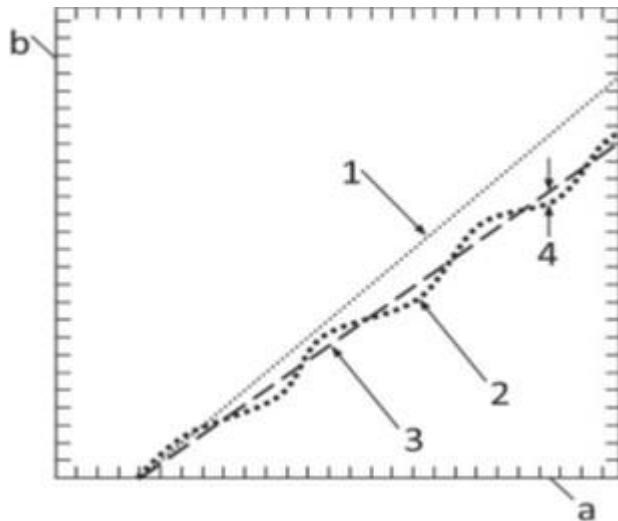


**Figure 4.7:** Example of an instrument response curve—: a- actual input quantities, b-measured quantities, 1- ideal response curve, 2-actual response curve of the instrument, 3-line from which the amplification coefficient is derived, 4-local linearity deviation. Reproduced from [131].

#### 4.1.3.2 Procedure; amplification coefficient and linearity deviation for z-axis

1. Four different step height artefacts are selected for the z-axis calibration. It is ensured that the artefacts cover the entire z-axis range of the measurement instrument to be calibrated.
2. Each artefact is placed parallel to the measurement instrument's lateral plane. This allows easy removal of tilts using mathematical algorithms (plane fitting). Thereby reducing the effects on the lateral plane on the measured height.
3. Each artefact is measured five times at five different positions. (i.e. 25 measurements in total)

4. The following are computed from the captured height values in step 3 to generate a residual plot in order to deduce the linearity deviation.

- Measurement error ( $\delta_{err}$ ) = average measured value - calibrated value.
- Repeatability ( $\delta_{repeat}$ ) = maximum standard deviation of measured values of step heights.
- Reproducibility ( $\delta_{reprod}$ ) = mean standard deviation of measured values of step heights.

5. The amplification coefficient is also calculated using the following equation.

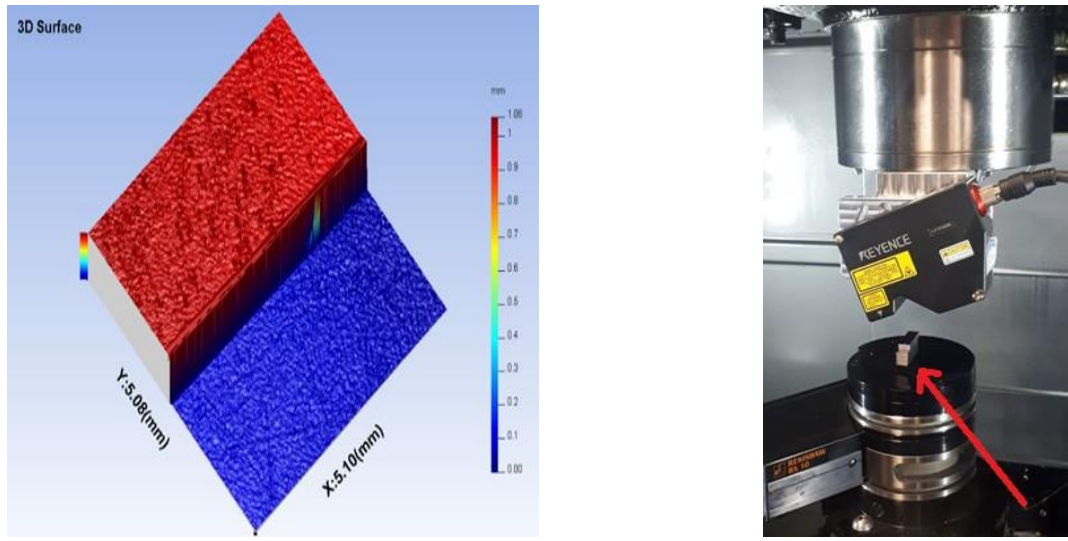
$$\alpha = \frac{\sum_{i=1}^n C_i I_i}{\sum_{i=1}^n C_i^2} \quad (4.5)$$

Where the amplification coefficient is denoted by  $\alpha$ ,  $C_i$  are the calibrated values,  $I_i$  the measured values and  $n$  denotes the number of different step height artefacts used.

#### **4.1.3.3 Calibration artefact; amplification coefficient and linearity deviation for z-axis**

In order to obtain the amplification coefficient and linearity deviation of z-axis scale, four step heights were utilised [137]. The artefacts were carefully selected to ensure that their nominal height values cover the vertical range of the technique under study; in this case the instrument has a relatively large range compared to typical surface metrology instruments of 4.6 mm (see **Appendix B**).

Although typical surface measurements would not use this range, it was deemed appropriate to calibrate over the full range in case freeform surfaces were measured, where the form deviation could easily be similar to typical profile measurement for which the instrument was originally designed.



**(a)** Surface topology of 1mm step height obtained using gauge blocks

**(b)** Step height using gauge blocks on CNC machine; arrow pointing to gauge blocks

**Figure 4.8:** Calibration of Z-axis of MDS using gauge blocks

In this thesis, calibrated gauge blocks were used to obtain the following step heights; 1 mm, 1.25 mm, 3.5 mm and 4 mm. One of the advantages of using gauge blocks (see figure 4.8b) is their ability to obtain higher step heights which are not available in most commercial standard calibration sets for surface metrology while maintaining very low uncertainty. The calibrated gauge blocks used have an expanded uncertainty of  $(0.014 + 0.5L/1000) \mu\text{m}$  at a coverage probability of 95% with coverage factor;  $k = 2$ . Where  $L$  is the nominal height of the block. Figure 4.8a shows measurement obtained from a step height whiles using MDS.

#### 4.1.3.4 Results; amplification coefficient and linearity deviation for z-axis

Table 4.4 and figure 4.9 are generated from the measurements obtained from the averaged profiles obtained from the step heights. The amplification coefficient of the z-axis scale of the MDS was computed using the equation 4.5 and was found to be 0.995. Also, from figure 4.9 it can be deduced that the linearity deviation for the z-axis scale,  $l_z$ , was in excess of  $2.9 \mu\text{m}$ .

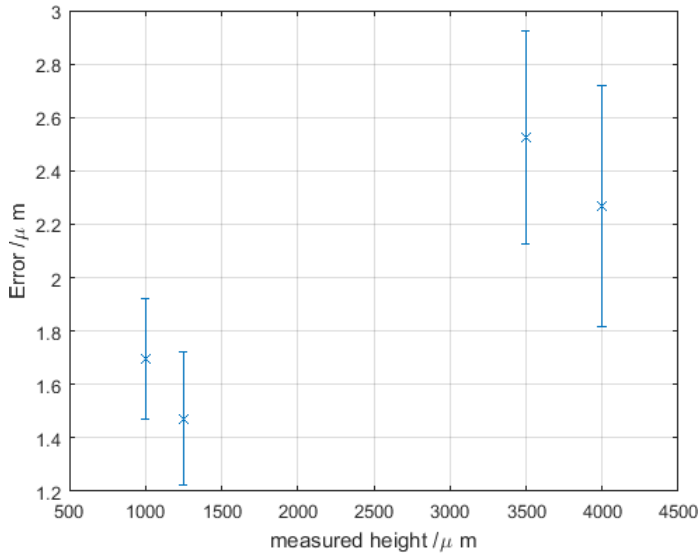


**Figure 4.9:** Bar Error chart of residual error obtained from MDS for calibration of its z-axis

**Table 4.4:** Results obtained from calibrating of the z-axis of MDS using step heights

Nominal height / $\mu\text{m}$	1000	1250	3500	4000
$\delta_{err}/\mu\text{m}$	1.78	1.55	2.65	2.39
$\delta_{repeat}/\mu\text{m}$	0.99	0.81	1.13	1.46
$\delta_{reprod}/\mu\text{m}$	0.58	0.68	1.06	1.32

#### 4.1.3.5 Procedure; amplification coefficient and linearity deviation for lateral axes of MDS

In order to obtain the amplification coefficient and the linearity deviation in the lateral axis of the measurement technique, a cross-grating artefact (see figure 4.1) was utilised. The following steps were employed;

1. The cross-grating is measured five times at the same position.
2. The distance between the centre of the first dimple and the other dimples are obtained from all the five measurements, i.e. in x-(horizontal), y- (vertical) and diagonal directions. The centre of the dimple is determined with the assistance of an image processing algorithm.
3. The measurement error ( $\delta_{err}$ ), repeatability ( $\delta_{repeat}$ ) and reproducibility ( $\delta_{rep}$ ) are obtained from the measurements in x- (horizontal), y- (vertical) and diagonal

directions.

4.Residual error plots are generated for the three results. The amplification coefficients;  $\alpha_x$   $\alpha_y$  and  $\alpha_{diagonal}$  and linearity deviation,  $l_x$   $l_y$  and  $l_{diagonal}$  are also computed.

#### **4.1.3.6 Calibration artefact; amplification coefficient and linearity deviation for lateral axes of MDS**

The calibration artefact used is the newly developed cross-grating described in section 4.1.1.1.

#### **4.1.3.7 Results; amplification coefficient and linearity deviation for lateral axes of MDS**

The locally designed cross-grating artefact was measured using the MDS technique to obtain its grid topography. With the assistance of MATLAB's image processing toolbox, the captured grid topography is converted into an image as shown in figure 4.10. Using an image processing algorithm, measurements are carried out to obtain the distances between the centres of the groove features in the x, y and diagonal directions as depicted in figure 4.10.

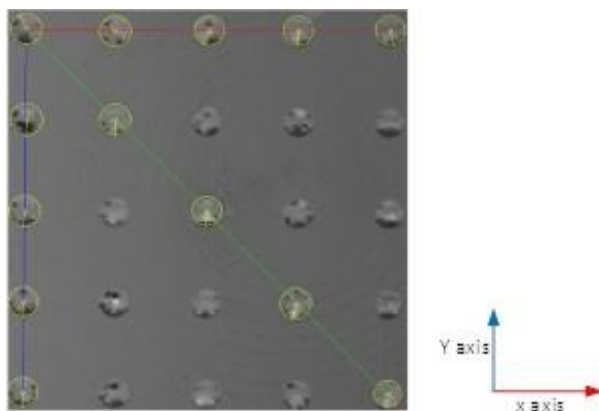


**Figure 4.10:** Lateral and diagonal direction measurements using image processing algorithm; red line represents data along the same profile axis, blue line represents data along the same time axis and green line represents data in diagonal direction

Table 4.5 and figure 4.11 are generated from the distance measurements obtained in the x-axis direction (marked with red line in figure 4.10). It should be mentioned that

the nominal distances; 1.5, 3.0, 4.5, 6.0, and 7.5 mm are obtained from the artefact design (Figure 4.1). That is 1.5 mm is the distance between the centre of the first groove feature and the second groove feature in the x- direction while 7.5 mm is the distance between the first groove feature and the centre of the sixth groove feature.

**Table 4.5:** Results obtained from calibrating of the x-axis of MDS using cross grating artefact

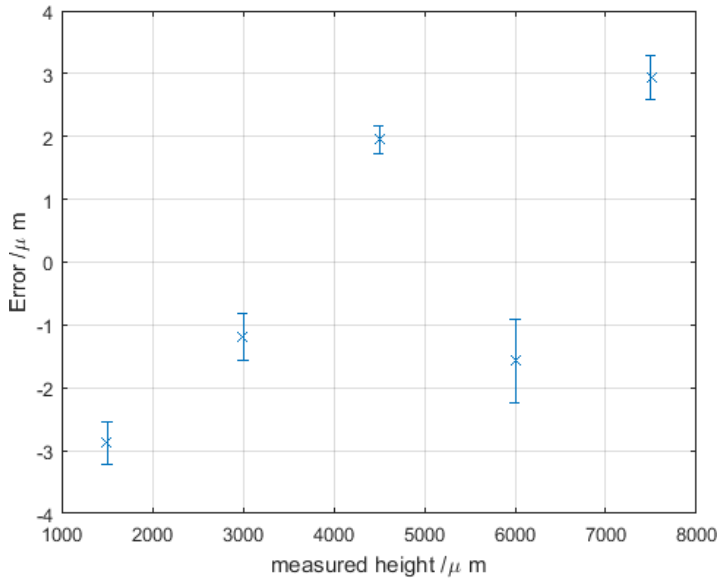
Nominal height/ $\mu\text{m}$	1500	3000	4500	6000	7500
$\delta_{err}/\mu\text{m}$	-2.88	-1.19	1.95	-1.57	2.94
$\delta_{repeat}/\mu\text{m}$	1.35	0.84	1.28	2.15	1.39
$\delta_{reprod}/\mu\text{m}$	1.26	0.09	0.10	1.75	0.03

The amplification coefficient of the MDS considering x-axis scale was computed using the equation 4.5 and was found to be 0.98. Moreover, from figure 4.11 it can be deduced that the linearity deviation for the x-axis scale,  $l_x$ , was in excess of 3.5  $\mu\text{m}$ .

Table 4.6 and figure 4.12 are generated from the measurements obtained from distance measurements obtained in the y-axis direction (marked with blue line in figure 4.10).

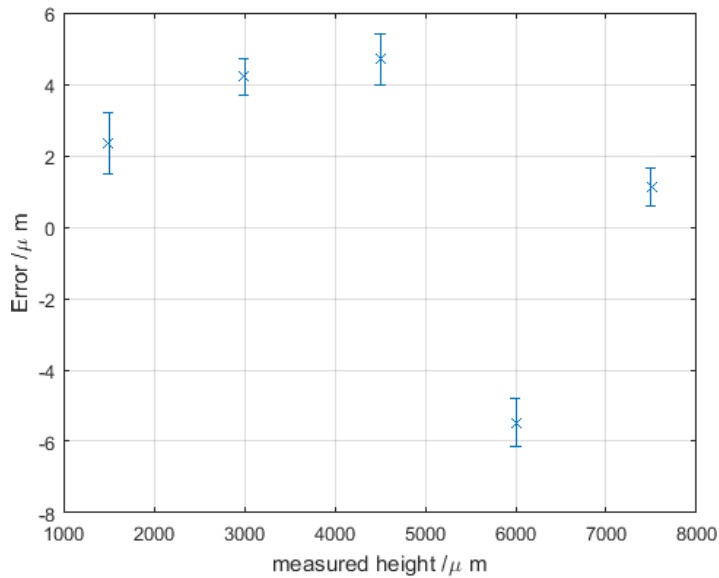
**Table 4.6:** Results obtained from calibrating of the y-axis of MDS using cross grating artefact

Nominal height/ $\mu\text{m}$	1500	3000	4500	6000	7500
$\delta_{err}/\mu\text{m}$	2.35	4.21	4.71	-5.48	1.31
$\delta_{repeat}/\mu\text{m}$	1.06	2.39	2.13	1.06	1.70
$\delta_{reprod}/\mu\text{m}$	0.53	2.09	1.46	0.46	0.99



**Figure 4.11:** Bar error chart of residual error obtained from MDS for calibration of its x-axis

The amplification coefficient of the y-axis scale of the MDS was computed using the equation 4.5 and was found to be 0.959. Also, from figure 4.12 it can be deduced that the linearity deviation for the y-axis scale,  $l_y$ , was in excess of  $5.2 \mu\text{m}$ .



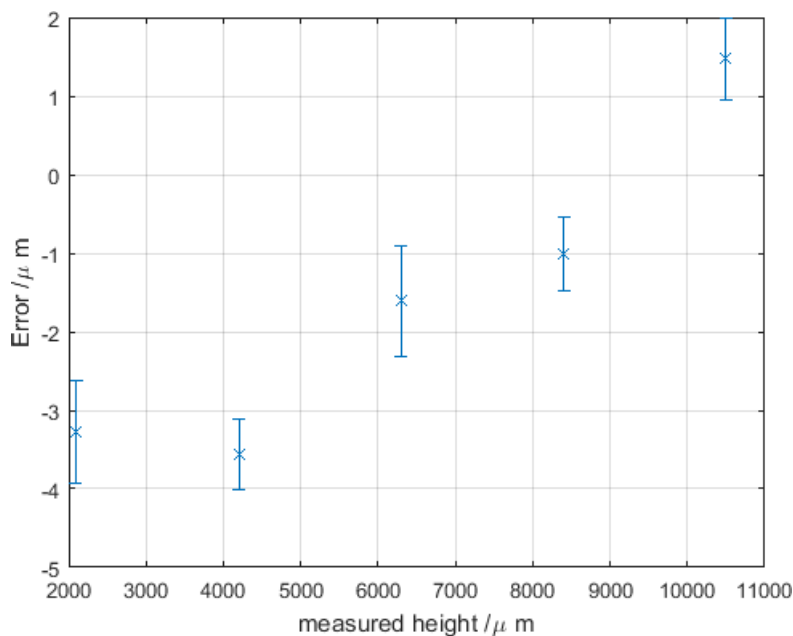
**Figure 4.12:** Bar error chart of residual error obtained from MDS for calibration of its y-axis

Table 4.7 and figure 4.13 are generated from the distance measurements obtained in the diagonal direction (marked with a green line in figure 4.10). The amplification coefficient

in the diagonal direction (dig) of the lateral scale of the MDS was computed found to be 1.07. Also, from figure 4.13 it can be deduced that the linearity deviation in the diagonal direction,  $l_{dig}$ , was in excess of  $1.95 \mu\text{m}$ .

**Table 4.7:** Results of the MDS error calculation in the diagonal direction

Nominal height/ $\mu\text{m}$	2100	4200	6300	8400	10500
$\delta_{err}/\mu\text{m}$	-3.28	-3.56	-1.61	-1.01	4.47
$\delta_{repeat}/\mu\text{m}$	3.12	2.16	1.24	3.21	3.71
$\delta_{reprod}/\mu\text{m}$	0.94	1.42	1.06	1.59	2.11



**Figure 4.13:** Bar error chart of residual error obtained from MDS for calibration (diagonal)

#### 4.1.4 Perpendicularity deviation

##### 4.1.4.1 Definition; perpendicularity deviation

It is defined as deviation from  $90^0$  of the angle between the x- and y-axes [131].

##### 4.1.4.2 Calibration artefact; perpendicularity deviation

The calibration artefact used is the newly developed cross-grating described in section 4.1.1.1.

#### **4.1.4.3 Procedure; perpendicularity deviation**

In order to obtain the perpendicularity deviation error of an instrument, the same results acquired from the x-(horizontal), y- (vertical) directions of the cross-gratings artefact in section 4.1.3.3 are used. The perpendicularity deviation is obtained by calculating the difference of the nominal and the measured angles between dimples on the cross-gratings.

#### **4.1.4.4 Results; perpendicularity deviation**

It was discovered that the perpendicularity deviation of the MDS technique was  $0.73^{\circ}$  which represents the average of all the perpendicularity deviations obtained by analysing the five measurements using an image processing algorithm. The perpendicularity error is therefore computed as the cosine error of measured length (the nominal distance between the groove features). The effect of the perpendicularity error was computed to be  $1.29 \mu\text{m}$ .

## **4.2 Measurement of uncertainty associated with MDS measurement**

It is a common practice to see statements on accuracy of surface metrology instrument on specification datasets or referred in documents if the instrument is used for measurement. However, statement on the uncertainty associated with surface topography measurements are rarely seen. The two main causes of this habit are most likely due to the complexity of the measurand and the measurement techniques usually employed. Research confirms that the greatest contributor to the variation in surface metrology results is the surface itself [118].

Regardless of this challenge, attempts have been made in estimating the uncertainty associated with surface measurement results when using MDS technique. This was achieved by considering the scale and noise contributions.

### 4.2.2 Scale contribution

This contribution is deduced from a combination of measurement error, traceability, repeatability and reproducibly obtained during the amplification coefficient and linearity deviation calculation in section 4.1.3. Considering a simple measurement model, by linearly summing the sources of errors in Table 4.8, the total contribution associated with each axis can be deduced using the following equation [138];

$$u_i = \sqrt{u_{trac}^2 + u_{repeat}^2 + u_{reprod}^2 + u_{err}^2} \quad (4.6)$$

Where  $i = x_{axis}, y_{axis}, z_{axis}$  and dig  $U_x \text{ axis}$ ,  $U_y \text{ axis}$  and  $U_z \text{ axis}$  were computed in the tables 4.9, 4.10 and 4.11 using information from tables 4.4, 4.5 and 4.6 respectively.

**Table 4.8:** Uncertainty budget for scale contribution

Source	Distribution	Formula
Measurement error	Rectangular	$u_{err}^2 = \delta_{err}^2 / 3$
Repeatability	Normal	$u_{repeat}^2 = \delta_{repeat}^2$
Reproductively	Normal	$u_{reprod}^2 = \delta_{reprod}^2$
Traceability	Normal	$u_{trac}^2 = \delta_{trac}^2$

**Table 4.9:** Standard measurement uncertainties associated with MDS calibration of the z-axis scale

Uncertainty contribution / $\mu\text{m}$	Uncertainty / $\mu\text{m}$			
	1000	1250	3500	4000
$u_{err}$	1.03	0.89	1.53	1.38
$u_{repeat}$	0.99	0.81	1.13	1.46
$u_{reprod}$	0.58	0.68	1.06	1.32
$u_{trac}$	0.72	0.80	1.33	1.42
$u_z \text{ axis}$	<b>1.70</b>	<b>1.60</b>	<b>2.55</b>	<b>2.79</b>

**Table 4.10:** Standard measurement uncertainties associated with MDS calibration of the x-axis

<b>Uncertainty contribution /<math>\mu\text{m}</math></b>	<b>Uncertainty /<math>\mu\text{m}</math></b>				
	<b>1500</b>	<b>3000</b>	<b>4500</b>	<b>6000</b>	<b>7500</b>
$u_{err}$	1.66	0.69	1.13	0.91	1.70
$u_{repeat}$	1.35	0.84	1.28	2.15	1.39
$u_{reprod}$	1.26	0.09	0.10	1.75	0.03
$u_{trac}$	0.21	0.21	0.21	0.21	0.21
<b><math>u_x \text{ axis}</math></b>	<b>2.49</b>	<b>1.11</b>	<b>1.72</b>	<b>2.92</b>	<b>2.20</b>

**Table 4.11:** Standard measurement uncertainties associated with MDS calibration of the y-axis

<b>Uncertainty contribution /<math>\mu\text{m}</math></b>	<b>Uncertainty /<math>\mu\text{m}</math></b>				
	<b>1500</b>	<b>3000</b>	<b>4500</b>	<b>6000</b>	<b>7500</b>
$u_{err}$	1.36	2.43	2.72	3.16	0.76
$u_{repeat}$	1.06	2.39	2.13	1.06	1.70
$u_{reprod}$	0.53	2.09	1.46	0.46	0.99
$u_{trac}$	0.21	0.21	0.21	0.21	0.21
<b><math>u_y \text{ axis}</math></b>	<b>1.81</b>	<b>4.00</b>	<b>3.76</b>	<b>3.37</b>	<b>2.12</b>

### 4.2.3 Perpendicularity contribution

The contribution of perpendicularity to the uncertainty of measurement ( $U_{PERP}$ ) is propagated in a rectangular distribution form, with an amplitude equal to the error of perpendicularity for the maximum length possible. Therefore, the contribution has been found to be equal to  $1.29 \mu\text{m}$  in section 4.1.4.4.

### 4.2.4 Noise contribution

This contribution is deduced from the measurement noise and the residual flatness. The combined effect of the measurement noise and residual flatness (see table 4.12) on the z-axis measurement standard uncertainty  $u_{NF}$  is given by

$$u_{NF} = \sqrt{Sq^2_{noise} + \frac{Sq^2_{flatness}}{12}} \quad (4.7)$$

**Table 4.12:** Uncertainty budget for noise contribution

Source	Distribution	Formula
Residual flatness	Rectangular	$u^2_{flat} = Sq^2_{flatness}/12$
Measurement noise	Normal	$u^2_{mn} = Sq^2_{noise}$

Therefore, it can be computed that,  $U_{NF} = 0.15 \mu\text{m}$

## 4.3 Comparison with another surface metrology instrument

Comparison of measurement obtained from the MDS technique with measurements obtained from a calibrated instrument play a vital role in the traceability and validation process.

### 4.3.1 Rules of comparison

At the time of writing this thesis, areal surface metrology, in general, can be classified to be at its infancy stage. This is because most standards are still being developed compared to other branches of metrology. Due to this reason, there is no available standard stipulating the procedures or rules required for comparing two measurements. Even though it is guaranteed that the ISO 25178 part 4 will cover the topic on board [118], the committee involved has not released any information at the moment.

Nevertheless, there have been few attempts to compare areal surface topologies. It could be concluded that ensuring the following factors match confirm fair comparison among areal surface metrology instruments.

- Size
- Filtering
- Resolution
- Evaluation area

To reduce the errors associated with the measurement of different areas on the same sample, a register was marked on all samples.

The benchmark instrument is carefully chosen for the comparison purpose in this thesis. This is because the comparison between techniques that operates on different physical principles are bound to have high discrepancies [139]. A typical example of such comparison is between an optical instrument and a stylus instrument. High discrepancies could be observed because the optical instrument measures the optical path of the sample; whiles the stylus instrument measures the geometry of the sample. If the sample is made up of different materials with different reflective index, the measurement obtained from the optical instrument will be highly affected but no significant influence will be noticed on the measurement obtained from the stylus instrument. Also, the hardness of the sample might affect the measurement results from a stylus instrument, possibility damaging the samples by scratching the surface or increasing wear on the tips of the stylus during scans. On the other hand, optical instruments are not faced with such challenges, hence the hardness of a sample will not have any significant impact on their measurement results. Even though the two instruments can be used to obtained surface measurements of samples, because different factors influence these instruments in different conditions, such comparisons are not encouraged.

Since the MDS utilises an optical approach to obtain data (laser triangulation); the selected benchmark instrument for this comparison also employs an optical technique.

### **4.3.2 Benchmark instrument**

The optical instrument used as a benchmark instrument for this comparison is a focal variation instrument (Alicona G4). The principle of operation of this instrument has been described earlier in chapter 2. The benchmark instrument used was located in a temperature-controlled environment;  $20 \pm 0.5^{\circ}\text{C}$ . All measurements were performed with a 20x objective lens. Based on the chosen lens; the maximum system lateral resolution was  $0.8 \mu\text{m}$ ; maximum system vertical resolution was 50 nm with a repeatability of 15 nm. The measurement area for all samples was set to 8 mm x 8 mm and the time spent during every single measurement was approximately 3 hours per measurement.

### **4.3.3 Samples used for comparison**

Six face-milled aluminium blocks; 35 mm x 35 mm x 10 mm; machined on a small three-axis CNC vertical machining centre were used. The milling process was performed with coolant (quakercool 7101 LF at a concentration of 7%) to aid the removal of heat from the material and to provide a stable temperature of the samples during the process. Different cutting parameters were used for cutting the samples to produce different surface finishes preferably all varying between very fine finish ( $0.8 \mu\text{m}$ ) and rough finish ( $3.2 \mu\text{m}$ ) as defined in section 1.5. This range covers surface finish for application i.e. precision machined surfaces typically produced by advanced manufacturing industry. It was also ensured that all the chosen cutting parameters are in the recommended range per the tooling manufacturer's guideline.

Two surface roughness artefacts; Microsurf 336, sample N4 which has an Ra of  $0.20 \mu\text{m}$  and Mitutyo SFM 001 which has a Ra of  $5.8 \mu\text{m}$ , were also measured using the two optical techniques. The purpose of using these artefacts is to confirm if the MDS could exceed the specification suggested in chapter 1.

## 4.3.4 Results from comparison

### 4.4.4.1 Visual comparison

The dataset captured when using the two surface metrology techniques were compared visually to check for any visible irregularities. This was achieved by importing the datasets into the Surfstand software package. The dataset was levelled, to remove any angular deviations as a result of the measurement table. No filtering or cut off frequencies were applied. Also, no threshold was applied whiles the dataset was being processed in the Surfstand software package. However, it should be mentioned that the MDS, has an internal feature for fixing missing dataset as explained earlier in section 3.3.1.5.

Figure 4.14 shows three images of the Microsurf 336, sample N4 artefact; the top image is the image captured with a camera, followed by a screenshot of topology obtained from MDS and the last obtained from the Alicona G4 instrument. Images of the other samples can be found in **Appendix D**.

### 4.4.4.2 Parametric comparison

In order to have more knowledge about the relationship between the two surface metrology techniques, a comparison between their parameters generated from the measured samples were conducted taking into account the rules in section 4.4.1. All the samples were measured 3 times using each technique. ISO 25178-2 areal texture parameters;  $S_a$  was computed from each measurement and its average was used for this comparison. This is because it is the most frequently used surface areal parameter both in industry and in research environment according to a recent survey published in [9]. Results from the standard artefacts and the milled surfaces are presented in table 4.13 and table 4.14 respectively which is discussed in the next section.

**Table 4.13:** Parametric comparison of artefacts; Sa in  $\mu\text{m}$ 

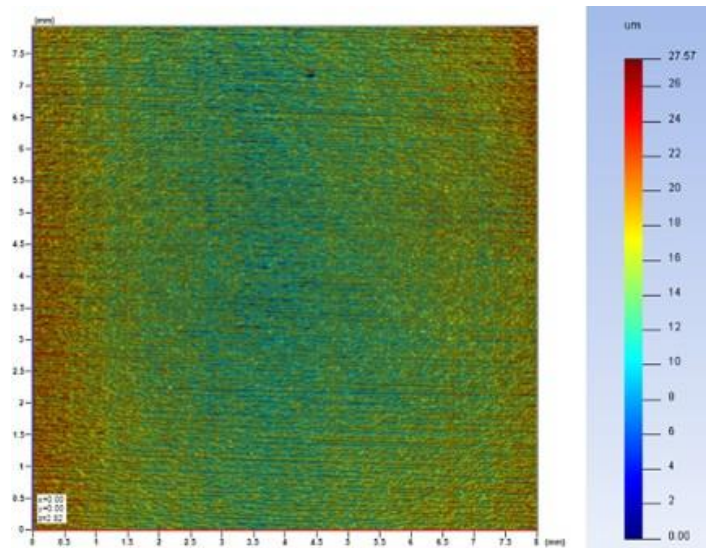
<b>Artefact Name</b>	<b>Alicona</b>	<b>MDS</b>	<b>Calibrated value</b>
<b>Microsurf 336, sample N4</b>	0.42	0.38	
	0.42	0.39	0.20
	0.41	0.34	
<b>Mitutoyo SFM 001</b>	7.01	6.40	
	6.99	6.38	5.80
	6.98	6.32	

**Table 4.14:** Parametric comparison of machined blocks; Sa in  $\mu\text{m}$ 

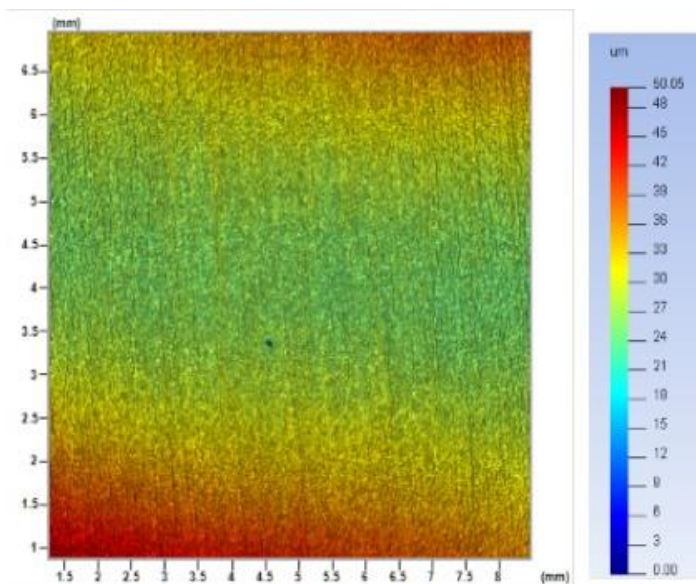
	<b>Sample Number</b>	<b>Alicona</b>	<b>MDS</b>
<b>Smooth face milled surface</b>	1	0.422	0.387
		0.419	0.387
		0.419	0.384
	2	0.701	0.640
		0.699	0.638
		0.698	0.637
<b>Rough face milled surface</b>	3	0.710	0.475
		0.710	0.465
		0.709	0.470
	2	1.256	1.105
		1.257	1.071
		1.254	1.067
	1	1.605	1.470
		1.605	1.330
		1.607	1.328
	3	2.023	2.075
		2.024	2.189
		2.015	2.271



(a) Image from camera



(b) Topology from MDS



(c) Topology from Alicona

**Figure 4.14:** Topologies and image of Microsurf 336, Sample N4

#### 4.4.4.3 Discussions of results

From the visual comparison, it can be confirmed that MDS can be used to detect malfunctions during a manufacturing process just as other lab-based surface metrology instruments such as the Alicona G4. This is because, by carefully observing the two topologies generated by both measurement techniques, (see figure 4.14 and **Appendix D**), both can measure distinctively close peaks, valleys and lays on a surface. On a typical machined surface, these features relate to machining parameters such as spindle speed and federate used for machining the component. Any abnormality in the machining process will cause a change in the surface topography of the component. Also, other imperfection features on the Artefact; Mitutoyo SFM 001 can also be easily identified in the topology obtained from MDS. These imperfection, mainly in the form of scratches, were as a result of a previous nail test or measurements using a stylus instrument. The ability to see these imperfection from MDS topologies confirms that MDS can be used to identify defects on a machined surface such as cracks, pore and buckle.

The parametric comparison on the other hand exposes the deviation of the  $S_a$  values of the measured artefacts and their nominal value. The percentage error for the smooth surface finish artefact (Microsurf 336, N4) was over 100% whiles for the rough surface finish artefact (Mitutyo SFM 001) was about 10%. These error margin can be attributed to the scratches. Also, the smooth artefact has a very high error margin because of the sensitivity of fine finishes in general.

However, a very significant observation which could be deduced from the parametric comparison is the close correlation between the parameters obtained from the MDS and Alicona G4. The percentage correlation between the two results was 99%. This conclusion could be made for both measurements from the artefacts and the machined samples.

It can also be deduced that there is a constant lag in the parameters obtained from MDS when compared to parameters obtained from Alicona G4. This might be because of the data filling-in process of the MDS merging process explained in section 3.3.1.5.

The MDS measurement can, therefore, be used to obtain an on-machine measurement which has a high correlation with the lab-based instrument and as well as quick on-machine analysis and detection of irregularities on a machined part.

## 4.5 Summary of chapter

This chapter supports the traceability of the novel MDS technique. The first part of this chapter present methods to obtain the following metrological characteristics of the MDS; measurement noise, residual flatness, amplification coefficient, linearity deviation and perpendicularity deviation. An attempt to estimate the uncertainties associated with all the scales were considered. It was confirmed that the MDS measurement technique is very useful in the micro-scale level.

The second part of this chapter compares the results obtained from MDS with standard lab-based optical surface metrology instrument. The outcome validated the reliability of results obtained from MDS technique for quick assessment of the surface quality of parts, directly on the machine tool and in a shop floor environment. The validation results show a strong correlation of 99% between the two results. It was also discovered that MDS can be used for the detection of irregularities on the surfaces of face milled parts. All of this capability is achieved with a much larger measurement area and low cost, in line with the high value manufacturing industries targeted by the application.

# Chapter 5

## Preliminary investigations for on-machine surface metrology modelling

The previous chapters have mainly focused on developing, evaluating and validating a new surface measurement technique suitable for on-machine metrology on a typical shop floor. The developed technique; MDS, provides an alternative to the challenges presented by off-machine measurement. These include eliminating the time spent on moving a machined component from the shop floor to a temperature-controlled room for metrology purpose.

To increase the probability of right-first-time production while using the surface integrity of the machined parts as a quality indicator; a predictive model is employed to assist with the exploited novel on-machine surface measurement technique in the earlier chapters. The model utilises cutting conditions to predict areal surface parameters so that pre-process optimisation can also be performed.

To develop the model, this chapter is dedicated to all the initial investigations conducted to ensure that the developed model is robust and reliable. At the end of this chapter, the appropriate areal parameters used to distinguish milled surfaces with different machining conditions are presented.

In addition,, the relationship between the machining condition and the selected areal

parameters is also discussed. Other investigations such as the degree of tool degradation in face milling and the best area on the machined surface to measure are also conducted.

## 5.1 Best measurement area to represent a milled surface

Whitehouse [139] explained the inconstancies in profile analysis of milled surfaces. These inconstancies arise because of the different surface patterns created on the surface during the machining process. By measuring profiles across different sections of the same surface machined under the same conditions, different Ra values were obtained. He [139] also confirmed that there is a common trend of 40% variation of Ra values on regular face-milled surfaces. These inconstancies can be traced in areal measurement as well, even though the variation of Sa value across a milled surface might not be as high as 40%.

To develop a robust model for prediction of surface areal parameters, it is necessary to consider ways to reduce or possibly eliminate these inconstancies. A critical study was conducted in order to select the appropriate area that can be used to best represent the surface under study after face milling. This study was based on visual inspection of the patterns on surfaces of face-milled parts.

Taking a critical look at the tool trails created on the machined part after a face milling process, it usually depicts the traces as shown in figure 5.1a or 5.1c [140].

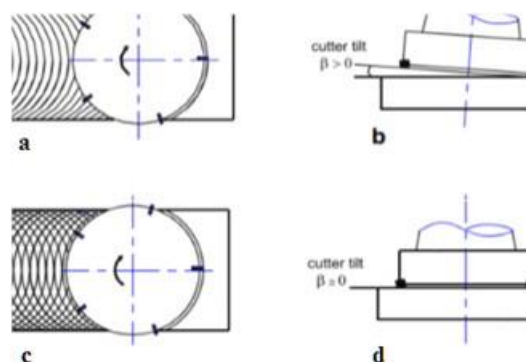


**Figure 5.1:** Effect of the tilted cutter on the surface topography. Taken from [140]

Based on visual observations by the author, the topologies can be categorized into three main groups as depicted in figure 5.2 considering the uniformity of the topology.

After measuring all the three different topologies and analysing them (results are tabulated in table 5.1 showing the different surface topology parameters on the same machined workpiece), it was noticed that surfaces with topologies as in figure 5.2b turns to have very high height surface topography parameters followed by figure 5.2a. It was concluded that figure 5.2a is the best topology, which will give the appropriate surface roughness parameters to represent the actual surface topography of the whole face-milled surface based on the following reasons.

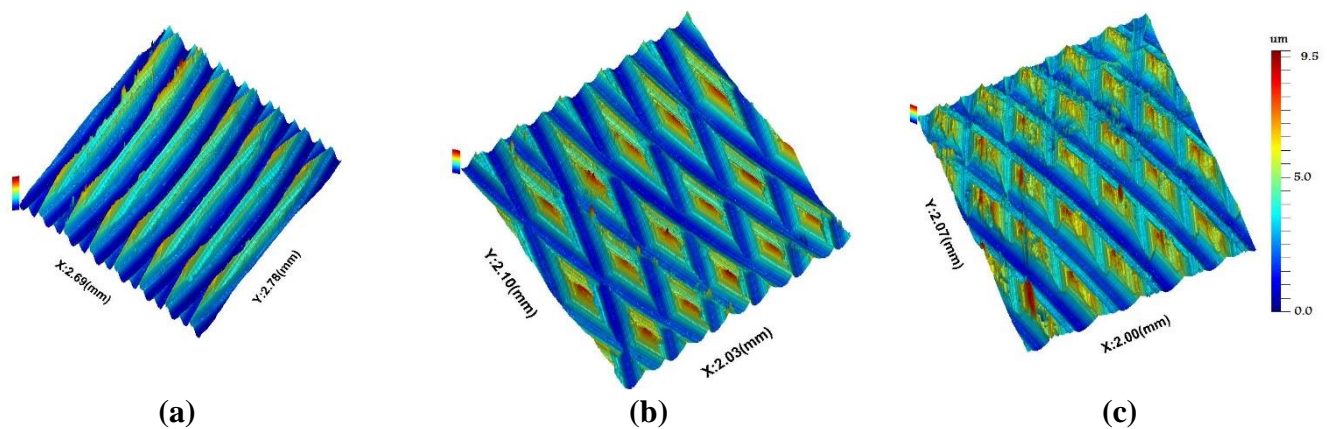


**Figure 5.2:** Different topology obtained from the same face milled workpiece

**Table 5.1:** Results of different topology on the same machined workpiece

Areal Parameters	Figure 5-2(a)	Figure 5-2(b)	Figure 5-2(c)	Average
<b>S<sub>a</sub> (μm)</b>	1.48	1.58	1.21	1.42
<b>S<sub>q</sub> (μm)</b>	1.81	1.93	1.47	1.74
<b>S<sub>z</sub> (μm)</b>	14.08	16.04	13.6	14.57

- When a part is machined with a larger tool diameter, the topology in figure 5.2a will tend to cover much of the surface area of the parts. This is because figure 5.2b and 5.2c are as a result of the overlapping of milling paths to ensure all the surface of the part is milled. This practice makes the topology in figure 5.2a the dominant topology over the others on most surfaces of face milled parts.

2. The average of all surface areal parameters; considering the parameters obtained from the three different topologies, is closer to the areal parameters obtained from the topology in figure 5.2a when compared to that of the topology in figure 5.2b and 5.2c as it can be seen in table 5.1, presenting the areal height surface parameters of the three topologies and their average.
3. Machine tools that do not suffer from the back cutting effects or chatter produce surface topology similar to that shown in figure 5.1a, only the topology in figure 5.2a could be found on surfaces machined with such cutting conditions.
4. The surface topology shown in figure 5.2a exhibits a periodic behaviour, hence it is easy to identify and characterize with unique features which can be related to the machining condition.

The primary causes of the different topology on the same surface milled with the same cutting conditions is the effect of back cutting by the cutter during the milling process in most situations. Back cutting results from tilt and the cutter-spindle. Figure 5.1 shows the effect of tilted angle on the surface topography [140]. Figure 5.1a illustrates the expected surface if the cutter is inclined at angle  $\beta$  to the surface of the machined part as shown in figure 5.1b. If the cutter is not tilted as illustrated in figure 5.1d, the expected surface finish is as depicted in figure 5.1c. The angle  $\beta$  of inclination is very difficult to measure and control especially in older machine tools.

## **5.2 Controlling degradation of the tool tip during face-milling**

The influence of tool degradation on the machined parts is inevitable. This is because of the brittleness and the hardness of the material that makes up the tool inserts and the workpiece. The influence of the tool degradation as well as the built-up edge formations can be observed throughout the machining process. Hence, much research such as documented in [141]–[144] has been geared toward its impact on surface finish. While

the most significant effect is tool wear, the term ‘degradation’ is used in this chapter to describe general condition change due to all factors.

Also, in the thesis, it was aimed to ensure that the influence of tool degradation on the surface quality of the training samples used for developing the models in chapter 6 is reduced or eliminated in cases where this is possible. This is not unrealistic for industrial applications when finishing cuts are used to minimise such influences.

Changing the tool inserts after face milling every sample would be an ideal way to avoid tool degradation for the training samples. However, it will be impractical because of the cost involved, as a high number of samples will be machined. Hence, changing the inserts as frequently as possible in order to avoid excessive tool degradation that may impact on the quality of the surface of the machined part was considered. To identify when to change the tool inserts, a series of experiments were conducted.

It is worth mentioning that all the samples used in this thesis were made up of the same material and size (30 mm x 30 mm x 20 mm). The aluminium alloy used was AL 6061. The mechanical properties and composition of AL 6061 are shown in table 5.2 and table 5.3 respectively. Moreover, the face milling was performed in a unidirectional manner on all the samples as well.

**Table 5.2:** Mechanical properties of the workpiece (AL 6061)

Mechanical Property	Value
Hardness, Rockwell A	40.00
Tensile Strength, Yield (MPa)	276.00
Elongation at Break(%)	17.00
Modulus of Elasticity (GPa)	68.90
Poisson’s Ratio	0.33
Shear Modulus(GPa)	26.00

In order to classify level of degradation of tool inserts after usage, the Alicona Infinite Focus G4 instrument was used to obtain the change between each tool insert before and after it is used. Measurement of the new tool insert was used as a reference form, and that of the used insert was inputted as the imperfect form. The area of defects ( $SIM_t$ )

**Table 5.3:** Composition (wt.%) of workpiece (AL 6061)

Content	Weight (%)
Al	97.30
Cr	0.30
Cu	0.20
Fe	0.10
Mg	1.00
Mn	0.10
Si	0.60
Ti	0.10
Zn	0.20

according to ISO 8785 [145] was obtained as the difference between the two measurements, which was used to represent the degree of degradation in this thesis. Also, with assistance of a locally-fabricated holder, the tool insert was always inclined at an angle of 45 degrees for all measurement, in order to measure the tip of the insert that was engaged with the workpiece during the machining process. As that gave the best measurement of the insert relative to the tip of the insert that had contact with the sample during the machining process and its subjection to degradation.

To understand how fast the tool degrades and/or wears during the milling process, ten samples were machined using the same cutting conditions. After each milling process, the inserts and machined samples were measured to obtain the  $SIM_t$  and the  $Sq$  respectively. Also, a digital indicator was used to check for tool degradation after every face milled sample on the machine tool. Two cutting conditions were used; for a relatively fine finish ( $Sq$  value  $< 1 \mu\text{m}$ ) and a rough finish ( $Sq$  value  $> 5 \mu\text{m}$ ) generated using typical finishing and roughing parameters respectively. It was discovered that different cutting conditions had different impact on tool degradation. Figure 5.3 shows the image of new insert (left); figure 5.3a and 5.3c and used insert (right); figure 5.3b and 5.3d. The following observations were discovered after analysing the tool degradation and its impact on the surface quality while face-milling ten samples of aluminium alloy block. Additional insight was also gained during this work through discussions with an experienced machinist.

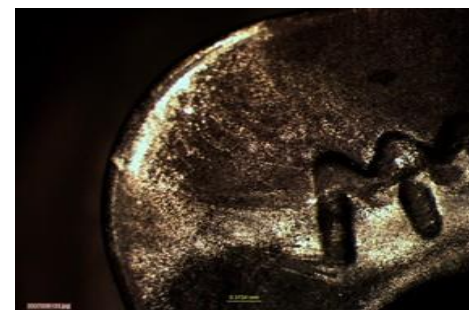


(a) Image captured using Alicona software;  
New insert tip

(b) Image captured using Alicona software;  
used insert tip



(c) New insert tips viewed under microscope



(d) Used insert tip viewed under microscope

**Figure 5.3:** Images of inserts; from the alicona software and microscope

1. There is a change in the volume of the tool insert after every revolution of the tool holder as it engages with the workpiece. This change could be as a result of wear, accumulation of residual on the tip of the tool (built-up edge) or the tip breaking.
2. Breakage of the tip of the insert rarely happens if the machining process is performed under the recommended cutting conditions of chosen workpiece's material which was followed in this research; hence breaking of the tip during machining was not experienced throughout this set of experiments.
3. Tool wear is most likely to occur in the initial milling process, and this was deduced from the  $SIM_t$  values obtained from the tool insert used for milling the first sample, which were approximately  $-97,100 \mu m^2$  (rough sample) and  $-12,000 \mu m^2$  (fine sample). The initial tool wear happens because the coatings covering the tool inserts were removed during the preliminary stages of the milling process. The difference in the  $SIM_t$  values differs in both fine and rough milling tool inserts

because of the area of engagement. For the fine milling, a cutting depth of 0.2 mm was used while for the rough milling, a cutting depth of 1.5 mm was utilised. Hence, a larger area of the tool insert is subjected to greater tool degradation during the rough sample milling process compared to the fine sample milling.

4. Also, during the milling process, as the tool inserts engage with the workpiece, heat is generated. The generated heat sometimes reaches the melting point of the workpiece. Hence, the use of coolant in the cutting process to reduce the heat. However, with soft materials such as aluminium alloys, it was noticed that residuals of the aluminium alloys after melting, solidifies quickly at the tool tip, increasing the volume of the used insert at the end of the face milling process forming the built-up edges.
5. The solidified mound at the tips of the inserts (built-up edges) could either chip off or increase in volume during subsequent milling. This is dependent on the cutting force, the temperature produced during the machining process and the cutting parameters. Unfortunately, no clear pattern was deduced on whether the built-up edge will chip off or increase in volume in subsequent milling.

The change in the surface quality ( $S_q$ ) of the samples over machining ten samples varied arbitrarily between  $5.41 \pm 0.27 \mu\text{m}$  and  $0.95 \pm 0.12 \mu\text{m}$  for the rough and finish samples respectively. This can be observed in figure 5.4 and 5.5 respectively.

Figure 5.4 display the results obtained from machining 10 aluminium alloy samples using the same cutting parameter with an aim of obtained a fine surface; Chart 1 (on top) is the deviation in  $S_q$  value (machined surface) as the number of sample increases. Chart 2 is results of SIM, obtained from the difference in tool inserts as machined sampled number increases. Chart 3 is a bar chart of the absolute deviation of height of tool insert on-machine using a digital indicator.

It can be observed from figure 5.4 that, the inserts first undergo losing of their coatings and slight degrades or/and wears (but enough to have an impact on the surface quality)

by observation of the first four samples. The fifth and sixth samples confirm the inserts' built-up edges. The built-up edges chips off and building up again as further samples are machined.

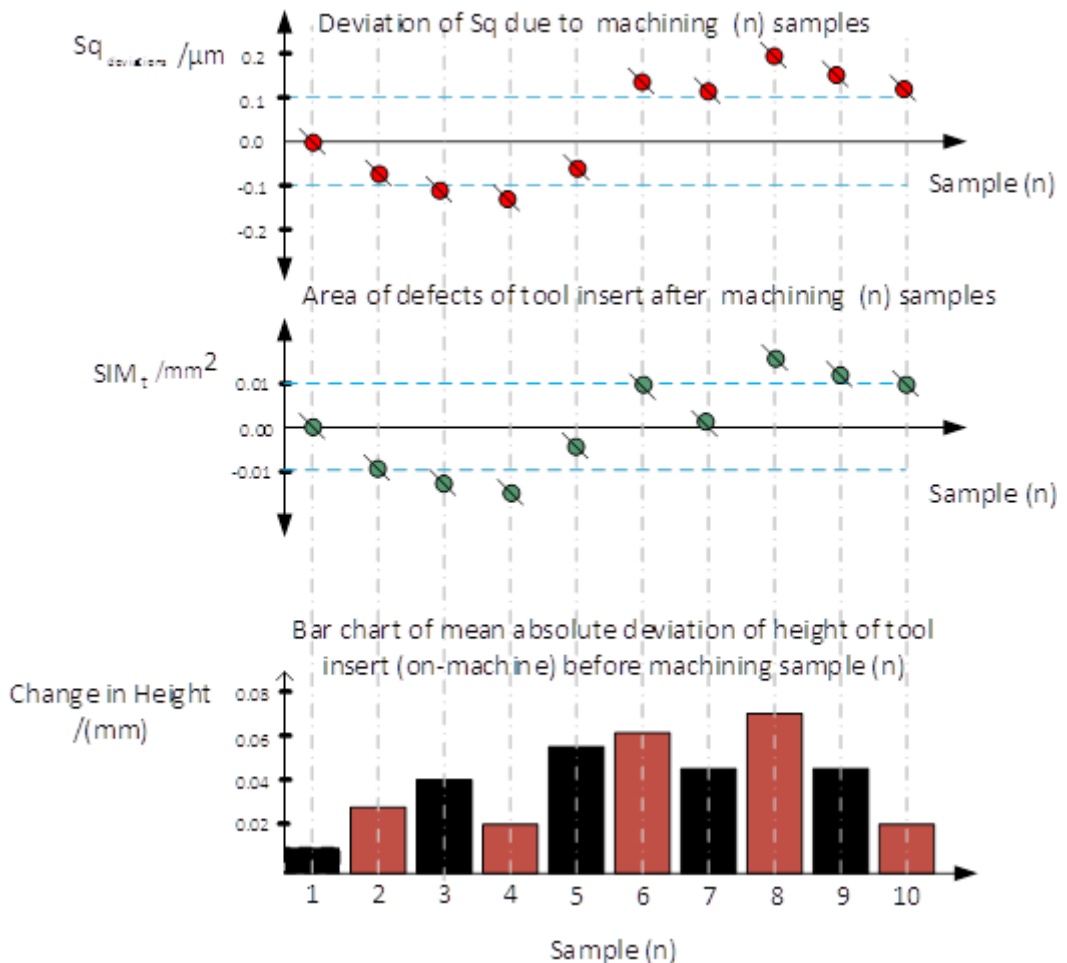


**Figure 5.4:** Effect of fine face milling on tool inserts as the number of samples increase

Figure 5.5 display results obtained from machining 10 aluminium alloy samples using the same cutting parameter with an aim of obtained a rough surface; Chart 1 is the deviation in  $Sq$  value (machined surface) as the number of sample increases. Chart 2 is results of  $SIM_t$  obtained from the difference in tool inserts as machined sampled number increases. Chart 3 is a bar chart of the absolute deviation of height of tool insert on-machine using a digital indicator.

An observation of the charts in figure 5.5 depicts that after the initial tool inserts

degradation/ wear caused by milling the first two samples, the volume of the inserts does not change rapidly compared to figure 5.4. Comparing figure 5.4 and 5.5 confirm that there is no similarity of the imparts of tool degradation when machining with different cutting parameters. This might be due to factors such as the speed of the cutting tool and the area of engagement of the tool. In conclusion, in order to reduce the influence of tool degradation on the surface of the sample during the machining process, a digital indicator was used to quick check for significant tool degradation after every face milled sample as shown in figure 5.6. The tool insert was changed if a change in the height of the deflection of 0.05 mm is detected. As it can be seen from figure 5.4 and 5.5, milling with tool inserts with height deflections above 0.05 mm has great impact on the surface quality.

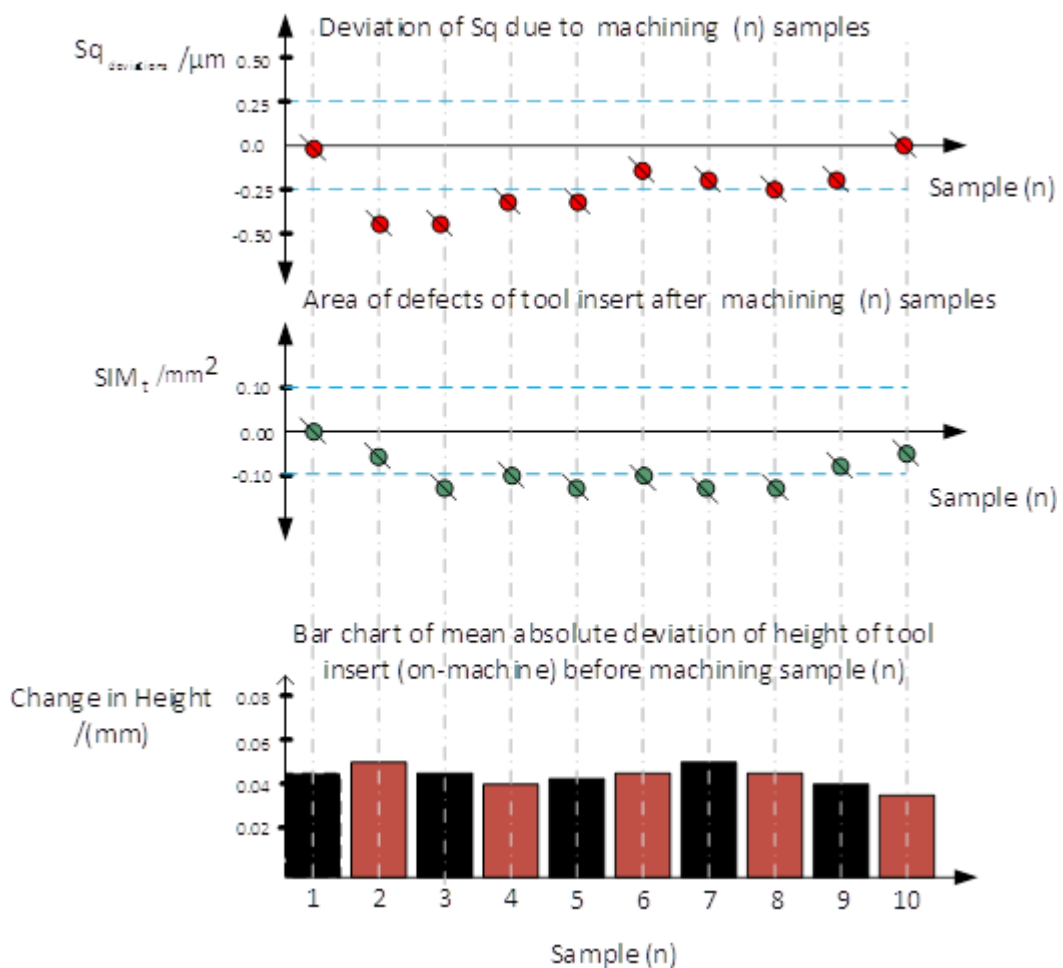


**Figure 5.5:** Effect of Rough face milling on tool inserts as the number of samples increase

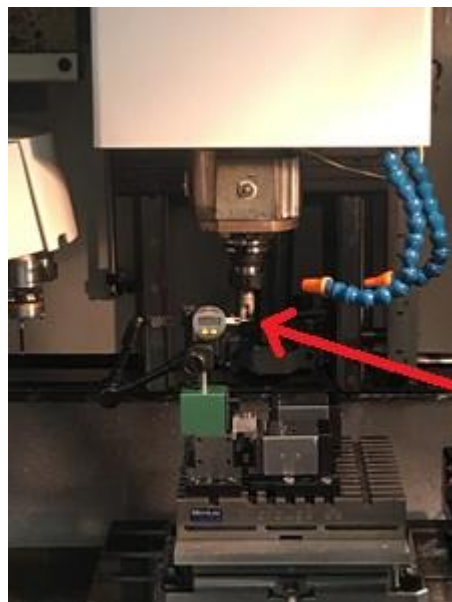


**Figure 5.6:** Image - checking tool degradation using a digital indicator; arrow pointing to tool holder during the checking process

### 5.3 Appropriate areal parameters to distinguish milled parts with different surface topologies

The introduction to the concept of areal surface measurements guarantees a more detailed description of the surfaces under study, giving a greater statistical significance and better repeatability between samples of the same surface; compared to the initial profile measurement [146].

Even though it is a fact that there is a relationship between the surface topology of a machined part and the functional performance of the part, it is still unclear which of the surface topography parameters are most useful in a unique manufacturing process such as face milling. This problem is as a result of the initial development of areal surface parameters, mainly for ultra-precision surfaces such as optics, the lack of research into the functional significance of sophisticated parameters [139] and the lack of a systemic approach to select a few appropriate surface roughness parameters that can be used to describe the surface quality of a machined part.

Different groups have used different surface parameters to define the surface quality of a product. A typical example would be the UK and USA using the average roughness

'Ra' as a control parameter whilst Germany, other eastern European countries and Russia employs the peak parameter for similar purposes [4]. This being one of the reasons for the lack of agreement on which parameters are best fit for representing a particular manufacturing process. Even though a single parameter could be used in indicating a variation in the manufacturing process, it may not be sufficiently discriminating or sensitive to pinpoint where the changes in the process have occurred. Moreover, a combination of parameters which are height related (Ra or Rq) cannot equally be used [147]. For the same reason areal surface parameters, such as Sa and Sq could potentially fail to discriminate between different manufacturing processes alone because both are height parameters [148].

In this section, a statistical approach is considered to suggest the most appropriate surface areal parameters for discrimination between different face-milled surfaces. The selected areal parameters will later be used as the output of the model in chapter 6.

### **5.3.1 Procedure for selection of best areal parameter**

The method of selecting the appropriate surface areal parameters which will be implemented in this study has been utilized by Helmlie *et al.* [149] to select significant areal parameters that can be used to discriminate between new and used abrasive papers. In their studies, they concluded that it is vital to select parameters based on their usefulness and significance; which is having disjoint intervals. The approach has been also been used by Das and Linke [150], to select surface roughness parameters that best distinguish between extruded surfaces and ground surfaces produced by #60 grit and #400 grit sizes. The technique used in the aforementioned works is referred to as cross-correlation coefficient; a tool for the classification of problems with only two events such as good or bad parts. In this study, it will be used to classify rough (on the left) or fine (on the right) face-milled surfaces shown in figure 5.7.

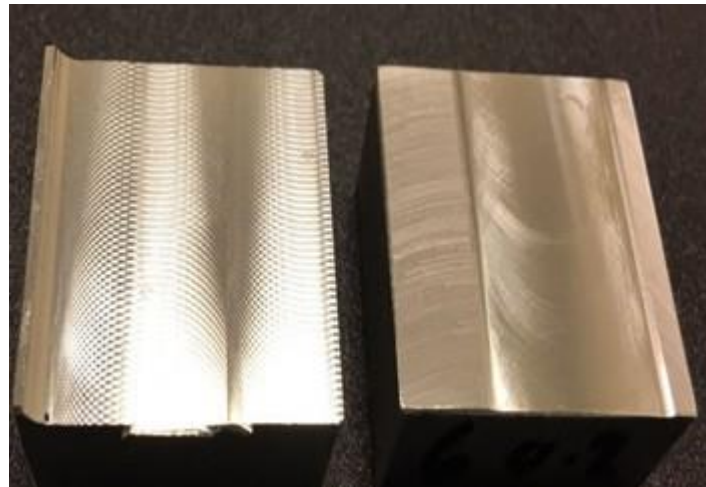


**Figure 5.7:** Faced-milled blocks with different surface topography; The rough sample on the left had an  $S_a$  value of  $5.7 \mu\text{m}$  whilst the fine face milled sample on the right had an  $S_a$  value of  $1.2 \mu\text{m}$

The cross-correlation coefficient ( $r_{FR}$ ) between the two face-milled surfaces will be calculated using the formula [149] below;

$$r_{FR} = \frac{\sum_{i=1}^n (S_v^{F,i} - \mu^F)(S_v^{R,i} - \mu^R)}{\sqrt{\sum_{i=1}^n (S_v^{F,i} - \mu^F)^2 \sum_{i=1}^n (S_v^{R,i} - \mu^R)^2}} \quad (5.1)$$

$S_v$  in equation 5.1 represents a surface topography parameter,  $\mu^F$  ( $\mu^R$ ) denotes the mean of the sample on a fine (rough) surface and  $S_v^{F,i}$  ( $S_v^{R,i}$ ) is the surface topography parameter  $S_v$  of the  $i^{th}$  sample on fine (rough) milled surface. “n” is the number of samples. The most significant parameter has the highest absolute cross correlation.

In order to utilise the above method for choosing the right surface areal parameter for the predictive model, a series of repeated measurements were carried out. Ten measurements were taken from each face-milled sample (fine and rough) using the same technique, instrument, operator, in the same environment, at the same spot. All 20 separate surface topologies were obtained with the same evaluation size, 8 mm x 8 mm.

### 5.3.2 Results and discussion; selection of appropriate areal parameter

After obtaining the twenty-four surface topography parameters for all the twenty measurements (10 per sample) using Surfstand V6 software package; the average and standard deviation were calculated, for the rough dataset and the fine dataset and in each case under a 95% confidence interval (coverage factor;  $K = 2$ ) as shown in **Appendix E**. To find the surface topography parameter that is the most significant, the significant value is first computed. The significance;  $S_i$  is calculated by using the intervals, and the mean of the two sample sets using the formula [149];

$$S_i = \frac{\partial(iR, iF)}{\frac{1}{2}(\mu^F + \mu^R)} \quad (5.2)$$

Where  $\partial(iR, iF)$  denotes the difference between the interval between the two datasets. Figure 5.8 shows the results of the significance against surface areal parameters between fine and rough face-milled surface.

From figure 5.8, it can be seen that the height parameters ( $S_a$ ,  $S_q$  and  $S_{pk}$ ) are most significant followed by the curves related parameters ( $V_{vc}$  and  $V_{mc}$ ) and then the spacing parameter,  $S_{al}$ .

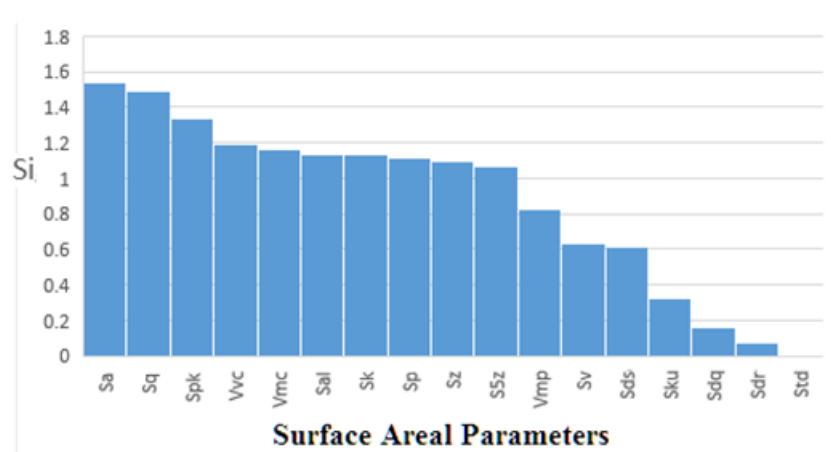


**Figure 5.8:** Significance of areal parameters between fine and rough face-milled surface

As explained earlier, even though the height parameters ( $S_a$  and  $S_q$ ) seem to have the highest value of significance, they may not be suitable to describe a machined surface alone.  $S_a$  and  $S_q$  are generally and widely used in many publications. This is because  $S_q$  is insensitive to differentiating peaks, valleys and the spacing of the surface as well as  $S_a$ . This has been demonstrated by Waterworth [148].  $S_{pk}$ , reduced peak height, is the next significant parameter after  $S_a$  and  $S_q$ .  $S_{pk}$  is an estimate of small peaks above the main plateau of the surface. It can be used to characterize the volume of material that is likely to be removed during running-in of a machined component [151].

The volume parameters ( $V_{vc}$  and  $V_{mc}$ ) have shown a good relationship with functional requirements in several applications [148]. The  $V_{vc}$  and  $V_{mc}$  can be used to describe the performance of a surface without considering its highest peaks. The highest peaks on a surface are usually lost in the earlier stage of wear of the machined component. These volume parameters represent the fluid retention ability of the surface.

The last parameter that will be considered from figure 5.8 is  $S_{al}$ . In using Fourier analysis, that is considering the surface topography of the machined workpiece is made up of a series of sine waves with different frequencies in all directions and amplitudes (see **Appendix A**), the power spectrum is a measure of the amplitude of each sine wave for a particular frequency, along a given direction. For an anisotropic surface (examples would be face-milled surfaces),  $S_{al}$  is in the direction perpendicular to the surface lay. A large value of  $S_{al}$  denotes that the surface is dominated by low spatial frequency components, while a small value for  $S_{al}$  denotes the opposite. Typically, the tool trace path in a milling process varies when there are changes in cutting conditions. The tool trace on a face milled surface has a relation with frequency components on the surface under study. This makes  $S_{al}$  a very important parameter in describing face-milled surfaces.

Based on the results and discussions above;  $S_a$ ,  $S_q$  and  $S_{al}$  were considered as the main areal surface roughness parameter to be used as indicators suitable for distinguishing between the different levels of roughness on surfaces caused by face-milling.

## 5.4 Influence of machining conditions on areal parameters

After identifying the appropriate areal parameters to be used for developing the predictive model, the next critical function that needs to be understood is the relationship between the milling conditions and the selected areal parameters. This is because different milling conditions causes different topologies on the surface of the machined parts as explained in chapter 2.

Previous research has shown that varying the cutting conditions such as cutting speed, depth of cut, feed rate and type of coolant, greatly affects the surface roughness of the machined part [152], [153]. Even though there are existing literature on the influence of cutting conditions on the surface finish, the predominant focus is on profile roughness parameters. This leaves a gap in understanding of the influence of cutting parameters on areal surface parameters. Therefore, this section aims to examine the influence of cutting parameters on areal surface parameters.

Many cutting conditions can influence the surface parameters as shown in chapter two. However, the most common cutting parameters identified via the reviewed literature in chapter two clearly shows that the depth of cut, cutting speed and feed rate are the most significant conditions that have great impact on the values of profile roughness parameters. While profile machining was the focus of the previous research it is assumed that the results are relevant to end milling processes. Henceforth, these three independent parameters are considered as the cutting parameters in this study.

Experiments were planned as per Taguchi's L'16 orthogonal array. Table 5.4 shows the investigating parameters used. These parameters were carefully chosen to ensure they all fall within the recommended cutting parameters provided by the manufacturer's technical guide for end milling using the cutting tool [154].

**Table 5.4:** Cutting parameters with levels

Cutting Parameter	Level 1	Level 2	Level 3	Level 4
Cutting Speed (RPM)	4000	5300	6600	8000
Feed Rate (mm/min)	750	1165	1580	2000
DoC (mm)	0.20	0.70	1.20	1.70

The Taguchi's L'16 design of experiment produces 16 face-milled samples machined with different combinations of the cutting conditions shown in table 5.4. The purpose of using Taguchi's L'16 instead of the traditional full factorial design of experiment is to reduce the number of resources used in the preliminary investigations and still achieve the aim of the study.

The 16 different cutting parameters used for face milling the samples and corresponding surface topography information after measuring the samples are presented in **Appendix F**. The corresponding surface topography parameters ( $S_a$ ,  $S_q$ , and  $S_{al}$ ) were extracted from the surface topology measured using the MDS technique, as explained in chapter 3, and parameterized using Surfstand software package.

The signal to noise ratio S/N ratios were calculated using the smaller-the-better characteristic proposed by Taguchi. With assistance from Minitab 17, a statistical analysis software, which is widely exploited in many engineering optimizations, analysis of variance (ANOVA) was carried out.

It should be mentioned that in order to maintain a constant temperature during the face-milling process, Coolant (Quakercool 7101 LF at a concentration of 7%) was used in the cutting process. Also, the tool degradation was also controlled as earlier.

### 5.4.1 Analysis of variance (ANOVA)

The experimental results of surface topography values were analysed with the Analysis of variance (ANOVA) method in order to identify the significant factors. During the

ANOVA process, a significance level of  $\alpha = 0.5$ , i.e., for a confidence level of 95%; of the signal to noise (S/N) ratios were evaluated. ANOVA also determined the contribution of individual cutting parameters. The source with the lowest P-value is considered to have a significant contribution to the surface roughness.

Table 5.5 and 5.6 show the results of the ANOVA for the areal parameters; Sq and Sal respectively. From the results, it can be observed that the feed rate is the most significant parameter followed by cutting speed. Depth of cut is the least significance in controlling Sq and Sal values of the machined part. From the results shown in table 5.5, the p-value of feed rate is 0.004 which is less than 0.05. This means that changing the feed rate while all other cutting parameters are constant will have higher impact on the value of Sq compared to when the other parameters are manipulated in the same manner.

**Table 5.5:** Analysis of variance for Sq ( $\mu\text{m}$ )

<b>Source</b>	<b>DF</b>	<b>Adj SS</b>	<b>Adj MS</b>	<b>F-Value</b>	<b>P-Value</b>
<b>Speed</b>	3	64.59	21.532	6.31	0.028
<b>Feed</b>	3	138.97	46.325	13.58	0.004
<b>DoC</b>	3	39.81	13.268	3.89	0.074
<b>Error</b>	6	20.47	3.411		
<b>Total</b>	15	263.84			

**Table 5.6:** Analysis of variance for Sal ( $\mu\text{m}$ )

<b>Source</b>	<b>DF</b>	<b>Adj SS</b>	<b>Adj MS</b>	<b>F-Value</b>	<b>P-Value</b>
<b>Speed</b>	3	174.66	58.219	11.64	0.007
<b>Feed</b>	3	276.28	92.093	18.41	0.002
<b>DoC</b>	3	23.74	7.913	1.58	0.289
<b>Error</b>	6	30.02	5.003		
<b>Total</b>	15	504.69			

Also, from the results shown in table 5.6, the p-value of feed rate is 0.002, which is also less than 0.05 and means that feed rate has a significant impact on Sal value compared to the other cutting parameters. Table 5.7 shows the results of the ANOVA for Sa. From the results, it can be observed that all the cutting parameters have relatively great influence on the Sa value i.e. changing any cutting parameter will have a significant impact on the Sa value. In other words, none of the chosen control parameters is more

significant than the other.

**Table 5.7:** Analysis of variance for Sa ( $\mu\text{m}$ )

Source	DF	Adj SS	Adj MS	F-Value	P-Value
<b>Speed</b>	3	31.11	10.369	2.04	0.209
<b>Feed</b>	3	68.94	22.98	4.53	0.055
<b>DoC</b>	3	42.57	14.19	2.8	0.131
<b>Error</b>	6	30.44	5.073		
<b>Total</b>	15	173.05			

#### 5.4.2 Main effects of cutting parameters on areal parameters

In statistics, a main effect is the effect of just one of the independent variables on the dependent variable i.e ignoring all other independent variables. In this section, the effects of the individual cutting parameters on the areal surface parameters were considered.

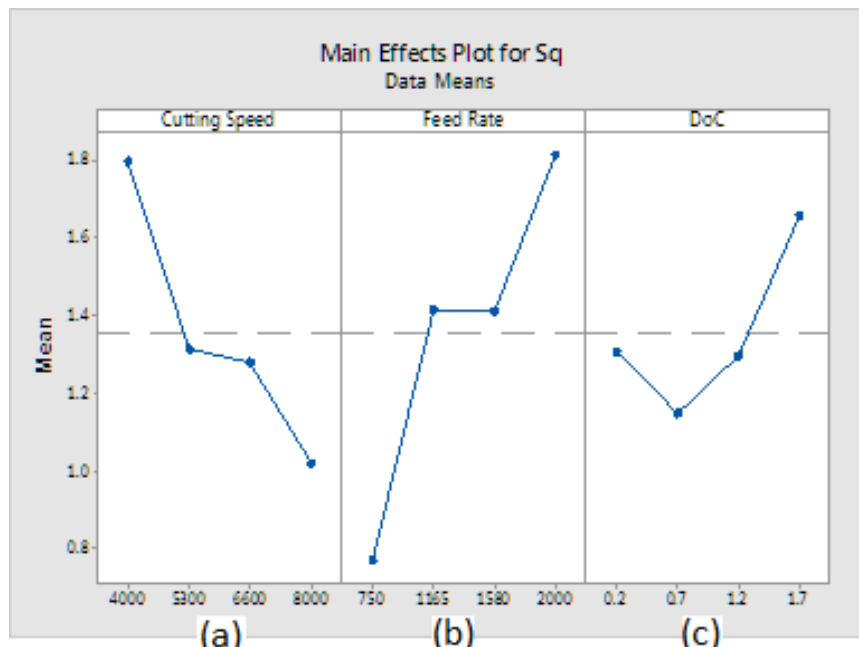


**Figure 5.9:** Main effects plot for Sq

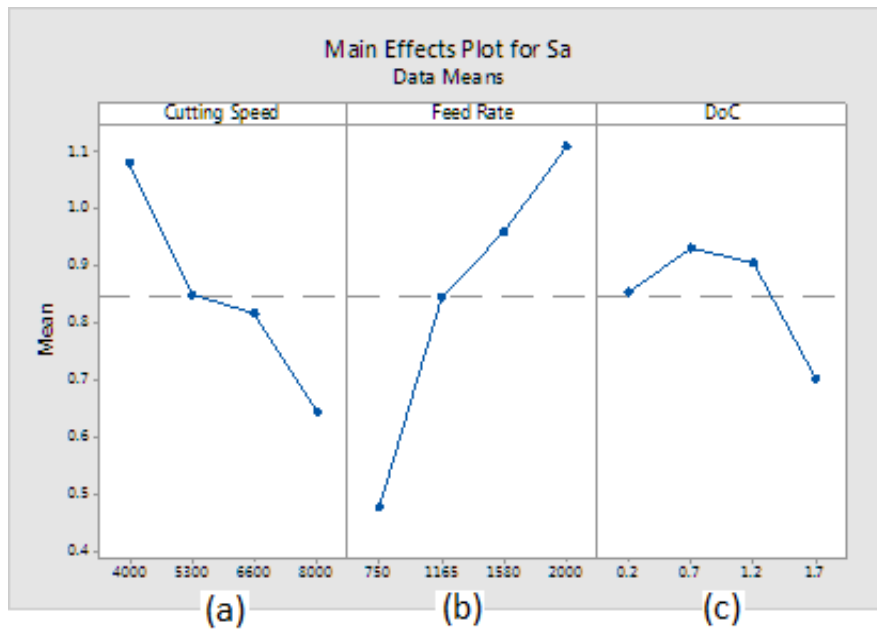


**Figure 5.10:** Main effects plot for Sa

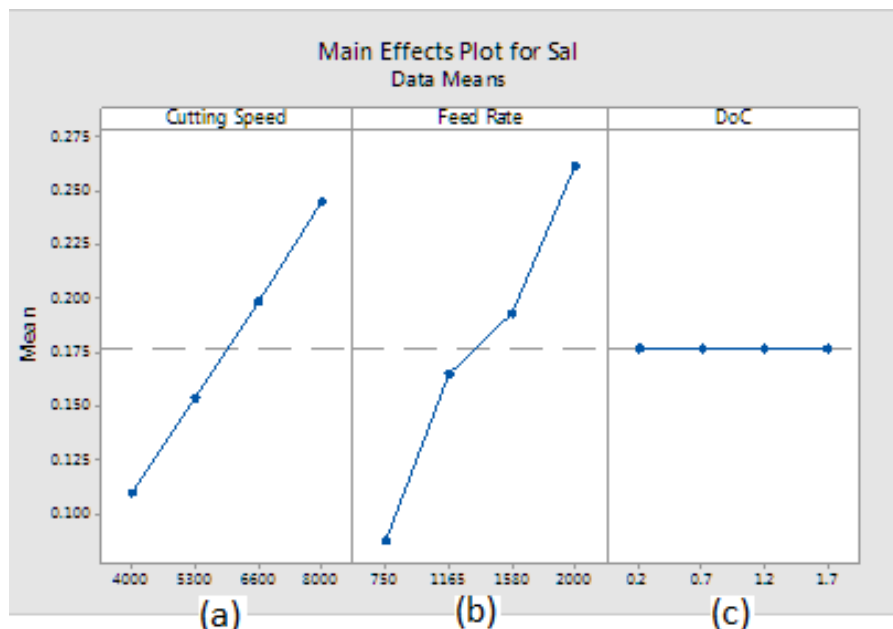
Figure 5.9a and 5.10a represent the main effect plots of cutting speed on Sq (Root mean square deviation of the surface) and Sa (arithmetical average of the surface) of a measured sample respectively. From the plots, both Sa and Sq reduce as cutting speed increases from 4000 to 8000 RPM. This is because, at the higher cutting speed, the tendency of built-up edge formation is decreased, more heat is carried away by the chip and less heat is dissipated to the sample, hence, the Sq is decreased. In order to achieve minimum Sq, the cutting speed should be kept at the highest level (8000 RPM). Similar results were obtained in previous research however they considered profile parameters; Rq [155].

Figure 5.9b and 5.10b represent the main effect plots of feed rate on Sa and Sq. From the plots, it is observed that the Sa and Sq increase with increasing feed rate from 750 to 2000 mm/min. Increasing the feed rate increases the area of contact between the cutting inserts and the sample. This increases the cutting forces and stimulates higher values of Sa and Sq. To achieve minimum Sa or Sq, the feed rate should be kept at the lowest level (750 mm/min).

Figure 5.9c and 5.10c represent the main effect plots of depth of cut on Sa and Sq. From the plots, it can be observed that the Sa and Sq value have an exponential relationship

with the depth of cut. Moreover, the effects of depth of cut on  $S_a$  and  $S_q$  are opposite in relation from 0.2 to 1.7 mm. It can be seen in both plots that after 0.7 mm depth of cut, there is a change in direction from increasing to decreasing or vice versa of the  $S_a$  or  $S_q$  value respectively.

Figure 5.11 shows the main effect plot of the cutting speed and feed rate on the  $S_{al}$  parameter. It can be observed that an increase in the cutting speed and feed rate increases the  $S_{al}$  of the surface. By increasing the cutting speed from 4000 – 8000 RPM and the feed rate from 750 – 2000 mm/min, the surfaces produced become dominated by low spatial frequency features. However, varying the depth of cut from (0.2 – 1.7) mm will not have any significant impact on the level of spatial frequencies on the surface.



**Figure 5.11:** Main effects plot for  $S_{al}$

## 5.5 Summary of chapter

From the investigations conducted in this chapter, the following conclusions were deduced:

1. In order to avoid inconsistencies in measurement results obtained from face-milled

surfaces, the middle section of the tool trails on the machined surface will be considered in this thesis. This is because this topology can be found in every face mill sample regardless of the cutting condition used. It is also easy to identify due to its periodic structure. Finally, areal surface topography parameters obtained from the middle section is closer to the average of parameter obtained from all potential topologies suitable to be used for representing the entire surface of the machined samples.

2. Even though tool degradation is inevitable in machining process due to the interaction between two different materials (the tool tip and the workpiece), it was discovered that in the cases were the workpiece is made of aluminium alloy, the tool can either wear (decreasing the overall tool insert volume) or incur built-up edges (increasing the overall tool insert volume). In order to avoid this phenomenon from impacting greatly on the surface quality of the machined samples used in this thesis, the tool inserts classified as useful were monitored to have a deflection height that does not exceed 0.05 mm.
3. The areal surface metrology parameters  $S_a$ ,  $S_q$  and  $S_{al}$  show results which confirm their ability to be used as indicators for various levels of surface topography in a milling process. The conclusion was made after a sensitivity analysis was conducted considering 24 areal surface topography parameters.
4. In an attempt to understand the cutting parameters influence on the selected surface areal texture parameters, an ANOVA was carried out using the cutting parameters (feed rate, depth of cut and cutting speed) as the factors and surface parameters ( $S_a$ ,  $S_q$  and  $S_{al}$ ) as responses. It was discovered that for  $S_q$  and  $S_{al}$ , the most significant parameter was the feed rate.

Based on the information revealed in this chapter, the next chapter develops a predictive model using the cutting parameters as input and areal surface topography parameters as the output.

# Chapter 6

## Development and evaluation of surface metrology models

On-machine metrology (bringing metrology onto the machine tool on the shop floor) has many benefits. One of its benefit is the elimination of challenges associated with realigning parts back on the machine tool for re-machining in case errors are identified during the post-process metrology analysis. Another important benefit is obtaining data in a short time. Often data from post-process inspection systems takes time, even days or weeks, to filter back for process improvement which will be greatly reduced if on-machine metrology is practiced.

In an attempt to increase the quality of machined parts; optimization of cutting parameters used for machining will increase the ability to control the surface quality which in turn is a key enabler for right-first- time production and reduces the quantity of defected parts that require re-machining. A system that combines a robust optimization model and on-machine metrology will not only increase productivity but also reduce the number of rejected parts as well.

Based on the review in chapter two, surface roughness models using cutting conditions in milling process have been in existence for several decades. However, the majority of models that have been developed have mainly focused on profile surface roughness

parameters and not areal parameters. The few that considered areal parameters as outputs were theoretical models only (reviewed in section 2.5 of this thesis).

The models developed in this chapter are data-driven models employing Artificial Intelligence (AI) methods to predict areal surface topography parameters ( $S_a$ ,  $S_q$  and  $S_{al}$ ) using cutting parameters (cutting speed, depth of cut and feed rate) because of its robustness and ease to develop.

## 6.1 Artificial Intelligence (AI) methods

An artificial intelligence (AI) model is a model that can make choices which would be viewed as intelligent if made by an individual. Artificial Intelligence is becoming more prominent and particularly amenable to modelling complex systems since it has exhibited better predictive ability compared to traditional methods.

The most common AI techniques for models that have been utilized in manufacturing include genetic algorithm (GA), fuzzy logic algorithm, and artificial neural network (ANN).

Neural networks use training data pairs representing the input and output of the system to learn a function that can be used to map the input to the output. Unlike methods such as linear regression, which only learn linear functions, feed forward neural networks can learn non-linear mappings [156]. They do this by transforming the input to another representation space using hidden layers that represent the parameters of a non-linear mapping function. The parameters of the hidden layers are then learned using gradient descent approach.

ANN models have been used in several areas of engineering applications. They have been proven as an excellent tool for predictive modelling in machining and processes. They also provide a more accurate prediction compared to conventional modelling tools such as regression models in many cases, especially when solving highly non-linear and

complex problems that cannot be easily modelled mathematically [157]. Hence, an ANN model was considered in this research.

### 6.1.1 Basic introduction to ANN

ANN models are made of layers that can be classified into three categories: input layer, hidden layer(s) and the output layer. Every ANN model must have at least one hidden layer. However, multiple hidden layers can also be used. The number of hidden layers must be chosen carefully to avoid limiting the networks' ability to generalise results for new input data.

Each layer consists of neurons, which are also referred to as the processing elements. The elements are connected to other elements in the adjacent layer. The strength of the connection is expressed by the weight. In a feed-forward network, the weighted connections feed activations only in one direction from the input to the output layer as shown in figure 6.1. Figure 6.1 is a preliminary design of the structure of a feed-forward neural network.

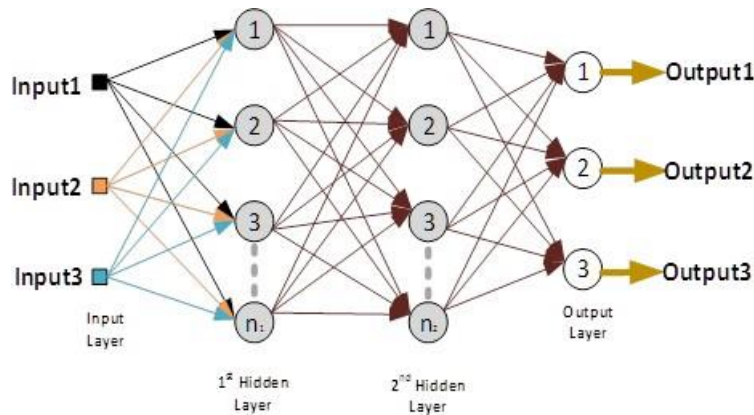


**Figure 6.1:** Structure of feed-forward neural network with four layers; one input layer, two hidden layers and one output layer

Each neuron in a layer initially performs a weighted amassing of the individual input values and then passes the results through an activation function, with the exception of

the input layer elements where no computation is performed. The net input to each neuron is the sum of the weighted output of the neurons in the previous layer. The output of the element  $j$  in layer  $k$  is

$$net_j^k = \sum W_{ji}^k O_i^{k-1} \quad (6.1)$$

$$O_k^j = f(net_j^k) = \frac{1}{1 + e^{-(net_j^k)}} \quad (6.2)$$

Where weight  $W_{ji}^k$  is between the  $i^{\text{th}}$  neuron in the  $(k-1)^{\text{th}}$  layer and the  $j^{\text{th}}$  neuron in the  $k^{\text{th}}$  layer,  $f(x)$  is the activation function and  $O_k^j$  is the output of the  $j^{\text{th}}$  neuron in the  $k^{\text{th}}$  layer.

In order to obtain a successful model of ANN, there is substantial reliance on trial and error process with the influencing functions [157]. The MATLAB neural network toolbox could be used as an assistant for designing and updating these functions efficiently. By using this toolbox, the influencing functions include network type, training function, learning function, performance function, transfer function and the number of hidden layers.

### **6.1.2 Selecting the right network structure and functions for ANN model**

The difficulty in building an ANN is to determine the number of hidden layers and neurons, the training and learning algorithm, the transfer function for each of the layers, and the network architecture to be used [158]. The transfer function could be any differentiable function such as hyperbolic tangent sigmoid (tansig), Log-sigmoid, (logsig) and linear (purelin). Also, there are over 14 training algorithms that could be

used when building an ANN, and only one can be utilized per model. Each of these parameters can have a significant impact on the network's performance, and care should be taken when choosing them to build a robust ANN.

Choosing the right network architecture also plays an important role in the performance as well. Unfortunately, the method of selection of the transfer functions and the network architecture during the modelling is based on trial and error. In the last decade, research has been undertaken which attempt to propose methods to fix this problem. A detailed review for the past 20 years can be found in [159] by Sheela and Deepa on the various attempts and techniques suggested to solve this problem. Based on their survey, it is appropriate to conclude that this challenging task can only be made simpler by eliminating the combinations of algorithms and functions that provide high errors for a unique application. This approach only solves one side of the problem leaving the challenge of selecting the right network architecture and hidden layers.

In order to solve the other half of the problem in this thesis, a guideline given by Zhang *et al.* [160] was considered in choosing the recommended number of neurons in the hidden layer and network architecture in this research. In accordance with Zhang *et al.*, the recommended number of neurons in the hidden layers to be considered during the trial and error experiments should be in the order; ' $n/2$ ', ' $1n$ ', ' $2n$ ', and ' $2n+1$ ', ' $3n$ ', and ' $3n+1$ ' where  $n$  is the number of input parameters. Also, it was considered the number of hidden layers should not exceed the number of inputs parameters. Henceforth, the following network architectures were considered;  $3 - X_1 - 3$  and  $3 - X_1 - X_2 - 3$ , where  $X_{ith}$  represents the number of neurons in the  $ith$  hidden layer.

To avoid the tedious trial and error approach, a MATLAB program was used to identify the best training algorithms, learning algorithms and transfer function for each layer in this thesis. The program considered all possible combinations of the algorithms, transfer functions, and confirmed the performances of each possible combination. The results from the program is described in section 6.2.

### **6.1.3 Quality assessment of developed models**

After a model has been developed, it is expedient to confirm the quality of predictions obtained from it to assess the models accuracy. This procedure gives the confidence behind the model. This process is referred to as model validation.

Two approaches are used in the validation of a model. The first examines the possibility of a model to predict dataset that was used in the training process. This is referred to as direct validation. If the model is not able to predict the dataset that has been used in the training procedure, it suggests that the model is not fit to be used to represent the system. The secondary test examines the possibility of the model to predict dataset that was not used in the training process, in other words, unseen dataset. This procedure is referred to as cross-validation. Cross-validation is mainly used to check the generalisation capability of the model [161].

In both tests, the predicted results by the model are compared with corresponding measured output to obtain its deviation. Usually a statistical index can be employed. The common statistical methods for this purpose include residual value, Root Mean Square Error ( $R_{MSE}$ ) and Correlation coefficient (R). These can also be referred to as performance criteria [162] .

Root Mean Square Error ( $R_{MSE}$ ) and correlation coefficient (R) were used in this study to assess the performance of the developed model as well as to assist in selecting the right model structure.

The coefficient of correlation (R) describes the degree of collinearity between predicted and measured data, which ranges between (-1, 1). This is an index of the degree of linear relationship between measured and predicted data. Systems with good correlations have an absolute magnitude approaching 1.

The root mean square error is used to measure the difference between values predicted by a model and those measured from the experimental test. Systems with high accuracy have  $R_{MSE}$  approaching 0. The coefficient of correlation (R) and  $R_{MSE}$  were calculated

using the equation below:

$$R = \frac{n \sum_{i=1}^n x_i y_i - \sum_{i=1}^n x_i \sum_{i=1}^n y_i}{\sqrt{(n \sum_{i=1}^n x_i^2 - (\sum_{i=1}^n x_i)^2)} \sqrt{(n \sum_{i=1}^n y_i^2 - (\sum_{i=1}^n y_i)^2)}} \quad (6.3)$$

$$R_{MSE} = \sqrt{\frac{\sum_{i=1}^n (x_i - y_i)^2}{n}} \quad (6.4)$$

Where n = total number of samples  $x_i$  = measured values  $y_i$  = predicted values

## 6.2 Development of the ANN

The description of key decisions required to develop a neural network was explained earlier. In this thesis, two ANNs were developed with each having a different network architecture. The first group has a single network with three inputs and three outputs as shown in figure 6.1. This model architecture will be referred to as conventional model in this thesis. The second model comprises of three networks enclosed to form a model. It has same inputs (three cutting parameters) but has a single output (either  $S_a$ ,  $S_{al}$ , or  $S_q$ ) connected to each network. This will be referred to as enclosed multiple network (EMN) model in this thesis. The structure of the EMN model is as shown in figure 6.2.

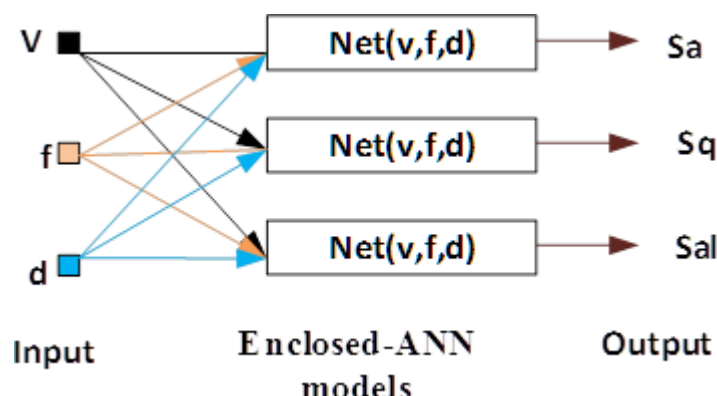


**Figure 6.2:** Structure of enclosed multiple network model

The purpose for developing two models with different structures is to confirm if the conventional model will be as reliable as the enclosed multiple network model. The enclosed model is expected to be more accurate than the conventional model. This is because, for the enclosed multiple network models, each embedded network is responsible for a single output parameter making each network dedicated to prediction only one output parameter. However, in a conventional model, a single network is responsible for all three-output parameters.

On the other side, the author also considered that, a conventional model with multiple outputs can be as reliable as an enclosed multiple network model, only if the output and input parameters are related that is, the stronger the relationship between the output parameters or/and input parameters; the higher the reliability of the conventional model. And since all three output parameters are surface areal parameters obtained from the same sample and the inputs parameters are all cutting parameters, it is worth investigating this possibility. And if per chance the conventional model is equally or better than the EMN model, it will be preferable over the enclosed multiple network model because it is less complex to develop.

It should be mentioned that 64 samples were machined using full factorial design of the cutting parameters in table 5.4 and following all the suggestions made in earlier chapters for both the machining process as well as the measurement process.

### **6.2.1 Conventional surface topography predictive model**

With the assistance of the MATLAB neural network toolbox and the programming codes for selecting the right network structure as well as the best transfer function explained in section 6.1.2, different conventional models were developed. The MATLAB program developed models with all possible combination of the algorithms and transfer functions and confirmed their performances using the direct validation approach and  $R_{MSE}$  as the performance criteria.

For conventional model with only one hidden layer, that is  $3 - X_1 - 3$ ; 1,512 models were developed from the possible combinations of function. For models with two hidden layers;  $3 - X_1 - X_2 - 3$ ; 27,216 were developed, where  $X_{ith}$  represents the number of neurons in the  $ith$ -hidden layer. Due to the high numbers of developed models in each category, only the top five is presented. Table 6.1 and 6.2 presents the top five conventional models selected based of earlier discussion in section 6.1.3.

**Table 6.1:** Best Models (Conventional Model  $3 - X_1 - 3$ ) Based on their  $R_{MSE}$  Values

	Model Name / Architecture	Training algorithm	Learning algorithm	Hidden Layer 1	Output Layer	$R_{MSE}$
1	net534/3-10-3	Trainlm	learngdm	Tansig	purelin	0.2876
2	net697/3-10-3	Trainscg	learngdm	Purelin	purelin	0.3251
3	net1206/3-3-3	Trainlm	learngdm	Logsig	purelin	0.3144
4	net1327/3-7-3	Trainrp	learngdm	Purelin	purelin	0.3251
5	net1390/3-9-3	Trainscg	learngdm	Purelin	purelin	0.3221

It is worth mentioning that the models presented in this section are made up of one network but have three outputs (areal surface parameters). Also, the  $R_{MSE}$  was used for the performance criteria and was obtained from the predicted and the real response of the same input dataset (cutting parameters).

**Table 6.2:** Best Models (Conventional Model  $3 - X_1 - X_2 - 3$ ) Based on their  $R_{MSE}$  Values

	Model Name / architecture	Training algorithm	Learning algorithm	Hidden Layer 1	Hidden Layer 2	Output Layer	$R_{MSE}$
1	net19578/3-1-10-3	Trainlm	learngdm	Tansig	Tansig	Purelin	0.0778
2	net19764/3-3-10-3	Trainlm	Learngdm	tansig	logsig	purelin	0.0885
3	net20237/3-9-10-3	Trainlm	Learngdm	Tansig	Purelin	purelin	0.0783
4	net7887/3-1-9-3	Trainlm	learngd	Tansig	Tansig	Purelin	0.0838
5	net8040/3-3-7-3	Trainlm	Learngd	Logsig	Tansig	purelin	0.0779

From table 6.1, the model assigned the name, net534 has the minimum  $R_{MSE}$  followed by net1206. Hence, they will be considered in the next section for cross-validation. From

table 6.2, the model assigned the name, net19578 has the minimum  $R_{MSE}$  followed by net8040. Hence, they will also be considered in the next section for cross validation.

### 6.2.2 Enclosed multiple network model for surface topography prediction

In this section, three groups of networks were created each predicting one areal surface topography parameters; Sa, Sq and Sal. For each surface parameter, 1512 networks with structure  $3 - X_1 - 1$  were created in order to observe the performance of different combinations of the transfer functions and algorithm. Likewise, 27216 networks with structure  $3 - X_1 - X_2 - 1$  were created for the same purpose which considering models

**Table 6.3:** Best Networks for the prediction of only Sa

	Model Name / architecture	Training algorithm	Learning algorithm	Hidden Layer 1	Hidden Layer 2	Output Layer	$R_{MSE}$
<b>Network with 1 hidden Layer; <math>3 - X_1 - 1</math></b>							
1	net1209/3-6-1	Trainlm	Learngdm	tansig		purelin	0.5076
2	net1206/3-3-1	Trainlm	Learngdm	logsig		purelin	0.3416
3	net504/3-3-1	Trainlm	Learngd	logsig		purelin	0.4667
4	net522/3-7-1	Trainlm	Learngd	logsig		purelin	0.7308
5	net678/3-7-1	Trainscg	Learngd	tansig		purelin	0.5416
<b>Network with 2 hidden Layer; <math>3 - X_1 - X_2 - 1</math></b>							
1	net21684/3-3-10-1	Trainlm	Learngdm	tansig	tansig	purelin	0.2463
2	net13734/3-1-9-1	Trainbr	Learngdm	logsig	logsig	purelin	0.2473
3	net8823/3-1-6-1	Trainlm	Learngd	logsig	tansig	purelin	0.1891
4	net8847/3-1-7-1	Trainlm	Learngd	logsig	logsig	purelin	0.212
5	net22073/3-9-3-1	Trainlm	Learngdm	tansig	purelin	purelin	0.3693

with two hidden layers. The best network obtained from each of the three groups is selected to develop the enclosed multiple network model as shown in figure 6.2. The best networks were therefore chosen based on results from the direct validation as explained in section 6.1.3. The best five networks under each category (for the prediction of Sa, Sq and Sal) are tabulated in table 6.3, table 6.4 and table 6.5 respectively.

**Table 6.4:** Best Networks for the prediction of only Sq

	Model Name / architecture	Training algorithm	Learning algorithm	Hidden Layer 1	Hidden Layer 2	Output Layer	$R_{MSE}$
<b>Network with 1 hidden Layer; <math>3 - X_1 - 1</math></b>							
1	net1107 3-6-1	Trainlm	Learngdm	logsig		tansig	0.3455
2	net471 3-9-1	Trainlm	Learngd	tansig		purelin	0.3840
3	net633 3-9-1	Trainscg	Learngd	tansig		purelin	0.3766
4	net459 3-6-1	Trainlm	Learngd	logsig		tansig	0.3605
5	net624 3-7-1	Trainscg	Learngd	tansig		purelin	0.2619
<b>Network with 2 hidden Layer; <math>3 - X_1 - X_2 - 1</math></b>							
1	net19575/3-1-9-1	Trainlm	Learngdm	tansig	logsig	purelin	0.3730
2	net19758/3-3-10-1	Trainlm	Learngdm	logsig	tansig	purelin	0.5671
3	net8046/3-3-7-1	Trainlm	Learngd	tansig	logsig	purelin	0.3640
4	net8550/3-9-9-1	Trainlm	Learngd	logsig	logsig	purelin	0.3778
5	net20352/3-10-7-1	Trainlm	Learngdm	logsig	tansig	purelin	0.4266

**Table 6.5:** Best Networks for the prediction of only Sal

	Model Name / architecture	Training algorithm	Learning algorithm	Hidden Layer 1	Hidden Layer 2	Output Layer	$R_{MSE}$
<b>Network with 1 hidden Layer; <math>3 - X_1 - 1</math></b>							
1	net1183/3-10-1	Traigda	Learngdm	purelin		purelin	0.9385
2	net247/3-7-1	Traincgp	Learngd	purelin		logsig	0.9176
3	net1138/3-1-1	Traigda	Learngdm	purelin		tansig	0.9113
4	net993/3-6-1	Traincgp	Learngdm	tansig		purelin	0.9094
5	net1327/3-7-1	Trainoss	Learngdm	purelin		purelin	0.9082
<b>Network with 2 hidden Layer; <math>3 - X_1 - X_2 - 1</math></b>							
1	net29152/3-6-6-1	trainlm	Learngdm	tansig	tansig	purelin	0.0026
2	net9566/3-10-1-1	Traincgp	Learngd	logsig	logsig	purelin	0.0035
3	net29371/3-7-10-1	Trainbr	Learngdm	logsig	tansig	purelin	0.0062
4	net1359/3-6-6-1	Trainlm	Learngd	logsig	logsig	purelin	0.0172
5	net12498/3-7-9-1	Trainlm	Learngd	tansig	purelin	purelin	0.0453

### 6.3 Validation of chosen models

Table 6.6 shows the cutting parameters which were used as the input data for cross-validation purpose. A comparison between table 5.4 and 6.6 clearly shows the cutting parameters outline in table 6.6 is acceptable for cross-validation of the model. In

otherwords, they (the parameters outlined in table 6.6 ) cannot be found in the dataset used for training the models (dataset from table 5.4). This is important because it is quite easy to get good results with standard ANN validation using a percentage of the training data set. This validation which does not use any of the training datasets ensure we have a robust model suitable for making predictions on dataset not seen before.

**Table 6.6:** Cross-verification cutting parameter

	<b>Speed (RPM)</b>	<b>Feed Rate (mm/min)</b>	<b>DoC (mm)</b>
1	3500.00	800.00	0.30
2	4000.00	700.00	0.40
3	5500.00	1300.00	1.00
4	6200.00	1400.00	1.80
5	7000.00	1900.00	2.00
6	7000.00	2100.00	1.00
7	5000.00	650.00	1.30
8	6400.00	650.00	2.10
9	8200.00	1200.00	0.50
10	8300.00	1300.00	0.80

The models selected in the earlier section are validated in this section using correlation coefficient (R) as the performance criterion. Cross-validation was performed on the models since the parameters in table 6.6 was considered. The results are tabulated in table 6.7 and 6.8. Table 6.7 and 6.8 also presents direct validation using R as the performance criterion.

From table 6.7, the best conventional ANN model to predict all the three surface areal parameters is net19764 which had a network architecture of 3 – 3 – 10 – 3. This is because it has the highest mean value (0.90). The training algorithm used was the Levenberg-Marquardt backpropagation and the transfer functions were tansig, logsig and purelin for the 1st and 2nd hidden layers and the output layer respectively. The values obtained from averaging R of both direct and cross validation under each areal parameters where Sq (0.93), Sal (0.83) and Sa (0.92).

**Table 6.7:** Performances of selected conventional model for prediction of surface texture parameters

Model Name	Coefficient of correlation (R)						<b>Average</b>
	Direct Validation			Cross-Validation			
Sq	Sal	Sa	Sq	Sal	Sa		
<b>Models with 1 hidden Layer; 3 – X<sub>1</sub> – 1</b>							
Net534	0.94	0.95	0.93	0.27	0.92	0.06	0.68
Net1206	0.75	0.63	0.67	0.84	0.67	0.86	0.74
<b>Models with 2 hidden Layer; 3 – X<sub>1</sub> – X<sub>2</sub> – 1</b>							
Net19764	0.97	0.89	0.98	0.89	0.77	0.87	<b>0.90</b>
Net7887	0.80	0.93	0.83	0.73	0.93	0.79	0.84

**Table 6.8:** Performances of selected networks for Enclosed multiple network Model for prediction of surface texture parameters

Model Name	Coefficient of correlation		<b>Average</b>
	Direct Validation	Cross Validation	
<b>Conventional Model - Sa hidden Layer; 3 – X<sub>1</sub> – 1</b>			
Net1206	0.95	-0.27	0.34
Net522	0.94	0.52	0.73
<b>Conventional Model - Sa hidden Layer; 3 – X<sub>1</sub> – X<sub>2</sub> – 1</b>			
Net21684	0.98	0.93	<b>0.95</b>
Net8823	0.94	0.63	0.79
<b>Conventional Model - Sal hidden Layer; 3 – X<sub>1</sub> – 1</b>			
Net1183	0.91	0.96	0.94
Net247	0.87	0.96	0.92
<b>Conventional Model - Sal hidden Layer; 3 – X<sub>1</sub> – X<sub>2</sub> – 1</b>			
Net9566	0.98	0.99	<b>0.99</b>
Net29152	0.98	0.98	0.98
<b>Conventional Model - Sq hidden Layer; 3 – X<sub>1</sub> – 1</b>			
Net624	0.81	0.92	0.87
Net459	0.86	0.83	0.85
<b>Conventional Model - Sq hidden Layer; 3 – X<sub>1</sub> – X<sub>2</sub> – 1</b>			
Net20352	0.99	0.93	<b>0.96</b>
Net8550	0.99	0.87	0.93

An enclosed multiple network model was also built using the networks in table 6.8. Net20352 was used to predict Sq which had R of 0.96. Net9566 for Sal with R of 0.99 and net21684 with R of 0.95 for prediction of Sa. It should be mentioned that the average coefficient of correlation is used.. Net 20352 had the architecture of 3 – 10 – 7 – 1 whilst net 9566 and net 21684 had an architecture of 3 – 10 – 1 – 1 and 3 – 3 – 10 – 1

respectively.

It is worth mentioning that a high correction coefficient does not mean the two measurements agree. In other words, a model with a correction coefficient of 1 does not mean the model can predict with 100% accuracy. The reasons for further comparison between the two chosen models and the real responses using other methods are as follows:

1. The correlation coefficient measures the strength of a relation between two variables. Results obtained from correlation cannot give any insight about the agreement between the measured valued and the predicted value.
2. A change in scale of measurement does not affect correlation values. Hence, high correlation such as 1 does not mean the model can predict with 100% accuracy. However, the scalar error can easily be compensated if it exist.
3. Correlation depends on the range of the samples used. Two datasets over a wider sample range (for example 20 samples) will turn to have a totally different correlation compared to the same datasets but using only a smaller sample range (for examples 5 samples). Since there are no clear rules about the number of samples required for validation of a model when using correlation, the correlation coefficient will vary when different number of samples are used. Hence, correlation cannot be the single measure to fully determine the accuracy of a models.

## **6.4 Comparison of results for models with measured results**

In this section, the two selected models are compared again by generated graphs that

depict their percentage deviation from the original measurement. This approach of comparing two models is referred to as Bland-Altman analysis. The samples used were machined using the same cutting parameters tabulated in table 6.6. Hence, ten samples were used. In order to understand the error associated with using the predictive models as well as the relationship between the samples; the percentage deviation of the predicted values from the measured values is used.

Figures 6.3, 6.4 and 6.5 show the Bland Altman Plot which illuminate the percentage deviation of the predicted values for both conventional model and EMN model.

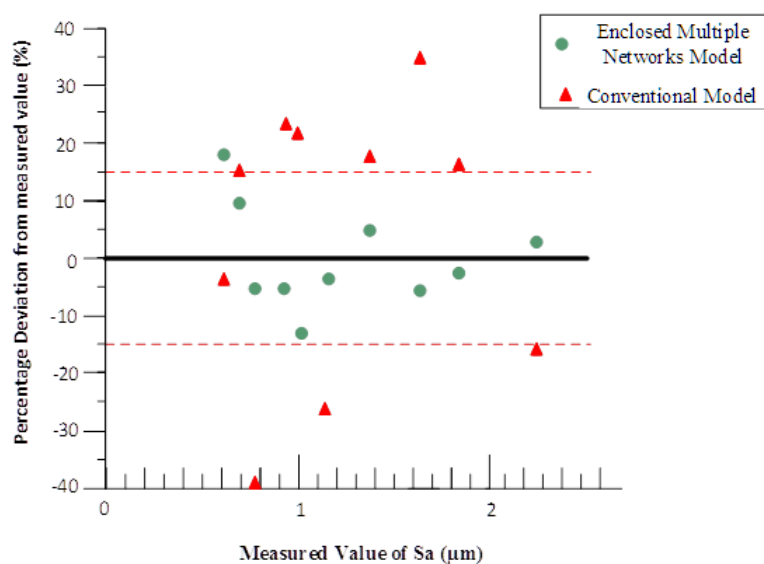


**Figure 6.3:** Bland-Altman plot for the chosen models against measured Sa value

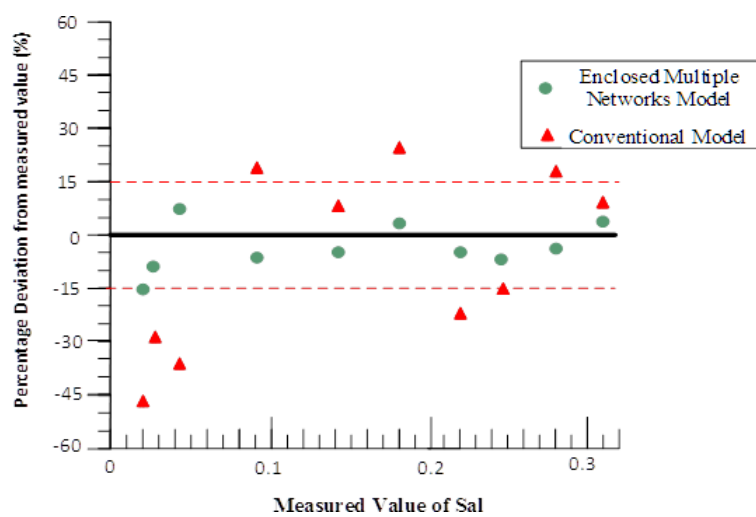


**Figure 6.4:** Bland-Altman plot for the chosen models against measured Sal value

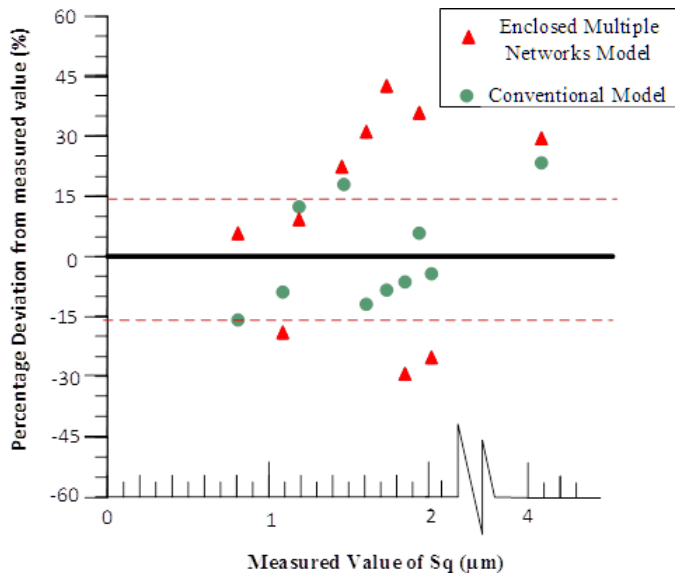


**Figure 6.5:** Bland-Altman plot for the chosen models against measured  $S_q$  value

It is worth mentioning that figure 6.5 has a contracted x-axis for clarity purposes. The following can be deduced from the above plots:

1. Majority of the predictions made by the EMN model falls within 85% interval confidence margin, unlike the prediction from the conventional model which is sporadic in nature. For example, a typical face-milled surface of  $S_a$  ( $1.5 \mu\text{m}$ ) which is commonly produced on a precision manufacturing shop floor; the conventional model predicted with a percentage deviation of 16 % which is equivalent to  $0.24 \mu\text{m}$  whilsts the EMN model predicted with a percentage deviation of 4 %, equivalent to  $0.06 \mu\text{m}$ . The deviations in the conventional model is too high and will not fall into any acceptance tolerance on a typical precision manufacturing shop floor.
2. Another keen observation that can be deduced from the plots is that the prediction of fine machined surfaces were very challenging for both models and accumulated high errors compared to rough machined surfaces. This trend was expected because the noise in the measurements increases when measuring fine surfaces with optical instruments. However, the results are still suitable for assisting with

predicting process parameters.

## 6.5 Summary of chapter

In this chapter, the possibility of using AI to assist in increasing the productiveness on a typical shop floor has been explored. This involved developing a novel neural network model which has the ability to predict areal surface parameters using cutting conditions as implementation of the developed model on a shop floor will increase right first-time machining.

Out of over 55,000 models, the EMN-ANN model comprising of net-9566 with structure  $3 - 10 - 1 - 1$ , net-21684 with structure  $3 - 3 - 10 - 1$  and net-20352 with structure  $3 - 10 - 7 - 1$  for prediction  $S_{\text{al}}$ ,  $S_{\text{a}}$  and  $S_{\text{q}}$  respectively emerged to be the best model for this application (prediction of surface areal parameters using machining conditions) based on the results.

The result of the average percentage deviation of the developed EMN-ANN model for  $S_{\text{q}}$ ,  $S_{\text{al}}$ , and  $S_{\text{a}}$  in figure 6.3, 6.4 and 6.5 were 9 %, 7 %, and 9 % respectively. This means that the EMN-ANN model could predict surface areal parameters with an accuracy of  $S_{\text{q}}$  (91 %),  $S_{\text{al}}$  (93 %) and  $S_{\text{a}}$  (91 %).

The error deviation can be further reduced by increasing the number of training trials. The ANN training performed in this thesis was only for testing (64 trials were used as stated in section 6.2) and more trials would be required to properly train an ANN for such purpose.

# Chapter 7

## Conclusion and future works

This chapter presents the summary of the thesis and the major contributions of the research preformed. Followed by future research that may be conducted in relation to this research area.

### 7.1 Thesis summary

One of the challenges faced on a typically manufacturing shop floor is the ability to ensure that the quality of manufactured parts is not compromised over quantity as the demand of manufacturing products arises. Post-process inspection of parts has been the keen approach to access the quality of products in most industries, however, its disadvantages, which includes, increasing the idle time in the manufacturing process and also difficulties associated with re-aligning products back on the workspaces if re-machining is required, outwards its benefits.

The main aim of this thesis was described in chapter 1 as,

*“to employ advanced techniques for increasing the quality of face-milled parts on a typical shop floor using areal surface roughness parameters as indicators”*

In order to achieve this aim, seven objectives were created. For an effective way of

summarizing this thesis, the objectives are outlined and under each objective, a summary of the work and the key results obtained from this thesis are presented.

### **1. To investigate into available surface metrology technique suitable for on-machine surface metrology for face milling.**

The intensive literature review presented in chapter 2 on surface metrology instruments resulted in the identification of the Keyence LV 7020k as a potentially suitable candidate for the task of rapid large area surface measurement. This instrument had never been used in such capacity before, but its specifications were appropriate for the machining tasks within the scope of this thesis. Several publications reviewed also supported this decision by proving the robustness of the instrument for on-machine measurement in other metrology branches such as form and dimension metrology. The technique which is employs by the instrument is laser triangulation. Which is also known to be very robust and less costly compared with other techniques such as WSI and FV.

The instrument can be used to measure an area of  $8 \text{ mm} \times "L" \text{ mm}$  with resolution  $10 \times "s" \mu\text{m}^2$ . where " $L$ " is the length which the instrument moves during the measurement and " $s$ " is its resolution which is mainly dependent on the sampling frequency and the speed of travel during the measurement. The variable axis of the instrument is due to its operating principle, providing it with a time axis in its measurements. Different sampling frequencies and speeds were considered in chapter 3. And it was revealed that setting the sampling frequency at 100 Hz and measuring at the speed of 18 mm/min provided stable and more reliable results appropriate for this research i.e. measurement of surface topography at the micro-scale level.

The main consideration for this decision was the level of noise induced into the measurement data by the measurement process. However, by measuring the surface of a part at the stated speed and frequency, the results obtained are subjected to reduced noise and a lateral resolution of  $10 \mu\text{m} \times 3 \mu\text{m}$  is also

achieved. It should be mentioned that the vertical resolution of the instrument used was  $0.1 \mu\text{m}$  which was also confirmed from the manufacturer as it was not clearly stated in the attached instrument specification (see **Appendix B**). Even though the desired evaluation area stated in chapter 1 is easy to achieve using the chosen instrument, achieving the targeted resolution in the lateral scale will require enhancement of the measuring sequence.

## **2. Develop a novel method to enhance the measurements captured by the selected instrument.**

Chapter 3 describes a novel methodology, which enhances the lateral resolution of the captured dataset and enables reduction in measurement noise. This technique was referred to as multidirectional scanning (MDS) technique in this thesis. MDS has the ability to increase the lateral resolution of the captured dataset to  $3 \mu\text{m} \times 3 \mu\text{m}$ . It also reduces the impact of environmental noise tremendously by exploiting the very high scan rate of the instrument. MDS technique operates based on averaging of two capture datasets of the same area, obtained in the same environment and measurement conditions. However, the scans are performed perpendicular to each other in relation to their profile data.

Due to the mismatch of lateral resolution in both captured datasets ( $10 \mu\text{m} \times 3 \mu\text{m}$  and  $3 \mu\text{m} \times 10 \mu\text{m}$ ), in other words, same but opposite lateral resolutions, the merging process ends up with a dataset with high and uniform lateral resolution ( $3 \mu\text{m} \times 3 \mu\text{m}$ ). This is achieved by enriching the profile axis resolution which is  $10 \mu\text{m}$ , using data obtained from the time axis of the secondary dataset which has a resolution of  $3 \mu\text{m}$ .

Also, since the scan is very fast i.e  $> 32 \mu\text{s}$  per profile, merging the two datasets also reduces noise the affected each scan.

Simulations were performed in chapter 3 to confirm the above claim. Which included the simulation of the impact of environmental noise on the dataset

obtained from the MDS technique. It was considered that the amplitude of environmental noise arbitrarily ranges from 0 to  $0.25 \mu\text{m}$  on a typical shop floor based on experimental results. And the surface finish of a typical milling process has  $R_z$  ranging between 0.5 to  $8 \mu\text{m}$ , which was confirm from a renowned precision manufacturing industry.

It was discovered that, smooth surfaces,  $R_z$  of  $0.5 \mu\text{m}$ , are very sensitive to the shop floor noise, and the MDS could not completely eliminate the noise but was able to reduce the impact of the noise by at least 50% when compared with datasets obtained from single measurement for the chosen instrument. Also, for very rough surface finish, say  $R_z$  of  $8 \mu\text{m}$ , it was possible to completely eliminate any induced errors which is introduced by the environmental noise within the stated range.

### **3. To validate the measurement technique for the on-machine surface measurement to establish traceability.**

For the purpose of traceability of the developed on-machine technique, chapter 4 presented investigations which utilised artefacts such as step height blocks, optical flat, and cross-grating artefacts to obtain the metrological characteristics (MCs) of the MDS technique. The following MCs were deduced: measurement noise, residual flatness, amplification coefficient, linearity deviation and perpendicularity deviation. The results exposed the possibility of MDS for micro-scale surface metrology. In that absence of an existing artefact suitable for MDS, a locally manufactured and calibrated artefact, using NPL primary instruments, was created.

A secondary traceability analysis was considered which involved the comparison (both visually and parametrically) of results captured by the MDS technique and a laboratory-based focus variation instrument. The results also demonstrated the potential of MDS to be used for on-machine detection of surface imperfections such as scratches.

After an in-depth review of predictive models for surface roughness in chapter 2, it was discovered that no attempt has been made to develop an AI model that predicts areal surface roughness parameters for face milling process. There has only been attempts to develop AI models for profile surface roughness parameters (parameters obtained from 1-dimensional scan of a line on the surface). In accordance with ISO 25178-3, it is not recommended to use the measured values from an equivalent areal parameter to compare with profile tolerance specifications. Generally, the measured values from equivalent profile and areal parameters are correlated, but are not directly comparable in an absolute sense, with areal parameters describing the quality of a manufactured surface more completely. Hence, the subsequent objectives are geared towards a secondary aim, which is “to predict areal surface roughness parameters on face milled surfaces from machine conditions using intelligent techniques”. The intelligent technique considered in this thesis was a feed-forward back propagation neural network. The following objective were followed to develop a very robust model suitable for the task at hand.

#### **4. Investigate the appropriate areal surface parameters suitable to represent face-milling process.**

The issue that drove an initial investigation of appropriate areal surface parameters suitable to be used to represent face-milling process was the availability of many areal surface roughness parameters (See **Appendix A**). In this thesis, the software used for computing the areal surface parameter is called SURFSTAND. The software package has the ability to compute for twenty-four areal surface roughness parameters. Using all the twenty-four areal surface roughness parameters as output of the predictive model will require a complex architectural structure which is out of the scope of this research. It was therefore needful to select a few areal surface roughness parameters that can be used to represent the surface topography of a milled surface.

In chapter 5, a statistical approach was considered which employed cross correlation coefficients and the significance of each parameter to determine the most appropriate parameters. The results were solely based on the ability of the parameter to distinguish between fine and rough face milled samples.

The areal surface parameters that came out as the best in order of performance were  $S_a$ ,  $S_q$ ,  $Spk$ ,  $V_{vc}$ ,  $V_{mc}$ , and  $Sal$ . The others had significance of less than 1, this demonstrated their inability to clearly differentiate between fine and rough face milled samples.  $S_a$ ,  $S_q$  and  $Sal$  were finally selected to be considered in this thesis as the suitable surface roughness parameters to represent the surface topography of a face milled sample.

$Spk$  was not considered because it is a height related parameter just as  $S_a$  and  $S_q$  and it is reviewed in chapter 2 that all height related parameters turned out to have a very strong relation with either  $S_a$  or  $S_q$ . Hence it was not expedient to consider all three height related parameters as output of the predictive model.

$Sal$  was also chosen over  $V_{vc}$  and  $V_{mc}$  because apart from the fact the  $Sal$  is a spacing parameter; it is also frequency dependant, making it a key parameter for easier indication of milling machine problems such as chatter.

## **5. To investigate the relationship between machining conditions and the selected areal surface parameters.**

During chapter 2, it was deduced from the reviewed literature that the machining parameters that have great influence on profile surface roughness are depth of cut, cutting speed and feed rate. In order to enlighten the reader about the influence these machining parameters have on areal surface roughness parameters in a typical milling process, an investigation (presented in Chapter 5) was conducted to understand the relationship pattern between the input and output of the model to be developed.

The aims of this investigation were first, to understand the degree to which the

cutting parameters affect the selected areal parameters and secondly to identify the most significant cutting parameters for each of the chosen areal surface parameters. This investigations were carried out with assistance from tools such as analysis of variance (ANOVA) and Taguchi's L'16 design of experiment.

From the results, it was discovered that for Sq and Sal of a machined surface, the feed rate is the most significant parameters. However, Sa value had no dominant cutting parameter the influence its value. Also, apart from the depth of cut, the other cutting parameters; cutting speed and feed rate has a linear relationship with the chosen surface roughness parameters.

Other preliminary investigations conducted that deemed relevant to the development of the model were as follows.

- Identification of the right area on a face milled surface to represent the entire surface topography.
- Effective ways to reduce tool degradation during machining process for training samples of the model.

The above investigations have been successfully conducted and presented in chapter 5 of this thesis.

## **6. To develop different neural network models with different training algorithms, learning algorithms, transfer functions for each layer and network architectures.**

The challenge when developing of neural network models involve taking decisions on the appropriate network architectural structure and the number of neurons in each layer in order to avoid generalisation of the model. In addition, identifying the appropriate transfer functions, training and learning algorithms to employ for a more reliable and robust model. There is no clear guidance on how to select these parameters, making it a difficult task. Majority of publication on this subject turn to use a trial and error approach to select these influential parameters for

developing a model.

The earlier sections of chapter 6, present a novel technique for making these decisions faster and easier. The technique employs a computing algorithm, which develops multiple models by considering all possible combinations of the influential parameters. After which a graph is plotted with information about the  $R_{MSE}$  obtained from direct validation procedure of all the developed models. The  $R_{MSE}$  value was used as the performance criterion for all the models. Based on the graph, the best influential parameters for developing the models for the application at hand can be easily selected.

Also, regarding the architectural structure of the models, two different classes of models were considered in this thesis. They were referred to as the conventional model and enclosed multiple network (EMN) model. The conventional models comprise of a single network with three input and three output. EMN models on the other hand were made up of three networks with each network having a unique output but all networks had the same three inputs. In total 28,728 models were developed under each category by using the developed computing algorithm.

Based on the performance criterion graph presented by the computing algorithm, the best five models under each category were selected for cross validation procedure.

## **7. To identify the best model for the prediction of areal surface roughness parameters of face milled parts using cutting conditions.**

In order to select the best model, a different performance criterion, correlation ( $R$ ) was utilised for cross validation using a new set of machined and measured dataset, which was not part of the training dataset of the models. This was done in order to avoid selecting an over fitted model. Over fitted model can predict only dataset that it has seen before (dataset used for training the model). The cross validation process was presented in chapter 6 as well.

Finally, two models; one conventional and the other EMN model were considered for further comparison using Bland-Altman analysis. It was concluded that the level of errors in the conventional model was larger and sporadic in nature whiles the predictions from the EMN model fell within 85% interval confidence margin when compared with the real measured results.

The result of the average percentage deviation of the developed EMN-ANN model for Sq, Sal, and Sa were 9%, 7%, and 9% respectively. This means that the EMN-ANN model could predict surface areal parameters with an accuracy of Sq (91%), Sal (93%) and Sa (91%).

## **7.2 Contribution and novelty**

This section summarises the novel solutions and contributions to knowledge.

1. Multidirectional Scanning (MDS) technique; this is a novel approach developed in this thesis which utilises a low-cost laser line scanner to obtain on-machine surface metrology dataset with high resolution and fast measurement suitable for micro-scale level metrology in advanced precision manufacturing industries.
2. Calibration of the MDS using artefacts; results obtained from the calibration of MDS expands the frontiers of knowledge. Other surface metrology techniques have been calibrated using the same procedures. The attempt to calibrate the MDS for surface metrology confirms the possibility to use laser triangulation for surface metrology and not only forms and dimensional metrology. It also increases the confidence of using laser triangulation on a typical manufacturing shop floor.
3. Developed an artefact (cross - grating artefact) suitable for obtaining the following metrological characteristics of MDS; the lateral amplification coefficient, linearity deviation and perpendicularity deviation.

4. Identified appropriate areal surface parameters for describing difference face-milled surfaces and established the relationship between face-milling parameters and areal surface parameters of face-milling parts.
5. Developed a new algorithm for the selection of optimised parameters for the development of a robust neural network model.
6. Developed a neural network model to predict areal surface parameters using cutting parameters. This is a novel model as there is AI model that can predict areal surface parameters for face milling process was not existing at the time of writing this thesis.

### **7.3 Future works**

#### **1. Recalibration of MDS after full publication of ISO standards 23168**

At the active period of this research, the ISO TC 213 committee was still debating the ISO standards for the procedure for calibration of surface metrology instruments as well as the rules of comparison between different instruments. The work presented in this thesis were based on the proposed ISO draft and other publications in the field. Henceforth, in future after the standards have been finalized and published, the MDS technique need to be calibrated as well as its results compared with other instruments. Also, since the uncertainty estimation presented in this thesis only covers the contributions associated with the instrument-surface interaction. To obtained the total combined uncertainty budget which considers the contribution of the software algorithm should be investigated as well.

#### **2. Automation of Delivery**

During this research, the measurement head of the blue line scanner was mounted on the spindle of the machine tool. This technique was improvised due to the absence of an adequate, robust and stable delivery system. Further investigation should be conducted on

the feasibility of integrating automated, possibly robotic, delivery of the measurement procedure in order to eliminate this challenge and increase efficiency.

In the current delivery technique, the sample needs to be removed from the worktable after machining to allow easy retrofitting of the measurement head of the sensor onto the spindle of the machine tool. The sample is placed back on the worktable of the machine tool after the measurement head has been setup before carrying out the MDS technique. By improving the delivery technique, issues such as tilting of the surface which is bound to occur if the sample is removed during the current delivery technique will be completely eliminated.

Due to the nature of the laser instrument employed, it may also be possible to repackage it to fit inside a machine tool change system so that it could be loaded automatically by the machine. Additional work on the robustness to high G-forces and coolant ingress would also be needed.

### **3. Modelling**

This thesis focused on the use of neural networks for the surface prediction modelling. Other AI models may be capable of providing higher accuracy. Hence, other AI models should be considered and proper comparison between the models should be considered in further works. Also, a theoretical model and increasing the scope of input parameters could be considered.

### **4. User-interface for models**

Further work would require developing a user-friendly interface for the developed model, which can be employed by a machinist to determine the right cutting parameters, required to achieve a unique or high quality face-milled surface for convenient right first time production or process improvement.

# References

- [1] K. Vacharanukul and S. Mekid, ‘In-process dimensional inspection sensors’, *Measurement*, vol. 38, no. 3, pp. 204–218, Oct. 2005.
- [2] F. Gao *et al.*, ‘In-situ defect detection systems for R2R flexible PV barrier films’, in *2015 International Conference on Optical Instruments and Technology: Optoelectronic Imaging and Processing Technology*, 2015, vol. 9622, p. 96220E.
- [3] X. Liu, ‘In situ metrology system for micro-milling machine’, *J. Manuf. Syst.*, vol. 31, no. 1, pp. 15–21, 2012.
- [4] D. J. Whitehouse, ‘Surface metrology. Measurement Science and Technology’, 1997.
- [5] X. Jiang, P. J. Scott, D. J. Whitehouse, and L. Blunt, ‘Paradigm shifts in surface metrology. Part I. Historical philosophy’, *Proc. R. Soc. A Math. Phys. Eng. Sci.*, vol. 463, no. 2085, pp. 2049–2070, 2007.
- [6] R. Leach, *Fundamental principles of engineering nanometrology*. Elsevier, 2014.
- [7] L. Blunt and X. Jiang, *Advanced techniques for assessment surface topography: development of a basis for 3D surface texture standards "surfstand"*. Elsevier, 2003.
- [8] R. Leach, *Optical measurement of surface topography*, vol. 14. Springer, 2011.
- [9] L. D. Todhunter, R. K. Leach, S. D. A. Lawes, and F. Blateyron, ‘Industrial survey of ISO surface texture parameters’, *CIRP J. Manuf. Sci. Technol.*, vol. 19, pp. 84–92, 2017.
- [10] Nanomend, ‘Enhanced in-line detection, cleaning and repair of nano-scale defects’. [Online]. Available: <http://nanomend.eu/>. [Accessed: 11-Apr-2018].
- [11] M. Elrawemi, L. Blunt, H. Muhamedsalih, F. Gao, and L. Fleming, ‘Implementation of in process surface metrology for R2R flexible PV barrier films’, *Int. J. Autom. Technol.*, vol. 9, no. 3, pp. 312–321, 2015.
- [12] T. J. Drozda, *Tool and manufacturing engineers handbook: machining*, vol. 1. Society of Manufacturing Engineers, 1983.
- [13] H. Kunzmann, T. Pfeifer, R. Schmitt, H. Schwenke, and A. Weckenmann, ‘Productive Metrology - Adding Value to Manufacture’, *CIRP Ann.*, vol. 54, no. 2, pp. 155–168, Jan. 2005.
- [14] E. Tomanik, M. El Mansori, R. Souza, and F. Profito, ‘Effect of waviness and roughness on cylinder liner friction’, *Tribol. Int.*, vol. 120, pp. 547–555, Apr. 2018.
- [15] E. Savio, L. De Chiffre, S. Carmignato, and J. Meinertz, ‘Economic benefits of metrology in manufacturing’, *CIRP Ann.*, vol. 65, no. 1, pp. 495–498, Jan. 2016.

- [16] B. A. Rodrigues Filho and R. F. Gonçalves, ‘Legal metrology, the economy and society: A systematic literature review’, *Measurement*, vol. 69, pp. 155–163, Jun. 2015.
- [17] British Standard Institute, ‘Geometrical Product Specification (GPS) -ISO 14638: Matrix Model’, 2015.
- [18] G. Bas, L. Stoev, and N. M. Durakbasa, ‘Assessment of the Production Quality in Machining by Integrating a System of High Precision Measurement’, *Procedia Eng.*, vol. 100, pp. 1616–1624, Jan. 2015.
- [19] A. M. Higginson and S. Handley, ‘The modelling and automatic commissioning of a high precision co-ordinate measuring machine’, *Mechatronics*, vol. 6, no. 3, pp. 261–281, Apr. 1996.
- [20] P. Yang *et al.*, ‘Development of high-precision micro-coordinate measuring machine: Multi-probe measurement system for measuring yaw and straightness motion error of XY linear stage’, *Precis. Eng.*, vol. 35, no. 3, pp. 424–430, Jul. 2011.
- [21] H. Schwenke, U. Neuschaefer-Rube, T. Pfeifer, and H. Kunzmann, ‘Optical Methods for Dimensional Metrology in Production Engineering’, *CIRP Ann.*, vol. 51, no. 2, pp. 685–699, Jan. 2002.
- [22] B. Muralikrishnan, S. Phillips, and D. Sawyer, ‘Laser trackers for large-scale dimensional metrology: A review’, *Precis. Eng.*, vol. 44, pp. 13–28, Apr. 2016.
- [23] H. Villarraga-Gómez, C. Lee, and S. T. Smith, ‘Dimensional metrology with X-ray CT: A comparison with CMM measurements on internal features and compliant structures’, *Precis. Eng.*, vol. 51, pp. 291–307, 2018.
- [24] J. P. Kruth, M. Bartscher, S. Carmignato, R. Schmitt, L. De Chiffre, and A. Weckenmann, ‘Computed tomography for dimensional metrology’, *CIRP Ann.*, vol. 60, no. 2, pp. 821–842, Jan. 2011.
- [25] H. N. Hansen, K. Carneiro, H. Haitjema, and L. De Chiffre, ‘Dimensional Micro and Nano Metrology’, *CIRP Ann.*, vol. 55, no. 2, pp. 721–743, Jan. 2006.
- [26] R. H. Schmitt *et al.*, ‘Advances in Large-Scale Metrology – Review and future trends’, *CIRP Ann.*, vol. 65, no. 2, pp. 643–665, Jan. 2016.
- [27] H. Sawano, T. Gokan, H. Yoshioka, and H. Shinno, ‘A newly developed STM-based coordinate measuring machine’, *Precis. Eng.*, vol. 36, no. 4, pp. 538–545, Oct. 2012.
- [28] J. Kwon, Y.-S. Kim, K. Yoon, S.-M. Lee, and S. Park, ‘Advanced nanoscale metrology of pole-tip recession with AFM’, *Ultramicroscopy*, vol. 105, no. 1–4, pp. 51–56, Nov. 2005.
- [29] B. Gapinski, M. Wieczorowski, L. Marciak-Podsadna, B. Dybala, and G. Ziolkowski, ‘Comparison of Different Method of Measurement Geometry Using CMM, Optical Scanner and Computed Tomography 3D’, *Procedia Eng.*, vol. 69, pp. 255–262, Jan. 2014.
- [30] L. Li, C. Li, Y. Tang, and Y. Du, ‘An integrated approach of reverse engineering aided remanufacturing process for worn components’, *Robot. Comput. Integrat. Manuf.*, vol. 48, pp. 39–50, Dec. 2017.

- [31] B. Bhushan, *Modern Tribology Handbook, Two Volume Set*. Taylor & Francis, 2000.
- [32] R. Adhikari, ‘Sensitivity and noise analysis of 4 km laser interferometric gravitational wave antennae’. Massachusetts Institute of Technology, 2004.
- [33] P. Hariharan, *Optical Interferometry*, 2nd ed. Elsevier, 2003.
- [34] K. Creath, ‘Phase-measurement of interferometry techniques for nondestructive testing’, in *Proc.SPIE*, 1991, vol. 1554.
- [35] J. A. Izatt and M. A. Choma, ‘Theory of Optical Coherence Tomography BT - Optical Coherence Tomography: Technology and Applications’, W. Drexler and J. G. Fujimoto, Eds. Berlin, Heidelberg: Springer Berlin Heidelberg, 2008, pp. 47–72.
- [36] M. N. Morris, ‘Dynamic Interferometry for On-Machine Metrology’, in *Frontiers in Optics 2010/Laser Science XXVI*, 2010, p. STuA3.
- [37] 4dtechnology, ‘Measure surface roughness on smooth and supersmooth surfaces’. [Online]. Available: <https://www.4dtechnology.com/products/optical-profilers/nanocam-sq/>. [Accessed: 22-Apr-2019].
- [38] J. Chen, Y. Ishii, and K. Murata, ‘Heterodyne interferometry with a frequency-modulated laser diode’, *Appl. Opt.*, vol. 27, no. 1, pp. 124–128, 1988.
- [39] S. Topcu, L. Chassagne, D. Haddad, Y. Alayli, and P. Juncar, ‘Heterodyne interferometric technique for displacement control at the nanometric scale’, *Rev. Sci. Instrum.*, vol. 74, no. 11, pp. 4876–4880, Nov. 2003.
- [40] J. C. Wyant, ‘White light interferometry In Holography: A Tribute to Yuri Denisyuk and Emmett Leith’, in *Proc.SPIE*, 2002, vol. 4737, pp. 98–108.
- [41] W. Kaplonek and C. Lukianowicz, ‘Coherence correlation interferometry in surface topography measurements’, in *Recent Interferometry Applications in Topography and Astronomy*, IntechOpen, 2012.
- [42] ‘CCI Talysurf 6000–The world’s highest resolution automated optical 3D profiler’, *Brochure, Taylor Hobson*, 2005.
- [43] D. Lin, X. Jiang, F. Xie, W. Zhang, L. Zhang, and I. Bennion, ‘High stability multiplexed fibre interferometer and its application on absolute displacement measurement and on-line surface metrology’, *Opt. Express*, vol. 12, no. 23, pp. 5729–5734, 2004.
- [44] G. Berger and J. Petter, ‘Novel technology for high precision, fast non-contact asphere metrology’, *tm–Technisches Mess.*, vol. 81, no. 1, pp. 2–7, 2014.
- [45] G. P. Barwood, P. Gill, and W. R. C. Rowley, ‘Laser diodes for length determination using swept-frequency interferometry’, *Meas. Sci. Technol.*, vol. 4, no. 9, p. 988, 1993.
- [46] G. P. Barwood, P. Gill, and W. R. C. Rowley, ‘High-accuracy length metrology using multiple-stage swept-frequency interferometry with laser diodes’, *Meas. Sci. Technol.*, vol. 9, no. 7, p. 1036, 1998.

- [47] Y. Ishii, ‘Wavelength-tunable laser-diode interferometer’, *Opt. Rev.*, vol. 6, no. 4, pp. 273–283, 1999.
- [48] R. Ohba, I. Uehira, and S. Kakuma, ‘Interferometric determination of a static optical path difference using a frequency swept laser diode’, *Meas. Sci. Technol.*, vol. 1, no. 6, p. 500, 1990.
- [49] J. Thiel, T. Pfeifer, and M. Hartmann, ‘Interferometric measurement of absolute distances of up to 40 m’, *Measurement*, vol. 16, no. 1, pp. 1–6, 1995.
- [50] I. Yamaguchi, A. Yamamoto, and S. Kuwamura, ‘Speckle decorrelation in surface profilometry by wavelength scanning interferometry’, *Appl. Opt.*, vol. 37, no. 28, pp. 6721–6728, 1998.
- [51] D. Xiaoli and S. Katuo, ‘High-accuracy absolute distance measurement by means of wavelength scanning heterodyne interferometry’, *Meas. Sci. Technol.*, vol. 9, no. 7, p. 1031, 1998.
- [52] J. Kato and I. Yamaguchi, ‘Phase-shifting fringe analysis for laser diode wavelength-scanning interferometer’, *Opt. Rev.*, vol. 7, no. 2, pp. 158–163, 2000.
- [53] A. P. Cabral and J. M. Rebordão, ‘Accuracy of frequency-sweeping interferometry for absolute distance metrology’, *Opt. Eng.*, vol. 46, no. 7, p. 73602, 2007.
- [54] S. Kuwamura and I. Yamaguchi, ‘Wavelength scanning profilometry for real-time surface shape measurement’, *Appl. Opt.*, vol. 36, no. 19, pp. 4473–4482, 1997.
- [55] M. Elrawemi, H. Muhamedsalih, L. Blunt, L. Fleming, H. Martin, and X. Jiang, ‘Comparative study between online and offline defect assessment methods for roll to roll flexible PV modules’, 2014.
- [56] X. Jiang, K. Wang, F. Gao, and H. Muhamedsalih, ‘Fast surface measurement using wavelength scanning interferometry with compensation of environmental noise’, *Appl. Opt.*, vol. 49, no. 15, pp. 2903–2909, 2010.
- [57] British Standard Institute, ‘Geometrical Product Specification (GPS) - ISO 25178-606: Surface Texture: Areal Nominal Characteristics of Non-Contact (Focus Variation) Instruments’, 2015.
- [58] R. Danzl, F. Helmli, and S. Scherer, ‘Focus Variation--a Robust Technology for High Resolution Optical 3D Surface Metrology.’, *Stroj. Vestnik/Journal Mech. Eng.*, vol. 57, no. 3, 2011.
- [59] W. O. Saxton, ‘What is the focus variation method? Is it new? Is it direct?’, *Ultramicroscopy*, vol. 55, no. 2, pp. 171–181, 1994.
- [60] R. Danzl, F. Helmli, and S. Scherer, ‘Focus variation—a new technology for high resolution optical 3D surface metrology’, in *The 10th international conference of the slovenian society for non-destructive testing*, 2009, pp. 484–491.
- [61] Alicona Imaging GmbH, ‘Alicona IF-Sensor R25’, *Dataset*, 2015.
- [62] Alicona Imaging GmbH, ‘IF - Portable’, *Dataset*, 2015.
- [63] British Standard Institute, ‘Geometrical Product Specifications (GPS) - ISO 25178-605: Surface Texture: Areal Nominal Characteristics of Non-contact (Point Autofocus Probe) Instruments’,

2014.

- [64] Mitaka Kohki Co. Ltd, ‘Laser Probe Unit’, *Dataset*, 2017.
- [65] M. P. Groover, *Fundamentals of modern manufacturing: materials processes, and systems*. John Wiley & Sons, 2007.
- [66] X. Zhao, M. Tootkaboni, and B. W. Schafer, ‘Development of a laser-based geometric imperfection measurement platform with application to cold-formed steel construction’, *Exp. Mech.*, vol. 55, no. 9, pp. 1779–1790, 2015.
- [67] M. G. Nygaard, ‘Triangulation-based, 3-d method and system for imaging the outer peripheral surface of a part’. Google Patents, 27-Nov-2014.
- [68] G. Guidi, M. Russo, G. Magrassi, and M. Bordegioni, ‘Performance evaluation of triangulation based range sensors’, *Sensors*, vol. 10, no. 8, pp. 7192–7215, 2010.
- [69] H. Mieno, ‘Method for predicting frictional resistance of rough surface, and apparatus for estimating surface performance’. Google Patents, 18-Jan-2018.
- [70] Y. Kozaki and K. Suzuki, ‘A facial wearable robot for supporting eye opening and closure movement’, in *2017 IEEE/RSJ International Conference on Intelligent Robots and Systems (IROS)*, 2017, pp. 1812–1817.
- [71] T. Mueller, A. Poesch, and E. Reithmeier, ‘Topography Measurement for Monitoring Manufacturing Processes in Harsh Conditions’, *Eng.* 8 (2016), Nr. 5, vol. 8, no. 5, pp. 292–300, 2016.
- [72] P. G. Benardos and G.-C. Vosniakos, ‘Predicting surface roughness in machining: a review’, *Int. J. Mach. tools Manuf.*, vol. 43, no. 8, pp. 833–844, 2003.
- [73] C. L. He, W. J. Zong, and J. J. Zhang, ‘Influencing factors and theoretical modeling methods of surface roughness in turning process: state-of-the-art’, *Int. J. Mach. Tools Manuf.*, vol. 129, pp. 15–26, 2018.
- [74] C. L. He, W. J. Zong, Z. M. Cao, and T. Sun, ‘Theoretical and empirical coupled modeling on the surface roughness in diamond turning’, *Mater. Des.*, vol. 82, pp. 216–222, 2015.
- [75] C. Felhő, B. Karpuschewski, and J. Kundrák, ‘Surface roughness modelling in face milling’, *Procedia CIRP*, vol. 31, pp. 136–141, 2015.
- [76] P. J. Arrazola, T. Öznel, D. Umbrello, M. Davies, and I. S. Jawahir, ‘Recent advances in modelling of metal machining processes’, *CIRP Ann.*, vol. 62, no. 2, pp. 695–718, Jan. 2013.
- [77] J. Peters *et al.*, ‘Contribution of CIRP to the Development of Metrology and Surface Quality Evaluation during the last fifty years’, *CIRP Ann.*, vol. 50, no. 2, pp. 471–488, Jan. 2001.
- [78] P. Muñoz-Escalona and P. G. Maropoulos, ‘A geometrical model for surface roughness prediction when face milling Al 7075-T7351 with square insert tools’, *J. Manuf. Syst.*, vol. 36, pp. 216–223, Jul. 2015.

- [79] D. K. Baek, T. J. Ko, and H. S. Kim, ‘Optimization of feedrate in a face milling operation using a surface roughness model’, *Int. J. Mach. Tools Manuf.*, vol. 41, no. 3, pp. 451–462, Feb. 2001.
- [80] M.-Y. Wang and H.-Y. Chang, ‘Experimental study of surface roughness in slot end milling AL2014-T6’, *Int. J. Mach. Tools Manuf.*, vol. 44, no. 1, pp. 51–57, Jan. 2004.
- [81] P. Franco, M. Estrems, and F. Faura, ‘Influence of radial and axial runouts on surface roughness in face milling with round insert cutting tools’, *Int. J. Mach. Tools Manuf.*, vol. 44, no. 15, pp. 1555–1565, Dec. 2004.
- [82] M. Tomov, M. Kuzinovski, and P. Cichosz, ‘Modeling and prediction of surface roughness profile in longitudinal turning’, *J. Manuf. Process.*, vol. 24, pp. 231–255, Oct. 2016.
- [83] S. M. O. Tavares, ‘Analysis of surface roughness and models of mechanical contacts’. Ph. D. dissertation (Università di Pisa, 2005), 2005.
- [84] J. A. Greenwood and J. B. P. Williamson, ‘Contact of nominally flat surfaces’, *Proc. R. Soc. London. Ser. A. Math. Phys. Sci.*, vol. 295, no. 1442, pp. 300–319, 1966.
- [85] W. R. Chang, I. Etsion, and D. B. Bogy, ‘An elastic-plastic model for the contact of rough surfaces’, *J. Tribol.*, vol. 109, no. 2, pp. 257–263, 1987.
- [86] Y. Zhao, D. M. Maietta, and L. Chang, ‘An asperity microcontact model incorporating the transition from elastic deformation to fully plastic flow’, *J. Tribol.*, vol. 122, no. 1, pp. 86–93, 2000.
- [87] C. Felho and J. Kundrak, ‘CAD-based modelling of surface roughness in face milling’, *Int. J. Mech. Aerospace, Ind. Mechatronics Eng.*, vol. 8, no. 5, pp. 814–818, 2014.
- [88] S. Manjeet and D. Kumar, ‘A Review on Artificial Intelligence Techniques Applied in End Milling Process’, *Int. J. Res. Appl. Sci. Eng. Technol. IJRASET*, vol. 2, no. III, 2014.
- [89] A. Yang, Y. Han, Y. Pan, H. Xing, and J. Li, ‘Optimum surface roughness prediction for titanium alloy by adopting response surface methodology’, *Results Phys.*, vol. 7, pp. 1046–1050, Jan. 2017.
- [90] A. J. Vallejo, R. Morales-Menendez, and R. Ramírez-Mendoza, ‘Surface Roughness Modelling in Machining Processes’, *IFAC Proc. Vol.*, vol. 42, no. 4, pp. 325–330, Jan. 2009.
- [91] M. Vishwakarma, V. Parashar, and V. Khare, ‘Optimization and regression analysis of surface roughness for electric discharge machining of EN-19 alloy steel using tungsten copper electrode’, *Int. J. Eng. Res. Appl.*, vol. 2, no. 6, pp. 785–792, 2012.
- [92] P. V. S. Suresh, P. Venkateswara Rao, and S. G. Deshmukh, ‘A genetic algorithmic approach for optimization of surface roughness prediction model’, *Int. J. Mach. Tools Manuf.*, vol. 42, no. 6, pp. 675–680, May 2002.
- [93] A. M. Zain, H. Haron, and S. Sharif, ‘Application of GA to optimize cutting conditions for minimizing surface roughness in end milling machining process’, *Expert Syst. Appl.*, vol. 37, no. 6, pp. 4650–4659, 2010.
- [94] A. M. Zain, H. Haron, and S. Sharif, ‘An overview of GA technique for surface roughness

optimization in milling process', in *2008 International Symposium on Information Technology*, 2008, vol. 4, pp. 1–6.

- [95] Y. M. Ali and L. C. Zhang, 'Surface roughness prediction of ground components using a fuzzy logic approach', *J. Mater. Process. Technol.*, vol. 89, pp. 561–568, 1999.
- [96] V. S. U. Konada, *A novel approach to predict surface roughness in machining operations using fuzzy set theory*. The University of Texas at El Paso, 2007.
- [97] D. Karayel, 'Prediction and control of surface roughness in CNC lathe using artificial neural network', *J. Mater. Process. Technol.*, vol. 209, no. 7, pp. 3125–3137, 2009.
- [98] M. S. J. Hossain and N. Ahmad, 'Artificial intelligence based surface roughness prediction modeling for three dimensional end milling', *Int. J. Adv. Sci. Technol.*, vol. 45, pp. 1–18, 2012.
- [99] B. P. Huang, J. C. Chen, and Y. Li, 'Artificial-neural-networks-based surface roughness Pokayoke system for end-milling operations', *Neurocomputing*, vol. 71, no. 4–6, pp. 544–549, 2008.
- [100] A. M. Zain, H. Haron, and S. Sharif, 'Prediction of surface roughness in the end milling machining using Artificial Neural Network', *Expert Syst. Appl.*, vol. 37, no. 2, pp. 1755–1768, 2010.
- [101] G. D'Mello, P. S. Pai, and R. P. Shetty, 'Surface roughness modeling in high speed turning of Ti-6Al-4V–Artificial Neural Network approach', *Mater. Today Proc.*, vol. 4, no. 8, pp. 7654–7664, 2017.
- [102] M. Mia and N. R. Dhar, 'Prediction of surface roughness in hard turning under high pressure coolant using Artificial Neural Network', *Measurement*, vol. 92, pp. 464–474, 2016.
- [103] M. Vrabel', I. Mankova, J. Beno, and J. Tuharský, 'Surface roughness prediction using artificial neural networks when drilling Udiment 720', *Procedia Eng.*, vol. 48, pp. 693–700, 2012.
- [104] M. Sivatte-Adroer, X. Llanas-Parra, I. Buj-Corral, and J. Vivancos-Calvet, 'Indirect model for roughness in rough honing processes based on artificial neural networks', *Precis. Eng.*, vol. 43, pp. 505–513, 2016.
- [105] P. G. Benardos and G. C. Vosniakos, 'Prediction of surface roughness in CNC face milling using neural networks and Taguchi's design of experiments', *Robot. Comput. Integrat. Manuf.*, vol. 18, no. 5–6, pp. 343–354, 2002.
- [106] U. M. R. Paturi, H. Devarasetti, and S. K. R. Narala, 'Application Of Regression And Artificial Neural Network Analysis In Modelling Of Surface Roughness In Hard Turning Of AISI 52100 Steel', *Mater. Today Proc.*, vol. 5, no. 2, pp. 4766–4777, 2018.
- [107] I. Asiltürk and M. Çunkaş, 'Modeling and prediction of surface roughness in turning operations using artificial neural network and multiple regression method', *Expert Syst. Appl.*, vol. 38, no. 5, pp. 5826–5832, 2011.
- [108] K. A. Patel and P. K. Brahmbhatt, 'A comparative study of the RSM and ANN models for predicting surface roughness in roller burnishing', *Procedia Technol.*, vol. 23, pp. 391–397, 2016.
- [109] N. S. K. Varma, I. Varma, S. Rajesh, K. S. R. Raju, and V. V. M. K. Raju, 'Prediction of surface

- roughness and MRR in grinding process on Inconel 800 alloy using neural networks and ANFIS', *Mater. Today Proc.*, vol. 5, no. 2, pp. 5445–5451, 2018.
- [110] U. Zuperl and F. Cus, 'Surface roughness fuzzy inference system within the control simulation of end milling', *Precis. Eng.*, vol. 43, pp. 530–543, 2016.
- [111] F. Dweiri, M. Al-Jarrah, and H. Al-Wedyan, 'Fuzzy surface roughness modeling of CNC down milling of Alumic-79', *J. Mater. Process. Technol.*, vol. 133, no. 3, pp. 266–275, 2003.
- [112] S.-Y. Ho, K.-C. Lee, S.-S. Chen, and S.-J. Ho, 'Accurate modeling and prediction of surface roughness by computer vision in turning operations using an adaptive neuro-fuzzy inference system', *Int. J. Mach. Tools Manuf.*, vol. 42, no. 13, pp. 1441–1446, 2002.
- [113] Y. Jiao, S. Lei, Z. J. Pei, and E. S. Lee, 'Fuzzy adaptive networks in machining process modeling: surface roughness prediction for turning operations', *Int. J. Mach. Tools Manuf.*, vol. 44, no. 15, pp. 1643–1651, 2004.
- [114] G. Kant and K. S. Sangwan, 'Predictive modelling and optimization of machining parameters to minimize surface roughness using artificial neural network coupled with genetic algorithm', *Procedia Cirp*, vol. 31, pp. 453–458, 2015.
- [115] G. Rangajanardhaa and S. Rao, 'Development of hybrid model and optimization of surface roughness in electric discharge machining using artificial neural networks and genetic algorithm', *J. Mater. Process. Technol.*, vol. 209, no. 3, pp. 1512–1520, 2009.
- [116] K. S. Sangwan and G. Kant, 'Optimization of machining parameters for improving energy efficiency using integrated response surface methodology and genetic algorithm approach', *Procedia CIRP*, vol. 61, pp. 517–522, 2017.
- [117] O. Lior, Horesh Ted Van Kessel; Conn, Andrew; Kormaksson, Matthias; Saliu, 'Should you derive? Or let the data drive? Towards a first-principles datadriven symbiosis', *Optim. Uncertain. Quantif. Energy Ind. Appl.*, 2016.
- [118] R. K. Leach, C. L. Giusca, H. Haitjema, C. Evans, and X. Jiang, 'Calibration and verification of areal surface texture measuring instruments', *CIRP Ann.*, vol. 64, no. 2, pp. 797–813, 2015.
- [119] Keyence Cooperation Ltd, 'User's Manual, Ultra-High Speed In-line Profilometer', Osaka, Japan, 2018.
- [120] J. Williamson, 'Dispersed reference interferometry for on-machine metrology', Apr. 2016.
- [121] T. J. Bruno and P. D. N. Svoronos, *CRC handbook of fundamental spectroscopic correlation charts*. CRC Press, 2005.
- [122] C. Jones, 'Red vs Blue Lasers: A Comparison of Triangulation Sensors', 2016. [Online]. Available: <https://www.automation.com/automation-news/article/red-vs-blue-lasers-a-comparison-of-triangulation-sensors>. [Accessed: 17-Mar-2018].
- [123] K. D. B. Akowua, S. Fletcher, A. P. Longstaff, and N. S. Mian, 'Areal surface measurement using multidirectional laser line scanning', euspen, 2017.

- [124] British Standard Institute, ‘Geometrical Product Specification (GPS) - ISO 4288: Surface Texture: Profile Method – Rules and Procedures for The Assessment of Surface Texture’, 1998.
- [125] British Standard Institute, ‘Geometrical Product Specification (GPS) - Surface Texture: Areal Part 601: Nominal characteristics of contact (stylus) instruments’, 2010.
- [126] L. Blunt and X. Jiang, ‘Numerical Parameters for Characterisation of Topography’, in *Advanced Techniques for Assessment Surface Topography Development of a Basis for 3D Surface Texture Standards “SURFSTAND”*, L. Blunt and X. B. T.-A. T. for A. S. T. Jiang, Eds. Oxford: Kogan Page Science, 2003, pp. 17–41.
- [127] S. J. Zhang, S. To, G. Q. Zhang, and Z. W. Zhu, ‘A review of machine-tool vibration and its influence upon surface generation in ultra-precision machining’, *Int. J. Mach. Tools Manuf.*, vol. 91, pp. 34–42, 2015.
- [128] P. M. Harris, I. M. Smith, C. Wang, C. Giusca, and R. K. Leach, ‘Software measurement standards for areal surface texture parameters: part 2—comparison of software’, *Meas. Sci. Technol.*, vol. 23, no. 10, p. 105009, 2012.
- [129] T. Li, *Software Measurement Standards in Surface Metrology: Basics, Concepts, Methods*. LAP LAMBERT Academic Publishing, 2012.
- [130] I. E. C. BiPM, Ila. IFcc, O. ISO, and O. IUPAP, ‘The international vocabulary of metrology—basic and general concepts and associated terms (VIM)’, *JcGM*, vol. 200, p. 2012, 2012.
- [131] British Standard Institute, ‘Geometrical Product Specifications (GPS) - ISO 25178-600: Surface Texture Areal Classification of Methods for Measuring Surface Texture’, 2010.
- [132] C. L. Giusca, R. K. Leach, F. Helary, T. Gutauskas, and L. Nimishakavi, ‘Calibration of the scales of areal surface topography-measuring instruments: part 1. Measurement noise and residual flatness’, *Meas. Sci. Technol.*, vol. 23, no. 3, p. 35008, 2012.
- [133] C. L. Giusca, R. K. Leach, and F. Helery, ‘Calibration of the scales of areal surface topography measuring instruments: part 2. Amplification, linearity and squareness’, *Meas. Sci. Technol.*, vol. 23, no. 6, p. 65005, 2012.
- [134] C. L. Giusca and R. K. Leach, ‘Calibration of the scales of areal surface topography measuring instruments: part 3. Resolution’, *Meas. Sci. Technol.*, vol. 24, no. 10, p. 105010, 2013.
- [135] A. Alburayt, W. P. Syam, and R. Leach, ‘Lateral scale calibration for focus variation microscopy’, *Meas. Sci. Technol.*, vol. 29, no. 6, p. 65012, 2018.
- [136] NPL, ‘Optical Dimensional Standard’. [Online]. Available: <http://www.npl.co.uk/measurement-services/dimensional/optical-dimensional-standard>. [Accessed: 11-Jun-2018].
- [137] R. K. Leach, ‘Is one step height enough?’, in *Proceedings of ASPE*, 2015.
- [138] I. E. C. BiPM and I. S. O. IFCC, ‘OIML, Guide to the Expression of Uncertainty in Measurement, Geneva, Switzerland: Int’, *Org. Stand.*, 1995.
- [139] D. J. Whitehouse, *Handbook of surface and nanometrology*. CRC press, 2010.

- [140] H. T. Nguyen, H. Wang, and S. J. Hu, ‘Modeling cutter tilt and cutter-spindle stiffness for machine condition monitoring in face milling using high-definition surface metrology’, *Int. J. Adv. Manuf. Technol.*, vol. 70, no. 5–8, pp. 1323–1335, 2014.
- [141] W. Zeng, X. Jiang, and L. Blunt, ‘Surface characterisation-based tool wear monitoring in peripheral milling’, *Int. J. Adv. Manuf. Technol.*, vol. 40, no. 3–4, pp. 226–233, 2009.
- [142] A. Polishetty, M. Alabdullah, and G. Littlefair, ‘Tool Wear Analysis due to Machining In Super Austenitic Stainless Steel’, in *MATEC Web of Conferences*, 2017, vol. 95, p. 5006.
- [143] M. S. H. Bhuiyan, I. A. Choudhury, and M. Dahari, ‘Monitoring the tool wear, surface roughness and chip formation occurrences using multiple sensors in turning’, *J. Manuf. Syst.*, vol. 33, no. 4, pp. 476–487, 2014.
- [144] P. Palanisamy, I. Rajendran, and S. Shanmugasundaram, ‘Prediction of tool wear using regression and ANN models in end-milling operation’, *Int. J. Adv. Manuf. Technol.*, vol. 37, no. 1–2, pp. 29–41, 2008.
- [145] British Standard Institute, ‘Geometrical Product Specification (GPS) - ISO 8785: Surface Imperfections. Terms, Definitions and Parameters’, 1999.
- [146] R. Leach, C. Giusca, and K. Naoi, ‘Traceability for areal surface texture measurement’, in *Key Engineering Materials*, 2010, vol. 437, pp. 121–125.
- [147] W. Grzesik, ‘Prediction of the functional performance of machined components based on surface topography: State of the art’, *J. Mater. Eng. Perform.*, vol. 25, no. 10, pp. 4460–4468, 2016.
- [148] A. Waterworth, ‘Quantitative characterisation of surface finishes on stainless steel sheet using 3D surface topography analysis’. University of Huddersfield, 2006.
- [149] F. Helmli, K. Pötsch, and C. Repitsch, ‘Choosing the Appropriate Parameter’, in *Characterisation of Areal Surface Texture*, Springer, 2013, pp. 155–177.
- [150] J. Das and B. Linke, ‘Evaluation and systematic selection of significant multi-scale surface roughness parameters (SRPs) as process monitoring index’, *J. Mater. Process. Technol.*, vol. 244, pp. 157–165, 2017.
- [151] F. Blateyron, ‘The areal field parameters’, in *Characterisation of areal surface texture*, Springer, 2013, pp. 15–43.
- [152] E. Rezvani, H. Ghayour, and M. Kasiri, ‘Effect of cutting speed parameters on the surface roughness of Al5083 due to recrystallization’, *Mech. Sci.*, vol. 7, no. 1, pp. 85–91, 2016.
- [153] I. Asiltürk, S. Neşeli, and M. A. Ince, ‘Optimisation of parameters affecting surface roughness of Co28Cr6Mo medical material during CNC lathe machining by using the Taguchi and RSM methods’, *Measurement*, vol. 78, pp. 120–128, 2016.
- [154] K. C. T. Catalogue, ‘KORLOY Inc., p’, F08, 2010.
- [155] T. Kıvak, ‘Optimization of surface roughness and flank wear using the Taguchi method in milling of Hadfield steel with PVD and CVD coated inserts’, *Measurement*, vol. 50, pp. 19–28, 2014.

- [156] J. Heaton, ‘Ian Goodfellow, Yoshua Bengio, and Aaron Courville: Deep learning’, *Genet. Program. Evolvable Mach.*, vol. 19, no. 1–2, pp. 305–307, 2017.
- [157] B. Anuja Beatrice, E. Kirubakaran, P. Ranjit Jeba Thangaiah, and K. Leo Dev Wins, ‘Surface roughness prediction using artificial neural network in hard turning of AISI H13 steel with minimal cutting fluid application’, *Procedia Eng.*, vol. 97, pp. 205–211, 2014.
- [158] D. Hunter, H. Yu, I. I. I. M. S. Pukish, J. Kolbusz, and B. M. Wilamowski, ‘Selection of Proper Neural Network Sizes and Architectures—A Comparative Study’, *IEEE Trans. Ind. Informatics*, vol. 8, no. 2, pp. 228–240, 2012.
- [159] K. G. Sheela and S. N. Deepa, ‘Selection of number of hidden neurons in neural networks in renewable energy systems’, *J. Sci. Ind. Res. (India)*, vol. 73, no. 10, pp. 686–688, 2014.
- [160] G. Zhang, B. E. Patuwo, and M. Y. Hu, ‘Forecasting with artificial neural networks: The state of the art’, vol. 14, pp. 35–62, 1998.
- [161] A. Donoso-Bravo, J. Mailier, C. Martin, J. Rodríguez, C. A. Aceves-Lara, and A. Vande Wouwer, ‘Model selection, identification and validation in anaerobic digestion: A review’, *Water Res.*, vol. 45, no. 17, pp. 5347–5364, Nov. 2011.
- [162] W. C. Wang, K. W. Chau, C. T. Cheng, and L. Qiu, ‘A comparison of performance of several artificial intelligence methods for forecasting monthly discharge time series’, *J. Hydrol.*, vol. 374, no. 3–4, pp. 294–306, Aug. 2009.
- [163] Keyence Cooperation Ltd, ‘Area Roughness Parameters’. [Online]. Available: <https://www.keyence.com/ss/products/microscope/roughness/surface/parameters.jsp>. [Accessed: 18-Oct-2018].

# Appendices

## **Appendix A      Surface Metrology Parameters**

### **A.1 Profile Parameters**

There are three types of surface profile parameters currently defined in the ISO standards (ISO 4287:1998+A1:2009). The classification is based on the filtration used, to obtain either, the form, waviness or roughness parameters. Below are commonly used profile roughness parameters.

**Table A.1 - Common profile parameters - name, definition and formula. Reproduced from Keyence [162].**

	<b>Name</b>	<b>Definition</b>	<b>Mathematical Formula</b>
1	R <sub>a</sub> Arithmetical mean deviation of the assessed profile	Arithmetic mean of the absolute ordinate values z(x) within a sampling length; l.  Where z(x) is the height of the assessed profile at any position x and l, is the length in the direction of the x-axis use for identifying the irregularities characterizing the profile under evaluation	$R_a = \frac{1}{l} \int_0^l  z(x)  dx$
2	R <sub>q</sub> Root mean Square deviation of the assessed profile	Root mean square value of the ordinate values z(x) within a sampling length, l.	$R_q = \sqrt{\frac{1}{l} \int_0^l Z^2(x) dx}$

3	Rsk  Skewness of the assessed profile	Quotient of the mean cube value of the ordinate values $z(x)$ and the cube of $Rq$ within a sampling length	$Rsk = \frac{1}{Rq^3} \left[ \frac{1}{l} \int_0^l Z^3(x) dx \right]$
4	Rku  Kurtosis of the assessed profile	Quotient of the mean quartic value of the ordinate values $z(x)$ and the fourth power of $Rq$ within a sampling length	$Rku = \frac{1}{Rq^4} \left[ \frac{1}{l} \int_0^l Z^4(x) dx \right]$
5	Rp  Maximum profile peak height	Largest profile peak height( $Z_{pj}$ )within a sampling length	$Rp = \max_{1 \leq j \leq m} Z_{pj}$  Where m is the number of profile peaks
6.	Rv  Maximum profile valley depth height	Largest profile valley height( $Z_{vj}$ )within a sampling length	$Rv = \max_{1 \leq j \leq m} Z_{vj}$  Where m is the number of profile peaks
7	Rz  Maximum height of the assessed profile	Sum of height of the largest profile peak height $Z_p$ and the largest profile valley depth $Z_v$ within a sampling length.	$Rz = Rp + Rv$
8	Rt  Total height of the assessed profile	Sum of height of the largest profile peak height $Z_p$ and the largest profile valley depth $Z_v$ within an evaluation length.	$Rz = Rp + Rv$

9	Rc  Mean height of profile elements of the assessed profile	Mean value of the profile elements heights Zt within a sampling length.  Where Ztj is the height of the jth profile element within the length.	$Rc = \frac{1}{m} \sum_{j=1}^m Zt_j$
10	RSm  Mean width of profile elements of the assessed profile	Mean value of the profile element widths Xs within a sampling length	$RSm = \frac{1}{m} \sum_{j=1}^m Xs_j$

## A.2 Surface texture Areal Parameters

The ISO 25178 series is dedicated to standardizing areal surface texture measurement. Below are the most commonly used areal surface texture areal parameters. The content in this appendix was extracted from [163]. This includes definitions of parameters and diagrams illustrating parameters.

### A.2.1 Height Parameters

#### 1. Sa (arithmetical mean height)

Sa is the extension of Ra (arithmetical mean height of a line) to a surface. It expresses, as an absolute value, the difference in height of each point compared to the arithmetical mean of the surface. This parameter is used generally to evaluate surface roughness.

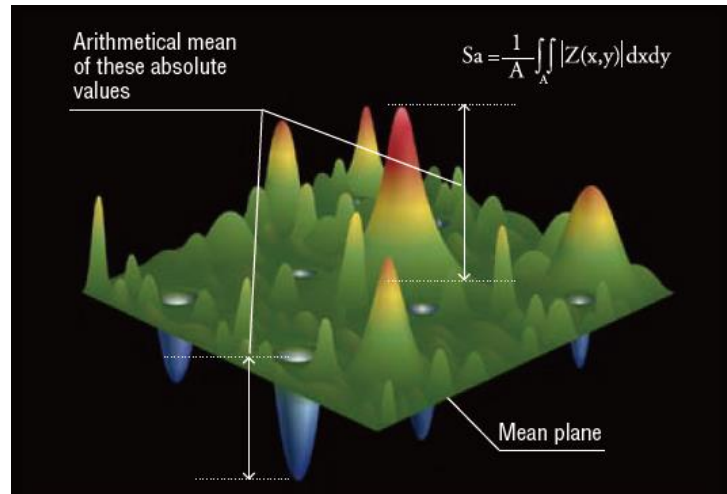


**Figure A.1** Arithmetical Mean Height. Reproduced from Keyence [162].

2. Sz (Maximum height)

Sz is defined as the sum of the largest peak height value and the largest pit depth value within the defined area.

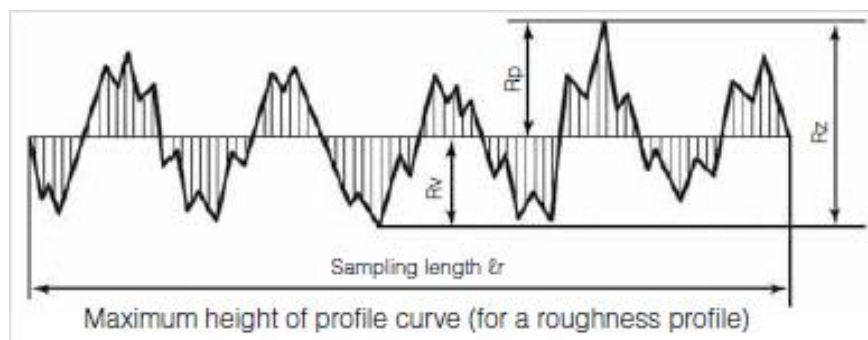


**Figure A.2** Maximum Height. Reproduced from Keyence [162]

3. Sp (Maximum peak height)

Sp is the height of the highest peak within the defined area.

4. Sv (Maximum pit height)

$S_v$  is the absolute value of the height of the largest pit within the defined area.

5.  $S_q$  (Root mean square height)

$S_q$  represents the root mean square value of ordinate values within the definition area. It is equivalent to the standard deviation of heights.

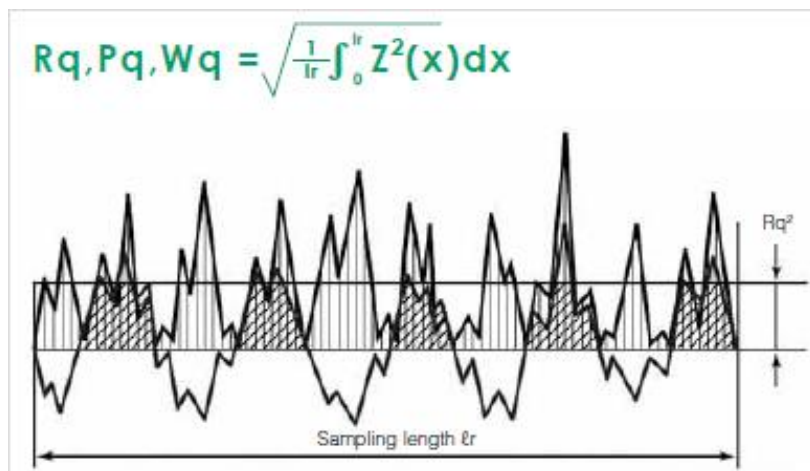


**Figure A.3** Root Mean Square Height. Reproduced from Keyence [162]

6.  $S_{sk}$  (Skewness)

$S_{sk}$  values represent the degree of bias of the roughness shape (asperity).

$S_{sk}<0$ : Height distribution is skewed above the mean plane.

$S_{sk}=0$ : Height distribution (peaks and pits) is symmetrical around the mean plane.

$S_{sk}>0$ : Height distribution is skewed below the mean plane.

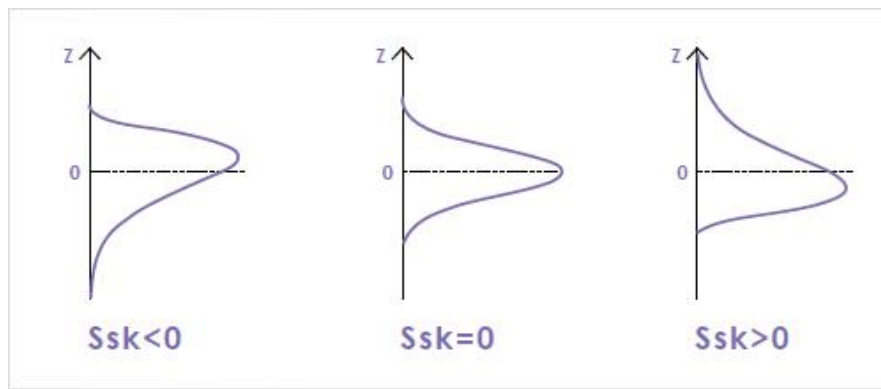


**Figure A.4** Skewness. Reproduced from Keyence [162]

#### 7. Sku (Kurtosis)

Sku value is a measure of the sharpness of the roughness profile.

Sku<3: Height distribution is skewed above the mean plane.

Sku=3: Height distribution is normal. (Sharp portions and indented portions co-exist.)

Sku>3: Height distribution is spiked.

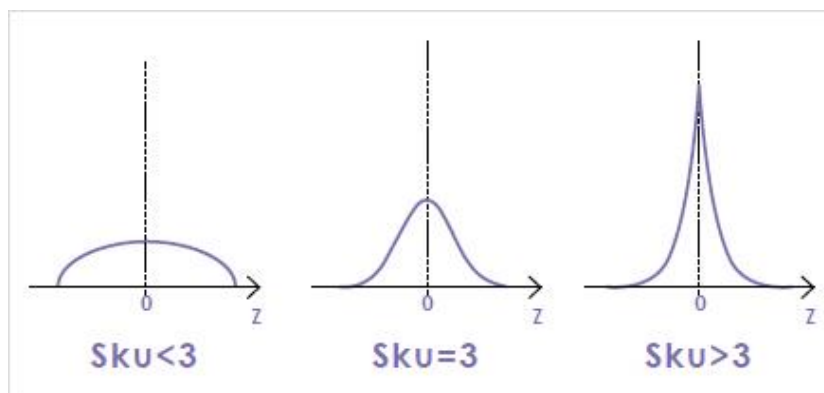


**Figure A.5** Kurtosis. Reproduced from Keyence [162]

#### A.2.2 ***Spatial Parameters***

##### 1. Sal (Auto-correlation length)

Sal represents the horizontal distance in the direction in which the auto-correlation function decays

to the value[s] (0.2 by default) the fastest.

## 2. Str (texture aspect ratio)

Str is a measure of uniformity of the surface texture. The value is obtained by dividing the horizontal distance in the direction in which the auto-correlation function decays to the value[s] (0.2 by default) the fastest (equivalent to Sal) by the horizontal distance in the direction of the slowest decay of auto-correlation function to the value[s].

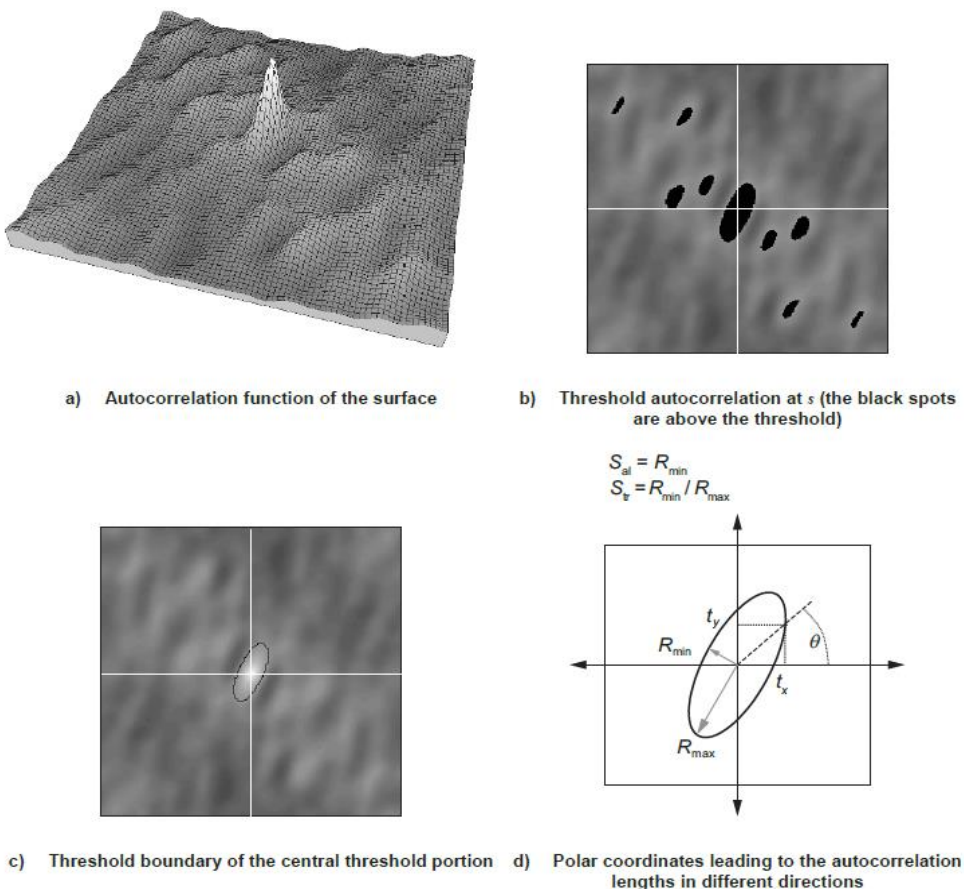


**Figure A.6** Procedure to calculate Sal and Str. Reproduced from Keyence [162].

### A.2.3 Hybrid Parameters

#### 1. Sdq (Root mean square gradient)

Sdq is calculated as a root mean square of slopes at all points in the definition area.

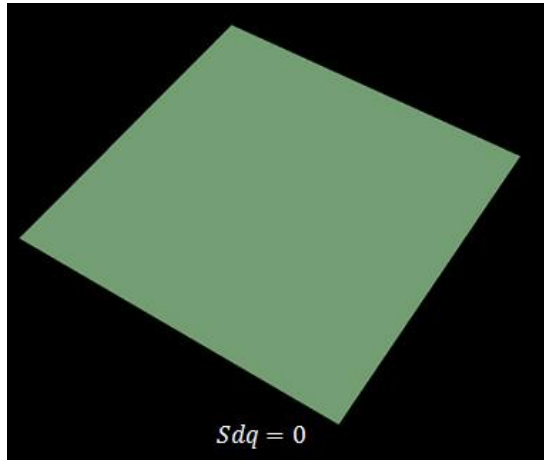


**Figure A.7** The Sdq of a completely level surface is 0. Reproduced from Keyence [162].

When a surface has any slope, its Sdq value becomes larger. The surface below is a plane with gradient components of 45 degrees and has an Sdq value of 1.

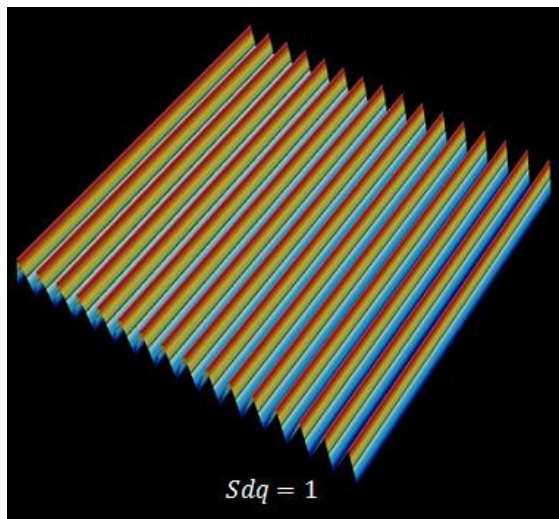


**Figure A.8** The Sdq of plane at 45 degrees. Reproduced from Keyence [162].

2 Sdr (Developed interfacial area ratio)

This parameter is expressed as the percentage of the definition area's additional surface area contributed by the texture as compared to the planar definition area.

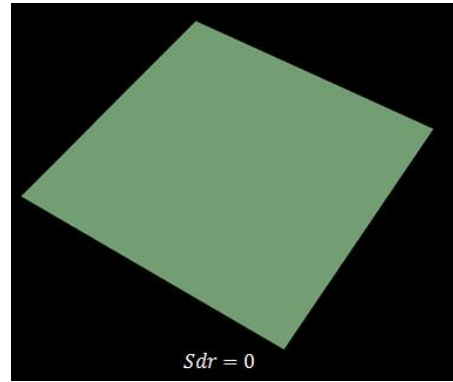


**Figure A.9** The Sdr of a completely level surface is 0. Reproduced from Keyence [162].

When a surface has any slope, its Sdr value becomes larger. The surface below is a plane with gradient components of 45 degrees and has an Sdr value of 0.414.

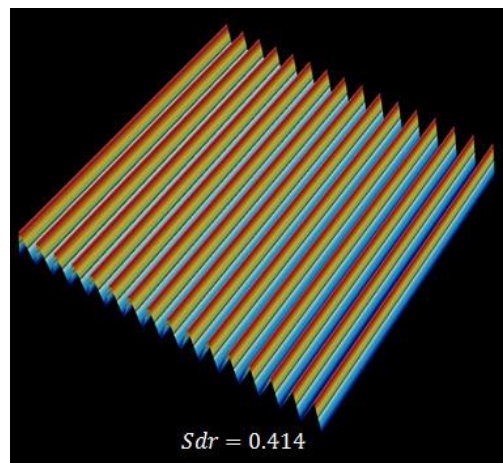


**Figure A.10** The Sdr of plane at 45 degrees. Reproduced from Keyence [162].

#### A.2.4 ***Functional Parameters***

1. Smr(c) (Areal material ratio)

The areal material ratio curve of an area is a curve representing heights at which the areal material ratio changes from 0% to 100%.

An areal material ratio represents the area with a specific height  $c$  or higher. The areal material ratio at height  $c$  corresponds to  $\text{Smr}(c)$  in the figure below.

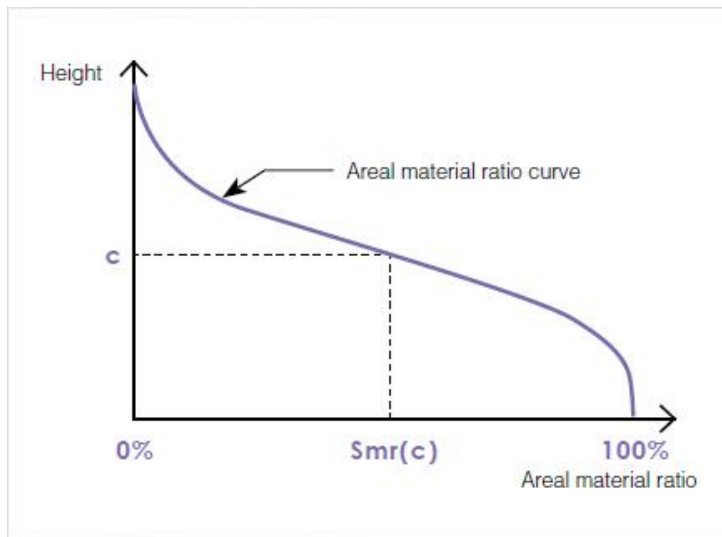


**Figure A.11** Areal material ratio curve. Reproduced from Keyence [162].

When a secant line of an areal material ratio curve, which covers 40% of the difference in the areal material ratio, is shifted from the areal material ratio of 0% the position at which the secant line has the smallest gradient is called the center portion of the areal material ratio curve.

The equivalent line is the line where the sum of the squared deviation in the vertical-axis direct is the smallest in the center portion.

The section of the equivalent line between the two height positions where the areal material ratio is 0% and 100% is called the core surface. The peaks with a height above the core surface are called reduced peaks, while the valleys below the core surface are called reduced valleys.

The core surface represents the height of the area that makes contact with other objects after initial abrasion.

2.  $\text{Smc}(\text{mr})$  (Inverse areal material ratio)

$\text{Smc}(\text{p})$  (inverse areal material ratio), is the height [c] that gives the areal material ratio p%.

3.  $\text{Sk}$  (Core roughness depth)

$\text{Sk}$  (core roughness depth) is calculated as the difference of heights at the areal material ratio values 0% and 100% on the equivalent line; specifically, it is a value obtained by subtracting the minimum height from the maximum height of the core surface.

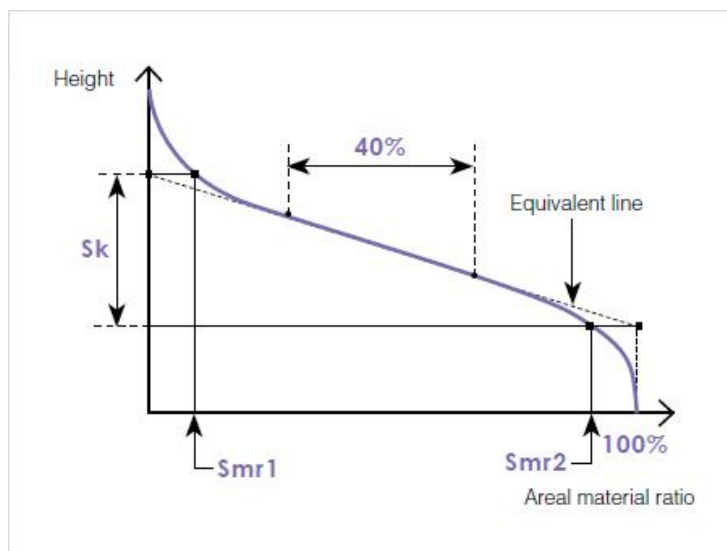


**Figure A.12** Core roughness depth. Reproduced from Keyence [162].

$\text{Sk}$  represents the height of the core surface,  $\text{Smr1}$  represents the areal material ratio that divides the reduced peaks from the core surface, and  $\text{Smr2}$  represents the areal material ratio that divides the reduced valleys from the core surface.

The reduced peaks are the areas that are removed by initial abrasion.  $\text{Spk}$  represents the average height of the reduced peaks.

The reduced valleys are the areas that hold liquid applied on the surface in order to improve lubricity.  $S_{vk}$  represents the average depth of the reduced valleys.

#### 4. Spk (Reduced peak height)

$Spk$  (reduced peak height) represents the mean height of peaks above the core surface.

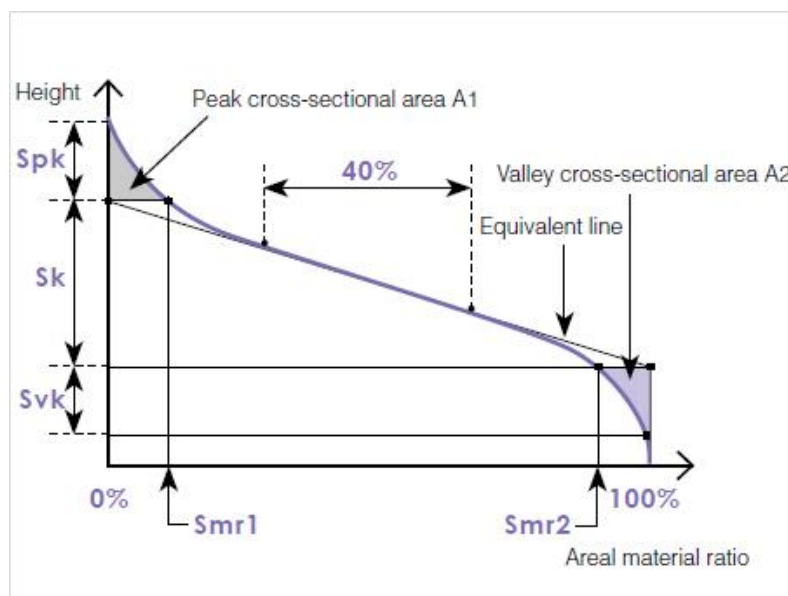


**Figure A.13** Reduced peak height. Reproduced from Keyence [162].

#### 5. $S_{vk}$ (reduced dale height, reduced valley depth)

$S_{vk}$  (reduced valley depth) expresses the arithmetical mean of the reduced valley depth of the areal material ratio curve. Essentially, this is a measure of the valley depth below the core roughness. This indicates the depth of the area in which fluid applied to the surface accumulates, which is information that can be used to improve the lubricating properties of the surface.

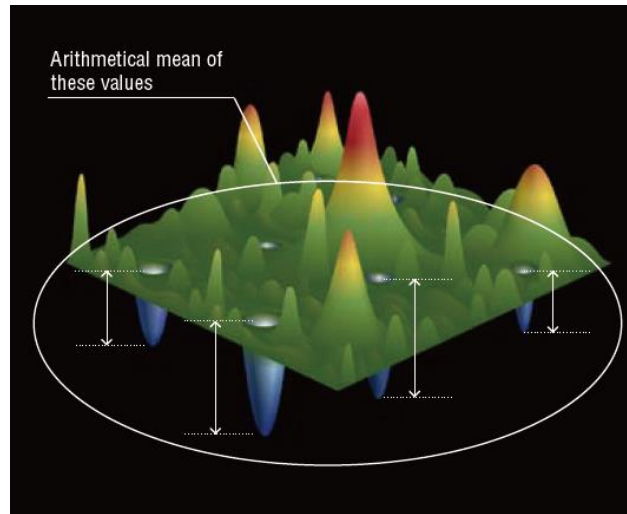


**Figure A.14** Reduced dale height, reduced valley depth. Reproduced from Keyence [162]

6. Smr (Peak material portion, percentage of material that comprises the peak structures associated with Spk)

Smr (peak material portion) is the percentage of material that comprises the peak structures associated with Spk.

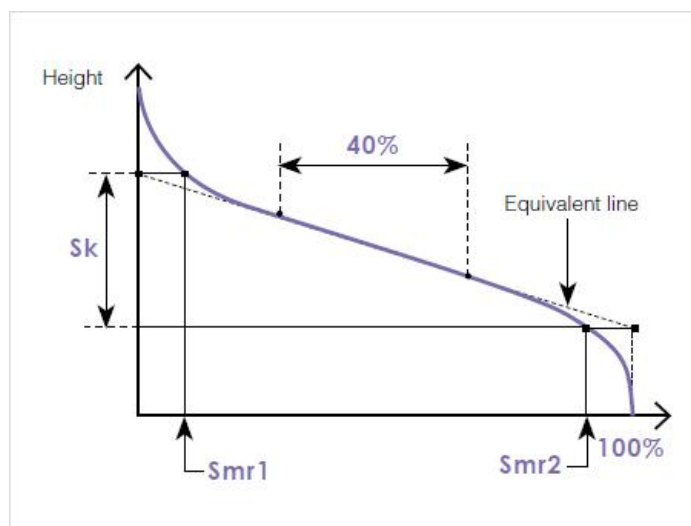


**Figure 9.15** Peak material portion. Reproduced from Keyence [162].

Sk represents the height of the core surface, Smr1 represents the areal material ratio that divides

the reduced peaks from the core surface, and Smr2 represents the areal material ratio that divides the reduced valleys from the core surface.

The reduced peaks are the areas that are removed by initial abrasion. Spk represents the average height of the reduced peaks.

The reduced valleys are the areas that hold liquid applied on the surface in order to improve lubricity. Svk represents the average depth of the reduced valleys.

#### 7. Smr2 (Valley material portion)

Smr2 (valley material portion) is the percentage of the measurement area that comprises the deeper valley structures associated with Svk.

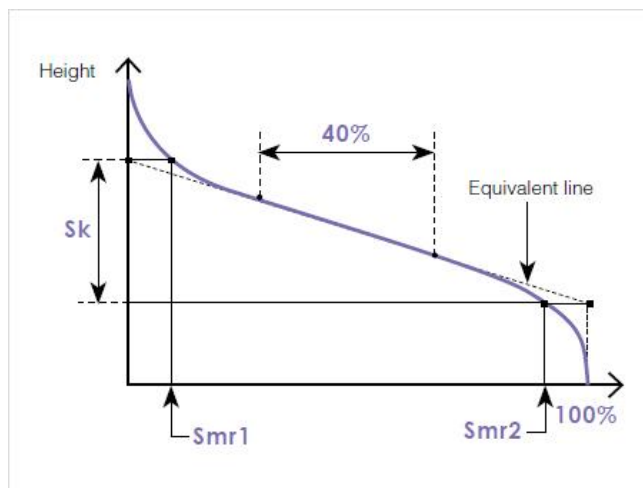


**Figure A.16** Valley material portion. Reproduced from Keyence [162]

Sk represents the height of the core surface, Smr1 represents the areal material ratio that divides the reduced peaks from the core surface, and Smr2 represents the areal material ratio that divides the reduced valleys from the core surface.

The reduced peaks are the areas that are removed by initial abrasion. Spk represents the average height of the reduced peaks.

The reduced valleys are the areas that hold liquid applied on the surface in order to improve lubricity. Svk represents the average depth of the reduced valleys.

#### 8. Sxp (Peak extreme height)

Sxp (peak extreme height) is the difference of heights at the areal material ratio values p% and q%. The areal material ratio curve is used for the calculation of Sxp.

Sxp represents the difference in the height between the average plane and peaks on the surface after especially high peaks on the surface are removed. By default, it is the height difference between the areal material ratio values 2.5% and 50%.

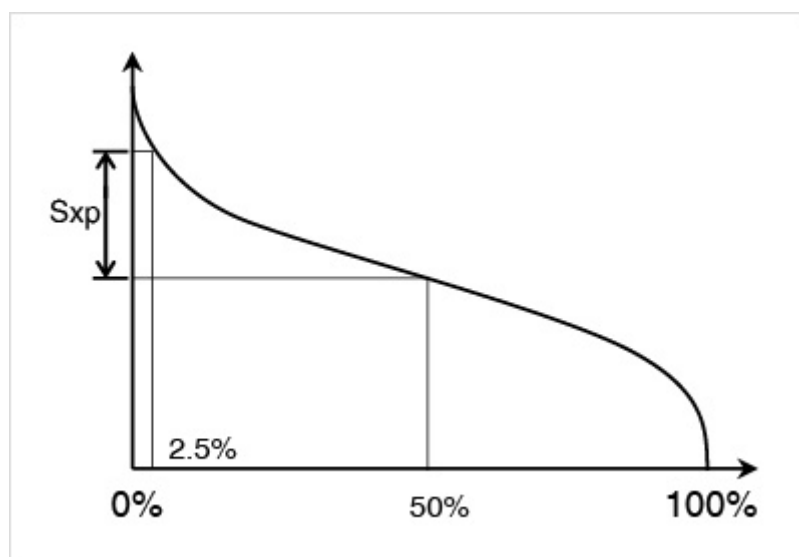


**Figure A.17** Peak extreme height. Reproduced from Keyence [162].

9. Vvv (Dale void volume)

Vvv (dale void volume) represents the void volume of dale at the areal material ratio p%. It can also be used to quantify the magnitude of the core surface, reduced peaks, and reduced valleys based on volume parameters.

Vmp, Vmc, Vvc, and Vvv represent the volumes of the reduced peaks, core material, core void, and valley void respectively.

To use volume parameters, the areal material ratio values that divide the reduced peaks and reduced valleys from the core surface must be specified. By default, 10% and 80% are used.

10. Vvc (Core void volume)

Vvc (core void volume) represents the difference between the void volume at areal material ratio p% and the void volume at areal material ratio q%. It can also be used to quantify the magnitude of the core surface, reduced peaks, and reduced valleys based on volume parameters.

Vmp, Vmc, Vvc, and Vvv represent the volumes of the reduced peaks, core material, core void, and valley void respectively.

To use volume parameters, the areal material ratio values that divide the reduced peaks and reduced valleys from the core surface must be specified. By default, 10% and 80% are used.

11. Vmp (Peak material volume)

Vmp (peak material volume) represents the volume of material at areal material ratio p%. It can also be used to quantify the magnitude of the core surface, reduced peaks, and reduced valleys based on volume parameters.

$V_{mp}$ ,  $V_{mc}$ ,  $V_{vc}$ , and  $V_{vv}$  represent the volumes of the reduced peaks, core material, core void, and valley void respectively.

To use volume parameters, the areal material ratio values that divide the reduced peaks and reduced valleys from the core surface must be specified. By default, 10% and 80% are used.

## 12. $V_{mc}$ (Core material volume)

$V_{mc}$  (core material volume) represents the difference between the material volume at areal material ratio  $q\%$  and the material volume at areal material ratio  $p\%$ . It can also be used to quantify the magnitude of the core surface, reduced peaks, and reduced valleys based on volume parameters.

$V_{mp}$ ,  $V_{mc}$ ,  $V_{vc}$ , and  $V_{vv}$  represent the volumes of the reduced peaks, core material, core void, and valley void respectively.

To use volume parameters, the areal material ratio values that divide the reduced peaks and reduced valleys from the core surface must be specified. By default, 10% and 80% are used.

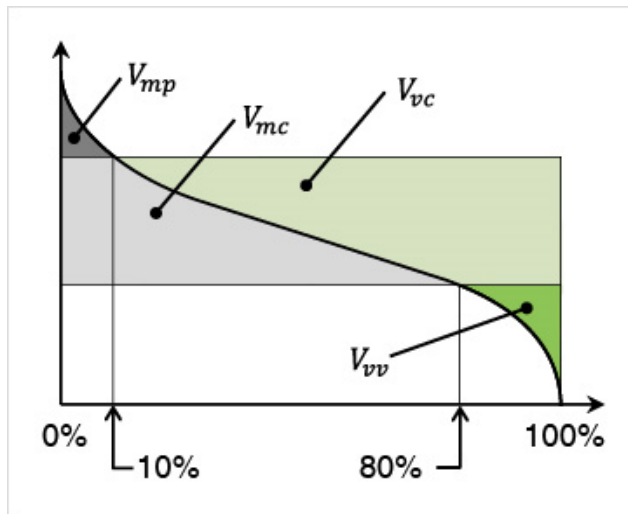


**Figure A.18** Material Volume. Reproduced from Keyence [162]

### A2.5 Feature

1. Spd (Density of peaks)

Spd (density of peaks) represents the number of peaks per unit area. A large number indicates more points of contact with other objects.

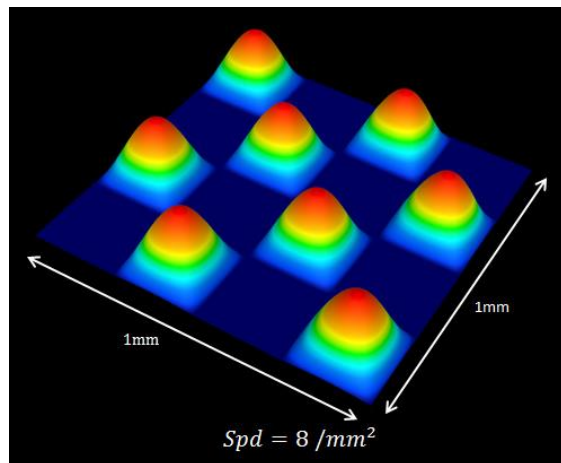


**Figure A.19** Density of peaks. Reproduced from Keyence [162]

2. Spc (Arithmetic mean peak curvature)

Spc (arithmetic mean peak curvature) represents the arithmetic mean of the principal curvature of the peaks on the surface. A smaller value indicates that the points of contact with other objects have rounded shapes; a larger value indicates that the points of contact with other objects have pointed shapes.

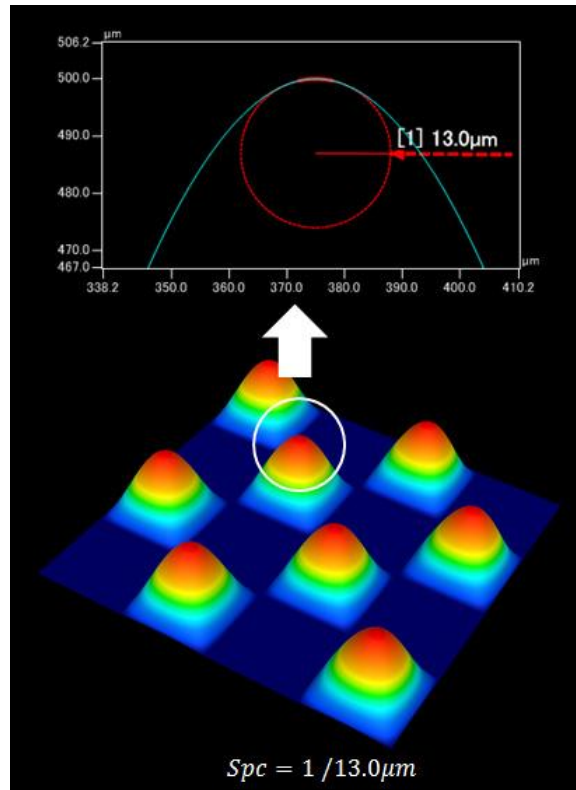


**Figure A.20** Arithmetic mean peak curvature. Reproduced from Keyence [162].

S10z (Ten-point height) / S5p (Five-point peak height) / S5v (Five-point pit height) / Sda(c) (Mean dale area) / Sha(c) (Mean hill area) / Sdv(c) (Mean dale volume) / Shv(c) (Mean hill volume)

### Segmentation

#### 3. Watershed algorithm

The watershed algorithm is employed to partition regions, which are used in the calculation of feature parameters.

Water is poured into the surface landscape and runs along the surface shape and reaches the pit. As more water continues to pour, the water surfaces of water filling different pits make contact

with each other. The set of these contact points is the ridge line that partitions the dale region. The same approach can be applied to the hill region by vertically inverting the process.

#### 4. Wolf pruning

Peaks and pits merely need to be higher or lower than other points in their respective neighborhoods. For this reason, a surface with fine asperity can have a vast number of peaks and pits. Applying the watershed algorithm to such surfaces can result in meticulous segmentation into minute peak and valley regions. In order to suppress this over-segmentation, the wolf pruning method is used to remove regions below a certain height/depth threshold.

The threshold is provided as a percentage of the maximum height ( $S_z$ ) of the surface. The default value is 5%.

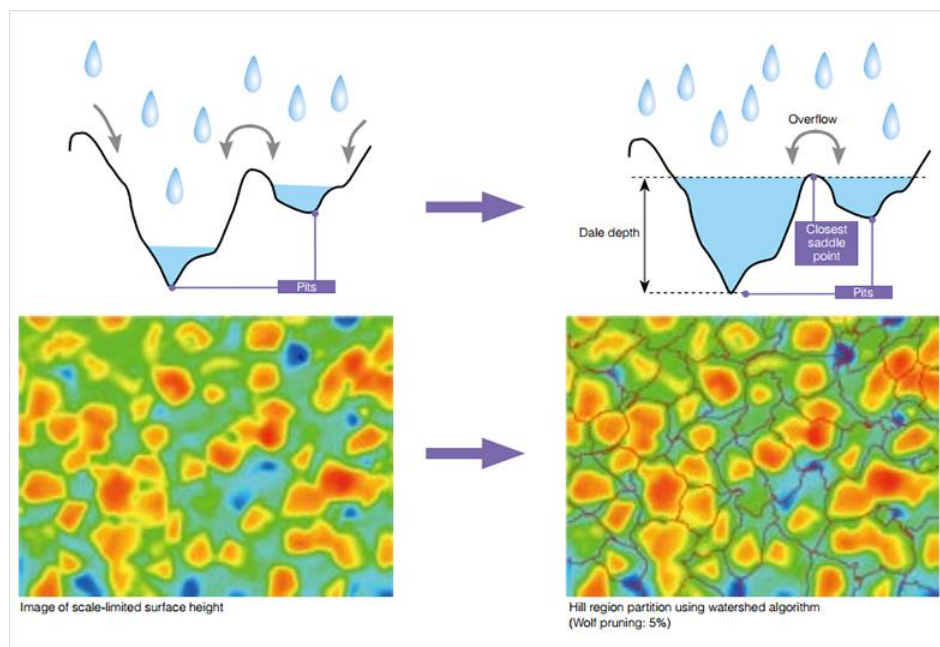


**Figure A.21** Wolf pruning. Reproduced from Keyence [162]

#### 5 Closed area, Open area

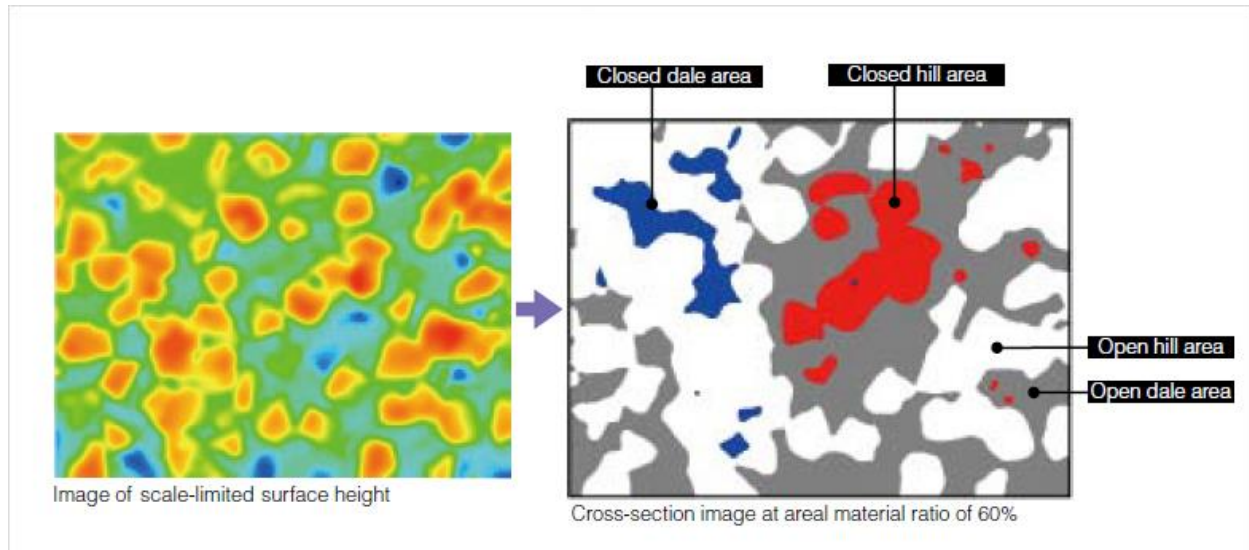


**Figure A.22** Closed area, Open area. Reproduced from Keyence [162]

A region that is in contact with the boundary of the definition area at the material height  $c$  is called an "open area," while a region that is not is called a "closed area." Height  $c$  is given in areal material ratio and the default value is 50%.

**Appendix B****Data sheet of Keyence LJ-V7020K sensor head**

The content in this appendix was extracted from [119].

**B.1 Specifications LJ-V7020K sensor head**

Model	LJ-V7020K <sup>1</sup>	
Mounting conditions	Specular reflection	
Reference distance	24.2 mm 0.95"	
Measurement range	Z-axis (height)	±2.3 mm 0.09" (F.S.=4.6 mm 0.18")
	X-axis (width)	NEAR side 6.5 mm 0.28" Reference distance 7 mm 0.28" Far side 7.5 mm 0.30"
	Type	Blue semiconductor laser
	Wavelength	405 nm (visible beam)
Light source	Laser class	Class 2M Laser Product <sup>2</sup> (IEC60825-1, FDA(CDRH) Part 1040.10 <sup>3</sup> )
	Output	10 mW
Spot size (reference distance)	Approx. 14 mm × 35 µm 0.55" × 0.001378"	
Repeatability	Z-axis (height)	0.2 µm 0.000008 <sup>4</sup> <sup>5</sup>
	X-axis (width)	2.5 µm 0.000099 <sup>4</sup> <sup>6</sup>
Linearity	Z-axis (height)	±0.1% of F.S. <sup>7</sup>
Profile data interval	X-axis (width)	10 µm 0.0004"
Sampling cycle (trigger interval)	Top speed: 16 µs (high-speed mode), Top speed: 32 µs (advanced function mode) <sup>8</sup>	
Temperature characteristics	0.01% of F.S./°C	
Environmental resistance	Enclosure rating	IP67 (IEC60529) <sup>9</sup>
	Ambient light	Incandescent lamp: 10,000 lux max. <sup>10</sup>
	Ambient temperature	0 to +45 °C 32 to 113 °F <sup>11</sup>
	Relative humidity	20 to 85 % RH (No condensation)
	Vibration resistance	10 to 57 Hz, Double amplitude 1.5 mm 0.06", 3 hours in each of the X, Y, and Z directions
	Shock resistance	15 G/6 ms
Material	Aluminum	
Weight	Approx. 410 g	

<sup>1</sup> The double polarization function cannot be used.

<sup>2</sup> Do not look into the beam directly using any optical instruments (such as eye loupes, magnifiers, microscopes, telescopes, or binoculars).

Viewing the laser output with an optical instrument may pose an eye hazard.

<sup>3</sup> The laser classification for FDA(CDRH) is implemented based on IEC60825-1 in accordance with the requirements of Laser Notice No. 50.

<sup>4</sup> This value is from a case in which measurement has been performed with a reference distance with 4,096 times of averaging.

<sup>5</sup> The measurement targets are KEYENCE standard targets. This value is from a case in which the average height of the default setting area has been measured in height mode. All other settings are default.

<sup>6</sup> The measurement target is a pin gauge. This value is from a case in which the position of the intersection between the rounded surface of the pin gauge and the edge level has been measured in position mode. All other settings are default.

<sup>7</sup> The measurement targets are KEYENCE standard targets. The profile data is from a case in which measurement has been performed with 64 times of smoothing and 8 times of averaging. All other settings are default.

<sup>8</sup> For high-speed mode, when the measurement area is at its minimum, binning is ON, image capture mode is set to standard, and parallel image capture is ON.

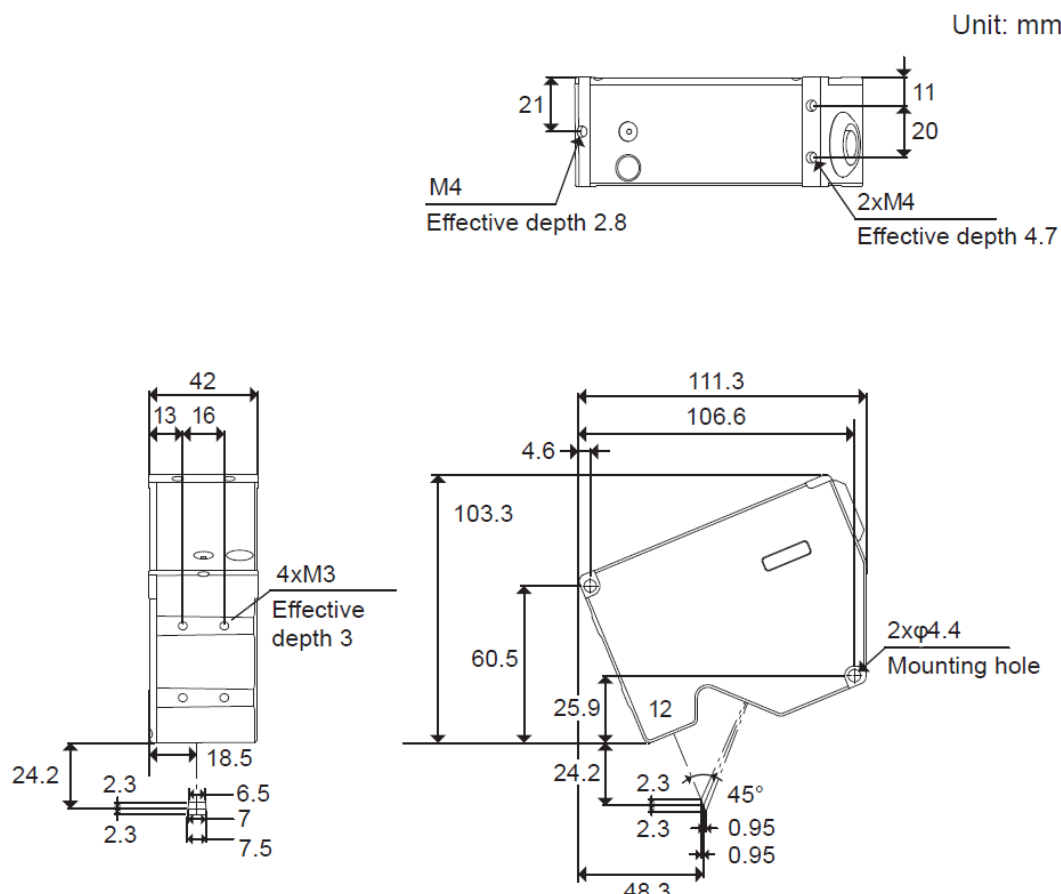
All other settings are default. For advanced function mode, when the measurement area is at its minimum, binning is ON and image capture mode is set to standard. All other settings are default.

<sup>9</sup> This value is from a case in which the sensor head cable (CB-B\*) or extension cable (CB-B\*E) has been connected.

<sup>10</sup> This is the illuminance for the light-receiving surface of the sensor head during white paper measurement when light has been shined onto the white paper.

<sup>11</sup> The sensor head must be mounted on a metal plate for use.

**B.2 Dimensions of LJ-V7020K sensor head. Reproduced from Keyence [119].**



## Appendix C Results from Optiv\_Classic CMM

### C.1 Results obtained from measuring distance between groove features on cross-grating

<b>pcdmis</b>			PART NAME : Student Block	July 02, 2018	13:10	
REV NUMBER :		SER NUMBER :	STATS COUNT :		1	
<b>↔ MM DIST1 - YAXIS_LH_X- TO YAXIS_RH_X+ (XAXIS)</b>						
AX	NOMINAL	+TOL	-TOL	MEAS	DEV	OUTTOL
M	11.500	0.010	0.010	11.511	0.011	0.001
<b>↔ MM DIST2 - XAXIS_TOP_Y+ TO XAXIS_BTM_Y- (YAXIS)</b>						
AX	NOMINAL	+TOL	-TOL	MEAS	DEV	OUTTOL
M	11.500	0.010	0.010	11.501	0.001	0.000
<b>↔ MM DIST3 - CIR1 TO YAXIS_LH_X- (XAXIS)</b>						
AX	NOMINAL	+TOL	-TOL	MEAS	DEV	OUTTOL
M	2.000	0.010	0.010	1.974	-0.026	0.016
<b>↔ MM DIST4 - CIR1 TO XAXIS_TOP_Y+ (YAXIS)</b>						
AX	NOMINAL	+TOL	-TOL	MEAS	DEV	OUTTOL
M	2.000	0.010	0.010	1.942	-0.058	0.048
<b>↔ MM DIST5 - CIR36 TO YAXIS_RH_X+ (XAXIS)</b>						
AX	NOMINAL	+TOL	-TOL	MEAS	DEV	OUTTOL
M	2.000	0.010	0.010	2.028	0.028	0.018
<b>↔ MM DIST6 - CIR36 TO XAXIS_BTM_Y- (YAXIS)</b>						
AX	NOMINAL	+TOL	-TOL	MEAS	DEV	OUTTOL
M	2.000	0.010	0.010	2.054	0.054	0.044
#	MM	LOC1 - CIR1				
AX	NOMINAL	+TOL	-TOL	MEAS	DEV	OUTTOL
X	0.000	0.020	0.020	-0.006	-0.006	0.000
Y	7.500	0.020	0.020	7.509	0.009	0.000
D	0.500	0.020	0.020	0.513	0.013	0.000
#	MM	LOC2 - CIR2				
AX	NOMINAL	+TOL	-TOL	MEAS	DEV	OUTTOL
X	1.500	0.020	0.020	1.494	-0.006	0.000
Y	7.500	0.020	0.020	7.505	0.005	0.000
D	0.500	0.020	0.020	0.512	0.012	0.000
#	MM	LOC3 - CIR3				
AX	NOMINAL	+TOL	-TOL	MEAS	DEV	OUTTOL
X	3.000	0.020	0.020	2.998	-0.002	0.000
Y	7.500	0.020	0.020	7.507	0.007	0.000
D	0.500	0.020	0.020	0.508	0.008	0.000
#	MM	LOC4 - CIR4				
AX	NOMINAL	+TOL	-TOL	MEAS	DEV	OUTTOL
X	4.500	0.020	0.020	4.496	-0.004	0.000
Y	7.500	0.020	0.020	7.509	0.009	0.000
D	0.500	0.020	0.020	0.513	0.013	0.000

#	MM	LOC5 - CIR5					
		NOMINAL	+TOL	-TOL	MEAS	DEV	OUTTOL
AX		6.000	0.020	0.020	6.000	0.000	0.000
X		7.500	0.020	0.020	7.509	0.009	0.000
Y		0.500	0.020	0.020	0.514	0.014	0.000
#	MM	LOC6 - CIR6					
		NOMINAL	+TOL	-TOL	MEAS	DEV	OUTTOL
AX		7.500	0.020	0.020	7.498	-0.002	0.000
X		7.500	0.020	0.020	7.509	0.009	0.000
Y		0.500	0.020	0.020	0.516	0.016	0.000
#	MM	LOC7 - CIR7					
		NOMINAL	+TOL	-TOL	MEAS	DEV	OUTTOL
AX		0.000	0.020	0.020	-0.003	-0.003	0.000
X		6.000	0.020	0.020	6.003	0.003	0.000
Y		0.500	0.020	0.020	0.520	0.020	0.000
#	MM	LOC8 - CIR8					
		NOMINAL	+TOL	-TOL	MEAS	DEV	OUTTOL
AX		1.500	0.020	0.020	1.499	-0.001	0.000
X		6.000	0.020	0.020	6.005	0.005	0.000
Y		0.500	0.020	0.020	0.524	0.024	0.004
#	MM	LOC9 - CIR9					
		NOMINAL	+TOL	-TOL	MEAS	DEV	OUTTOL
AX		3.000	0.020	0.020	2.996	-0.004	0.000
X		6.000	0.020	0.020	6.005	0.005	0.000
Y		0.500	0.020	0.020	0.515	0.015	0.000
#	MM	LOC10 - CIR10					
		NOMINAL	+TOL	-TOL	MEAS	DEV	OUTTOL
AX		4.500	0.020	0.020	4.497	-0.003	0.000
X		6.000	0.020	0.020	6.003	0.003	0.000
Y		0.500	0.020	0.020	0.517	0.017	0.000
#	MM	LOC11 - CIR11					
		NOMINAL	+TOL	-TOL	MEAS	DEV	OUTTOL
AX		6.000	0.020	0.020	6.001	0.001	0.000
X		6.000	0.020	0.020	6.009	0.009	0.000
Y		0.500	0.020	0.020	0.513	0.013	0.000
#	MM	LOC12 - CIR12					
		NOMINAL	+TOL	-TOL	MEAS	DEV	OUTTOL
AX		7.500	0.020	0.020	7.501	0.001	0.000
X		6.000	0.020	0.020	6.008	0.008	0.000
Y		0.500	0.020	0.020	0.515	0.015	0.000

#	MM	LOC13 - CIR13					
		NOMINAL	+TOL	-TOL	MEAS	DEV	OUTTOL
AX		0.000	0.020	0.020	-0.002	-0.002	0.000
X		4.500	0.020	0.020	4.503	0.003	0.000
Y		0.500	0.020	0.020	0.512	0.012	0.000
#	MM	LOC14 - CIR14					
		NOMINAL	+TOL	-TOL	MEAS	DEV	OUTTOL
AX		1.500	0.020	0.020	1.502	0.002	0.000
X		4.500	0.020	0.020	4.504	0.004	0.000
Y		0.500	0.020	0.020	0.517	0.017	0.000
#	MM	LOC15 - CIR15					
		NOMINAL	+TOL	-TOL	MEAS	DEV	OUTTOL
AX		3.000	0.020	0.020	2.997	-0.003	0.000
X		4.500	0.020	0.020	4.504	0.004	0.000
Y		0.500	0.020	0.020	0.516	0.016	0.000
#	MM	LOC16 - CIR16					
		NOMINAL	+TOL	-TOL	MEAS	DEV	OUTTOL
AX		4.500	0.020	0.020	4.500	0.000	0.000
X		4.500	0.020	0.020	4.507	0.007	0.000
Y		0.500	0.020	0.020	0.522	0.022	0.002
#	MM	LOC17 - CIR17					
		NOMINAL	+TOL	-TOL	MEAS	DEV	OUTTOL
AX		6.000	0.020	0.020	6.000	0.000	0.000
X		4.500	0.020	0.020	4.505	0.005	0.000
Y		0.500	0.020	0.020	0.517	0.017	0.000
#	MM	LOC18 - CIR18					
		NOMINAL	+TOL	-TOL	MEAS	DEV	OUTTOL
AX		7.500	0.020	0.020	7.500	0.000	0.000
X		4.500	0.020	0.020	4.510	0.010	0.000
Y		0.500	0.020	0.020	0.520	0.020	0.000
#	MM	LOC19 - CIR19					
		NOMINAL	+TOL	-TOL	MEAS	DEV	OUTTOL
AX		0.000	0.020	0.020	-0.003	-0.003	0.000
X		3.000	0.020	0.020	3.002	0.002	0.000
Y		0.500	0.020	0.020	0.511	0.011	0.000
#	MM	LOC20 - CIR20					
		NOMINAL	+TOL	-TOL	MEAS	DEV	OUTTOL
AX		1.500	0.020	0.020	1.498	-0.002	0.000
X		3.000	0.020	0.020	3.007	0.007	0.000
Y		0.500	0.020	0.020	0.521	0.021	0.001

#	MM	LOC21 - CIR21					
		NOMINAL	+TOL	-TOL	MEAS	DEV	OUTTOL
AX		3.000	0.020	0.020	3.000	0.000	0.000
X		3.000	0.020	0.020	3.006	0.006	0.000
Y		0.500	0.020	0.020	0.528	0.028	0.008
D							
#	MM	LOC22 - CIR22					
		NOMINAL	+TOL	-TOL	MEAS	DEV	OUTTOL
AX		4.500	0.020	0.020	4.499	-0.001	0.000
X		3.000	0.020	0.020	3.002	0.002	0.000
Y		0.500	0.020	0.020	0.522	0.022	0.002
D							
#	MM	LOC23 - CIR23					
		NOMINAL	+TOL	-TOL	MEAS	DEV	OUTTOL
AX		6.000	0.020	0.020	5.997	-0.003	0.000
X		3.000	0.020	0.020	3.003	0.003	0.000
Y		0.500	0.020	0.020	0.524	0.024	0.004
D							
#	MM	LOC24 - CIR24					
		NOMINAL	+TOL	-TOL	MEAS	DEV	OUTTOL
AX		7.500	0.020	0.020	7.499	-0.001	0.000
X		3.000	0.020	0.020	3.001	0.001	0.000
Y		0.500	0.020	0.020	0.517	0.017	0.000
D							
#	MM	LOC25 - CIR25					
		NOMINAL	+TOL	-TOL	MEAS	DEV	OUTTOL
AX		0.000	0.020	0.020	-0.002	-0.002	0.000
X		1.500	0.020	0.020	1.500	0.000	0.000
Y		0.500	0.020	0.020	0.507	0.007	0.000
D							
#	MM	LOC26 - CIR26					
		NOMINAL	+TOL	-TOL	MEAS	DEV	OUTTOL
AX		1.500	0.020	0.020	1.497	-0.003	0.000
X		1.500	0.020	0.020	1.501	0.001	0.000
Y		0.500	0.020	0.020	0.513	0.013	0.000
D							
#	MM	LOC27 - CIR27					
		NOMINAL	+TOL	-TOL	MEAS	DEV	OUTTOL
AX		3.000	0.020	0.020	3.001	0.001	0.000
X		1.500	0.020	0.020	1.504	0.004	0.000
Y		0.500	0.020	0.020	0.515	0.015	0.000
D							
#	MM	LOC28 - CIR28					
		NOMINAL	+TOL	-TOL	MEAS	DEV	OUTTOL
AX		4.500	0.020	0.020	4.498	-0.002	0.000
X		1.500	0.020	0.020	1.501	0.001	0.000
Y		0.500	0.020	0.020	0.474	-0.026	0.006
D							

#	MM	LOC29 - CIR29					
		NOMINAL	+TOL	-TOL	MEAS	DEV	OUTTOL
AX		6.000	0.020	0.020	6.002	0.002	0.000
X		1.500	0.020	0.020	1.502	0.002	0.000
Y		0.500	0.020	0.020	0.512	0.012	0.000
#	MM	LOC30 - CIR30					
		NOMINAL	+TOL	-TOL	MEAS	DEV	OUTTOL
AX		7.500	0.020	0.020	7.504	0.004	0.000
X		1.500	0.020	0.020	1.501	0.001	0.000
Y		0.500	0.020	0.020	0.515	0.015	0.000
#	MM	LOC31 - CIR31_X0_Y0					
		NOMINAL	+TOL	-TOL	MEAS	DEV	OUTTOL
AX		0.000	0.020	0.020	0.000	0.000	0.000
X		0.000	0.020	0.020	0.000	0.000	0.000
Y		0.500	0.020	0.020	0.514	0.014	0.000
#	MM	LOC32 - CIR32					
		NOMINAL	+TOL	-TOL	MEAS	DEV	OUTTOL
AX		1.500	0.020	0.020	1.500	0.000	0.000
X		0.000	0.020	0.020	0.003	0.003	0.000
Y		0.500	0.020	0.020	0.479	-0.021	0.001
#	MM	LOC33 - CIR33					
		NOMINAL	+TOL	-TOL	MEAS	DEV	OUTTOL
AX		3.000	0.020	0.020	3.000	0.000	0.000
X		0.000	0.020	0.020	0.002	0.002	0.000
Y		0.500	0.020	0.020	0.518	0.018	0.000
#	MM	LOC34 - CIR34					
		NOMINAL	+TOL	-TOL	MEAS	DEV	OUTTOL
AX		4.500	0.020	0.020	4.505	0.005	0.000
X		0.000	0.020	0.020	-0.001	-0.001	0.000
Y		0.500	0.020	0.020	0.515	0.015	0.000
#	MM	LOC35 - CIR35					
		NOMINAL	+TOL	-TOL	MEAS	DEV	OUTTOL
AX		6.000	0.020	0.020	6.003	0.003	0.000
X		0.000	0.020	0.020	-0.001	-0.001	0.000
Y		0.500	0.020	0.020	0.517	0.017	0.000
#	MM	LOC36 - CIR36					
		NOMINAL	+TOL	-TOL	MEAS	DEV	OUTTOL
AX		7.500	0.020	0.020	7.504	0.004	0.000
X		0.000	0.020	0.020	0.004	0.004	0.000
Y		0.500	0.020	0.020	0.523	0.023	0.003

## C.2 Results obtained from measuring the optical dimensional standard

			PART NAME : STK095 short				August 28, 2018	12:32
			REV NUMBER :		SER NUMBER : 10241709	STATS COUNT : 1		
<b>#</b> MM LOC74 - LINS_C_1_2								
AX	MEAS		NOMINAL	+TOL	-TOL	DEV	OUTTOL	
X	1.002		1.000	0.005	0.005	0.002	0.000	
<b>#</b> MM LOC99 - LINS_C_1_3								
AX	MEAS		NOMINAL	+TOL	-TOL	DEV	OUTTOL	
X	2.002		2.000	0.005	0.005	0.002	0.000	
<b>#</b> MM LOC100 - LINS_C_1_4								
AX	MEAS		NOMINAL	+TOL	-TOL	DEV	OUTTOL	
X	3.001		3.000	0.005	0.005	0.001	0.000	
<b>#</b> MM LOC101 - LINS_C_1_5								
AX	MEAS		NOMINAL	+TOL	-TOL	DEV	OUTTOL	
X	4.002		4.000	0.005	0.005	0.001	0.000	
<b>#</b> MM LOC102 - LINS_C_1_6								
AX	MEAS		NOMINAL	+TOL	-TOL	DEV	OUTTOL	
X	5.002		5.000	0.005	0.005	0.002	0.000	
<b>#</b> MM LOC103 - LINS_C_1_7								
AX	MEAS		NOMINAL	+TOL	-TOL	DEV	OUTTOL	
X	6.002		6.000	0.005	0.005	0.002	0.000	
<b>#</b> MM LOC104 - LINS_C_1_8								
AX	MEAS		NOMINAL	+TOL	-TOL	DEV	OUTTOL	
X	7.001		7.000	0.005	0.005	0.001	0.000	
<b>#</b> MM LOC105 - LINS_C_1_9								
AX	MEAS		NOMINAL	+TOL	-TOL	DEV	OUTTOL	
X	8.001		8.000	0.005	0.005	0.001	0.000	
<b>#</b> MM LOC106 - LINS_C_1_10								
AX	MEAS		NOMINAL	+TOL	-TOL	DEV	OUTTOL	
X	9.002		9.000	0.005	0.005	0.001	0.000	
<b>#</b> MM LOC107 - LINS_C_1_11								
AX	MEAS		NOMINAL	+TOL	-TOL	DEV	OUTTOL	
X	10.002		10.000	0.005	0.005	0.002	0.000	

## Appendix D Images and topologies

### D.1 Mitutoyo SFM 001

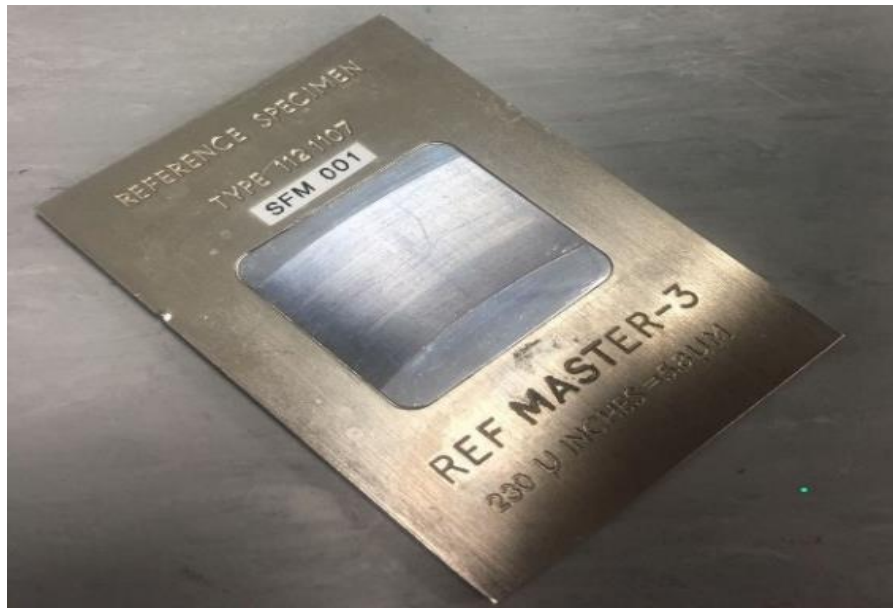


Figure D.1.1 Image from camera

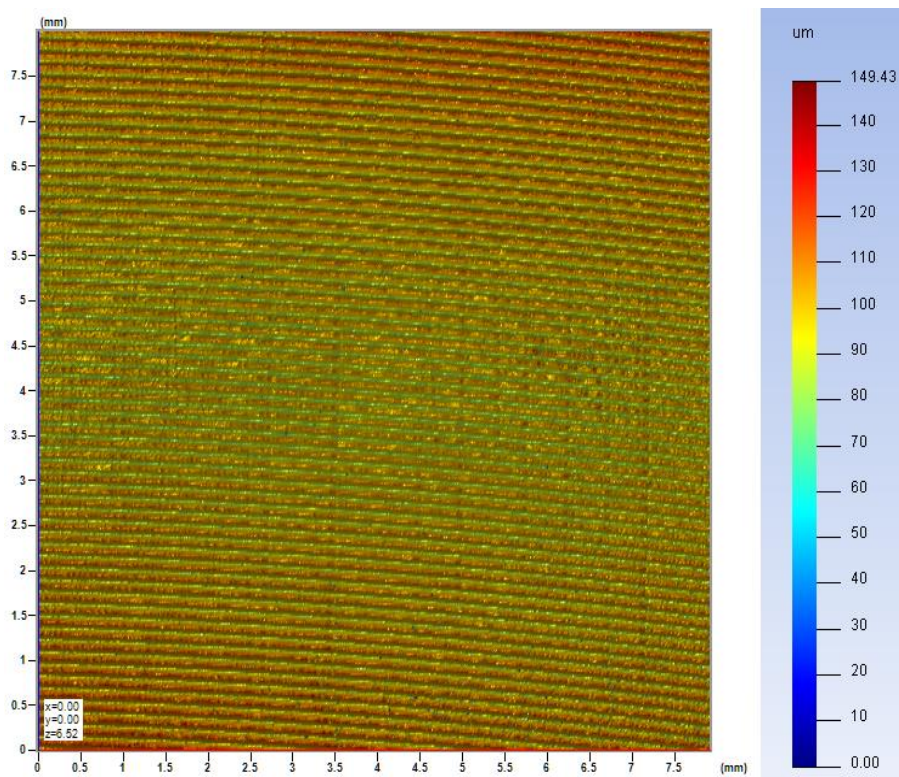
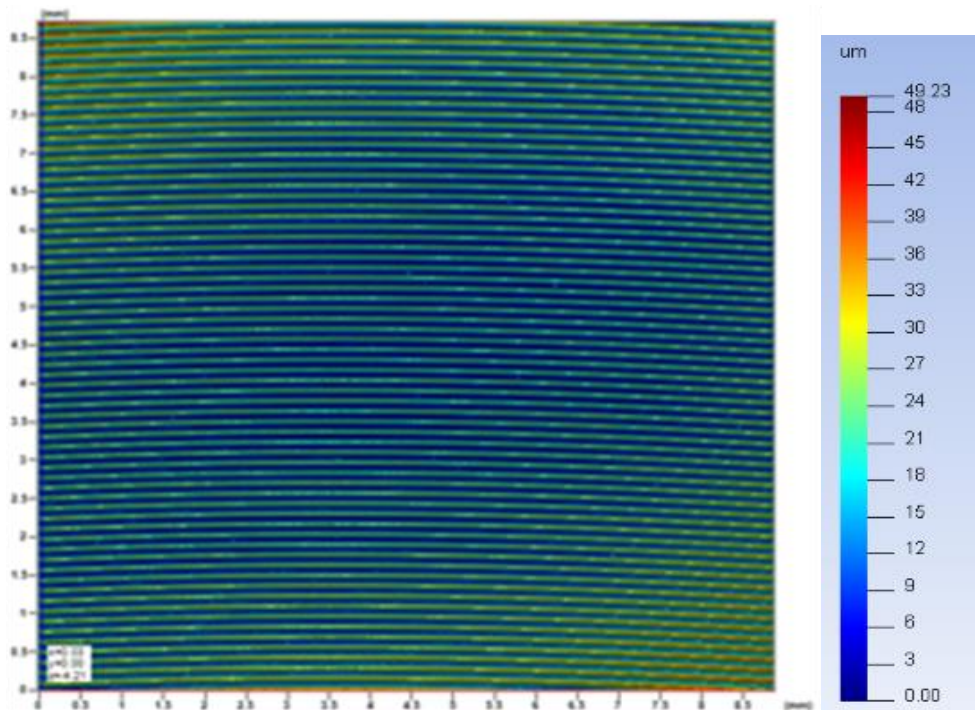
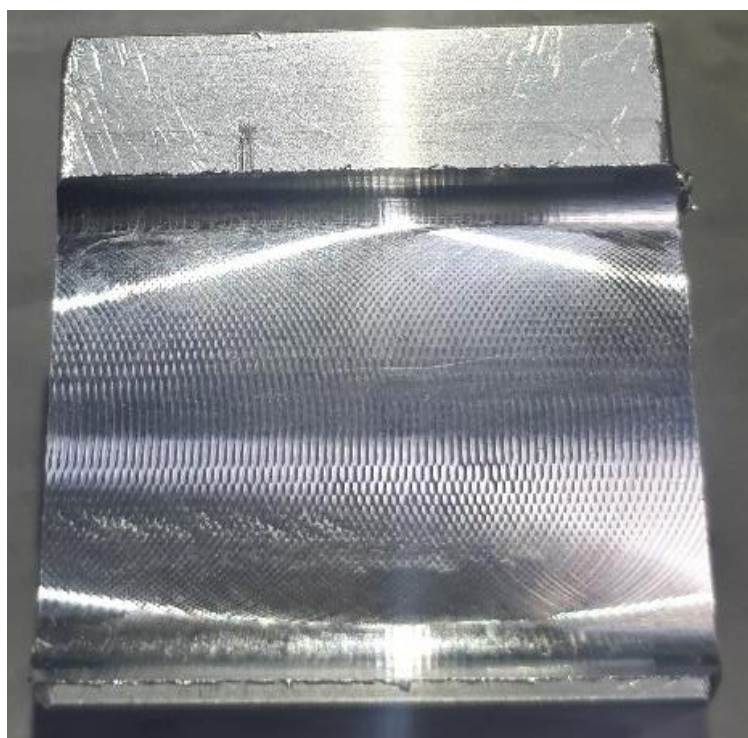


Figure D.1.2 Topology from MDS



**Figure D.1.3** Topology from Alicona

## D.2 Rough sample face milled surface



**Figure D.2.1** Image from camera

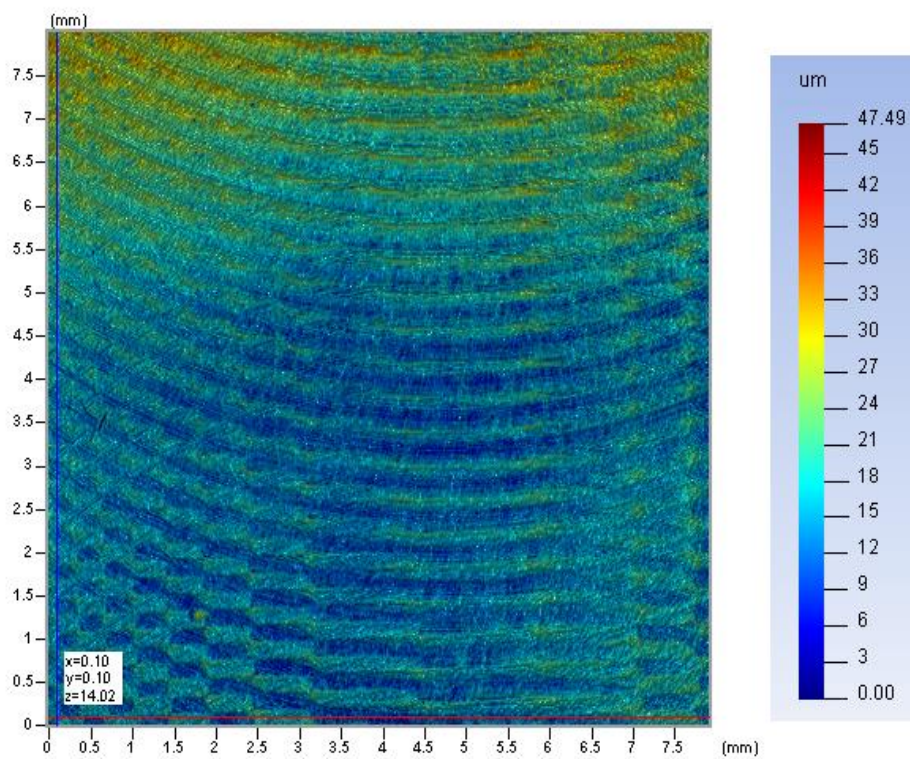


**Figure D.2.2** Topology from MDS

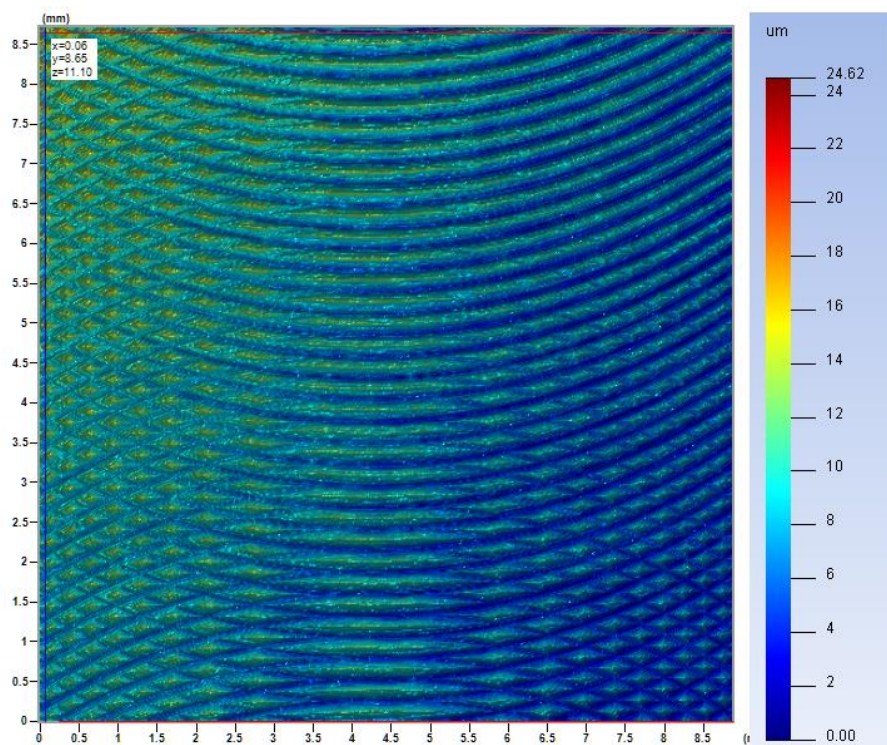


**Figure D.2.3** Topology from Alicona

### D.3 Smooth sample face milled surface

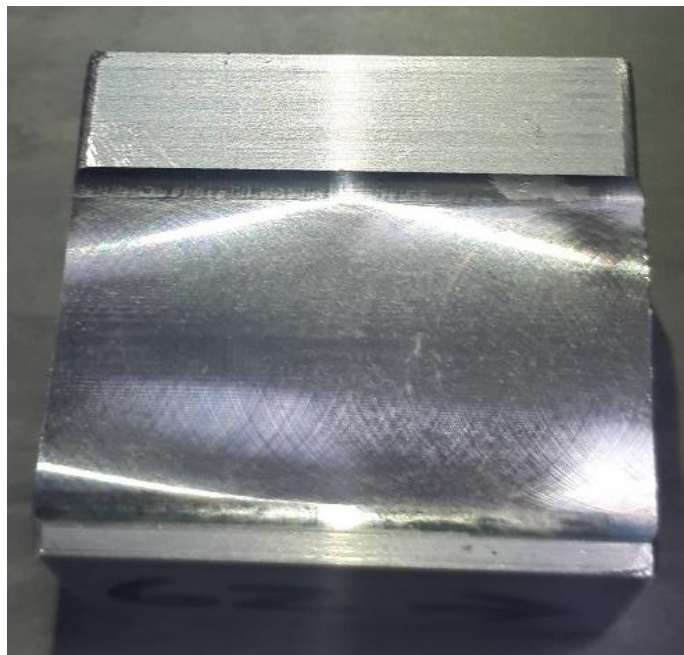


**Figure D.3.1** Image from camera

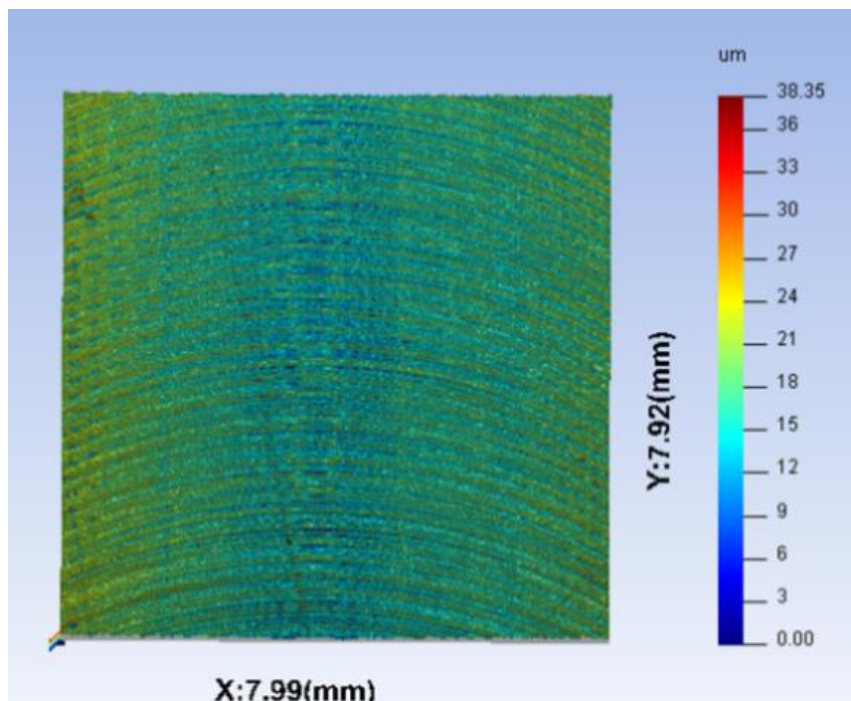


**Figure D.3.2** Topology from MDS

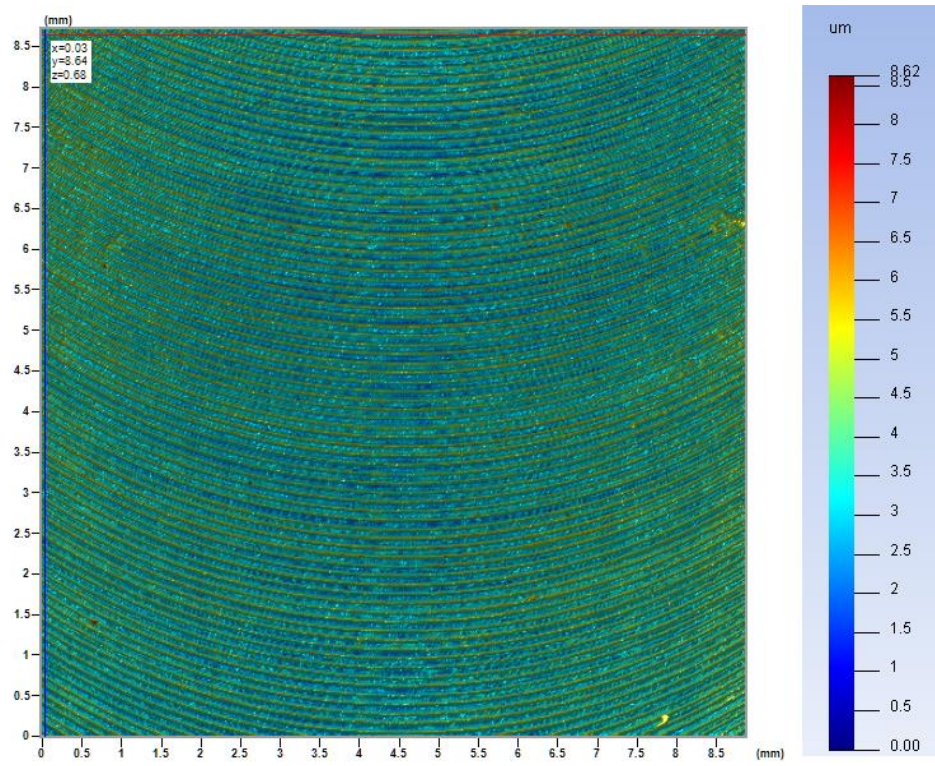


**Figure D.3.3**

Topology from Alicona

**Appendix E****Cross-correlation table**

Table E.1: Average and standard deviation method

	<b>Parameters</b>	<b>Mean, <math>\mu^R</math></b>	<b>Standard Deviation, <math>\sigma^R</math></b>	<b>95% Confidence Interval for Rough samples</b>	<b>Mean, <math>\mu^F</math></b>	<b>Standard Deviation, <math>\sigma^F</math></b>	<b>95% Confidence Interval for fine Samples</b>
1	Sq( $\mu\text{m}$ )	2.83	0.04	$\pm 0.07$	0.36	0.02	$\pm 0.03$
2	Ssk	0.20	0.15	$\pm 0.29$	-0.37	0.13	$\pm 0.26$
3	Sku	2.30	0.07	$\pm 0.15$	3.70	0.15	$\pm 0.30$
4	Sp( $\mu\text{m}$ )	8.40	0.26	$\pm 0.52$	1.72	0.27	$\pm 0.55$
5	Sv( $\mu\text{m}$ )	5.67	0.15	$\pm 0.30$	1.58	0.07	$\pm 0.14$
6	Sz( $\mu\text{m}$ )	14.07	0.35	$\pm 0.69$	3.30	0.27	$\pm 0.54$
7	Sds( $\text{mm}^{-2}$ )	287.63	263.65	$\pm 527.30$	5071.75	1312.83	$\pm 2625.66$
8	Str	0.08	0.06	$\pm 0.11$	0.08	0.01	$\pm 0.03$
9	Sal( $\text{mm}$ )	0.12	0.004	$\pm 0.007$	0.03	0.002	$\pm 0.004$
10	Sdq	0.05	0.001	$\pm 0.002$	0.08	0.01	$\pm 0.02$
11	Ssc( $\mu\text{m}^{-1}$ )	0.009	0.0006	$\pm 0.001$	0.07	0.03	$\pm 0.06$
12	Sdr(%)	0.14	0.003	$\pm 0.005$	0.37	0.10	$\pm 0.21$
13	Vmp( $10^3 \mu\text{m}^3/\text{mm}^2$ )	61.41	5.27	$\pm 10.55$	14.38	2.48	$\pm 4.96$
14	Vmc( $10^4 \mu\text{m}^3/\text{mm}^2$ )	155.10	6.81	$\pm 13.63$	30.54	1.61	$\pm 3.22$
15	Vvc( $10^4 \mu\text{m}^3/\text{mm}^2$ )	187.96	4.49	$\pm 8.97$	39.86	1.71	$\pm 3.42$
16	Vvv( $10^3 \mu\text{m}^3/\text{mm}^2$ )	62.92	10.30	$\pm 20.60$	46.84	1.24	$\pm 2.48$
17	Spk( $\mu\text{m}$ )	2.52	0.13	$\pm 0.26$	0.28	0.05	$\pm 0.10$
18	Sk( $\mu\text{m}$ )	6.70	0.7	$\pm 1.40$	0.90	0.05	$\pm 0.09$
19	Svk( $\mu\text{m}$ )	1.73	0.84	$\pm 1.67$	0.49	0.04	$\pm 0.07$
20	Smr1(%)	9.93	1.00	$\pm 2.00$	8.23	0.54	$\pm 1.09$
21	Smr2(%)	78.20	7.28	$\pm 14.56$	90.20	0.68	$\pm 1.37$
22	Std(deg)	0.00	0.00	0.00	-3.00	6.00	$\pm 12.00$
23	S5z( $\mu\text{m}$ )	13.14	0.37	$\pm 0.73$	3.20	0.25	$\pm 0.50$

**Appendix F*****Cutting Parameters, corresponding surface Roughness, and Their S/N***

	Speed (RPM)	Feed (mm/sec)	DOC (mm)	Sq ( $\mu\text{m}$ )	Sal ( $\mu\text{m}$ )	Sa ( $\mu\text{m}$ )	S/N-Sq	S/N-Sal	S/N-Sa
1	4000.00	750.00	0.20	0.61	0.022	0.46	4.29	33.11	6.74
2	4000.00	1165.00	0.70	1.67	0.097	1.00	-4.45	20.23	0.00
3	4000.00	1580.00	1.20	1.67	0.126	1.10	-4.45	18.03	-0.83
4	4000.00	2000.00	1.70	2.28	0.196	0.94	-7.16	14.17	0.54
5	5300.00	750.00	0.70	0.49	0.065	0.41	6.20	23.70	7.74
6	5300.00	1165.00	0.20	0.71	0.144	0.52	2.97	16.83	5.68
7	5300.00	1580.00	1.70	1.24	0.172	0.34	-1.87	15.31	9.37
8	5300.00	2000.00	1.20	2.09	0.240	1.31	-6.40	12.39	-2.35
9	6600.00	750.00	1.20	0.83	0.110	0.58	1.62	19.18	4.73
10	6600.00	1165.00	1.70	1.51	0.187	0.50	-3.58	14.58	6.02
11	6600.00	1580.00	0.20	1.21	0.212	0.68	-1.66	13.48	3.35
12	6600.00	2000.00	0.70	1.72	0.282	0.95	-4.71	10.99	0.45
13	8000.00	750.00	1.70	0.72	0.154	0.50	2.85	16.27	6.02
14	8000.00	1165.00	1.20	0.83	0.234	0.68	1.62	12.62	3.35
15	8000.00	1580.00	0.70	0.61	0.263	0.47	4.29	11.61	6.56
16	8000.00	2000.00	0.20	1.00	0.331	0.65	0.00	9.59	3.74